

Lignin-based nanoparticles with antibacterial properties and their nanocomposite materials for wound healing

Angela Gala Morena Gatus



UNIVERSITAT POLITÈCNICA
DE CATALUNYA
BARCELONATECH



UNIVERSITAT POLITÈCNICA DE CATALUNYA
BARCELONATECH

Departament d'Enginyeria Química

Lignin-based nanoparticles with antibacterial properties and their nanocomposite materials for wound healing

Angela Gala Morena Gatius

This thesis is submitted in fulfilment of the requirements for the degree of

Doctor of Philosophy

at the

Universitat Politècnica de Catalunya

Supervised by Prof. Tzanko Tzanov

Grup de Biotecnologia Molecular i Industrial

Departament d'Enginyeria Química

Programa de Doctorat de Polímers i Biopolímers

Universitat Politècnica de Catalunya

This thesis has been financially supported by:

PhD Grant (2019FI_B 01004) *Agència de Gestió d'Ajuts Universitaris i de Recerca* (AGAUR) of the *Generalitat of Catalunya*



European Project *Reinvent* H2020-BBI-JTI-2017 (Bio-Based Industries), Grant Agreement Number 792049



Molecular and Industrial Biotechnology Group (GBMI)



Abstract

Abstract

Lignocellulosic biomass is an abundant renewable resource considered a suitable carbon raw material for the synthesis of chemicals¹ and as an alternative to fossil fuels energy supply source.² Cellulose, hemicellulose, and lignin are the primary components of lignocellulosic biomass, among which lignin, the most abundant aromatic molecule on earth, represents from 15 to 30 % of its dry mass in woody plants.^{3,4} Lignin has been traditionally considered a low value by-product from paper manufacturing. Around 70 million tons of lignin are generated annually from the pulp and paper industry,⁵ whereof only 2–5 % is reused in its macromolecular form.⁶ Its underutilization is mainly caused by its heterogeneous molecular structure, which highly depends on the extraction and purification methods, and its low compatibility with polymeric matrices in composite production. In recent years, the potential of lignin for the synthesis of value-added materials has been considered in various fields. Lignin features multiple functionalities, including aromatic and aliphatic hydroxyl groups, providing antibacterial, antioxidant, and ultraviolet (UV)-blocking capacities, in addition to carboxylic, carbonyl, and methoxyl groups.^{6,7} Nanotransformation of lignin yields nano-entities with higher reactivity compared to their bulk counterparts, which inclusion in composites endows them with enhanced mechanical properties and bioactivities.⁸ Nano-formulation of lignin is an emerging valorization approach, yielding lignin nanoparticles (LigNPs) that have been used as mechanical reinforcement in polymeric matrices,⁹ as UV absorbers,¹⁰ as antibacterial and antioxidant agents in food packaging,¹¹ and as carriers for drug delivery.¹² The increasing interest in LigNPs is reflected in the numerous recent reviews addressing the bioactivities of macromolecular lignin^{13,14} in biomedical applications,¹⁵ the methods for the synthesis of LigNPs^{16–21} and their different applications,^{22–26} and the combination of lignin with other materials or actives to obtain hybrid nanocomposites.²⁷

In light of the rapid surge of antimicrobial resistance (AMR), driven by the misuse and overuse of antibiotics, research has been focused on developing novel antimicrobials for substituting conventional antibiotics. The use of LigNPs as antibacterial agents is a suitable alternative to traditional antibiotics owing to their

antibacterial properties and their biocompatibility, coupled to additional bioactivities such as antioxidant and UV-blocking.

The present thesis aims to develop novel antibiotic-free, lignin-based NPs with antibacterial properties for biomedical applications. To achieve this, different hybrid LigNPs have been designed by combining the biopolymer with metals, metalloids, and natural phenolic compounds. Such particles were used as active and structural elements in materials for biomedical uses, especially for chronic wound treatment.

The first chapter of the thesis describes the preparation of silver/phenolated lignin NPs (AgPheLigNPs), tellurium lignin NPs (TeLigNPs), and phenolated lignin NPs (PheLigNPs) that have been synthesized using high-intensity ultrasound and/or enzymatic functionalization. The antibacterial properties against medically-relevant Gram-positive and Gram-negative strains, the biocompatibility toward human cells, and the mechanism of action of the NPs were studied.

In the second chapter of the thesis, the preparation of active materials for wound healing with incorporated lignin-based NPs is described. In particular, AgPheLigNPs were used as active fillers in soft polyurethane foams, while PheLigNPs were used as both active and structural agents for preparing hydrogels based on silk fibroin and thiolated hyaluronic acid. The AgPheLigNPs incorporated in the foams are expected to be a part of the material's structure through covalent immobilization, whereas in the second case they are driving elements for self-assembling *via* non-covalent interactions. The potential of these materials as wound dressings was assessed by measuring their antibacterial and antioxidant capacity, ability to inhibit deleterious wound enzymes, and capacity to absorb exudates.

Resum

La biomassa lignocel·lulòsica és un recurs renovable abundant considerat com una font de carboni adequada per a la síntesis productes químics¹ i com a alternativa als combustibles fòssils per proveir energia.² La cel·lulosa, l'hemicel·lulosa i la lignina són els components primaris de la biomassa lignocel·lulòsica. La lignina és la molècula aromàtica més abundant al planeta i representa un 15–30 % del pes sec en les plantes llenyoses.^{3,4} Tradicionalment, la lignina s'ha considerat un subproducte de baix valor resultant de la indústria de la pasta i del paper.⁵ Cada any es generen al voltant de 70 milions de tones de lignina com a conseqüència de l'activitat de la indústria paperera, i només un 2–5 % es reutilitza en la seva forma macromolecular.⁶ La seva infrautilització és causada principalment per l'heterogeneïtat de la seva estructura molecular, la qual varia en funció dels mètodes d'extracció i de purificació, i per la seva baixa compatibilitat amb matrius polimèriques en la producció de compòsits. En els últims anys, el potencial de la lignina per sintetitzar materials de valor afegit s'ha considerat en diferents camps d'aplicació. La lignina té diversos grups funcionals, d'entre els quals destaquen els grups hidroxils aromàtics i alifàtics, responsables d'aportar propietats antibacterianes, antioxidants i capacitat de bloquejar la penetració dels rajos UV, juntament amb els grups carboxil, carbonil i metoxil.^{6,7} La nanotransformació de la lignina resulta en nanopartícules (NPs) amb una reactivitat més elevada que el seu homòleg macroscòpic, i la seva incorporació en compòsits suposa una millora de les propietats mecàniques i de les bioactivitats.⁸ La nanoformulació és una via emergent per valoritzar la lignina en la qual les nanopartícules de lignina (LigNPs) resultants ja s'han utilitzat com a reforç mecànic en matrius polimèriques,⁹ com a absorbents de la radiació UV,¹⁰ com a agents antioxidants i antibacterians en envasos d'ús alimentari¹¹ i com a portadors per al lliurament de fàrmacs.¹² El creixent interès en les LigNPs es reflecteix en els nombrosos articles de revisió sobre les bioactivitats de lignina macromolecular en aplicacions biomèdiques,^{13–15} els mètodes per a la síntesi de LigNPs^{16–21} i les seves diferents aplicacions,^{22–26} i la combinació de lignina amb altres materials o agents actius per obtenir nanocompòsits híbrids.²⁷

Considerant el ràpid augment de la resistència antimicrobiana (AMR), impulsat per l'excessiu i incorrecte ús d'antibiòtics, el focus de la recerca s'ha centrat en el desenvolupament de nous agents antimicrobians per substituir els antibiòtics convencionals. L'ús de les LigNPs com a agents antibacterians és una alternativa adequada als antibiòtics tradicionals gràcies a les seves propietats antibacterianes i la seva biocompatibilitat, juntament amb altres bioactivitats com l'antioxidant i la capacitat de bloquejar els rajos UV.

Aquesta tesi pretén desenvolupar noves NPs basades en lignina sense antibiòtics i amb propietats antibacterianes per a aplicacions biomèdiques. Per aconseguir-ho, diferents LigNPs híbrides han estat dissenyades combinant la lignina amb metalls, metal·loides i compostos fenòlics naturals. Aquestes partícules s'han utilitzat com a elements actius i estructurals en materials per a usos biomèdics, concretament pel tractament de ferides cròniques.

El primer capítol de la tesi descriu la preparació de NPs de plata i lignina fenolada (AgPheLigNPs), de NPs de lignina i tel·luri (TeLigNPs), i de NPs de lignina fenolada (PheLigNPs) les quals s'han sintetitzat mitjançant la funcionalització amb ultrasons i/o enzimàtica. Es van estudiar les propietats antibacterianes contra soques grampositives i gramnegatives rellevants en la medicina, la biocompatibilitat cap a les cèl·lules humanes i el mecanisme d'acció de les NPs.

En el segon capítol de la tesi es descriu la preparació de materials actius per a la curació de ferides que incorporen les NPs basades en lignina a la seva formulació. Concretament, les AgPheLigNPs s'han utilitzat com a additius funcionals en escumes flexibles de poliuretà, mentre que les PheLigNPs s'han utilitzat com a agents actius i d'entrecreuament per preparar hidrogels basats en fibroïna de seda i àcid hialurònic tiolat. S'espera que les AgPheLigNPs incorporades a les escumes de poliuretà siguin una part de l'estructura del material a través de la immobilització covalent, mentre que en el segon cas són elements que condueixen a l'autoassemblatge dels polímers a través d'interaccions no covalents. El potencial d'aquests materials per al tractament de ferides es va avaluar mesurant la seva capacitat antibacteriana i antioxidant, l'habilitat d'inhibir certs enzims perjudicials present en les ferides i la capacitat d'absorbir exsudats.

Contents

Abstract	i
Contents	1
Abbreviation list.....	5
Introduction	11
Occurrence, structure, extraction, and bioactivities of lignin.....	11
Lignin in plants.....	11
Lignin structure and biosynthesis.....	11
Technical lignins and extraction methods	14
Bioactivities of lignin.....	16
Lignin in antibacterial nanoformulations.....	17
Lignin as an antibacterial agent in nanoformulations.....	17
Lignin as a reducing and capping agent of metal and metal oxide NPs	22
Lignin nanocarriers.....	29
Antibacterial composite materials containing lignin NPs.....	35
Food packaging	37
Biomedical applications	41
Coatings.....	43
Wound healing	44
Objectives.....	51
Chapter 1. Antibacterial lignin-based NPs.....	56
Introduction.....	56
Materials and methods	58
Reagents, cells, and enzymes	58
Characterization of laccase.....	59
Synthesis of AgPheLigNPs.....	60
Synthesis of TeLigNPs.....	60
Synthesis of PheLigNPs and LigNPs.....	61
Characterization of the lignin-based NPs.....	61
Phenolic content	61
Hydrodynamic size, polydispersity index and ζ -potential.....	62
FTIR spectra.....	62
UV-vis absorbance scan.....	62

Growth inhibition of bacteria by the lignin-based NPs	63
Cytotoxicity assay	64
Generation of ROS by bacteria and human cells treated with lignin NPs	65
TEM of bacterial samples incubated with lignin-based NPs.....	66
Interaction of lignin-based NPs with bacteria assessed by SEM.....	66
Interaction of lignin-based NPs with bacteria assessed by QCM	66
Interaction of NPs with model membranes assessed by Langmuir isotherms	67
Determination of membrane integrity by fluorescence imaging.....	68
Resistance development assay.....	69
Data analysis	69
Results and discussion	70
Silver phenolated lignin nanoparticles.....	70
AgPheLigNPs synthesis and characterization	70
Antibacterial properties of AgPheLigNPs.....	72
<i>In vitro</i> cytotoxicity assessment of AgPheLigNPs	73
Tellurium lignin nanoparticles	75
TeLigNPs synthesis and characterization	75
Antibacterial activity of TeLigNPs	77
<i>In vitro</i> cytotoxicity assessment of TeLigNPs	81
Antibacterial mode of action of TeLigNPs.....	82
Phenolated lignin nanoparticles.....	85
Synthesis and characterization of PheLigNPs	85
Antibacterial activity of PheLigNPs.....	88
<i>In vitro</i> cytotoxicity assessment of PheLigNPs.....	90
Antibacterial mechanism of action of PheLigNPs	91
Resistance development of PheLigNPs by bacteria	97
Chapter 2. Lignin-based NPs in composite materials for wound healing.....	101
Introduction.....	101
Materials and methods	103
Reagents, cells, and enzymes	103
Preparation of polyurethane foams embedded with AgPheLigNPs.....	104
Characterization of PUFs	104
FTIR analysis of the foams	104
SEM and energy dispersive X-ray spectroscopy analysis.....	105

Mechanical properties of the foams.....	105
Swelling kinetics.....	105
Silver content and silver release from the PUFs.....	105
Antibacterial activity of PUFs.....	106
<i>Ex vivo</i> evaluation of MPO inhibition.....	106
Antioxidant activity of PUFs.....	107
<i>In vitro</i> cytotoxicity evaluation.....	107
Modification and characterization of HA.....	108
Synthesis of HA-SH/SF hydrogels.....	109
Characterization of HA-SH/SF hydrogels.....	110
Rheological characterization.....	110
Cryogenic Scanning Electron Microscopy (Cryo-SEM).....	110
Swelling capacity.....	110
Stability in PBS.....	111
pH responsiveness of the hydrogels.....	111
Biodegradability and NPs release in the presence of hyaluronidase.....	112
Antioxidant activity.....	112
Antibacterial activity.....	112
Morphology of bacterial cells.....	113
Evaluation of MPO and MMPs inhibition.....	113
Cytotoxicity toward human cells.....	114
Data analysis.....	115
Results and discussion.....	115
Antibacterial polyurethane foams with incorporated lignin-capped silver NPs for chronic wound treatment.....	115
Structural and mechanical characterization of PUFs.....	115
Swelling profiles of PUFs containing AgPheLigNPs.....	118
Silver release kinetics.....	120
Antibacterial activity of PUFs.....	121
Antioxidant property.....	122
<i>Ex vivo</i> inhibition activity of PUFs against deleterious wound enzyme.....	123
Cytotoxicity evaluation of the PUFs.....	125
Nano-enabled hydrogels self-assembled with phenolated lignin NPs.....	126
Synthesis of Self-assembling HA-SH/SF_PheLigNPs hydrogels.....	126

Rheological properties of HA-SH/SF_PheLigNPs hydrogels	129
Swelling capacity	132
Stability of the hydrogels	133
Release of PheLigNPs and hydrogel stability in response to the pH and hyaluronidase	134
Multiple features of the hydrogels for promoting wound healing	137
Cytotoxicity evaluation of the hydrogels	141
General discussion	144
Conclusions.....	151
Bibliography.....	156
Annex	182
Supplementary information of Chapter 1	182
Supplementary information of Chapter 2	184
Scientific contribution.....	186

Abbreviation list

	3iT	3-interval thixotropic test
A	<i>A. baumannii</i>	<i>Aspergillus baumannii</i>
	<i>A. fumigatus</i>	<i>Aspergillus fumigatus</i>
	<i>A. niger</i>	<i>Aspergillus niger</i>
	<i>A. penicilloides</i>	<i>Aspergillus penicilloides</i>
	AA	acrylic acid
	ADH	adipic acid dihydrazide
	AcLi	acetylated lignin
	AgCLPs	silver colloidal lignin particles
	AgLigNPs	silver lignin nanoparticle
	AgNO ₃	silver nitrate
	AgNPs	silver nanoparticles
	AgPheLigNPs	silver phenolated lignin nanoparticles
	AL	alkali-extracted lignin
	aLNP	acetylated LigNPs
	AML	amphoteric lignin
	AMR	antimicrobial resistance
	ANOVA	analysis of variance
APS	ammonium persulfate	
ATCC	American type culture collection	
ATP	adenosine triphosphate	
ATR	attenuated total reflection	
B	<i>B. cereus</i>	<i>Bacillus cereus</i>
	<i>B. circulans</i>	<i>Bacillus circulans</i>
	<i>B. megaterium</i>	<i>Bacillus megaterium</i>
	<i>B. subtilis</i>	<i>Bacillus subtilis</i>
C	<i>C. albicans</i>	<i>Candida albicans</i>
	<i>C. coronatus</i>	<i>Conidiobolus coronatus</i>
	<i>C. diphtheriae</i>	<i>Corynebacterium diphtheriae</i>
	CA	cellulose acetate
	CA	citric acid
	caLNP	citric acid-treated LigNPs
	CEL	cellulolytic enzyme lignin
	CFU	colony forming unit
	CLPs	colloidal lignin particles
	CNC	cellulose nanocrystals
	CNF	cellulose nanofibrils
	CryoSEM	cryogenic scanning electron microscopy
	CS	chitosan

D	DABCO	1,4-diazabicyclo(2.2.2)octane
	DES	deep eutectic solvents
	DLS	dynamic light scattering
	DMEM	Dulbecco's modified Eagle's medium
	DNA	deoxyribonucleic acid
	DPPH	2,2-diphenyl-1-picrylhydrazyl
E	<i>E. casseliflavus</i>	<i>Enterococcus casseliflavus</i>
	<i>E. coli</i>	<i>Escherichia coli</i>
	<i>E. faecalis</i>	<i>Enterococcus faecalis</i>
	ECM	extracellular matrix
	EDC	N-(3-dimethylaminopropyl)-N'-ethylcarbodiimide
	EDX	energy dispersive X-ray diffraction
	EE	encapsulation efficiency
	EFSA	European Food Safety Authority
F	FDA	Food and Drug Administration
	FESEM	field emission scanning electron microscopy
	FITC	fluorescein isothiocyanate
	FTIR	Fourier-transform infrared
G	GA	gallic acid
	GAE	gallic acid equivalents
	GS	gentamicin sulfate
	GVL	γ -valerolactone
	GWBS	γ -valerolactone/water binary solvent
H	HA	hyaluronic acid
	HA-ADH	hyaluronic acid modified with adipic acid dihydrazide
	HAADF	high-angle annular dark field
	HA-SH	thiolated hyaluronic acid
K	<i>K. pneumoniae</i>	<i>Klebsiella pneumoniae</i>
L	<i>L. monocytogenes</i>	<i>Listeria monocytogenes</i>
	LB	Luria Bertani
	LCSN	lignin-coated silver nanoparticles
	LED	light emitting diode
	Lig	lignin
	LigNPs	lignin nanoparticles
	LNP	lignin nanoparticle
	LNSR	lignin nanospray
	LPUF	lignin-based polyurethane foam
	LS	lignosulfonate

M	<i>M. abscessus</i>	<i>Mycobacterium abscessus</i>
	<i>M. cookei</i>	<i>Microsporium cookei</i>
	<i>M. luteus</i>	<i>Micrococcus luteus</i>
	MDI	4,4'-methylenebis(phenyl isocyanate)
	MDR	multi-drug resistant
	MHB	Mueller Hinton Broth
	MIC	minimum inhibitory concentration
	MMPs	matrix metalloproteinases
	MPO	myeloperoxidase
	MRSA	methicillin-resistant <i>Staphylococcus aureus</i>
MWL	milled wood lignin	
N	NB	nutrient broth
	n-LCSN	nanolignin-coated silver nanoparticles
	NMR	nuclear magnetic resonance
	NPs	nanoparticles
O	OD	optical density
P	<i>P. aeruginosa</i>	<i>Pseudomonas aeruginosa</i>
	<i>P. carotovorum</i>	<i>Pectobacterium carotovorum</i>
	<i>P. italicum</i>	<i>Penicillium italicum</i>
	<i>P. syringae</i>	<i>Pseudomonas syringae</i>
	P(AAm-co-AA)	poly(acrylamide-co-acrylic acid)
	PAA	poly(acrylic acid)
	PAHC	phenylboronic acid-modified hydroxypropyl cellulose
	PAN	polyacrylonitrile
	PANI-LIG	polyaniline grafted lignin
	PBS	phosphate buffered saline
	PDI	polydispersity index
	PE	phosphatidylethanolamine
	PEG	poly(ethylene glycol)
	PEG-DGE	poly(ethylene glycol) diglycidyl ether
	PG	phosphatidylglycerol
	PheLig	phenolated lignin
	PheLig NPs	phenolated lignin nanoparticles
	PI	propidium iodide
	PLA	poly(lactic acid)
	PNMA	poly(N-me-thylaniline)
	PPy-PDa	polypyrrole glutinous nanofibrils crosslinked with dopamine
PU	polyurethane	
PUF	polyurethane foam	
PVA	poly(vinyl alcohol)	
Q	QAL	quaternized alkali lignin
	QCM-D	quartz crystal microbalance with dissipation

R	<i>R. eutropha</i>	<i>Ralstonia eutropha</i>
	<i>R. ornithinolytica</i>	<i>Raoultella ornithinolytica</i>
	ROS	reactive oxygen species
S	<i>S. aureus</i>	<i>Staphylococcus aureus</i>
	<i>S. enterica</i>	<i>Salmonella enterica</i>
	<i>S. epidermidis</i>	<i>Staphylococcus epidermidis</i>
	<i>S. equi</i>	<i>Streptococcus equi</i>
	<i>S. haemolyticus</i>	<i>Streptococcus haemolyticus</i>
	<i>S. paratyphi</i>	<i>Salmonella paratyphi</i>
	<i>S. typhimurium</i>	<i>Salmonella typhimurium</i>
	SD	standard deviation
	SDS	sodium dodecyl sulfate
	SEM	scanning electron microscopy
	SESC	simultaneous enzymatic saccharification and communitation
SF	silk fibroin	
STEM	scanning transmission electron microscopy	
T	TA	tannic acid
	TEAC	Trolox equivalent antioxidant capacity
	TeLig NPs	tellurium lignin nanoparticles
	TEM	transmission electron microscopy
	THPP	5,10,15,20-tetrakis (4-hydroxyphenyl)-21H,23H- porphine
TNBSA	2,4,6-trinitrobenzenesulfonic acid	
U	US	ultrasound
	UV	ultraviolet
W	WPU	waterborne polyurethane
X	<i>X. arboricola</i>	<i>Xanthomonas arboricola</i>
	<i>X. axonopodis</i>	<i>Xanthomonas axonopodis</i>
Z	ZnO	zinc oxide
	ZOI	zone of inhibition

Introduction

This section is based on the following publication:

Morena A G, Tzanov T. “Antibacterial lignin-based nanoparticles and their use in composite materials”. *Nanoscale Advances*, 2022, doi: 10.1039/d2na00423b



Introduction

Occurrence, structure, extraction, and bioactivities of lignin

Lignin in plants

Lignin is found in the secondary cell wall and in the middle lamella of vascular plants.²⁸ Lignin and hemicellulose encase the cellulose fibrils, providing mechanical support to the plant and allowing water conduction (**Figure 1**). Besides its structural role, the polyphenolic composition of lignin and its hydrophobic nature ensure the resistance of plants to biological and chemical degradation,²⁹ and assists in their defense against pathogens.³⁰

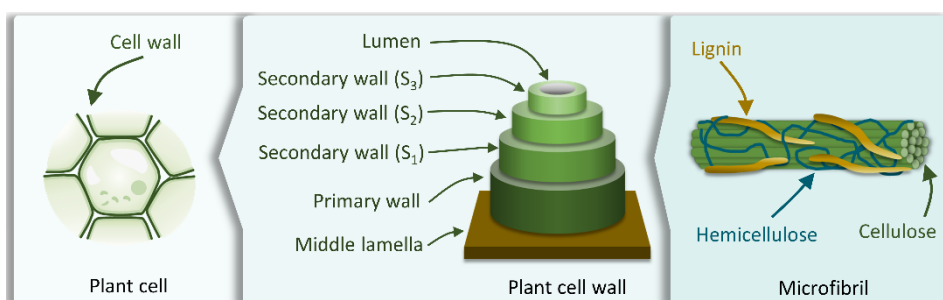


Figure 1. Schematic representation of the cellular plant structure, comprising plant cell, cell wall, and microfibrils. Adapted from Ref. 22.

The content of lignin differs between plants and varies depending on the tissue, location in the cell, and the environmental conditions. For instance, hardwood and softwood plants are lignin-rich, containing 16–24 and 25–31 % of lignin, respectively, while herbaceous plants such as hemp and cotton present low contents of this polymer (~6 %). The major component of coir fibers in coconut husk is lignin (43–49 %), in contrast to lower amounts found in other parts of the plant.⁴

Lignin structure and biosynthesis

The chemical structure, molecular weight, functional groups, and properties of lignin highly depend on the origin and the extraction method. The complex nature and low solubility of native lignin provoke inherent difficulties in its

analysis, which hampers the development of an accurate structural model.³¹ Lignins isolated by enzymatic digestion (cellulolytic enzyme lignin, CEL), and by ball milling (milled wood lignin, MWL) followed by dioxane extraction are considered the most representative of native lignins since these processes minimize the structural changes and increase the solubility of the molecule.³²

The structure of lignin has been studied through numerous techniques, including nuclear magnetic resonance (NMR) spectroscopy, Fourier-transform infrared (FTIR) spectroscopy, Raman spectroscopy, and X-ray photoelectron spectroscopy.^{33,34} It is generally accepted that lignin is a three-dimensional, highly branched, amorphous molecule composed of three basic phenylpropanoid units: p-hydroxyphenyl (H), guaiacyl (G), and syringyl (S) (Figure 2).

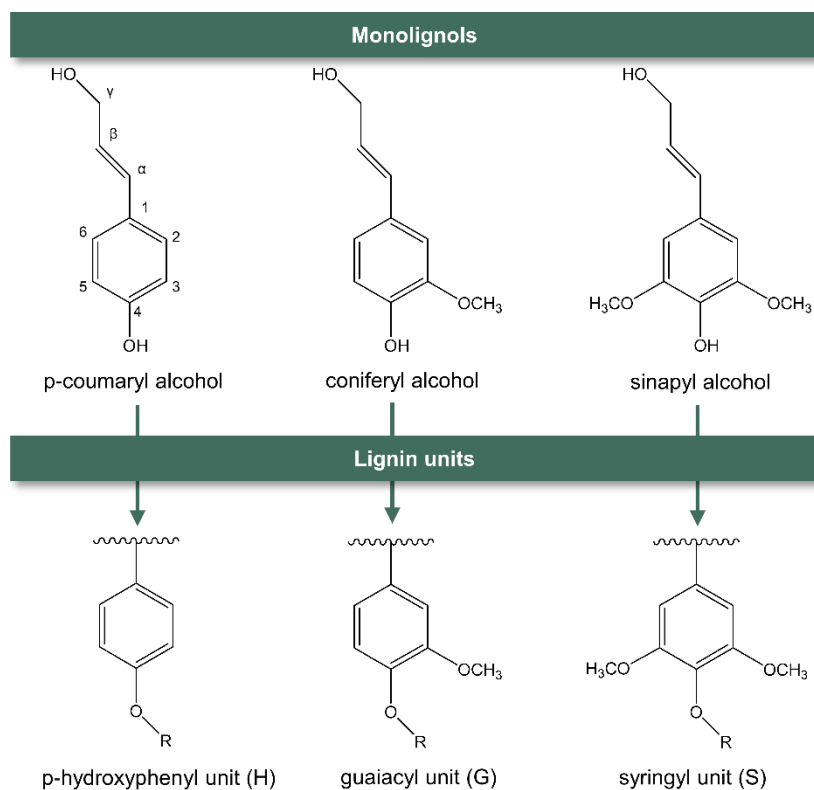


Figure 2. Representation of the main monolignols and their units in lignin.

The biosynthetic pathway of lignin stems from the radical polymerization of three main monolignols, namely p-coumaryl alcohol, conyferyl alcohol, and sinapyl alcohol (**Figure 2**), which are derived from phenylalanine and differ in their degree of methoxylation. When monolignols are oxidized by laccase or peroxidase, they form radicals which undergo coupling reactions to form dilignols through C-C and C-O linkages, such as β -O-4, β -5, and β - β bonds (**Figure 3**).^{35,36} The biosynthesis of lignin results in heterogeneous interactions with S, G, and H units, whose content differs as a function of the plant species. For instance, in softwood lignins (from gymnosperms), G units are predominant, whereas hardwood lignins (from angiosperms) comprise equal amounts of G and S units, and herbaceous lignins are constituted by all three units, being H the less abundant.³⁷ The most stable bonds are 5-5 and β -5, which occur mainly between G units since S units have more methoxylated groups that block the C-5 position of the aromatic ring. Therefore, the lignin found in gymnosperms is more recalcitrant to chemical and microbial degradation, while angiosperm lignin is more likely to be less branched which can improve its processibility.^{38,39}

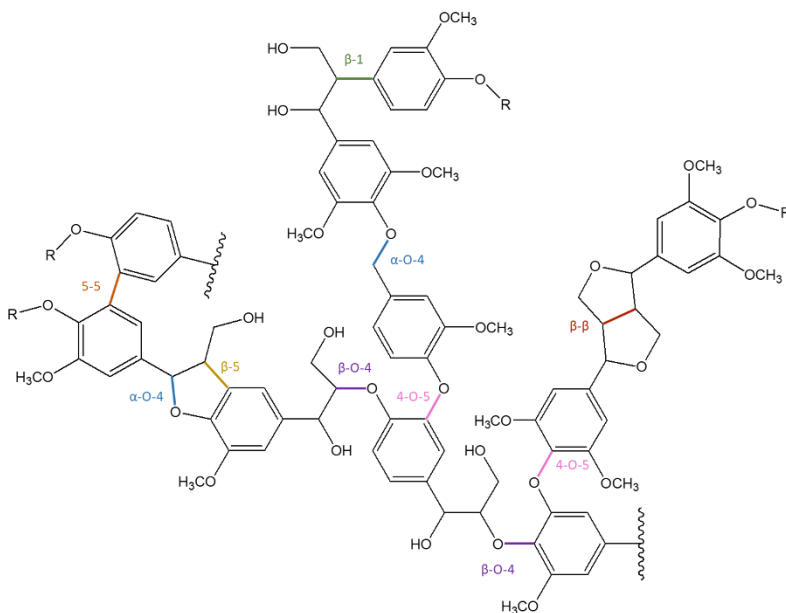


Figure 3. Lignin structure. Adapted from Refs. 299 and 37.

Technical lignins and extraction methods

Lignins extracted from biomass feedstock after chemical processing are called technical lignins. The main industrial lignin extraction methods, originated from pulp and paper processes, are Kraft pulping, soda pulping, and sulfite pulping, which yield Kraft, soda, and lignosulfonate (LS) lignin, respectively (**Figure 4**).^{40,41} The Kraft method consists in alkaline hydrolysis with sodium hydroxide and sodium sulfide at high temperatures (150–170 °C), which cleaves the bonds between lignin and cellulose, and dissolves lignin. The product resulting from this process is hydrophobic lignin containing 1–3 % sulfur in the form of aliphatic thiol groups, besides other functional groups including methoxy (14 %), aliphatic (10 %) and phenolic (2–5 %) hydroxyl, and carboxylic acid (4–7 %).^{5,42} The sulfite process involves reactions between sulfur dioxide and sulfite salts in aqueous media at 125–150 °C and acid pH. The lignin produced by this procedure is hydrophilic due to its high content in sulfonate groups (up to 13 %).⁴³ The soda process uses alkaline hydrolysis with sodium hydroxide at high temperatures (140–170 °C) in the absence of sulfur-containing molecules, yielding hydrophobic lignin. These pulping methods are widely established in the industry and produce highly pure lignin at elevated yields. However, due to the multiple chemical reactions occurring during these extraction processes, the structure of technical lignins differs significantly from that of native lignin. Partial biopolymer degradation also occurs during lignin extraction, thus decreasing its molecular weight. Moreover, harsh pH and temperature conditions are required, and toxic effluents are generated. Organosolv is another sulfur-free method that uses organic solvents such as ethanol in combination with acids and bases. This method allows the recovery of the organic solvents, while highly pure, sulfur-free lignin is obtained. The native lignin structure with β -O-4 linkages is partially preserved after the treatment.⁴⁴

Other processes that are in ways of being established in the industry are acid hydrolysis, steam explosion, enzymatic hydrolysis, and ammonia fiber expansion

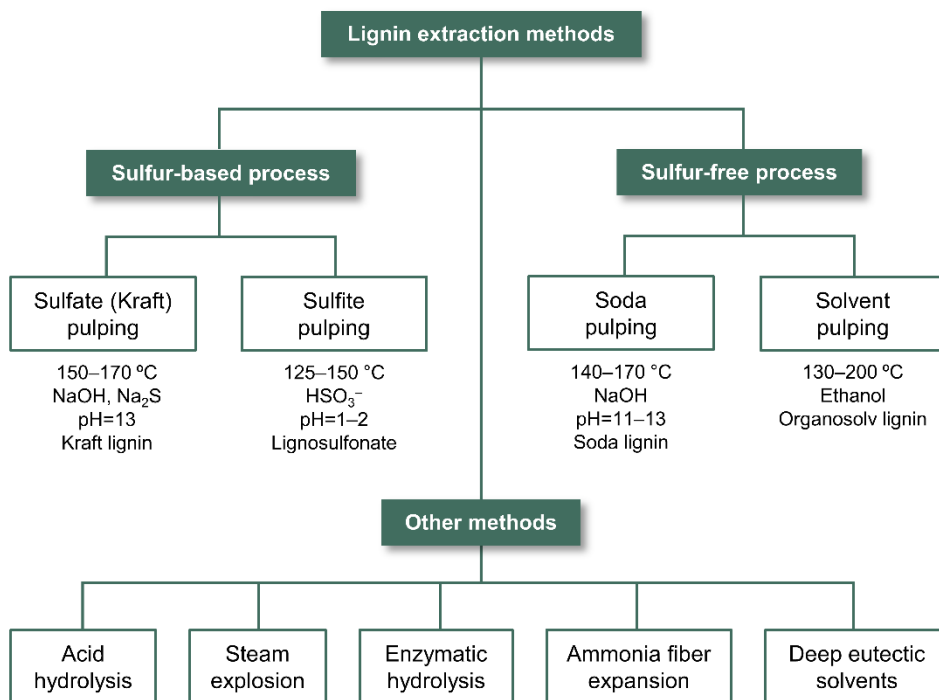


Figure 4. Lignin extraction methods. Adapted from Ref. 44.

pretreatments (**Figure 4**). Recently, emerging processes using deep eutectic solvents (DES)⁴⁵⁻⁴⁷ and biomass-derived organic solvents such as γ -valerolactone^{48,49} demonstrated potential for lignin isolation. These methods are able to preserve the lignin structure (i.e. β -O-4 and β - β linkages), while the solvents can be recovered and recycled,^{50,51} thus moving toward a sustainable biorefinery concept by decreasing the amount of toxic solvents and pollutants. Selective enzymatic hydrolysis of the biomass carbohydrates is used to purify lignin. Through this method, lignin is obtained in a quite high yield and its structure is considered to be chemically unaltered.⁵² The main drawback of this method, however, is the presence of carbohydrate and protein impurities. The properties of lignin such as molecular weight, functional groups, and solubility are important factors to be considered for the selection of a lignin type suitable for a desired application. Nevertheless, it is extremely difficult to correlate the lignin properties with the performance of the final material.²⁷

Bioactivities of lignin

Besides its structural role, native lignin also prevents the degradation of carbohydrates in plants by inhibiting the activity of bacteria and fungi. By analyzing plants with silenced genes participating in lignin biosynthesis, it has been demonstrated that the absence of lignin reduces the resistance against bacterial and fungal pathogens.³⁰ Therefore, lignin is an important plant defense against microbial pathogens. The antimicrobial effect of the lignin structure has been associated with the presence of phenolic hydroxyl and methoxy groups.⁵³ When lignin is isolated from the plant, the extraction conditions can influence its antimicrobial potential due to the differences in molecular weight, functional groups, and solubility. For example, bacterial growth inhibition has been found in Kraft lignin, while lignin extracted by simultaneous enzymatic saccharification and communitation (SESC) has not shown such inhibitory effect.¹⁴ Other works reported that lignin with isoeugenol structures possesses higher antibacterial activity than lignin with phenolic moieties containing oxygen (-OH, -CO, -COOH) in the side chain.¹⁴

The mechanism of action of lignin against bacteria has not been completely elucidated. Some studies attribute the antibacterial activity of phenolic compounds to their ability to inhibit essential enzymes by generating hydrogen peroxide and complexing with metal ions,⁵⁴ in addition to their ability to destabilize bacterial membranes.^{55,56} In the case of macromolecular lignin, it has been suggested that the phenolic hydroxyl groups promote a pH decrease around the cell, which destabilizes the membrane and eventually leads to the rupture of the cell.⁵⁷ These non-specific modes of action might reduce the possibility of resistance development in bacteria, thus contributing to overcome the antimicrobial resistance (AMR) both in biomedical and phytosanitary applications.

Besides their antibacterial effect, the phenolic moieties of lignin also confer antioxidant and UV-blocking capacities. In an oxidative stress environment, phenolic structures can act as proton donors, converting free radicals into non-

radical molecules. As a consequence, phenols convert into phenoxy radicals that can react with another free radical to form a quinone.⁵⁸ For this reason, lignin can act as a scavenger preventing the adjacent molecules from oxidation. This characteristic of lignin is of special interest in packaging to preserve the food properties, in dressing products for wound healing, and in cosmetic formulations for anti-aging.⁵⁹ On the other hand, the aromatic structures and carbonyl groups in lignin absorb visible and UV light (250–400 nm), acting as UV-blockers. Taking advantage of this property, lignin has been tested as an active ingredient in sunscreen formulations.^{60,61}

Lignin in antibacterial nanoformulations

The different roles of lignin in the synthesis of nano-enabled antibacterial agents could be outlined as: (i) an antibacterial active in the nanoformulation, (ii) a reducing and capping agent for antimicrobial metals and metal oxides, and (ii) a carrier of antibacterial agents.

Lignin as an antibacterial agent in nanoformulations

In view of the potential of lignin as an antibacterial agent, several works reported the development of LigNPs dispersions capable of inhibiting bacteria (**Table 1**). There are different methods to synthesize these particles, among which solvent displacement, acid treatment, sonochemistry, and their combinations are the most common (**Figure 5**). Solvent displacement consists in mixing an organic solvent containing solubilized lignin with an excess of water, resulting in a gradual decrease of lignin solubility which rearranges into NPs.²⁰ Solvent displacement is a versatile technique that allows accurate control of the setting conditions, hence obtaining NPs with the desired characteristics. However, the low yield of NPs (~1 wt %) limits its application, especially at large scale.¹⁹ The acid precipitation method, developed by Frangville *et al.*, consisted in adding hydrochloric acid into a solution of lignin dissolved in ethylene glycol.⁶² The method is based on initial lignin nucleation followed by particle growth from

its molecular solution, which is promoted by the gradual addition of an aqueous solution of acid.

In ultrasonication, LigNPs are formed by fractioning the large lignin macromolecule due to the cavitation phenomena.⁶³ This process, however, induces the formation of radical oxygen species that can result in lignin oxidation. The morphology and size of LigNPs vary in function of the synthetic method and the experimental settings (**Figure 5, Table 1**). Spherical particles are commonly obtained from solvent displacement methods,^{64–66} while acid treatment and ultrasonication yield irregular-shaped particles.^{63,67,68}

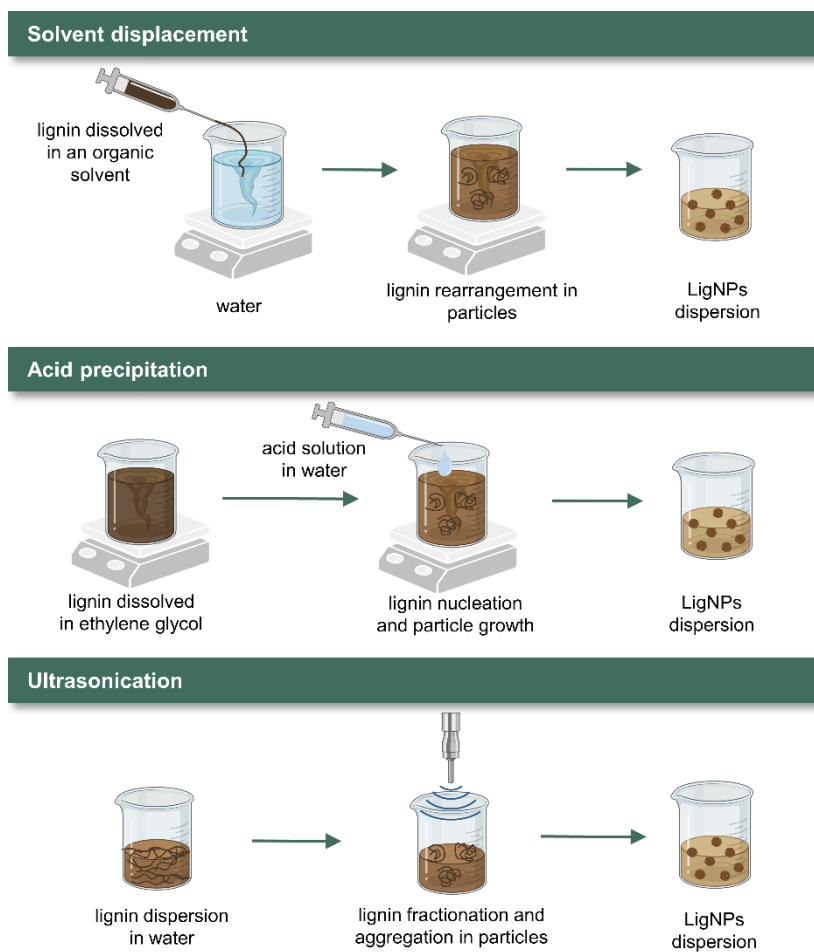


Figure 5. Schematic representation of the most common methods employed to synthesize antibacterial lignin-based nanoparticles.

Table 1 LigNPs in suspension used as antibacterial agents

Type of lignin	Preparation method	Particle shape	Particle size	Antibacterial activity	Ref.
Alkali	Acidolysis combined with sonochemistry	Irregular	33–120 nm ^{a,c}	<i>P. syringae</i> pv <i>tomato</i> , <i>X. axonopodis</i> pv <i>vesicatoria</i> , <i>X. arboricola</i> pv <i>pruni</i>)	68
Organosolv	Solvent displacement	Spherical	149–324 nm ^{b,c}	<i>E. coli</i> O157:H7, <i>S. enterica</i> Typhimurium	64
Kraft	Solvent displacement combined with sonochemistry	Spherical	122.5 nm ^a	<i>E. coli</i> , <i>B. megaterium</i>	65
Alkali, aminated	Acidolysis combined with sonochemistry	Irregular	580 nm ^a	<i>S. aureus</i>	69
LS	Ultrasonication in oil/water	N.D.	221–234 nm ^{a,c}	<i>E. coli</i> , <i>S. aureus</i> , <i>B. subtilis</i>	70

^aObtained by dynamic light scattering

^bObtained by measuring transmission electron microscopy (TEM) images

^cDepending on experimental conditions

Alkali lignin dissolved in ethylene glycol was subjected to different acidic conditions to prepare LigNPs (**Figure 6a i**).⁶⁸ The particles presented different sizes ranging from 33 to 120 nm depending on the acid treatment with HCl, H₂SO₄, or H₃PO₄. The antibacterial activity of the particles was assessed using three methodologies, namely spot diffusion assay, incorporation of lignin nanoparticles assay, and growth in broth assay. The results showed the capacity of the LigNPs to inhibit the growth and reduce the amount of viable plant pathogen Gram-negative bacteria (*Pseudomonas syringae* pv *tomato*, *Xanthomonas axonopodis* pv *vesicatoria*, and *X. arboricola* pv *pruni*). Therefore, the particles can be considered antibacterial agents for plant pathogens control. The authors proposed two mechanisms to explain the antibacterial behavior of the LigNPs: (i) damage of the bacterial cell wall by the lignin polyphenols, causing

lysis, leaking of the cytoplasmic content and induction of reactive oxygen species (ROS), and (ii) penetration of the LigNPs inside the cell followed by depletion of adenosine triphosphate (ATP) by monophenolic compounds originated from lignin (**Figure 6c**).

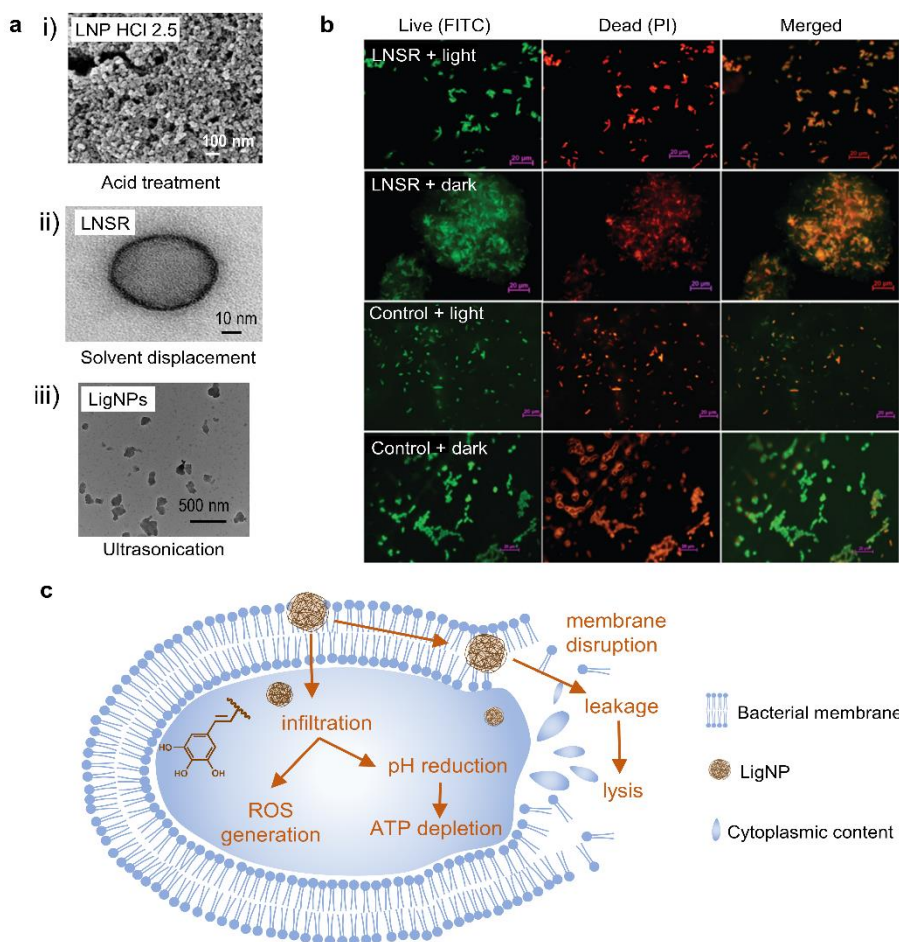


Figure 6. (a) (i) FESEM image of clustered structured lignin nanoparticles after acidolysis (reproduced from Ref. 68. Copyright (2018) American Chemical Society), (ii) HRTEM image of the lignin nanospray (LNSR) (reproduced from Ref. 65 with permission from the Royal Society of Chemistry). (b) Fluorescence microscopy images of *E. coli* treated with the LNSR and untreated (control) in the light, stained with FITC and PI (at scale 20 μm) (reproduced from Ref. 65 with permission from the Royal Society of Chemistry). (c) Mechanisms for antibacterial behavior of extracted LNP. Adapted from Ref. 68.

Spherical LigNPs with different sizes were obtained by solvent displacement approach, dropping ethanol-solubilized organosolv lignin into water.⁶⁴ The NPs displayed radical scavenging capacity and bacteriostatic effect at 1 mg·mL⁻¹ against *Escherichia coli* O157:H7 and *Salmonella enterica* Typhimurium. Contrary to what was expected, the larger particles (324 nm) presented a higher inhibitory effect than the smaller ones (149 nm). Other physiochemical properties of the particles, such as roughness, ζ-potential, and reactivity should be studied to explain the different antibacterial properties of these particles. The particles did not show cytotoxic effects on epithelial Caco-2 cells, and also showed an antioxidant cellular effect by reducing the natural ROS level of the cells. Paul *et al.* combined the solvent displacement method with sonochemistry to develop stable photodynamic lignin nanospheres in an aqueous medium to be used as lignin nanospray (LNSR) for microbial disinfection (**Figure 6a ii**).⁶⁵ Under blue light emitting diode (LED) irradiation, the LNSR presented enhanced inhibition capacity toward the Gram-negative *E. coli* and the Gram-positive *Bacillus megaterium* compared to LNSR in dark conditions (**Figure 6b**). Studies on singlet oxygen generation revealed that the particles induced the formation of ROS under blue LED irradiation, which might explain the antibacterial activity of LNSR under this condition. The LNSR coated onto a glass slide prevented the growth of bacteria after blue LED exposure, which evidenced their suitability as a photodynamic coating material.

Lignin can be chemically modified in order to achieve superior antibacterial and antioxidant effects. Aminated LigNPs (a-LigNPs), prepared by acid precipitation followed by Mannich reaction surface modification, showed enhanced antioxidant activity in comparison with unmodified LigNPs.⁶⁹ However, the inhibition capacity toward *Staphylococcus aureus* was higher for LigNPs in comparison with a-LigNPs, which could be explained by the morphology of the particles: while LigNPs were quasi-spherical, a-LigNPs seemed glued by a substance, and this might impede their penetration inside the

cells. Given their improved UV-blocking capacity, a-LigNPs could find their application in sunscreen lotions.

Lignin has also been combined with polymers or inorganic materials to enhance the antibacterial activity of nanoformulations. For instance, hybrid chitosan/lignosulfonate (CS-LS) NPs were prepared by sonochemistry taking advantage of the electrostatic interaction between the polymers.⁷⁰ The NPs inhibited the growth of Gram-negative *E. coli* and Gram-positive *S. aureus* and *Bacillus subtilis* in a higher rate than CS or LS alone.

Several works studied the effect of small phenolic compounds on bacteria,^{56,71,72} however, very few studies analyzed the mechanism of action of macromolecular lignin or LigNPs. Despite being commonly accepted as antioxidants, phenolic compounds can exhibit pro-oxidant activity depending on their concentration and environmental factors.⁷³ In fact, polyphenols induce the generation of hydrogen peroxide, causing oxidative stress in bacterial cells.⁵⁴ Their antibacterial activity has been also related to their capacity to suppress the activity of essential enzymes.^{74,75} Other studies have reported their capacity to weaken the bacterial membrane, increasing the permeability of the cell.^{55,56}

Lignin as a reducing and capping agent of metal and metal oxide NPs

The combination of lignin with metal NPs has been extensively explored in the biomedical field, especially using lignin as a reducing agent (**Figure 7a, Table 2**). The large amounts of phenolic groups of lignin make possible the reduction of metal ions to form NPs. Among the antibacterial metals, silver has received special attention due to its ability to eradicate a broad range of microorganisms, and its easiness to be reduced to form NPs.

Table 2 Lignin as a reducing and capping agent for the synthesis of hybrid antibacterial NPs

Type of lignin	Metal	Particle shape ^a	Particle size ^{a, b}	Antibacterial activity	Ref.
Alkali	Ag	Spherical	~20 nm	<i>S. aureus</i> , <i>S. epidermidis</i> , <i>E. coli</i> , <i>P. aeruginosa</i> , <i>K. pneumoniae</i> , <i>A. baumannii</i> (MDR isolates and commercial)	76
Alkali	Ag	Spherical	~20 nm	<i>M. abscessus</i> in infected macrophage	77
Alkali	Ag	Spherical	~20 nm	<i>S. aureus</i> , <i>E. coli</i>	78,79
Kraft	Ag	Spherical	13 nm	<i>A. baumannii</i> , <i>P. aeruginosa</i> , <i>S. aureus</i> , <i>S. epidermidis</i> , <i>E. casseliflavus</i> , <i>K. pneumoniae</i> , <i>A. baumannii</i> (MDR isolates)	80
Alkali	Ag	Spherical	10–50 nm	<i>S. aureus</i> , <i>E. coli</i> , <i>A. niger</i>	81
N.D.	Ag	Quasi-spherical	50–80 nm ^c	<i>S. aureus</i> , <i>E. coli</i>	82
Organosolv	Ag	Spherical	10–50 nm	<i>S. aureus</i> , <i>B. circulans</i> , <i>P. aeruginosa</i> , <i>E. coli</i> , <i>B. subtilis</i> , <i>R. eutropha</i>	83
Acid-alkaline	Ag	Spherical	15–25 nm	<i>E. coli</i>	84
Alkali, quaternized	Ag	Spherical	10–20 nm	<i>S. aureus</i> , <i>E. coli</i>	85
Alkali, quaternized	Ag	Spherical	25 nm	<i>S. aureus</i> , <i>E. coli</i>	86
Alkali, ZHL and alkali-	Ag, Au	Spherical	8–25 nm ^c	<i>S. aureus</i> , <i>E. coli</i>	87
Waste from paper	Cu ₂ O	Quasi-spherical	100–200 nm	<i>S. aureus</i> , <i>E. coli</i>	88

^aRefers to metallic core^bObtained by measuring TEM images^cDepending on experimental conditions

In a recent work, alkali lignin served as a reducing and capping agent for the formulation of AgLigNPs by simply stirring the precursors for 3 days at 60 °C.⁷⁶ The resulting particles of ~20 nm (**Figure 7b i**) were able to inhibit the growth of a broad range of bacterial strains, including multi-drug resistant (MDR) clinical isolates (*S. aureus*, *Staphylococcus. epidermidis*, *Pseudomonas aeruginosa*, *Klebsiella pneumoniae*, *Acinetobacter baumannii*, *E. coli*), while a 5-fold higher amount of commercial AgNPs was needed for a comparable efficacy. The increased antibacterial efficacy of the lignin-capped silver NPs was attributed to the ability of lignin to interact and disturb bacterial membranes, hence facilitating the penetration of Ag⁺ ions inside the cell. Following the above-described work, the authors incorporated the AgLigNPs into niosomes to target

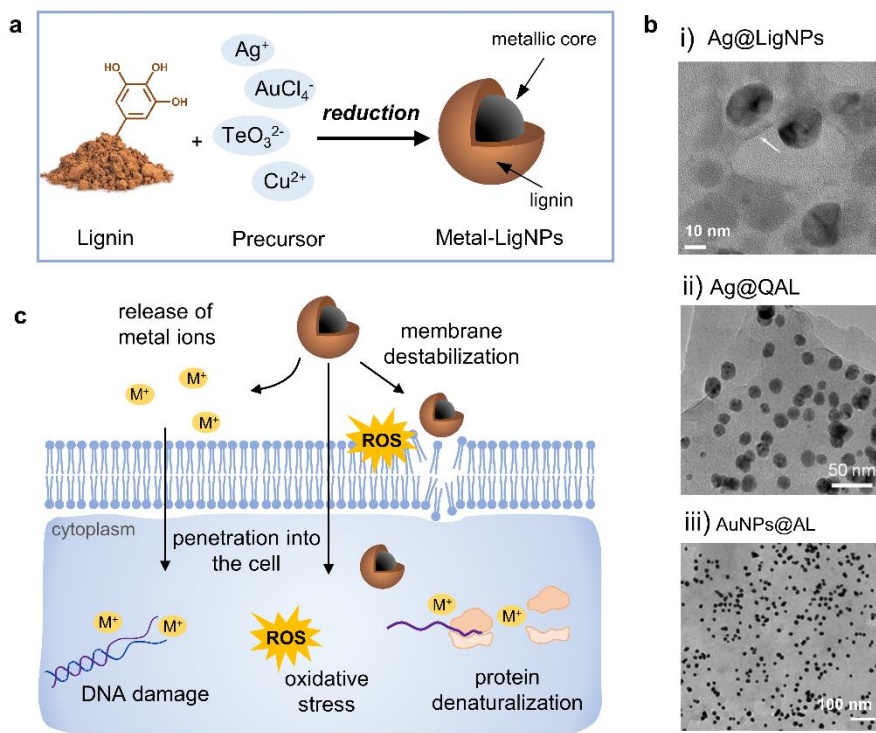


Figure 7. (a) Schematic representation of the synthesis of metal-lignin NPs. (b) TEM images of (i) Ag@LigNPs (reproduced from Ref. 76 with permission from the American Chemical Society) (ii) Ag@QAL (reproduced from Ref. 85. Copyright (2021) Elsevier), and (iii) AuNPs@AL (reproduced from Ref. 87 with permission from the Royal Society of Chemistry), (c) Schematic representation of the antibacterial modes of action of metal lignin NPs.

mycobacteria.⁷⁷ Niosomes are vesicles fabricated with biomimetic cell membrane, which promotes their interaction with eukaryotic cells and the delivery of their cargo into the cytoplasm. *In vitro* assays against *Mycobacterium abscessus*, an intracellular pathogen causing lung infections, showed that it was resistant to the treatments with the NP-loaded niosomes, suggesting that the nanoniosomes did not merge with the bacterial cell wall. Antimicrobial effect was only observed in *M. abscessus*-infected macrophage, probably due to the fusion of the niosome with the eukaryotic cell membrane and the subsequent delivery of the bactericide cargo in macrophages.

Saratale *et al.* used alkali lignin extracted from wheat straw as a reducing, capping, and stabilizing agent for the synthesis of AgNPs by stirring for 60 min at 50 °C.⁷⁸ The lignin capping enhanced the free radical scavenging capacity of the AgLigNPs in comparison with the antioxidant capacity of AgNPs alone. The minimum inhibitory concentration (MIC) against *S. aureus* and *E. coli* was 25 and 20 µg·mL⁻¹, respectively. The combination of AgLigNPs with commercial antibiotics showed a synergistic antibacterial effect, suggesting the potential of this combination to combat MDR infections. Later, the authors studied the reusability of AgLigNPs in photocatalytic degradation, and also demonstrated their growth inhibition capacity against *S. aureus* and *E. coli*.⁷⁹ A different methodology for the Kraft lignin-mediated synthesis of AgNPs was reported by Pletzer *et al.*, who described a fast microwave-assisted technique yielding lignin-capped AgNPs of 13 nm in diameter.⁸⁰ The NPs were tested against MDR clinical isolates. The highest antibacterial activity was found against the Gram-negative *A. baumannii* and *P. aeruginosa*, with a MIC of ≤1.0 µg·mL⁻¹, while MICs of 2.5 and 5.0 µg·mL⁻¹ were found for the other tested bacteria (*S. aureus*, *S. epidermidis*, *Enterococcus casseliflavus*, and *K. pneumoniae*). *In vitro* cytotoxicity studies with monocytic THP-1 leukemia cells demonstrated a lack of toxicity of these NPs at their antibacterial concentrations. In addition, *in vivo* studies using a skin abscess infection model in mice against MDR *P. aeruginosa* and methicillin-resistant *S. aureus* (MRSA) showed a significant reduction in abscess sizes, while the Gram-

negative bacteria load was reduced by 5-fold. The antibacterial effect of AgLigNPs demonstrated higher efficiency on Gram-negative bacteria than on Gram-positive. This tendency, which supports other AgLigNPs studies,^{76,82} is attributed to the thicker peptidoglycan wall in Gram-positive bacteria which hinders the penetration of the NPs into the cell.

Marulasiddeshwara *et al.* used high molecular weight alkali lignin as a reducing and capping agent for AgLigNPs.⁸¹ The resulting spherical in shape NPs, with an average size of 10–50 nm, were able to inhibit the growth of *S. aureus* and *E. coli*, and the fungi *Aspergillus niger*. Following the same procedure, Tran *et al.*⁸² prepared AgNPs coated with rice-husk-extracted lignin or nano-lignin (LCSN and n-LCSP). It was found that lignin and nano-lignin were more antibacterial against Gram-positive *S. aureus* than Gram-negative *E. coli*, while the (nano)-lignin-coated AgNPs presented a higher antibacterial effect against the Gram-negative bacterium. The proposed mechanism of action of these particles involves: (i) adhesion of AgNPs on the bacterial membrane causing structural damage, (ii) interaction with cytoplasmic biomolecules, (iii) generation of ROS, increasing the oxidative stress level of the cell, and (iv) interference with the signal transduction pathways by forcing the cell to intake extracellular signaling molecules when exposed to AgNPs

Aadil *et al.* used lignin extracted from Acacia wood dust by organosolv method to reduce silver and produce spherical AgNPs sizing 10–50 nm.⁸³ The NPs displayed antibacterial properties against Gram-positive and negative strains, including the pathogens *S. aureus*, *Bacillus circulans*, *P. aeruginosa*, and *E. coli*. These NPs were also tested as colorimetric sensors for heavy metal ions, and as a redox catalyst, being able to reduce the methylene blue dye. Zevallos Torres *et al.* reported the acid-alkaline extraction of lignin from oil palm empty fruit bunches, which are by-products of the process to extract edible and industrial oils, and its use as a reducing agent of silver ions.⁸⁴ After putting in contact a solution of the extracted lignin with a solution of AgNO₃, spherical particles of 15–25 nm in diameter embedded in lignin were produced. The resulting NPs

presented a MIC of $62.5 \mu\text{g}\cdot\text{mL}^{-1}$ against *E. coli*, while the MIC of silver in ionic form was $31.25 \mu\text{g}\cdot\text{mL}^{-1}$. This difference was explained by the fact that AgNPs act as slow-release devices that prolong the antibacterial effect, while AgNO_3 in solution is already in form of ions available for bacteria.

Microwave-assisted reduction of AgNO_3 by quaternized alkali lignin was reported by Wang *et al.*⁸⁵ The functionalization of lignin with the quaternary ammonium reagent (3-chloro-2-hydroxypropyltrimethylammonium chloride, CHMAC) provided positive charges that enhance the electrostatic interaction of the nanocomposite with negatively-charged bacteria. The composites containing AgNPs and quaternized alkali lignin (Ag@QAL) (**Figure 6b ii**) were able to reduce viable *E. coli* by $3.72 \log_{10}$ (>99.9 %) and *S. aureus* by $5.29 \log_{10}$ (>99.999 %) CFU·mL⁻¹. The results indicated that quaternary ammonium lignin contributed to the antibacterial activity of the composites by enhancing the NP-bacteria interaction. The proposed antibacterial mechanism of action is based on the direct contact of Ag@QAL with the bacteria, induced by the positively charged quaternized lignin, followed by the generation of ROS by the nanosilver. Similarly, Li *et al.* prepared amphoteric lignin (AML)/nanosilver (AML@AgNPs) using lignin quaternized with CHMAC as a reducing and stabilizing agent.⁸⁶ Unmodified lignin presented a slight antibacterial effect against *S. aureus*, while AML showed increased antibacterial properties that were attributed to the strong interactions between positively charged AML and negatively charged bacteria. The highest antibacterial capacity was observed for AML@AgNPs, which were able to completely eradicate *S. aureus* and *E. coli* at 60 and 30 ppm of Ag, respectively. Additionally, AML@AgNPs provided waterborne polyurethane (WPU) films with antibacterial properties. The authors demonstrated the adsorption of positively charged AML onto bacteria, which could enable the AgNPs to rapidly contact bacterial cells and then exert their antibacterial effect.

Besides silver, lignin has also been used for reducing other metals and metal oxides to produce hybrid NPs. Rocca *et al.* provided a one-pot thermal and

photochemical approach for the synthesis of lignin-doped silver and gold nanoparticles (**Figure 6b iii**).⁸⁷ In general, all the tested lignins, namely low-sulfonate alkali lignin, ZHL lignin (depolymerized and 27 % sugar content), and AL lignin (alkali-extracted, 16 % sugar content), were able to reduce both metals and form spherical and monodispersed NPs. However, the antibacterial effect of the nanocomposites was clearly influenced by the nature of lignin, and only alkali and AL lignin produced antibacterial NPs. The AgNPs produced with alkali and AL lignin (AgNP@alkali, AgNPs@AL) exhibited antibacterial properties under light and dark conditions, with MIC values of 0.2 $\mu\text{g}\cdot\text{mL}^{-1}$ and 24.2 $\mu\text{g}\cdot\text{mL}^{-1}$, respectively. Contrarily, the lignin-coated AuNPs (AuNP@alkali and AuNPs@AL) only presented antibacterial activity under light irradiation and the MIC values were significantly higher (223–499 $\mu\text{g}\cdot\text{mL}^{-1}$). The AgNP@alkali and AgNPs@AL nanocomposites were able to completely eradicate *E. coli* and *S. aureus* within 30–40 min, while a longer time was required for the lignin-coated AuNPs (6 h). Results on ROS quantification in bacteria suggested that the mechanism of action of the NPs involved a photochemical process since elevated ROS values were detected after exposing the bacteria to the NPs under light conditions. Moreover, it was hypothesized that the sugars present in AL lignin might adhere to the peptidoglycan of the bacterial cell wall. Importantly, the particles were non-cytotoxic toward human cells at the bactericidal concentrations. Preliminary assays show these AgNPs as potential antimicrobial agents towards *S. aureus* biofilm eradication. The lignin-mediated synthesis of crystalline Cu_2O NPs sizing 100–200 nm was reported by Li *et al.*⁸⁸ Lignin derived from papermaking waste liquid reduced the Cu(II) ions from $\text{Cu}(\text{OH})_2$ to Cu (I) oxide NPs, and established a uniform coating onto the surface of the particles. The NPs presented high antibacterial efficiency, being able to completely eradicate *E. coli* and *S. aureus* within 30 min.

Lignin nanocarriers

One of the emerging applications of lignin is its use as nanocarriers for biologically active substances, including antimicrobial agents, anti-cancer drugs, enzymes, and pesticides that should be delivered in a specific location under controlled conditions.²³ The advantage of using lignin as a nanocarrier is the increase in the stability of the loading substance, especially in the case of poorly water-soluble molecules. The most common approaches for loading bioactives in lignin carriers include entrapment (by infusion, solvent displacement, ion exchange, or coating), and adsorption (**Figure 8**). The loading of the active substance can take place during or after the formation of NPs. For instance, in the solvent displacement approach, the cargo is entrapped into lignin during the NPs formation process. In the adsorption approach, the cargo is adsorbed onto previously synthesized LigNPs. The location of the cargo in the LigNP (i.e. inside

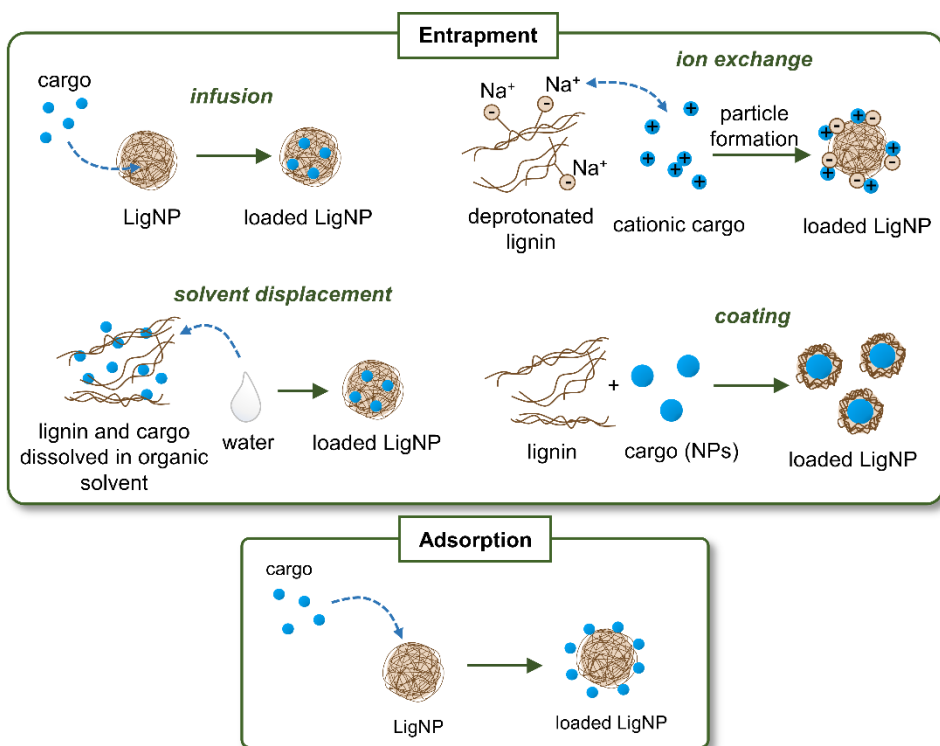


Figure 8. Main strategies for loading actives into lignin nanocarriers.

the particle or onto its surface) may affect the functionality of the nanocarrier. For instance, encapsulation of the cargo inside the carrier may result in a slow release of the active substance and prolong antibacterial effect, while an active located on the surface is expected to have a burst release and shorter antibacterial effect. However, other factors such as cargo-NP interaction, hydrophobicity of the cargo, and covalent crosslinking should be also considered for predicting the behavior of the active substance. **Table 3** is an overview of LigNPs used as carriers of different antibacterial agents.

Maldonado-Carmona *et al.* described the encapsulation of a porphyrin (5,10,15,20-tetrakis (4-hydroxyphenyl)-21H,23H-porphine, THPP) in acetylated lignin (AcLi) NPs by solvent displacement in dialysis membranes, achieving up to 87.6 % encapsulation rate.⁸⁹ Porphyrins are used as photosensitizers in antibacterial photodynamic therapy. Upon light irradiation, these molecules produce singlet oxygen which causes bacterial cell damage.⁹⁰ When exposed to light, the THPP@AcLi were able to drastically reduce the growth of Gram-positive bacteria (*S. aureus*, *S. epidermidis*, and *E. faecalis*) at low concentrations of porphyrin, while were ineffective against Gram-negative *E. coli* and *P. aeruginosa*. The researchers found that acetylated lignin NPs possess bacteriostatic effect, thus the antibacterial effect was attributed to the presence of porphyrin. It was shown that the NPs exerted their antibacterial action on the bacterial wall, without penetrating inside the cell. Given their antibacterial activity and light responsiveness, the porphyrin-loaded acetylated lignin NPs were proposed for photodynamic antimicrobial chemotherapy in wastewater purification. Later, in the same group, four different derivatives of THPP with different physicochemical characteristics (charge, size, and solubility) were encapsulated into AcLi.⁹¹ The cationic porphyrins were able to reduce the growth of *E. coli* only in free form, but not after being encapsulated in AcLi NPs. Interestingly, for some porphyrins, the antibacterial efficacy against *S. aureus* increased in their encapsulated form in comparison with their free form.

Table 3 LigNPs as carriers of antibacterial agents

Type of lignin	NP preparation method	Loading strategy	Cargo	Particle shape	Particle size ^a	Antimicrobial activity	Ref.
Kraft, acetylated	Solvent displacement	Entrapment	Porphy-rins	Spherical	160–1348 nm ^b	<i>S. aureus</i> , <i>S. epidermidis</i> , <i>E. faecalis</i>	89, 91
Alkali	Solvent displacement	Emulsion	Essential oils	Spherical	~200 nm	<i>P. italicum</i>	92
LS modified with an azo dye	Chemical reduction to form ZnO	Coating	ZnO	Quasi-spherical	21–32 nm	<i>S. haemolyticus</i> , <i>B. cereus</i> , <i>C. diphtheriae</i> , <i>M. cookei</i> , <i>R. ornithinolytica</i> , <i>S. typhimurium</i> , <i>S. paratyphi</i> , <i>A. fumigatus</i> , <i>A. penicilloides</i> , <i>C. albicans</i> , <i>C. coronatus</i>	93
Organosolv	Chemical reduction to form AgNPs	Adsorption	AgNPs	Quasi-spherical	28 to 54 nm ^b	<i>E. coli</i>	94
LS, PNMA-modified	Self-assembling, chemical reduction	Adsorption	AgNPs	Spherical	11 nm	<i>S. aureus</i> , <i>E. coli</i>	95
Kraft	Coating and chemical reduction	Adsorption	AgNPs	Irregular	30–36 nm	<i>B. subtilis</i> , <i>S. aureus</i> , <i>P. aeruginosa</i> , <i>E. coli</i> , <i>K. pneumoniae</i>	96
Kraft	Acid precipitation	Infusion	Ag ⁺	Irregular	40–70 nm	<i>S. aureus</i> , <i>S. epidermidis</i> , <i>E. coli</i> , <i>P. aeruginosa</i>	97
Kraft	Solvent displacement	Ion exchange	Ag ⁺	Spherical	60–200 nm ^b	<i>S. aureus</i> , <i>E. coli</i> , <i>P. aeruginosa</i>	98

^aObtained by measuring TEM images, ^bDepending on setting conditions

Despite the potential of solvent displacement for the synthesis of lignin nanocarriers, volatile and flammable solvents such as tetrahydrofuran, acetone, and ethanol are typically used to produce these particles. These inherently hazardous chemicals might remain in the NPs, limiting their application in the biomedical field.⁹⁹ Alternative biomass-derived solvents are a greener option that would avoid safety issues. In this line, Chen *et al.* synthesized LigNPs using a recycled γ -valerolactone (GVL)/water binary solvent (GWBS) system and two different nanoprecipitation methods—dropping and dialysis.⁹² GVL is a non-toxic, non-volatile solvent obtained from cellulose feedstock that has been proposed as an alternative to toxic solvents in solvent displacement techniques. The resulting spherical lignin particles were used to prepare Pickering emulsions of essential oils, which are emulsions stabilized by surface active solid particles. The encapsulation of essential oils is expected to increase their stability, enhance their efficacy against microbes and hamper their volatilization. The antibacterial assay consisted in inoculating the fruit pathogen fungus *Penicillium italicum* in wounded oranges treated with essential oils dispersed in solvents or stabilized with LigNPs. The results showed that LigNPs promoted the growth inhibition activity of the essential oils towards the fungus.

Lignin has been also used to entrap previously synthesized metal oxide NPs. In a recent study, ZnO nanoparticles were entrapped by lignin modified with 2-[(E)-(2-hydroxy naphthalen-1-yl) diazenyl] benzoic acid, a photoactive azo dye, to obtain photoresponsive NPs for antimicrobial photodynamic therapy.⁹³ The antimicrobial activity assessed by the agar diffusion method showed that the hybrid particles after light irradiation presented high antibacterial activity against the Gram-positive *Streptococcus haemolyticus*, *Corynebacterium diphtheriae*, and *Bacillus cereus*, presenting a zone of inhibition (ZOI) of 29–34 mm, and against Gram-negative *Raoultella ornithinolytica*, *Salmonella typhimurium*, and *Salmonella paratyphi* (ZOI ~26 mm). In addition, the particles were capable of inhibiting the growth of different fungal strains (*Aspergillus fumigatus*, *Aspergillus penicilloides*, *Candida albicans*, *Conidiobolus coronatus*, and

Microsporium cookei), achieving ZOI varying from 20 to 43 mm. In both antibacterial and antifungal tests, light irradiated particles showed greater antimicrobial activity than non-irradiated particles.

Researchers have used LigNPs as carriers to entrap AgNPs as well. In these works, lignin was not a reducing agent, but served as a carrier for AgNPs. For instance, Zhong *et al.* prepared lignin/AgNPs using citric acid or sodium borohydride as reducing agents to obtain AgNPs that remained adsorbed onto the surface of organosolv lignin.⁹⁴ The nanocomposites were able to inhibit the growth of *E. coli* after 2 and 4 h of exposure. In another work, self-assembled poly(N-me-thylaniline)–lignosulfonate (PNMA–LS) composite microspheres with Ag⁺ adsorbability were prepared.⁹⁵ After chelating Ag⁺, the reducing capacity of PNMA served to produce NPs of 11.2 nm that remained adsorbed onto the spheres. The PNMA–LS–Ag composite exhibited strong bactericidal effect, with bactericidal rates of 99.95 and 99.99 % for *E. coli* and *S. aureus* cells, respectively, which were higher than those obtained with free lignin and AgNPs. Another approach was used by Klapiszewski *et al.*⁹⁶ who combined Kraft lignin with silica NPs as supports for AgNPs. The preparation route to composite NPs consisted in chemical reduction of Ag⁺ by NaBH₄ followed by incorporation of the resulting AgNPs into previously hybridized and functionalized silica/lignin particles. Interestingly, increasing the amount of lignin in the hybrid materials resulted in higher adsorption rates of nanosilver onto their surface. The silica/lignin/AgNPs were able to inhibit the growth of *B. subtilis*, *S. aureus*, *P. aeruginosa*, *E. coli*, and *K. pneumoniae* achieving ZOI of up to 12 mm for the highest concentration of NPs tested. The highest antibacterial effect was against *P. aeruginosa*, while *K. pneumoniae* was slightly inhibited by the particles. Correlation between Gram-staining and bacterial susceptibility to the antibacterial properties of the silica/lignin/AgNPs was not found in this work.

Despite the widespread use of silver as antimicrobial agent in biomedical products, concerns have been raised about their environmental persistence and potential effects on human health.^{100,101} When it comes to Ag-containing NPs, it

is thus important to tightly control the amount and the size of the NPs in order to avoid the cytotoxic effects of such NPs toward humans and the environment. Aiming to avoid the persistence of metal reservoirs after the intended use of such NPs, Richter *et al.* synthesized biodegradable Ag⁺ infused NPs.⁹⁷ More specifically, nanoprecipitation of Kraft lignin was used to prepare LigNPs which, in turn, were used as a core to infuse silver ions. Then, the resulting NPs were coated with a cationic electrolyte that increases their adhesion to the bacterial surface. In this work, instead of being the reducing agent of silver to produce AgNPs as described in the previous section, lignin was used as a nanocarrier of Ag⁺. The NPs, with sizes ranging 40–70 nm, presented high antibacterial activity against the Gram-negative *E. coli* and *P. aeruginosa*, and the Gram-positive *S. epidermidis* after a short time of exposure (1–30 min). The NPs outperformed the AgNPs and Ag⁺ solutions, even at lower Ag equivalents, suggesting an enhanced antibacterial effect due to the combination of Ag⁺ and LigNPs. The silver-infused LigNPs were dialyzed against water to simulate their depletion process, and only 18 % of the total Ag remained in the particles after 24 h. It should be noted that the particles presented less cytotoxic effects than the free silver ions.¹⁰² However, the fast release of Ag⁺ from the lignin core reduces the shelf-life of these particles. Following a similar concept, Lintinen *et al.*⁹⁸ produced colloidal lignin particles (CLPs) where Ag⁺ was ionically bounded (AgCLPs). The synthetic procedure consisted in the deprotonation of Kraft lignin, which led to sodium carboxylate and phenolate groups, followed by the bounding of Ag⁺ by ion exchange. Finally, the mixture of lignin with ionically bounded Ag⁺ was used to form NPs by solvent displacement. In this process, the recovered solvents can be reused for further synthesis cycles. Release of Ag⁺ from the CLPs was not observed in water, but only in physiological conditions. The growth of *P. aeruginosa*, *E. coli* and *S. aureus* was inhibited by 94–96 % in the presence of the AgCLPs. Interestingly, a synergistic effect of CLP and Ag⁺ was observed for the Gram-positive bacteria.

Antibacterial composite materials containing lignin NPs

Due to their higher specific surface area, NPs are known to improve the stiffness, strength, toughness, thermal stability, and barrier properties of polymeric materials better than traditional fillers, even at low concentrations (1–5 wt %).¹⁰³ In recent years, LigNPs have been incorporated in a variety of composite materials not only for improving the mechanical properties of the material, but also to provide antibacterial, antioxidant, anticorrosion, and UV-blocking activities, and metal adsorbent capacity (**Figure 9**).¹⁰⁴

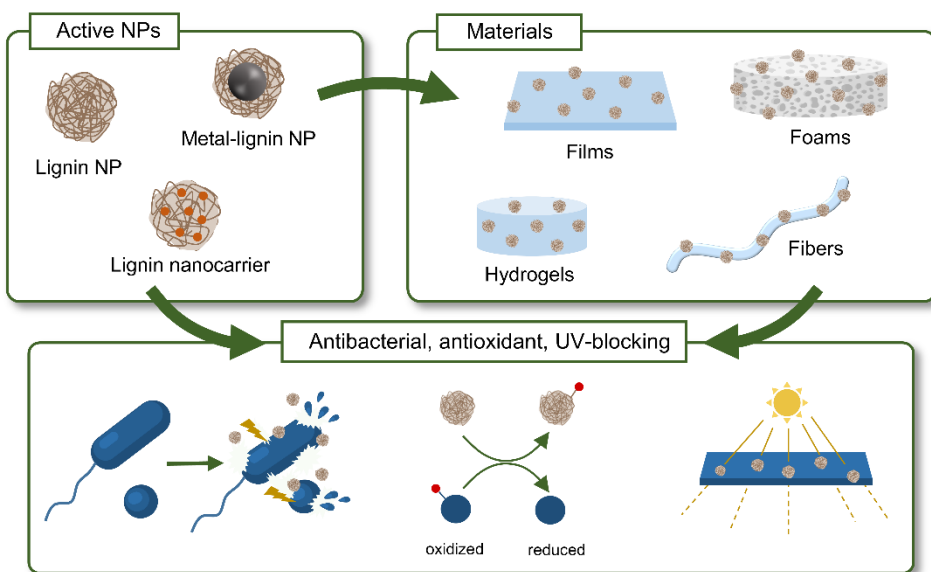


Figure 9. Schematic representation of the activities of LigNPs and their nanocomposite materials.

In this section, the different antibacterial composite materials containing LigNPs, alone or in combination with other polymers or metals, will be reviewed. Such materials can be prepared by incorporating previously synthesized NPs,^{105–107} or using an *in situ* approach where the NPs synthesis takes place in the material.^{108–111} Some of these materials include films, hydrogels, fibers, and foams, which have been validated as food packaging materials, wound dressings, medical coatings, or other biomedical applications (**Figure 10**). Especial

attention is paid to materials designed as dressings for the treatment of chronic wounds.

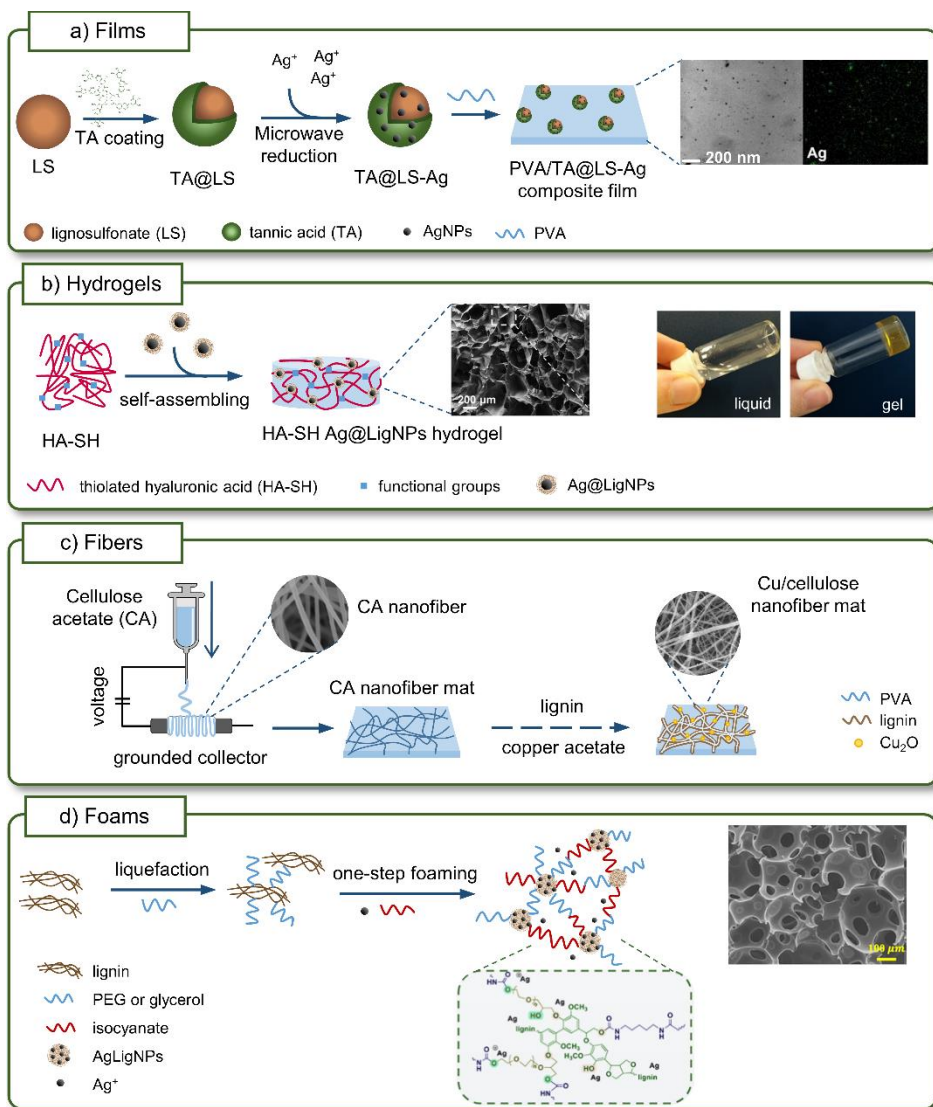


Figure 10. Schematic representation of antibacterial materials containing LigNPs. (a) Films (adapted from Ref 107. Copyright (2020) John Wiley & Sons), (b) fibers (adapted from Ref. 138. Copyright (2021) Elsevier), (c) hydrogels (adapted from Ref 105 with permission from the American Chemical Society) and (d) foams (adapted from Ref. 108. Copyright (2022) American Chemical Society).

Food packaging

The growth of microorganisms in food is a serious concern because it causes a reduction in the shelf-life of food and increases the risk of acquiring food-borne infections causing illness to almost 1 in 10 people in the world.¹¹² Hence, preventing the contamination of food to avoid food-borne infections is crucial. Ideal advanced materials for food packaging should be antimicrobial and antifouling to avoid the proliferation of bacteria and fungi, antioxidant to preserve the properties of food, and resistant to humidity. Moreover, biomass sources for environmentally-friendly and biodegradable packaging are interesting since they can potentially substitute traditional petroleum-based plastics. Lignin, as a natural antioxidant and antibacterial polymer, is a suitable filler for food packaging materials, especially in form of NP that additionally improves the mechanical performance of the material.¹¹³ **Table 4** gives an overview of the film materials in which LigNPs or their derivatives have been used as multifunctional fillers.

An example of these packaging materials is found in the work by Yang *et al.*, who incorporated LigNPs obtained by hydrochloric acidolysis into poly(vinyl alcohol) (PVA) and PVA/CS films produced by solvent casting.¹¹⁴ The phenolic and aliphatic hydroxyl groups of LigNPs interacted with the hydroxyl groups of PVA and the amino groups of CS. The DPPH assay revealed that the nanocomposites presented a radical scavenging activity of 70.5–91.7 %, with a clear dependence on the amount of LigNPs. The growth of plant pathogenic *Pectobacterium carotovorum* and *X. arboricola* was reduced in the presence of PVA/LigNP and PVA/CS/LigNP, while no growth inhibition was observed with the PVA and PVA/CS films without NPs. LigNPs not only conferred bioactivities to the films but also improved their mechanical performance, showing an increase in the tensile strength from 45.8 to 51.5 MPa in PVA/LigNP films. Moreover, the thermal analysis showed that the LigNPs enhanced the crystallization of the PVA, probably acting as heterogeneous nucleating agents.

Table 4 Nanolignin-based film materials for food packaging applications

Type of lignin	Filler	Polymer matrix	Antimicrobial activity	Ref.
Extracted by steam explosion and enzymatic treatment	LigNPs	PVA, CS	<i>P. carotovorum</i> , <i>X. arboricola</i>	114
Steam explosion and enzymatic treatment	LigNPs, CNC	PLA	<i>P. syringae</i>	115
Alkali	aLigNPs, caLigNPs	PLA	<i>E. coli</i> , <i>M. luteus</i>	11
Soda	LigNPs	CNC, CNF	<i>S. aureus</i>	106
N.D.	LigNPs	CNF	<i>S. aureus</i> , <i>E. coli</i>	116
Alkali	LigNPs and metal oxide NPs	PLA	<i>S. aureus</i> , <i>E. coli</i>	117
N.D.	LigNPs and ZnO/Ag NPs	PLA	<i>S. aureus</i> , <i>E. coli</i>	118
Alkali	AgLigNPs	Cellulose	<i>E. coli</i>	119
Alkali	AgLigNPs	Agar	<i>L. monocytogenes</i> , <i>E. coli</i>	120
Organosolv	AgLigNPs	PLA	<i>L. monocytogenes</i> , <i>E. coli</i>	121
LS	TA@LS-Ag NPs	PVA	<i>S. aureus</i> , <i>E. coli</i>	107

The incorporation of LigNPs and cellulose nanocrystals (CNC) into poly(lactic acid) (PLA) films was also explored by Yang and coworkers.¹¹⁵ The combination of the two nanofillers in the polymeric film increased its crystallinity and the tensile strength, and imparted UV-blocking capability. Only the films containing LigNPs were able to reduce the growth of the plant pathogen *Pseudomonas syringae*, indicating the role of LigNPs in the antibacterial activity. However, the binary PLA/LigNP film presented higher antibacterial activity than PLA/CNC/LigNP. The presence of CNC clearly contributed to the high degree of crystallinity of the films, which may decrease the diffusion of LigNPs and their antibacterial response. Similarly, with the aim of improving the dispersibility of the fillers in PLA/LigNPs formulations, Cavallo *et al.* used acetylated LigNPs (aLNP) and citric acid-treated LigNPs (caLNP) as nanofillers in PLA films.¹¹ The incorporation of acetyl in aLNP, and ester and ether in caLNP had a significant

effect on their compatibility with the PLA matrix, and the aggregation of the modified fillers at 1 wt % in PLA films decreased in comparison with pristine LigNPs. However, self-aggregation was observed in increasing concentrations of filler regardless of the chemical modification. The growth of *E. coli* and *Micrococcus luteus* was reduced after incubation with PLA films containing LigNPs, aLNP, and caLNP, however, the antibacterial effect was more pronounced in the case of the Gram-positive *M. luteus*. The aLNP significantly increased the antibacterial activity of the composites, whereas their antioxidant and UV blocking capacities were not improved with the chemical modification of lignin.

In a recent work, the effect of the polymerization degree and the functional groups of lignin on the properties of films based on CNC and cellulose nanofibrils (CNF) was studied.¹⁰⁶ The two forms of lignin, i.e. phenol-enriched oligomer fractions and colloidal LigNPs, showed different effects on the antioxidant activity of the cellulose films. Lignin oligomers enhanced the radical scavenging capacity, while LigNPs reduced it, probably as a consequence of the less accessible phenolic groups in the colloidal particles. In contrast, the antibacterial properties were not affected by the molecular weight: all the formulations reduced the growth of *S. aureus* by 0.3–0.5 log, however, the growth of *E. coli* was not affected. In view of the properties of cellulose and lignin films, both LigNPs and lignin oligomers can be potentially used as active additives in food packaging. In another work, LigNPs obtained from corncob lignin via anti-solvent precipitation method were blended with CNF to prepare biodegradable films.¹¹⁶ The presence of LigNPs increased the hydrophobicity of the films and provided UV and visible light blocking capacities, which are desirable features of food packaging. However, the tensile stress and elongation of CNF-based composite films decreased after the addition of LigNPs. The hybrid films reduced the growth of *S. aureus* and *E. coli* in comparison to the CNF films.

Lizundia *et al.* showed the benefits of the incorporation of metallic NPs into transparent PLA films to be used in the packaging industry.¹²² Later, the authors

introduced LigNPs and inorganic metal oxide NPs into these films.¹¹⁷ The combination of metal oxides and LigNPs provided high UV-protection capacity and antioxidant activity, with superior results obtained only with inorganic NPs. Another study combining metal/metal oxide NPs (ZnO/Ag) with LigNPs in PLA composites was carried out by Deng *et al.*, obtaining nanocomposites with multiple functionalities.¹¹⁸ To overcome the common dispersion issues in the PLA matrix, polypyrrole glutinous nanofibrils crosslinked with dopamine (PPy-PDa) were used as particle dispersants. The films containing LigNPs did not produce a ZOI in agar plates where *E. coli* and *S. aureus* were grown. However, after adding the hybridized PPy-PDa-ZnO/Ag, a ZOI of both bacteria was observed. Therefore, ZnO/Ag were responsible for the antibacterial properties of the films, while LigNPs increased the thermal stability and improved the mechanical properties of the composites.

As mentioned in the previous sections, one of the most efficient methods for controlling the growth of microorganisms is the use of AgNPs. However, concerns about the safety for human health and the environment appear related to the diffusion of such NPs to food, thus, the release of AgNPs from food packaging materials should be rigorously controlled. According to the European Food Safety Authority (EFSA), using AgNPs additives at low concentrations (up to 0.025 % w/w) in polymers that do not swell should not raise safety concerns for the consumer, since under these conditions the release of silver is below the acceptable daily intake.¹²³

Lignin-capped AgNPs were used as active fillers in cellulose fibrous membranes,¹¹⁹ agar films,¹²⁰ and PLA films,¹²¹ achieving antibacterial properties against food-borne pathogens such as *E. coli* and *Listeria monocytogenes*. Zhang *et al.* prepared TA@LS-Ag NPs using tannic acid (TA) as a reducing agent and LS as a carrier and dispersing agent (**Figure 10a**).¹⁰⁷ By comparing the different hybrid NPs (TA-Ag, LS-Ag, TA@LS, and TA@LS-Ag), the authors demonstrated the important role of lignin in the antibacterial activity of the particles, since it significantly reduced the minimum inhibitory and bactericidal concentrations of

TA@LS–Ag in comparison with TA–Ag. The ternary particles provided PVA films with antibacterial activity, being able to inhibit the growth of *S. aureus* and *E. coli*. The TA@LS–Ag also improved the mechanical performance of the films, showing very high toughness and tensile strength values, which were attributed to the dense hydrogen bonding interactions between the particles and the PVA matrix.

Biomedical applications

The interest in utilizing lignin as a functional additive for biomedical applications has increased over the past years, demonstrating the suitability of lignin for the development of advanced and sustainable biomaterials. LigNPs have been studied as vehicles for drug and gene delivery, as biosensors, for tissue engineering, etc.^{124,125} This section focuses on antibacterial biomedical materials containing LigNPs, comprising hydrogels, films, nanofibers, and foams (Table 5). Long-lasting antibacterial properties of these materials are required, which are usually achieved by a sustained release of the active NPs over time. However, such release of NPs together with the degradation products of the polymeric matrix may cause cell inflammation.¹²⁶ Thus, an in-depth investigation of the cytotoxicity and biocompatibility of these materials should be conducted before their application for human health.

A facile approach for the development of antibacterial nanolignin-based materials is to use LigNPs as fillers in a polymeric matrix. For instance, hydrogels of PVA and CS embedding LigNPs as antibacterial fillers were prepared by Puglia *et al.*¹²⁷ The resulting PVA/Ch/LigNPs gels were able to reduce the number of viable *E. coli* and *S. aureus* by 2 log. Bacterial reduction was also observed in the PVA/Ch gels prepared without NPs, especially against *E. coli*, probably due to the presence of antibacterial CS. On the other hand, the growth of planktonic *S. epidermidis* was only reduced by the hydrogels containing LigNPs, even though the reduction was modest (~0.3 log). However, the gels were not efficient against *S. epidermidis* biofilms, which reflects the much higher resistance of biofilm-forming bacteria to antibacterial agents.

Table 5 Nanolignin-embedded antibacterial polymeric materials for biomedical applications

Type of lignin	Filler	Polymer matrix	Material	Antimicrobial activity	Application	Ref.
Steam explosion and enzymatic treatment	LigNPs	PVA, chitosan	Hydrogel	<i>S. aureus</i> , <i>E. coli</i>	Biomedical, generic	127
LS	PANI-LIG:Fe ₃ O ₄ @GS	N.A.	Coating onto titanium	<i>S. aureus</i> , <i>E. coli</i> , <i>C. albicans</i>	Coating	128
Alkali	AgLigNPs	CA, AA, P(AAm-co-AA)	Hydrogel fibers	<i>E. coli</i>	Coating	129
Lignocellulosic biomass	AgLigNPs	Lignocellulose	Hydrogel	<i>E. coli</i>	Wound healing	111
Alkali	AgLigNPs	Pectin, PAA	Hydrogel	<i>S. aureus</i> , <i>E. coli</i>	Wound healing	130
Alkali	AgLigNPs	HA-SH	Hydrogel	<i>S. aureus</i> , <i>P. aeruginosa</i>	Wound healing	105
Alkali	AgLigNPs	PAHC	Hydrogel	<i>E. coli</i> , <i>S. aureus</i> , MRSA, <i>C. albicans</i>	Wound healing	131
Alkali	AgLigNPs	Carrageenan	Hydrogel	<i>S. aureus</i> , <i>E. coli</i>	Wound healing	132
Alkali	LNP-Ag, CNC	PVA	Hydrogel	<i>S. aureus</i> , <i>E. coli</i>	Wound healing	133
Kraft	Ag/Au NPs	PAA	Hydrogel	<i>C. albicans</i>	Wound healing	134
LS	AgNPs	Aminated lignin, PVA	Hydrogel	<i>S. aureus</i> , <i>E. coli</i>	Wound healing	135
Organosolv	AgNPs	Lignin, PVA	Nanofiber mats	<i>E. coli</i> , <i>B. circulans</i>	Wound healing	136
Alkali	AgLigNPs	PAN	Nanofibers	<i>S. aureus</i> , <i>E. coli</i>	Wound healing	137
Alkali	CuO	CNF	Nanofibers	<i>S. aureus</i> , <i>E. coli</i>	Wound healing	138
Extracted by enzymolysis	AgLigNPs	PU	Foam	<i>S. aureus</i> , <i>E. coli</i>	Wound healing	108

For some biomedical applications, such as implantable medical devices and their packaging, an environment completely free from bacteria is required. To this end, the medical devices should possess a strong antibacterial effect that prevents the colonization of bacteria and biofilm formation. The combination of biocompatible LigNPs with strong antibacterial metals is a common approach for achieving such performance.

Coatings

Bacterial adhesion on biomedical devices and subsequent biofilm formation is a major concern from health and economic perspectives. An approach to prevent bacterial contamination and proliferation is the surface coating with antibacterial NPs. An example of antibacterial coating for implantable titanium devices is found in the work of Visan *et al.*, who developed nanostructured coatings based on polyaniline grafted lignin (PANI-LIG) embedded with magnetite nanoparticles loaded with aminoglycoside gentamicin sulfate (GS) ($\text{Fe}_3\text{O}_4\text{@GS}$).¹²⁸ The coatings were anticorrosive, antioxidant, and more hydrophilic than the bare titanium surface. The formation of *E. coli* and *S. aureus*, and *C. albicans* biofilms on the coatings were inhibited by ~ 3 , ~ 1.5 , and ~ 1.5 log, respectively, in 24 h. On the other hand, human osteoblast-like cells did not lose viability when were grown onto the surface of the PANI-LIG: $\text{Fe}_3\text{O}_4\text{@GS}$ coatings, which makes feasible the application of these materials as medical implants. In another work, highly-stretchable hydrogel fibers based on AgLigNPs, citric acid (CA), acrylic acid (AA), and poly(acrylamide-co-acrylic acid) (P(AAm-co-AA)) were prepared by He *et al.*¹²⁹ The AgLigNPs, obtained by lignin-mediated reduction, participated in the gelation process by initializing the radical polymerization of monomers and, owing to the quinone-catechol reversible reactions, provided the hydrogel with adhesion properties. CA was added to the formulation to create reversible bonds that improve the deformability and stretchability of the gel, enabling its manufacturing in form of fibers with a diameter of 50 μm . The hydrogels demonstrated antibacterial activity against *E. coli*, achieving 1.8 log reduction after 24 h. When the hydrogel fibers were coated

onto a mask (i.e. personal protective equipment) by electrospinning, a 100 % eradication of *E. coli* was achieved.

Wound healing

Chronic wounds are injuries that fail to progress through the normal stages of healing¹³⁹ and generally result from diabetes ulcer, leg ulcer and burns, but conditions such as vascular diseases and cancer also contribute to wound chronicity.¹⁴⁰ Actually, complications related to diabetic ulcers affect 1.51 per 1000 population¹⁴¹ and precede the majority of nontraumatic amputations.¹⁴² The dynamic process of wound healing takes place in three overlapping phases, i.e. hemostasis (blood clotting), inflammation (immune cells recruitment), proliferation (fibroblast growth and extracellular matrix (ECM) regeneration), and tissue remodeling (degradation of excess of collagen and maturation) (**Figure 11**).¹⁴³ The healing process is regulated by many factors including immune cells, growth factors, cytokines, and enzymes. The defective regulation of these complex events delays healing and results in the development of wound chronicity, with the healing process stalled in the inflammatory phase.¹⁴⁴ Chronic wounds are susceptible to infection by resident opportunistic bacteria normally

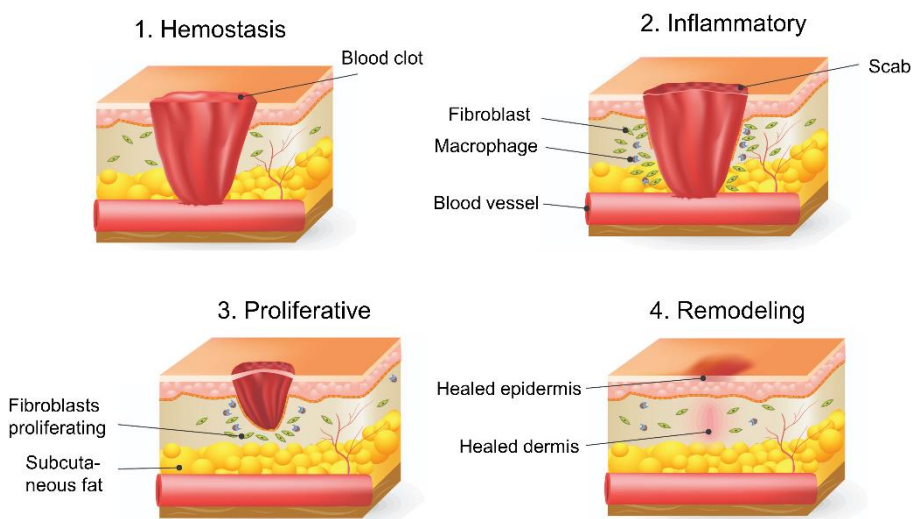


Figure 11. Schematic representation of the main phases of wound healing (adapted from Ref. 300 with permission from the American Chemical Society).

found in the skin, but also by exogenous pathogenic bacteria. All chronic wounds are heavily contaminated with microorganisms, among which *S. aureus*, *P. aeruginosa*, *E. faecalis*, *S. epidermidis*, and anaerobic bacteria are the most common.^{145,146} In addition, non-healing wounds are also characterized for having elevated levels of ROS, which promotes biofilm formation¹⁴⁷ and deregulates the enzymes responsible for tissue remodeling, i.e. matrix metalloproteinases (MMPs). The elevated inflammation in chronic wounds over activates myeloperoxidase (MPO) which produces elevated levels of hypochlorous acid. As a result, the tissue inhibitors of MMPs (TIMMPs) are degraded, and in turn, the latent form of MMPs is activated.¹⁴⁸ The ECM is excessively degraded when the MMPs/TIMMPs ratio is shifted towards overexpression of MMPs, which hinders the wound healing process.¹⁴⁹

Considering the pathophysiology of chronic wounds, an efficient wound dressing material should simultaneously inhibit the growth of pathogenic bacteria, reduce oxidative stress and promote wound healing by reducing the activity of deleterious enzymes. In the design of materials for wound treatment, lignin is frequently found in combination with metals to enhance the antibacterial activity of the dressing to achieve efficient pathogen elimination (Table 5). Different nanolignin-based materials for wound healing have been developed, mainly hydrogels, nanofibers, and polyurethane foams.

Hydrogels

Polymer hydrogels are three-dimensional (3D), porous, hydrophilic networks capable of retaining large amounts of water. Hydrogels can be synthesized by covalent crosslinking induced by radical polymerization, redox reactions, and enzymatic catalysis, among others,^{150,151} which yield non-reversible covalent bonds between the polymer chains. In physically crosslinked hydrogels, the polymeric matrix is formed by non-covalent interactions such as hydrogen bonds, ionic interactions, crystallization, metal coordination, and hydrophobic-hydrophilic interactions that usually occur at mild reaction conditions.¹⁵² These

dynamic and reversible interactions allow the hydrogels to adapt to complicated geometries of the site for their application and to self-heal after a stress causing network rupture.

Advanced hydrogel dressings should incorporate multifunctional agents to ensure antibacterial and antioxidant capacities.¹⁵³ In the case of hybrid silver/lignin NPs as actives in hydrogels for wound treatment, examples of use can be found in Gan *et al.* where novel pectin and poly(acrylic acid) (PAA) hydrogel was built using AgLigNPs as antibacterial and crosslinking agents.¹³⁰ Ammonium persulfate (APS) produced free radicals in lignin, which initiated the polymerization of the hydrogel. The hydrogels presented bactericidal properties *in vitro*, being able to reduce cultures of *S. aureus* and *E. coli* by 98 and 97 %, respectively, and *in vivo* in a rabbit model. The catechol-based chemistry was the main responsible for the durable adhesiveness of the gels. The *in vitro* studies showed the capacity of the gels to promote cell adhesion and proliferation, while the *in vivo* tests with rats validated the wound healing and skin tissue regeneration capacities of the hydrogel.

Our group developed a self-assembling injectable hydrogel based on modified thiolated hyaluronic acid (HA-SH) and Ag@LigNPs (**Figure 10b**).¹⁰⁵ The lignin-capped NPs were responsible for the gelation through multiple polymer-NP interactions, comprising hydrogen bonding, thiol- π , and cation- π . These dynamic non-covalent interactions imparted self-healing and injectability to these materials. The hydrogels displayed a strong bactericidal activity, achieving 7 and 4.5 log reduction of *P. aeruginosa* and *S. aureus*, respectively, while cytotoxicity toward human keratinocytes was not observed. Interestingly, the release of silver was sustained over time (following zero-order kinetics), which is expected to prolong the antibacterial activity and reduce possible side effects. *In vivo* studies in mice showed a rapid closure of the wound after the treatment with the gel, complete regeneration of the skin and lack of signs of inflammation or bacterial infection. Similarly, using an *in situ* synthetic approach, AgNPs obtained by lignin-mediated reduction were used as crosslinking agents to construct

hydrogels based on phenylboronic acid-modified hydroxypropyl cellulose (PAHC).¹³¹ The dynamic borate ester bonds of catechol groups of lignin with the phenylboronic acid groups in PAHC provided self-healing and shape adaptive properties. Moreover, the hydrogels were capable of adhering to different tissues and inorganic materials through hydrogen bonding, electrostatic, and ion coordination interactions. The gels presented radical scavenging ability and completely eradicated *E. coli*, *S. aureus*, the yeast *C. albicans*, and MRSA. *In vivo* studies with a MRSA-infected wound model showed that the hydrogels accelerated the epithelial tissue regeneration, reduced the inflammatory cell infiltration, and significantly promoted the wound healing. The *in situ* reduction of silver into hydrogels was also achieved using the lignin from lignocellulosic biomass as a reducing and capping agent.¹¹¹ By adjusting the content of lignin in the hydrogel, AgLigNPs of different size were obtained (10–40 nm). The hydrogels inhibited the growth of *E. coli*, obtaining larger ZOI with the increase of lignin content in the material.

The one-pot synthesis of carrageenan-based AgLigNPs-enabled hydrogels was performed by Jaiswal *et al.* using lignin as a reducing and capping agent, and divalent cations (CaCl_2 , CuCl_2 , MgCl_2) as crosslinking agents.¹³² The presence of AgLigNPs increased the tensile strength and elongation of the hydrogel while completely eradicating *E. coli* and *S. aureus* within 3–6 h. The hydrogels showed good biocompatibility with dermal fibroblasts *in vitro* and were capable of improving the healing of wounds in rats. Yang *et al.* studied the effect of silver/lignin NPs and CNC in PVA hydrogels.¹³³ The hydrogels were prepared by firstly embedding AgNPs onto the surface of LigNPs by a direct reduction of silver nitrate, then PVA was crosslinked by glutaraldehyde in presence of CNC and Ag loaded LigNPs (LNP-Ag). The addition of the nanofillers allowed to tune the pore structure and mechanical properties of the material. The hydrogels containing LigNPs presented a slight antibacterial effect against *S. aureus* and *E. coli*, tested by the agar diffusion method, that was significantly improved when LNP-Ag were added. The gels containing LigNPs and LNP-Ag exhibited radical scavenging

activity unlike the PVA and PVA/CNC hydrogels alone. The wound healing and skin regeneration tested *in vivo* in mice was accelerated by the Ag-containing hydrogel, which was attributed to the gradual release of LNP-Ag from these hydrogels.

An *in situ* approach for the synthesis of AgNPs into a lignin-based hydrogel was chosen by Li *et al.*¹³⁵ First, LS was aminated through Mannich reaction and was then crosslinked with PVA to form the hydrogel. Afterwards, silver nitrate was added and AgNPs were formed by reduction within the hydrogel. The hydrogel completely eradicated *E. coli* and *S. aureus* within 6 and 9 h, respectively, and reduced the cell viability of mouse fibroblast cells (L929 cell line) by 25 %.

The use of hybrid lignin-bimetallic NPs in hydrogels for wound healing has been explored by Chandna *et al.*¹³⁴ using Kraft lignin as a reducing and stabilizing agent for the synthesis of Ag/Au NPs conjugated with the photosensitizer Rose Bengal and doped into a PAA hydrogel. A rapid release of the nanoactives occurred at acid pH due to degradation of the hydrogel under this condition. After excitation with a green laser, the number of viable yeast (*C. albicans*) decreased. These results demonstrated the applicability of the hydrogels in antimicrobial photodynamic therapies for infected acute wounds, where the environment is mostly acidic.

Nanofibers

AgNPs were synthesized *in situ* onto the surface of polyacrylonitrile (PAN) nanofibers using lignin as a reducing agent.¹³⁷ The presence of lignin did not only provide antioxidant capacities but also significantly promoted the NPs' anchoring onto the nanofibers. The antibacterial activity of the PAN/AgNPs composites tested by the agar diffusion method showed ZOI of ~13–21 mm against *S. aureus* and *E. coli*, achieving higher values increasing the concentration of the silver precursor. On the contrary, PAN nanofibers without NPs did not inhibit the growth of bacteria. The antibacterial activity of the nanocomposites

was attributed to the burst release of silver within the first 2 h, followed by a sustained release over several days. These nanofibrous materials were considered suitable for the treatment of acute wounds.

The *in situ* lignin-mediated synthesis of CuO nanoparticles on the surface of electrospun CNF as potential wound dressings was also explored by Haider *et al* (**Figure 10c**).¹³⁸ The CuO/CNF released 80 % of the copper ions within the first 24 h, reaching a plateau in the release during the next 5 days. The growth of *S. aureus* and *E. coli* was inhibited by the CuO/CNF (ZOI 1.9–2.8), while the viability of a NIH3T3 fibroblast cell line was over 80 % after 7 days of incubation in the presence of the nanofibers. Moreover, the presence of lignin conferred antioxidant properties to the nanofibers. The incorporation of AgNPs into lignin/PVA nanofibrils was carried out by Aadil *et al.*¹³⁶ In this work, lignin was not in form of NPs but as a polymer matrix together with PVA in the electrospun nanofibers. The material was capable of inhibiting the growth of *E. coli* and *B. circulans* in the agar diffusion test, showing larger ZOI than antibiotic discs.

Polyurethane foams

Polyurethane is a synthetic material made of polyols and isocyanate bonded by urethane linkages through polyaddition polymerization. Flexible polyurethane foams (PUFs) are of particular interest for wound management due to their high capacity to absorb fluids, mechanical stability, softness, flexibility, and low cytotoxicity.^{142,154} Due to these properties, PUF dressings have the capacity to absorb large amounts of wound exudates and can be easily adapted to different wound shapes. Despite PUFs act as a physical barrier between the wound and the environment, the incorporation of antimicrobial NPs within this material would provide functionalities, yielding high-performance antibacterial wound dressings.

An *in situ* approach for the synthesis of lignin-based PUFs (LPUFs) was adopted by Li *et al.*,¹⁰⁸ where AgNPs were formed reduced by lignin during polyurethane polymerization (**Figure 10d**). The synthetic procedure of these

composite foams comprised liquefaction of lignin with poly(ethylene glycol) and glycerol, following simultaneous foaming and AgNPs formation. The swelling behavior of the resulting AgNP-LPUFs was influenced by the presence of hydrophobic lignin and AgNPs by decreasing the water uptake ability of the foams. The AgNP-LPUFs gradually reduced the number of viable *S. aureus* and *E. coli* over time, achieving above 99 % reduction after 8 h. However, the antibacterial activity of the foams against *S. aureus* was significantly lower than against *E. coli*. The LPUF without AgNPs did also present some antibacterial activity against *E. coli*, which was attributed to the intrinsic antibacterial activity of lignin. *In vivo* studies in mice wound model showed that the group treated with AgNP-PUF exhibited better wound area closure than those treated with PUF, LPUF, and a commercial dressing without antibacterial agents.

Objectives

The **main objective** of this thesis is to engineer antibacterial lignin-based nanoparticles and multifunctional nano-composite materials for biomedical applications. Different strategies, such as enzymatic functionalization and ultrasonication, or a combination thereof, will be applied in the context of green chemistry by using lignin as a key functional and structural element for building the novel nanomaterials. Given the antimicrobial and antioxidant capacities of lignin, the developed NPs are expected to improve the treatment of chronic wounds. For this purpose, the NPs need to be embedded or crosslinked in a scaffold material that would serve as a wound dressing.

The **specific objectives** towards the design of lignin-based nano-enabled materials for medical applications are the following:

- **To develop efficient antibacterial NPs combining lignin with natural phenolic compounds, metals, and metalloids** using enzymatic or sonochemical technologies. Despite lignin being considered an antibacterial biomolecule, the enhancement of its antibacterial properties by means of nanotransformation, functionalization, and combination with other antibacterial agents would lead to nanoentities with high potential in the biomedical field.
- **To expand the knowledge on the antibacterial mode of action of lignin-based nanomaterials.** Regardless of the broad information available about the mechanism of action of metal NPs, very few have been explored in biopolymer-based NPs. Understanding how such NPs interact with bacteria would ease the engineering of efficient antibacterial NPs.
- **To incorporate lignin-based NPs into synthetic polyurethane foams as materials for wound healing.** Wound dressings are usually inert materials that serve as absorbents of wound exudate and as a physical barrier to avoid infection, but do not promote wound healing. The development of active dressing materials is crucial for accelerating the healing of wounds. The addition of lignin-based NPs into foams formulations is expected not only to provide bioactivities, but also to

improve their mechanical properties due to covalent crosslinking with the polyols.

- **To use lignin-based NPs as active and crosslinking agents for the synthesis of biopolymer hydrogels for wound healing.** Taking advantage of the functional groups of lignin, the developed lignin nanoparticles could be used not only as active agents, but also as driving elements for self-assembling in the formation of novel hydrogel materials through non covalent interactions. The combination of the NPs with specific biopolymers would result in efficient hydrogel materials for wound healing.

Chapter 1

Antibacterial lignin-based nanoparticles

This chapter is based on the following publications:

Morena A G, Stefanov I, Ivanova K, Pérez-Rafael S, Sánchez-Soto M, Tzanov T. “Antibacterial Polyurethane Foams with Incorporated Lignin-Capped Silver Nanoparticles for Chronic Wound Treatment”. *Industrial and Engineering Chemistry Research*, 2020, doi: 10.1021/acs.iecr.9b06362

Morena A G, Bassegoda A, Hoyo J, Tzanov T. “Hybrid Tellurium-Lignin Nanoparticles with Enhanced Antibacterial Properties”. *ACS Applied Materials & Interfaces*, 2021, licensed under CC-BY 4.0, doi: 10.1021/acsami.0c22301

Morena A G, Bassegoda A, Natan M, Jacobi G, Banin E, Tzanov T. “Antibacterial Properties and Mechanisms of Action of Sonoenzymatically Synthesized Lignin-Based Nanoparticles”. *ACS Applied Materials & Interfaces*, 2022, licensed under CC-BY 4.0, doi: 10.1021/acsami.2c05443

Chapter 1. Antibacterial lignin-based NPs

Introduction

In recent years, lignin has drawn increasing attention for different applications due to its intrinsic antibacterial and antioxidant properties, coupled with biodegradability and biocompatibility.⁵⁹ Despite those different green methods to produce LigNPs, including solvent exchange,⁶² water-in-oil microemulsions,¹⁵⁵ and ultrasonication,^{63,67} are used for biomedical and food applications where biocompatibility and biodegradability are crucial features, chemical modification of lignin and its combination with metals is usually a requirement to potentiate the functionalities of the NPs and extend their application range.⁷⁶

Several techniques have been used to enhance the antibacterial and antioxidant properties of lignin and LigNPs, including chemical phenolation^{156,157} and amination⁶⁹. Traditional functionalization strategies often involve toxic reagents or metal catalysts and require harsh conditions. An eco-friendly alternative to enhance the antibacterial activity of lignin is the use of enzymatic catalysis for grafting functional molecules. This biotechnological approach provides clear environmental advantages over chemical modification, allowing it to work at mild conditions and avoiding the use of hazardous chemicals, ultimately reducing the amount of toxic residues.¹⁵⁸ Laccases are oxidoreductases found in plants, fungi, and bacteria that catalyze the oxidation of a wide range of substrates, including phenolic lignin-related compounds. Once oxidized, the phenolic group yields radicals that rapidly form reactive phenoxy radicals, which are able to form covalent bonds with other molecules.

On the other hand, the chemical reduction of metal ions to produce NPs is frequently achieved by toxic reducing agents, such as borohydride, and requires stabilizers such as PEG to prevent particle aggregation.¹⁵⁹ Alternatively, lignin

can be used both as a reducing and capping agent of metals due to its large content of phenolic and aliphatic hydroxyl groups.^{34,76}

In this chapter, the synthesis and characterization of different formulations of antibacterial lignin-based NPs are described. Concretely, lignin –pristine or enzymatically modified with phenolic groups– was used as a reducing agent of metals and metalloids, or as an antibacterial agent itself, for the synthesis of hybrid NPs (**Figure 12**). The three formulations of lignin-based particles are described below:

- **Tellurium lignin NPs (TeLigNPs)**. Pristine lignin was used to reduce sodium tellurite to elemental tellurium (Te^0) under US, which yielded TeLigNPs.
- **Phenolated lignin NPs (PheLigNPs)**. Lignin-based particles were produced by a sonoenzymatic approach that allowed to simultaneously functionalize and nano-transform lignin, resulting in PheLigNPs.
- **Silver phenolated lignin NPs (AgPheLigNPs)**. Lignin enriched with phenolic compounds via laccase oxidation was used to reduce silver nitrate to elemental silver (Ag^0) under US and produce AgPheLigNPs.

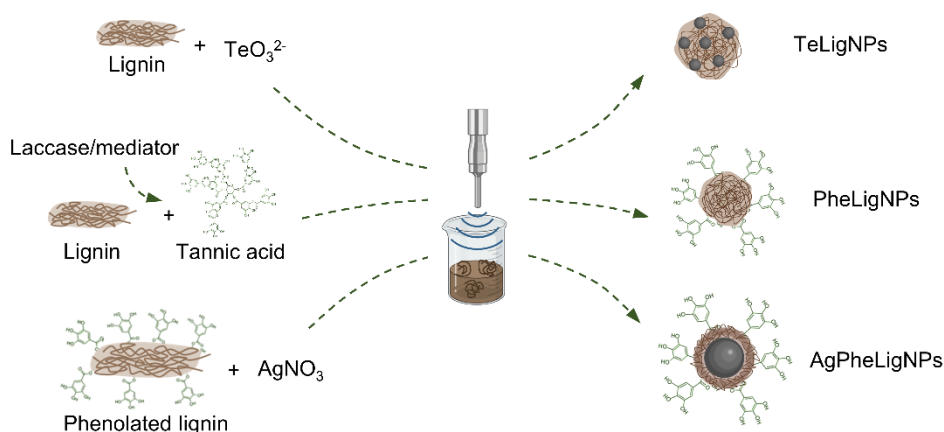


Figure 12. Schematic representation of the synthesis of lignin-based NPs *via* ultrasound.

The antibacterial activity of these NPs against Gram-positive and Gram-negative bacteria, as well as their mode of action, were studied. Their biocompatibility with human cell lines, which is a prerequisite for their application in the medical field, was also assessed.

Materials and methods

Reagents, cells, and enzymes

Protobind 6000 sulfur-free soda lignin powder was purchased from Green Value (Switzerland). Tannic acid (TA), gallic acid (GA), and 3',5'-dimethoxy-4'-hydroxyacetophenone (acetosyringone) were obtained from ACROS Organics (Belgium). Silver nitrate, sodium tellurite, hydrogen peroxide, chloroform, 2,2'-azino-bis(3-ethylbenzothiazoline-6-sulfonic acid) diammonium salt (ABTS), phosphate buffered saline (PBS), Folin-Ciocalteu's phenol reagent, resazurin sodium salt, and Dulbecco's Modified Eagle's Medium (DMEM) were purchased from Sigma-Aldrich (Spain). Nutrient broth (NB) was provided by Sharlab (Spain). Luria-Bertani (LB) with agar, Coliform ChromoSelect agar, Cetrimide agar, and Baird Parker agar were obtained from Sigma-Aldrich (Spain). Ciprofloxacin and ampicillin were purchased from Fluka and Duchefa, respectively. AlamarBlue cell viability reagent and molecular probe H₂DCFDA, and Live/Dead BacLight kit (Molecular probes L7012) were purchased from Invitrogen, Life Technologies Corporation (Spain). Avanti Polar Lipids provided phosphatidylethanolamine (PE, #840027) and phosphatidylglycerol (PG, #841188) extracted from *E. coli*.

Bacterial strains *S. aureus* (ATCC 25923), *B. cereus* (14579), *E. coli* (ATCC 25922) and *P. aeruginosa* (ATCC 10145), human fibroblast cells (ATCC-CRL-4001, BJ-5ta), and human keratinocyte cells (HaCaT cell line) were obtained from the American Type Culture Collection (ATCC LGC Standards, Spain).

Novozym 51003 laccase from *Miceliophthora termophila* was provided by Novozymes (Denmark). The enzymatic activity of laccase was 529 U·mL⁻¹ defined

as the amount of enzyme converting 1 μmol ABTS to its cation radical ($\epsilon_{436}=29\ 300\ \text{M}^{-1}\cdot\text{cm}^{-1}$) in sodium acetate buffer (0.05 M, pH 5) at 25 °C.

The water used in all experiments was purified by MilliQplus system (Millipore) with 18.2 $\text{M}\Omega\cdot\text{cm}$ resistivity prior to its use.

Characterization of laccase

Laccase activity was determined by monitoring the oxidation of ABTS by changes in absorbance. Briefly, 10 μL of diluted laccase was mixed with 215 μL of sodium acetate buffer (0.05 M, pH 5.0) and 25 μL of 10 mM ABTS. The increase in the absorbance was measured at 436 nm and 25 °C. For the blank, laccase was substituted by buffer. The activity of laccase was defined as the amount of enzyme converting 1 μmol of ABTS to its cation radical ($\epsilon_{436} = 29\ 300\ \text{M}^{-1}\cdot\text{cm}^{-1}$) in sodium acetate buffer (0.05 M, pH 5.0) at 25 °C and was calculated as follows:

$$\text{Activity (U}\cdot\text{mL}^{-1}) = \frac{(\Delta A_{\text{test}} - \Delta A_{\text{blank}}) \times \text{final volume (mL)} \times \text{dilution factor of enzyme}}{\text{time (min)} \times \epsilon (\text{mM}^{-1}\text{cm}^{-1}) \times \text{pathlength (cm)} \times \text{volume of enzyme}} \quad (\text{Eq. 1})$$

The optimum pH and temperature of the enzyme was studied using ABTS as a substrate. First, 10 μL of diluted laccase was mixed with 215 μL of 0.05 M Britton-Robinson buffer (pH 3.0–10.0) and 25 μL of 10 mM ABTS. The increase in the absorbance was measured at 436 nm and 25 °C. The highest increase in absorbance of laccase was taken as the 100 % relative activity.

Once the optimum pH was established, the optimum temperature was determined by mixing 10 μL of diluted laccase, 215 μL of sodium acetate buffer (0.05 M, pH 5.0), and with and 25 μL of 10 mM ABTS. The mixture was subjected to a range of temperatures (25–75 °C) and the increase in absorbance at 436 nm was measured. The highest increase in absorbance of laccase was taken as the 100 % relative activity.

The stability of laccase at 50 °C under stirring or US was also studied. Laccase diluted in sodium acetate buffer (0.05 M, pH 5.0) was subjected to stirring at 200 rpm, or high-intensity US (20 kHz, 50 % amplitude, Ti-horn, VCX 750 ultrasonic

processor, Sonics, USA) for 1 h at 50 °C. Aliquots of 100 μL were withdrawn to measure the laccase activity as previously described. The activity of laccase in the initial point was considered 100 % relative activity.

Synthesis of AgPheLigNPs

Previous to the NPs' synthesis, lignin was enzymatically grafted with phenolic compounds to increase its reactivity. Protobind 6000 lignin ($10 \text{ mg}\cdot\text{mL}^{-1}$) was soaked in sodium acetate buffer (0.05 M, pH 5), where the mediator acetosyringone ($1.5 \text{ mg}\cdot\text{mL}^{-1}$) was previously dissolved. Laccase at a final concentration of $5.29 \text{ U}\cdot\text{mL}^{-1}$ was added and the mixture was stirred for 1 h at 50 °C to pre-activate lignin. Then, GA ($10 \text{ mg}\cdot\text{mL}^{-1}$) and TA ($10 \text{ mg}\cdot\text{mL}^{-1}$) were added to the mixture and stirred at 50 °C for 2 h. The enzymatic reaction was stopped by increasing the temperature to 95 °C for 15 min. The phenolated lignin was separated from the non-reacted phenolic compounds by centrifugation for 20 min at $4000g$, and freeze-dried.

Phenolated lignin was dissolved in water ($10 \text{ mg}\cdot\text{mL}^{-1}$) and the pH was adjusted to 8. The solution was mixed with $4 \text{ mg}\cdot\text{mL}^{-1}$ AgNO_3 (3:2 lignin : silver ratio) and subjected to high-intensity US (20 kHz, 50 % amplitude, Ti-horn) for 2 h at 60 °C (VCX 750 ultrasonic processor, Sonics, USA). The NPs were purified by centrifugation of the reaction mixture at $18000g$ for 40 min. The obtained pellet was resuspended in miliQ water and centrifuged at $500g$ for 10 min to remove the non-reacted lignin molecules. The suspension was further subjected to low-intensity US to disaggregate the nanoparticles.

Synthesis of TeLigNPs

First, lignin was dispersed in water ($10 \text{ mg}\cdot\text{mL}^{-1}$) and the pH was raised to 9 by addition of 1 M NaOH. Thereafter, sodium tellurite powder was diluted in the prepared lignin solution at 100 mM final concentration. The resulting solution was subjected to high-intensity US (20 kHz, 50 % amplitude, Ti-horn) for 30 min at 60 °C (VCX 750 ultrasonic processor, Sonics, USA). The generated NPs were purified by centrifugation at $25000g$ for 30 min. The pellet was washed for

complete removal of tellurite ions by resuspension in Milli-Q water and further centrifugation at 25000*g* for 30 min. Afterwards, the washed pellet was resuspended again in Milli-Q water and low-intensity US was used to completely disaggregate the NPs in the suspension. Finally, centrifugation at 500*g* for 5 min removed larger particles and remaining insoluble lignin.

Synthesis of PheLigNPs and LigNPs

Lignin (10 mg·mL⁻¹) was soaked in sodium acetate buffer (0.05 M, pH 5) where acetosyringone was previously dissolved (1.5 mg·mL⁻¹). Laccase at a final concentration of 5.29 U·mL⁻¹ was added and the mixture was stirred for 1 h at 50 °C to pre-activate lignin. Then, TA was added to a final concentration of 10 mg·mL⁻¹, and the solution was subjected to high-intensity US (20 kHz, 50 % amplitude, Ti-horn) for 1 h at 50 °C to produce the PheLigNPs (VCX 750 ultrasonic processor, Sonics, USA). The mixture was centrifuged at 18000*g* for 20 min to remove unreacted TA molecules present in the supernatant. The pellet was resuspended in water and concentrated 10-times, then, disaggregation of the particles was achieved by applying low-intensity US. Lastly, the NPs were centrifuged at 500*g* for 10 min to remove larger aggregates. The PheLigNPs were stored at 4 °C.

The LigNPs were synthesized by sonicating a solution of lignin in water (10 mg mL⁻¹) at 50 % amplitude and 50 °C for 2 h, following an adapted protocol previously reported.⁶³

Characterization of the lignin-based NPs

Phenolic content

The phenolic content of the lignin samples was determined spectrophotometrically, measuring the absorbance at 765 nm of a water solution containing 20 µL of lignin dispersion (1 mg·mL⁻¹), 100 µL of 20 %w/v Na₂CO₃ and 80 µL of 0.2 N Folin-Ciocalteu phenol reagent, after 10 min incubation in dark. GA was used to build the calibration curve. All samples were measured in

triplicated, and results are expressed in in GA equivalents (GAE) per gram of sample.

Hydrodynamic size, polydispersity index and ζ -potential

The hydrodynamic size, polydispersity index (PDI), and ζ -potential of the NPs were measured using a Zetasizer Nano Z (Malvern Instruments Inc., U.K.). Transmission electron microscopy (TEM) was used to study the morphology and distribution of the NPs by placing 10 μL of diluted sample onto holey carbon films on copper grids (for AgPheLigNPs and PheLigNPs) or carbon-coated silicon dioxide grids (for TeLigNPs). The samples were observed in a JEOL JEM-2100 LaB6 microscope operating at an accelerating voltage of 200 kV. Energy dispersive X-ray diffraction (EDX) was used for the elemental analysis, and chemical maps were acquired using the high-angle annular dark-field (HAADF) scanning TEM (STEM). Nanoparticle size was measured using the ImageJ software (version 1.52a).

FTIR spectra

FTIR spectra of lignin samples over the 600–4000 cm^{-1} range were collected by a PerkinElmer Spectrum 100 FTIR spectrometer (PerkinElmer, MA, USA) with an attenuated total reflection (ATR) accessory of germanium crystal with a high-resolution index (4.0), performing 64 scans for each spectrum at 4 cm^{-1} resolution. The peak at 2920 cm^{-1} , corresponding to the C-H stretching in aromatic methoxyl groups, was used for normalization.¹⁶⁰ For the semi-quantitative analysis of PheLigNPs, the relative intensities of the respective bands were calculated taking the band at 2920 cm^{-1} as the reference. The ratio of A_x/A_{2920} was taken as the quotient between specific intensity and the reference band.

UV-vis absorbance scan

UV-vis absorbance scan of the AgPheLigNPs was performed using a microplate reader Infinite M200 (Tecan, Austria) to study the presence of silver in its elemental form (Ag^0). The content of tellurium in the TeLigNPs and silver in the

AgPheLigNPs was quantified by inductively coupled plasma mass spectrometry (ICP-MS 7800, Agilent Technologies, USA) calibrated by an internal standard with ^{45}Rh and a standard curve of ^{125}Te or ^{107}Ag . Prior to the analysis, the samples were digested with 20 % (v/v) HNO_3 at 100 °C for 1 h, diluted until a final concentration of 2 % HNO_3 and filtered through a 0.2 μm pore size filter.

Growth inhibition of bacteria by the lignin-based NPs

The antibacterial activity of the lignin-based NPs was assessed toward Gram-positive *S. aureus* and *B. cereus*, and Gram-negative *E. coli* and *P. aeruginosa* following the serial dilution method. Overnight bacterial cultures were diluted in NB to an $\text{OD}_{600}=0.01$ ($\sim 10^5$ – 10^6 CFU·mL $^{-1}$). Then, 50 μL of the NPs at different concentrations were mixed with 50 μL of bacterial suspension in 96-well polystyrene plates. The samples were incubated for 24 h at 37 °C with 230 rpm shaking. Bacterial growth in the presence of NPs was assessed measuring the OD_{600} in a microplate reader (Infinite M200, Tecan, Austria). Bacterial inoculum without NPs was used as a growth control (no inhibition). The OD_{600} of the samples at time 0 h was used as a blank. The growth inhibition was calculated following Eq. 2:

$$\text{Bacterial growth inhibition (\%)} = 100 - \left(\frac{\text{OD}_{\text{sample}} - \text{OD}_{\text{blank}}}{\text{OD}_{\text{growth control}} - \text{OD}_{\text{blank}}} \times 100 \right) \quad (\text{Eq. 2})$$

The MIC was taken as the lowest concentration of NPs that inhibited the growth of the bacteria after 24 h of incubation at 37 °C. The minimum bactericidal concentration (MBC) was determined by plating 10 μL of the suspensions onto specific agar and further incubation for 24 h at 37 °C. The MBC was considered the lowest concentration of particles at which growth was not observed. In addition, the number of survived bacteria during NPs treatment was determined after plating 10 μL of the diluted suspensions onto specific agar and further incubation for 24 h at 37 °C. After counting the colonies, the log reduction and the percentage of reduction were calculated (Eq. 3 and 4).

For the kinetic growth curves, bacteria grown overnight in NB were diluted in NB medium to an $OD_{600}=0.01$ ($\sim 10^5$ – 10^6 CFU·mL⁻¹). Then, 250 μ L of bacterial suspension were incubated with 250 μ L of the lignin samples in 2 mL tubes at 37 °C with 230 rpm shaking. Growth controls were bacteria cultured in NB without lignin samples. After different incubation times, samples were taken and the number of survived bacteria (CFU·mL⁻¹) was obtained using the drop plate method. Briefly, serial dilutions of the samples were performed in PBS, and 10 μ L drops were plated in Baird-Parker, LB, Cetrimide, and Coliform ChromoSelect agar plates for *S. aureus*, *B. cereus*, *P. aeruginosa* and *E. coli*, respectively. After 24 h incubation of the agar plates at 37 °C, the grown colonies were counted. The log reduction and bacterial viability reduction (%) was calculated as follows:

$$\text{log reduction} = \log_{10}(A/B) \quad (\text{Eq. 3})$$

$$\text{bacterial viability reduction (\%)} = [(A - B)/A] \times 100 \quad (\text{Eq. 4})$$

where A and B are the average number of bacterial colonies before (0 h) and after (24 h) the treatment, respectively.

Cytotoxicity assay

Cytotoxicity of the lignin-based NPs was tested toward human fibroblasts (cell line BJ5ta) and human keratinocytes (cell line HaCaT). The cells were grown in 100 μ L of DMEM in a 96-well plate (60000 cells per well) at 37 °C in a humidified atmosphere with 5 % CO₂. After 24 h of cell growth, NPs at different concentrations were incubated in contact with the cells for 24 h. Afterwards, the NPs were removed from the wells, and washed three times with PBS. The cell viability assessment was performed using the AlamarBlue reagent, which is a redox indicator dye used for evaluation of the metabolic activity of cells. After removing the culture medium, 100 μ L of AlamarBlue reagent diluted in culture medium (10 % v/v) was added to each well. After 3 h incubation at 37 °C, the fluorescence was measured ($\lambda_{\text{ex/em}}=550/590$ nm). The percentage of cell viability was calculated using the fluorescence values of the wells containing only cells and AlamarBlue reagent as reference (growth control). Wells containing

only AlamarBlue reagent were used as the blank group. The percentage of cell viability was calculated following Eq. 5:

$$\text{cell viability (\%)} = \frac{(F_{\text{sample}} - F_{\text{blank}})}{(F_{\text{growth control}} - F_{\text{blank}})} \times 100 \quad (\text{Eq. 5})$$

Cell viability was further assessed with fluorescence microscopy using the Live/Dead Viability/Cytotoxicity kit that stains the live cells in green and the dead ones in red. After 24 h incubation of the cells with the NPs, the culture medium was removed and 20 μL of staining solution (0.1 % calcein AM and 0.1 % ethidium homodimer-1 in PBS) were added. After 20 min incubation in the dark, the samples were visualized under fluorescence microscopy using a 100x objective lens.

Generation of ROS by bacteria and human cells treated with lignin NPs

ROS generated by bacterial cultures exposed to the lignin-based NPs were evaluated using the oxidation-sensitive probe H_2DCFDA , which is activated by intracellular oxidants such as hydrogen peroxide and the hydroxyl radical.^{161,162} In the assay, carried out in triplicate, bacteria were grown in NB to an OD_{600} of ~ 0.8 and were exposed to TeLigNPs (2.39 ppm of Te) or PheLigNPs ($2.5 \text{ mg}\cdot\text{mL}^{-1}$) for 30 min at 37 °C. The samples were centrifuged at 4000g and washed twice with PBS. The bacteria in the pellet were incubated with a solution of 20 μM H_2DCFDA in PBS for 30 min in the dark. Thereafter, fluorescence measurements ($\lambda_{\text{ex/em}}=490/520 \text{ nm}$) were performed and normalized to OD_{600} . Bacteria incubated without NPs were used as controls.

ROS generated in human keratinocytes and fibroblasts were assessed after growing the cells in 100 μL of DMEM in a 96-well plate (60000 cells per well) at 37 °C in a humidified atmosphere with 5 % CO_2 . After 24 h, the cells were washed with PBS and were exposed to TeLigNPs (2.39 ppm of Te) for 30 min at 37 °C. After removing the particles, 100 μL of 2 mM H_2DCFDA was added. After 30 min incubation in the dark, the fluorescence measurements ($\lambda_{\text{ex/em}}=490/520 \text{ nm}$) were performed. Cells incubated without TeLigNPs were used as controls.

TEM of bacterial samples incubated with lignin-based NPs

TeLigNPs were incubated under shaking with *E. coli* and *S. aureus* ($OD_{600}=0.01$) for 2 h at 37 °C. The samples were centrifuged at 2000g for 5 min at 4 °C and resuspended in a fresh fixative solution containing 2.5 % (v/v) glutaraldehyde and 2 % (v/v) paraformaldehyde in 0.1 M phosphate buffer, pH 7.4. The samples were incubated with the fixative solution for 1 h at 4 °C, washed three times with 0.1 M phosphate buffer, pH 7.4 and fixed in 1 % (w/v) osmium tetroxide. Afterwards, the samples were stained with 2 % (w/v) uranyl acetate, dehydrated in ethanol, and embedded in Spurr resin. Ultrathin sections were obtained with an Ultracut E (Reichert-Jung) ultramicrotome and counterstained with lead citrate. Then, the slices were deposited on bare mesh copper grids and the sections were observed using JEOL 1100 transmission electron microscope at 80 kV.

Interaction of lignin-based NPs with bacteria assessed by SEM

In order to study the interaction of PheLigNPs with bacteria and their effect on cell structure, overnight bacterial cell cultures in NB grown at 37 °C were diluted to an $OD_{600}=0.01$ ($\sim 10^5$ – 10^6 CFU·mL⁻¹) and mixed with PheLigNPs (final concentration 1.25 mg·mL⁻¹). After 4 h incubation at 37 °C and 230 rpm, the volume was transferred to a 48-well plate containing silicon wafers. The samples were further incubated overnight at room temperature. Then, the liquid was carefully removed and the bacteria remaining in the grid were fixed overnight in a 2 % paraformaldehyde and 2.5 % glutaraldehyde buffered solution. The samples were dehydrated incubating the wafers with ascending concentrations of ethanol for 1 h each (25, 50, 75, and 100 %). The samples were observed using a field emission scanning electron microscope (FESEM) at 1kV (Merlin Zeiss).

Interaction of lignin-based NPs with bacteria assessed by QCM

The interaction of PheLigNPs with bacteria was assessed using a quartz crystal microbalance with dissipation monitoring (QCM-D, E4 system, Q-Sense, Sweden), following a previously reported procedure with some modifications.¹⁶³

The experiments were performed on gold sensors (QSX 301, QSense, Sweden) at 37 °C. A peristaltic pump was used to flow the liquids at a constant rate of 20 $\mu\text{L min}^{-1}$. At first, sterile PBS (100 mM, pH 7.4), was used for 30 min to establish a stable baseline. The deposition of bacteria on the sensor was achieved by circulating the *S. aureus* inoculum ($\text{OD}_{600}=0.2$) in NB for 3 h. In order to remove the non-deposited bacteria, PBS was flowed through the system for 1 h and a second baseline was established. Thereafter, PheLigNPs ($2.5 \text{ mg}\cdot\text{mL}^{-1}$ in PBS) were circulated for 45 min. Finally, the third baseline was established by further flowing PBS.

Interaction of NPs with model membranes assessed by Langmuir isotherms

For studying the interaction of TeLigNPs with bacterial model membranes, an insertion of the NPs into a previously established lipid monolayer was performed. First, a mixture of PE and PG was prepared at 8:2 (v:v) ratio in CHCl_3 ($0.5 \text{ mg}\cdot\text{mL}^{-1}$) to mimic a Gram-negative bacterial membrane.¹⁶⁴ The Langmuir films were formed in a Langmuir trough equipped with two mobile barriers (KSV NIMA Langmuir-Blodgett Deposition Troughs, model KN2002, Finland) mounted on an anti-vibration table housed in an insulation box at 23 ± 1 °C. Prior to subphase addition (MilliQ water), Langmuir trough was cleaned with CHCl_3 and water, and the surface was further cleaned by suction. Afterwards, 40 μL of the lipid mixture solution were added dropwise into the trough filled with the subphase, and after 10 min evaporation of CHCl_3 , the barriers were compressed at $15 \text{ cm}^2\cdot\text{min}^{-1}$ until reaching $33 \text{ mN}\cdot\text{m}^{-1}$, the equivalent of the natural membranes lateral surface pressure.¹⁶⁵ After the stabilization of the membrane for at least 30 min, 500 μL of TeLigNPs in MilliQ water were inserted beneath the Langmuir film and the changes of the surface pressure (π) derived from their interactions with the already formed bacterial model membrane were recorded. Blank experiments were carried out using the same procedure, but inserting 500 μL of MilliQ water instead.

The interaction of the PheLigNPs with bacterial model membranes was studied using Langmuir isotherms. A mixture of PE and PG in an 8:2 ratio (v:v) at $0.5 \text{ mg}\cdot\text{mL}^{-1}$ in chloroform was used to simulate the *E. coli* bacterial membrane. Monolayers were formed in the Langmuir trough at a constant temperature of $23 \pm 1^\circ\text{C}$. The surface pressure was measured using a Wilhelmy plate connected to the trough. After cleaning the system with chloroform and water, the subphase (PBS or PBS with PheLigNPs) was added and $30 \mu\text{L}$ of lipids was gently added. After the chloroform from the lipid mixture was evaporated, the surface pressure-area per molecule (π -A) isotherm was recorded under a barrier closure rate of $15 \text{ cm}^2\cdot\text{min}^{-1}$. The experiments were carried out three times, and one representative measure is reported.

Determination of membrane integrity by fluorescence imaging

Membrane integrity of bacteria incubated with PheLigNPs was assessed using the Live/Dead BacLight bacterial viability kit according to the manufacturer's instructions. Overnight bacterial cell cultures in NB grown at 37°C were diluted to an $\text{OD}_{600}=0.01$ and mixed with PheLigNPs (final concentration $0.6 \text{ mg}\cdot\text{mL}^{-1}$). After 24 h incubation at 37°C and 230 rpm, the cells were washed by centrifugation at $10000g$ for 2 min and the pellet was resuspended in NaCl 0.9 %. The bacterial suspension was stained with an equal mixture of SYTO 9 and propidium iodide, and observed using a fluorescence microscope (Nikon/Eclipse Ti-S, the Netherlands) after 15 min incubation in the dark. Bacteria grown in the absence of PheLigNPs were used as controls. Damage to the bacterial membrane was also assessed by measuring the fluorescence of the suspensions using a microplate reader (Infinite M200, Tecan, Austria). The excitation wavelength was 485 nm for both dyes, and the fluorescence was read at 530 nm for SYTO 9 and at 645 nm for propidium iodide. Fluorescence values of untreated and treated bacteria without the dyes were used as blanks. The ratio of SYTO-9 to propidium iodide ($R=\text{Emission SYTO 9}/\text{Emission propidium iodide}$) was calculated.

Resistance development assay

The ability of the PheLigNPs to cause resistance development among pathogenic bacteria was evaluated by determining first the MIC value using *S. aureus* ATCC 29213 and *E. coli* 25922. The stock solution of the NPs was diluted in two-fold serial dilutions in LB medium in a 96-well plate (Greiner Bio-one), and bacteria were added to a final concentration of bacteria of 10^5 CFU·mL⁻¹. The control was bacteria treated with water. The bacterial growth was monitored by measuring the absorbance at OD₅₉₅ using a microplate reader (Synergy 2, BioTek instruments). On the following day, each bacterium was serially passaged in two-fold antibiotic or NPs gradients in a 96-well plate, performing a MIC assay as described above except that the bacteria concentration was set on 10^5 CFU·mL⁻¹ from the second growth cycle. At the end of each growth cycle (20–24 h) following the determination of the MIC, the culture in the highest drug concentration having turbidity, suggestive of bacterial growth, was taken and diluted at 1:50. The newly diluted bacterial suspension was grown overnight in a new 96-well plate, conducting a new MIC assay, following which the absorbance was monitored. This assay was conducted daily for a period of 30 days to determine a change in the MIC value of the antibiotic or the NPs.

Data analysis

Three replicate samples were used in each measurement. Results are presented as mean values with standard deviation (SD) error bars. Data were analyzed using Graph Pad Prism version 8.0.1 (Graph Pad Software, CA, USA). Statistical significances were determined using the unpaired two-tailed Student's t-test or one-way ANOVA. *p* values <0.05 were considered statistically significant.

Results and discussion

Silver phenolated lignin nanoparticles

AgPheLigNPs synthesis and characterization

Lignin has attracted considerable attention as a renewable resource to produce chemicals or value-added materials. However, the low reactivity of lignin usually hinders its processability. Soda lignin (with intrinsic phenolic content of 206.9 ± 29 mg GAE per g lignin) was enzymatically modified with laccase to increase its reactivity by introducing phenolic groups from two natural phenolic compounds, GA and TA. The conditions of the enzymatic modification of lignin (reaction time, pH, and temperature) were set according to the characterization results of laccase (Annex – **Figure S1**).

Due to the enzymatic functionalization, the phenolic content of lignin increased 2-fold (397.2 ± 64 mg GAE·g⁻¹ lignin). The enzyme laccase oxidized the phenolic and non-phenolic lignin structures *via* the mediator acetosyringone.^{166,167} Upon the addition of GA and TA, these were also oxidized by laccase generating phenoxy radicals that converted to quinones and grafted on lignin^{168,169} increasing its phenolic content (**Figure 13**).

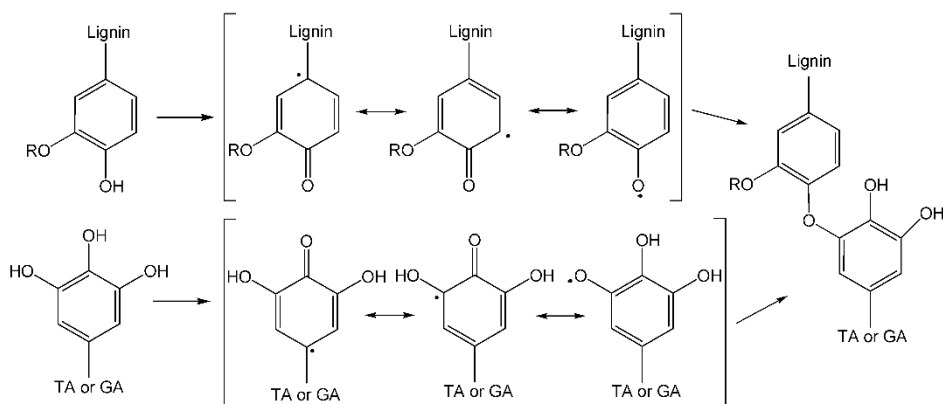


Figure 13. Proposed crosslinking reaction of lignin and TA or GA during the laccase-assisted phenolation.

The phenolated lignin was used as both reducing and capping agent to synthesize AgPheLigNPs in an US-assisted effective process. After supplying US energy to the solution of phenolated lignin and AgNO₃, its color changed from brown to dark yellow. The appearance of an absorbance peak at 428 nm confirmed the presence of Ag in metallic form (**Figure 14**). Contrarily, such absorbance peak was not observed in phenolated lignin without Ag⁺ or in Ag⁺ treated with non-modified lignin. The results indicated that higher phenolic content, and thus reactivity of lignin, was needed to reduce the silver ions.

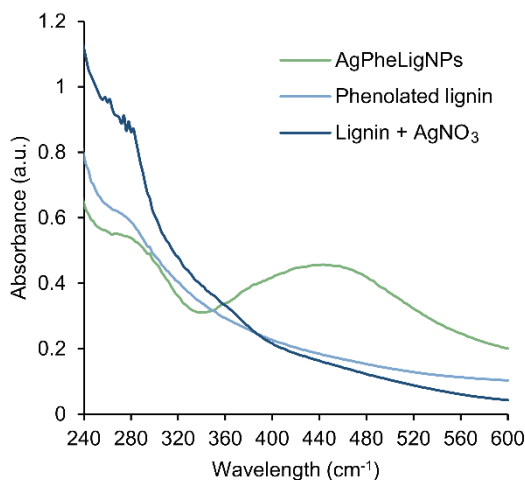


Figure 14. UV-vis scan of AgPheLigNPs, phenolated lignin, and a mixture of lignin and silver nitrate after ultrasound treatment.

Due to silver reduction and formation of AgPheLigNPs the phenolic content of lignin decreased from 397.2 ± 64 to 138.8 ± 80 mg GAE per g of lignin. After purification, the synthesized AgPheLigNPs were characterized by TEM in terms of size and morphology. The TEM images showed an organic matrix where metallic nanostructures of 13.29 ± 3.53 nm were embedded and evenly dispersed (**Figure 15a–c**). The composition of the Ag cores was confirmed by EDX analysis (**Figure 15d**) and the content of Ag in 1 mL of AgPheLigNPs, quantified by ICP, was 380 ppb. The NPs presented a ζ -potential of -34.7 mV, indicating their colloidal stability.¹⁷⁰ These results confirmed the roles of lignin as reducing and capping agent in the synthesis of the hybrid NPs.

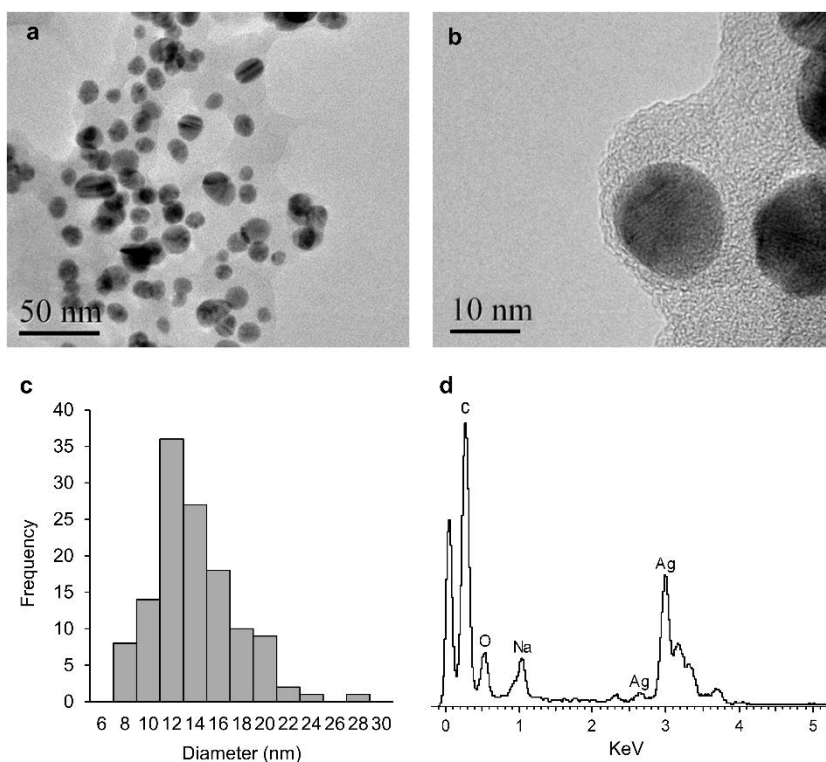


Figure 15. TEM images (a, b), EDX spectrum (c) and size distribution (d) of AgPheLigNPs. Nanoparticles size and distribution were derived from imaging 200 particles using software ImageJ.

Antibacterial properties of AgPheLigNPs

The antibacterial activity of the AgPheLigNPs was evaluated against *S. aureus* and *P. aeruginosa* by measuring the OD₆₀₀ before and after 24 h treatment with different concentrations of AgPheLigNPs. The MIC for *S. aureus* and *P. aeruginosa* was 34 and 17.03 $\mu\text{g NPs}\cdot\text{mL}^{-1}$, respectively, revealing high antibacterial efficacy of the novel AgPheLigNPs even at low concentration (**Figure 16a**). Experimental studies suggest that concentrations of 50–200 ppb Ag⁺ and 4000–8000 ppb AgNPs are needed to inhibit the growth of bacterial pathogens.¹⁷¹ The Ag content of AgPheLigNPs at MIC was 5.4 ppb, which is significantly lower than the antibacterial concentration of Ag⁺ and AgNPs.

The bactericidal activity of PheLigNPs was confirmed by plating the bacterial suspensions incubated with AgPheLigNPs in agar plates (**Figure 16b**). In the case of *S. aureus*, colonies were not observed after 24 h exposure to AgPheLigNPs at 34.06 – 272.50 $\mu\text{g}\cdot\text{mL}^{-1}$, indicating that these concentrations of particles are capable of completely eradicate the bacteria. Higher bactericidal effect was found against *P. aeruginosa*, since bacterial colonies were not grown in the presence of AgPheLigNPs at a concentration of 17.03 $\mu\text{g}\cdot\text{mL}^{-1}$ or higher. The MBC of the particles against *S. aureus* and *P. aeruginosa* was 34.06 and 17.03 $\mu\text{g}\cdot\text{mL}^{-1}$, respectively, which coincided with their MIC.

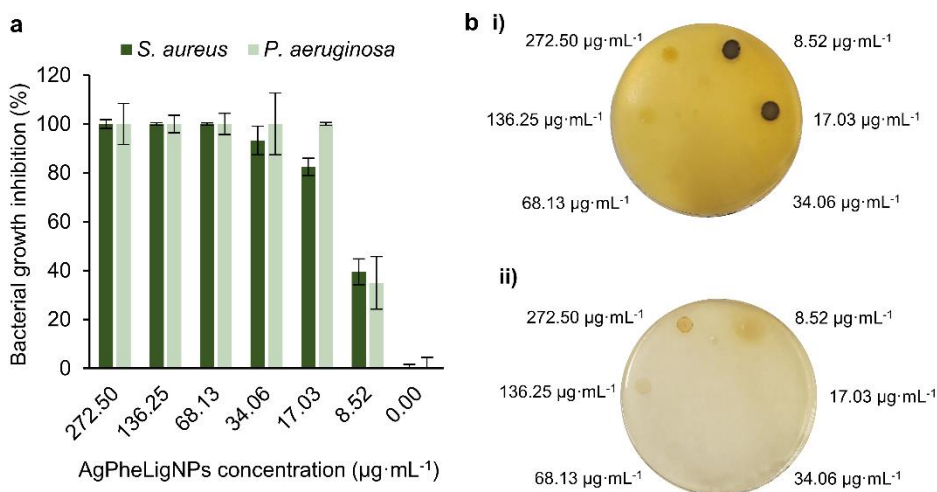


Figure 16. (a) Growth inhibition effect of AgPheLigNPs against *S. aureus* and *P. aeruginosa*. Results are reported as mean values \pm SD (n=3). (b) Representative images after culturing on agar plates i) *S. aureus* and ii) *P. aeruginosa* samples after incubation with different concentrations of AgPheLigNPs.

In vitro cytotoxicity assessment of AgPheLigNPs

Despite the wide use of AgNPs as antibacterial agents in biomedical products,¹⁷² their persistence in the environment coupled to their potential human health implications have raised some concerns.^{100,101} Silver ions released from NPs were considered as the main contributors to the cytotoxicity of AgNPs. However, studies show that Ag^+ released from AgNPs does not explain the

toxicity effects caused by exposure to AgNO_3 at the same concentration.¹⁰¹ Probably, the nanosize and specific properties of AgNPs also contribute to their cytotoxicity. The AgNPs toxicity is both concentration and size-dependent, being high concentrations and smaller sizes more toxic.¹⁷³ Hence, the evaluation of AgNPs' toxicity is crucial for their application in medical products.

In this work, the potential cytotoxicity of the AgPheLigNPs was assessed *in vitro* against human keratinocytes and fibroblasts (**Figure 17a**). The viability of

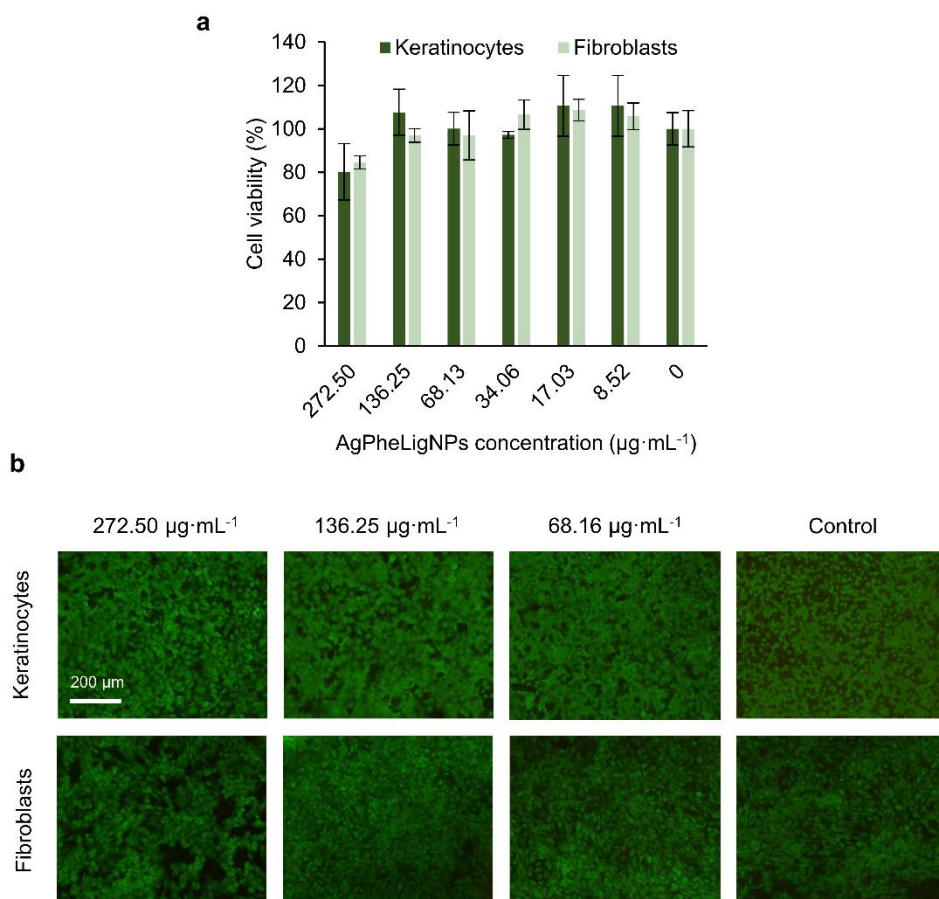


Figure 17. (a) Cell viability (%) of human keratinocytes and fibroblasts treated with different concentrations of AgPheLigNPs for 24 h assessed by the AlamarBlue assay. Results are reported as mean values \pm SD ($n = 3$). (b) Live/dead assay of human keratinocytes and fibroblasts treated with different concentrations of AgPheLigNPs. The assay stains the live cells in green and the dead ones in red.

these cell lines was above 80 % for all the tested AgPheLigNPs concentrations (272.50 – 34.06 $\mu\text{g}\cdot\text{mL}^{-1}$). Moreover, the morphology of the cells incubated with the particles did not differ from the control cells (**Figure 17b**). The presence of a biocompatible polymer surrounding the Ag core may contribute to decrease the toxicity of AgNPs and the released Ag^+ .⁹⁷

Tellurium lignin nanoparticles

TeLigNPs synthesis and characterization

In the search of antibiotic alternatives against AMR bacteria, antimicrobial metal or metalloid NPs, which mode of action circumvents the evolve of resistance mechanisms, are of high interest for the development of novel antimicrobials. Among them, TeNPs have emerged as promising antimicrobial agents. However, these NPs have been mostly obtained by traditional chemical synthesis yielding TeNPs with low biocompatibility and an associated environmental burden. Previously explored environmentally-friendly synthetic approaches mostly rely on extraction and purification of plant-derived reducing agents, thus, despite of being green, are competing with food and healthcare industries.

Herein, lignin, which is rarely valorized in its macromolecular form, was chosen as a reducing agent for tellurite. This polymer possesses a variety of chemical groups, including phenolic and aliphatic hydroxyl groups,³⁴ and it was previously used for reducing silver ions into NPs.¹⁶⁴ However, initial attempts to reduce tellurite by incubation with a lignin solution did not result in NPs formation. In order to increase the reduction capacity of lignin and increase the NPs synthesis yield, a sonochemically-assisted approach was adopted. In high-intensity US field, reducing species formed from the sonolysis of organic additives and water accelerate the reduction of the metalloid and increasing the yield of produced NPs.¹⁷⁴⁻¹⁷⁶ Moreover, it has been described that the application of US on lignin causes both side chain depolymerization and oxidative coupling/polymerization of phenoxy radicals,^{12,63,155} which in turn may complex

with metals.¹⁷⁷ The darkening of the lignin-tellurite mixture upon application of US suggested the reduction of tellurite (TeO_3^{2-}) to elemental tellurium (Te^0).¹⁷⁸

The synthesized NPs were negatively charged, with a ζ -potential of -32.7 mV and an average NP size of 182 ± 85 nm (**Figure 18a**). The NPs were comprised of an amorphous matrix embedding several electrodense spherical clusters containing defined crystalline domains (red lines in **Figure 18b**). The elemental map showed that tellurium was mainly located in the electrodense clusters (**Figure 18c-d**), while the high intensity oxygen signal observed in the amorphous matrix indicated the presence of lignin containing numerous methoxy and hydroxyl groups (**Figure 18e**). These images evidenced that in the sonochemical synthesis of TeLigNPs, lignin not only acted as a reducing agent, but also as a NPs matrix embedding Te clusters.

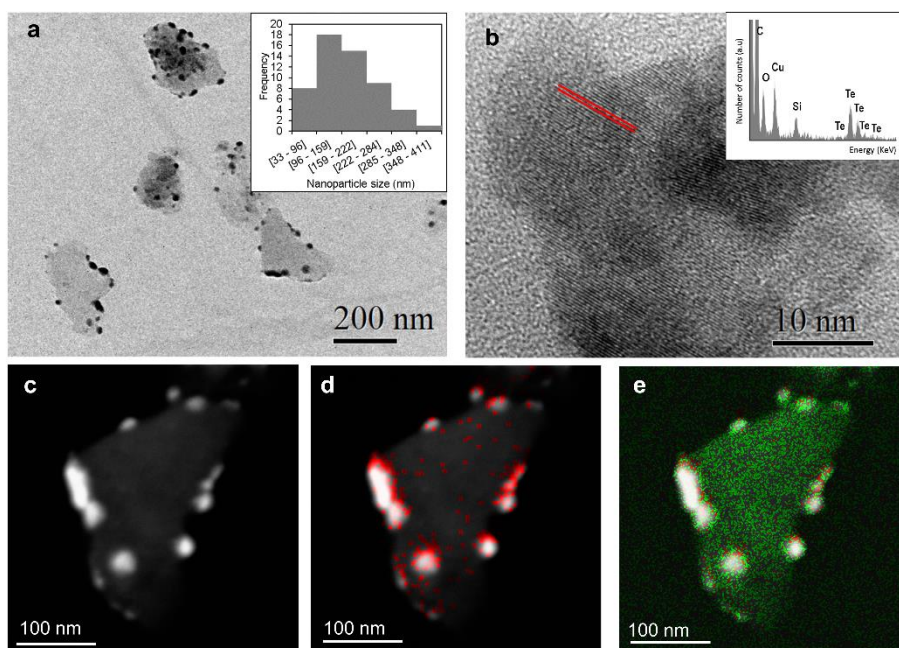


Figure 18. (a) TeLigNPs image at $\times 150000$ magnification by TEM, size distribution of TeLigNPs (inset), (b) detail image of Te cluster at $\times 500000$ magnification by high-resolution TEM observing the defined crystalline domains (red lines), EDX spectrum of the clusters (inset), (c) HAADF-STEM image of TeLigNPs, (d) overlapped HAADF-STEM image with tellurium mapping (red), and (e) overlapped HAADF-STEM image of TeLigNPs with tellurium (red) and oxygen (green) mapping.

Antibacterial activity of TeLigNPs

TeLigNPs at 2.39 ppm of Te were able to completely inhibit the growth of *E. coli* and *P. aeruginosa* (**Figure 19a-b**), while only 13 % growth inhibition could be achieved against the Gram-positive *S. aureus* (**Figure 19c**). These results are in agreement with previous studies reporting higher antibacterial activity of TeNPs against Gram-negative than Gram-positive bacteria,¹⁷⁸⁻¹⁸¹ a trend also observed for AgNPs.¹⁸² In particular, *S. aureus* is able of thriving in the presence of high concentrations of tellurite ions due to its capacity to reduce them.¹⁷⁹

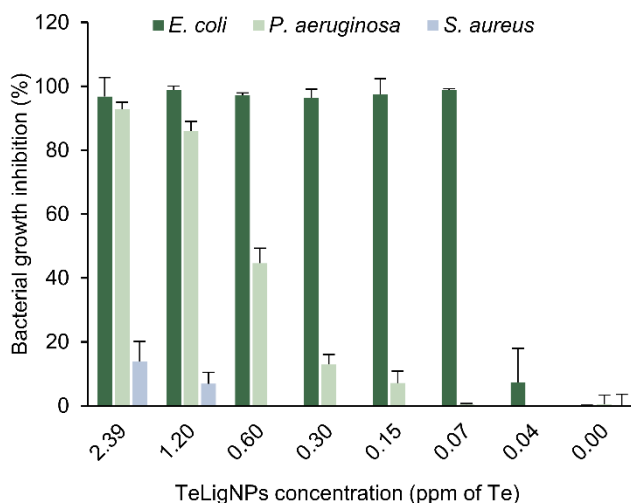


Figure 19. Growth inhibition effect of TeLigNPs against (a) *E. coli*, (b) *P. aeruginosa* and (c) *S. aureus*. Results are reported as mean values \pm SD (n=3).

The evaluation of the MIC of TeLigNPs took into account the concentration of Te, the bactericidal agent in the synthesized hybrid NPs, thus allowing a comparison with its bulk counterpart, the tellurite ion (TeO_3^{2-}). While a MIC corresponding to 0.07 and 2.39 ppm of Te was determined for *E. coli* and *P. aeruginosa*, respectively, the same Te concentrations in form of tellurite did not reduce the growth of these Gram-negative bacteria (**Figure 20**). Indeed, the MIC of tellurite for *E. coli* and *P. aeruginosa* was 0.31 and 15.60 ppm, respectively (**Table 6**). These results indicated that the nanoformulation of Te into hybrid TeLigNPs increased the antimicrobial activity of the metalloid.

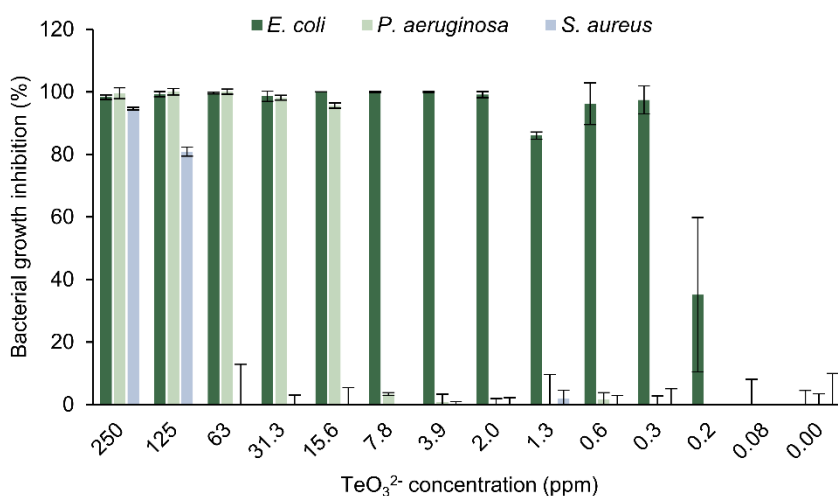


Figure 20. Growth inhibition effect of tellurite (TeO_3^{2-}) against (a) *E. coli*, (b) *P. aeruginosa* and (c) *S. aureus*. Results are reported as mean values \pm SD (n=3).

Table 6 Minimum inhibitory concentration (MIC) values of TeLigNPs and tellurite ion (TeO_3^{2-}) (ppm) assessed toward *E. coli*, *P. aeruginosa* and *S. aureus*.

	TeLigNPs	TeO_3^{2-}
<i>E. coli</i>	0.07	0.31
<i>P. aeruginosa</i>	2.39	15.60
<i>S. aureus</i>	> 2.39	250.00

TeLigNPs showed a strong bactericidal effect against *E. coli* and *P. aeruginosa*, achieving 100 and 99.9995 % reduction, respectively, corresponding to more than 5 log reduction (**Table 7**). To the best of our knowledge, this complete bacterial eradication has not been achieved for previously reported TeNPs, which, in contrast to TeLigNPs, lack a structural polymeric component.¹⁷⁸⁻¹⁸⁰ Thus, these results suggest that lignin not only acts as a green reducing agent, but also as a nanoparticle structural component that synergistically enhances the antibacterial activity of the Te clusters.⁵⁹

Table 7 Log reduction and equivalent bacterial viability reduction (%) of *E. coli* and *P. aeruginosa* exposed to different concentrations of TeLigNPs for 24 h at 37 °C. Results are reported as mean values \pm SD (n=3).

	<i>E. coli</i>		<i>P. aeruginosa</i>	
	Log reduction	% reduction	Log reduction	% reduction
2.39 ppm	6.54 \pm 0.00	100.0000	5.42 \pm 0.35	99.9995
1.20 ppm	6.05 \pm 0.85	100.0000	0.43 \pm 0.53	65.2941
0.60 ppm	1.96 \pm 1.49	81.7810	0	0
0.30 ppm	2.06 \pm 0.14	99.1136	0	0
0.15 ppm	2.26 \pm 1.41	97.2455	0	0
0.07 ppm	0.77 \pm 0.20	81.8182	0	0

The killing kinetics of the TeLigNPs were assessed to study the bactericidal effect of the hybrid NPs against Gram-negative bacteria as a function of time. The killing curves revealed that TeLigNPs with Te concentrations of 2.39 and 1.2 ppm were bactericidal against *E. coli* within 4 h, and achieved complete eradication after 24 h (**Figure 21a**), in agreement with previous results (**Table 7**). Regarding *P. aeruginosa*, the bactericidal efficacy of TeLigNPs at a concentration of 2.39

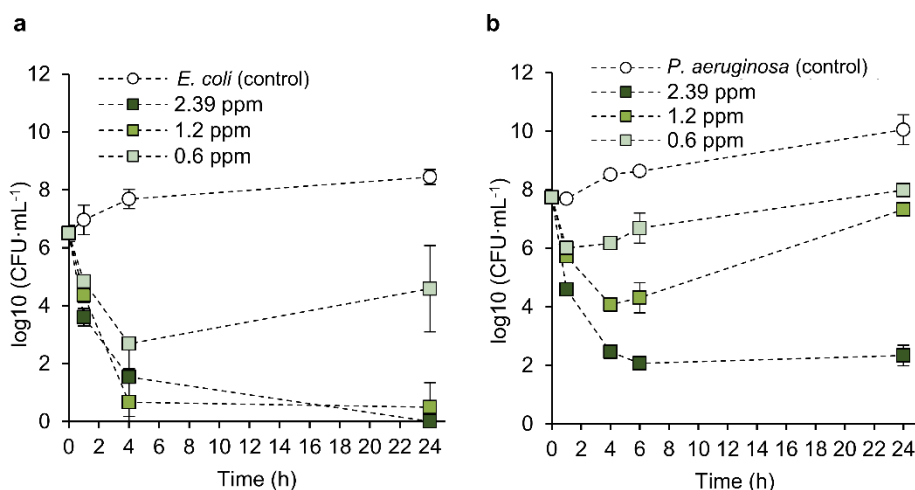


Figure 21. Kinetic growth curves of TeLigNPs at different concentrations (Te content 0.6, 1.2 and 2.39 ppm) against (a) *E. coli* and (b) *P. aeruginosa*. Results are reported as mean values \pm SD (n=3).

ppm was achieved after 6 h, corresponding to 5.7 log reduction, and was maintained after 24 h (**Figure 21b**). However, lower concentrations of the NPs exerted only bacteriostatic effect. Despite an initial reduction was observed after 4 h (4 log), *P. aeruginosa* was able to recover and grew up to the initial CFU values.

Ultrastructural analysis of bacteria was performed to study the morphological changes of the cells exposed to TeLigNPs. A clear difference was observed between control *E. coli* cells and those exposed to the hybrid NPs. Untreated *E. coli* presented a smooth surface and an electron-dense cytoplasmic content (**Figure 22a**), while *E. coli* cells treated with TeLigNPs showed different signs of cellular damage such as loss of cytoplasmic integrity, disrupted cell envelope, and aggregation of intracellular content (arrows in **Figure 22b–c**). Contrarily, *S. aureus* exposed to TeLigNPs were undamaged (**Figure 22d**) and did not present morphological differences compared to the control *S. aureus* cells (**Figure 22e–f**).

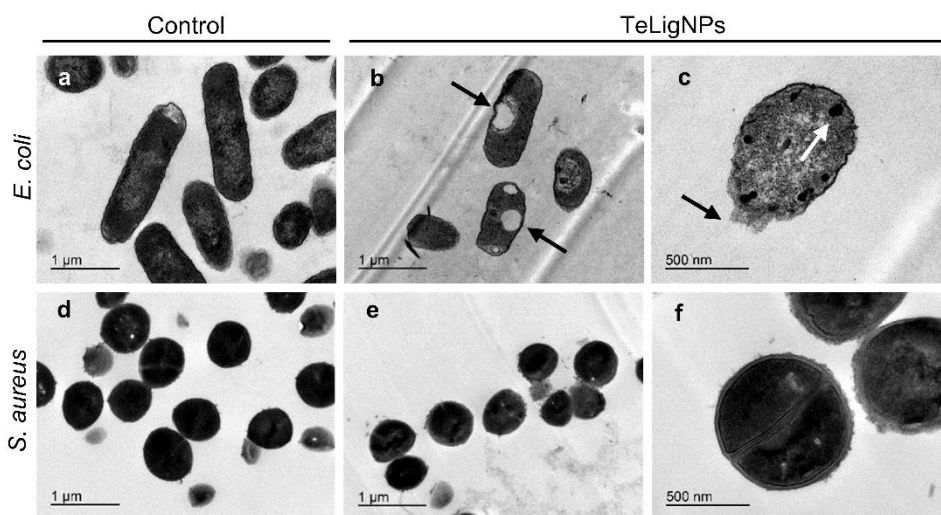


Figure 22. TEM images of *E. coli* (a) before and (b, c) after exposure to TeLigNPs, and *S. aureus* (d) before and (e, f) after exposure to TeLigNPs.

In vitro cytotoxicity assessment of TeLigNPs

The biocompatibility of metal- and metalloid-based antibacterial agents is a major issue for biomedical applications in humans. The cytotoxic mechanism of NPs toward eukaryotic cells is associated with oxidative stress, damage to cell membrane and DNA, and consequently apoptosis.^{183,184} These cytotoxic effects are aggravated when the NPs are chemically synthesized since toxic solvents and reducing agents may remain in the NPs.^{185,186} The TeLigNPs were synthesized

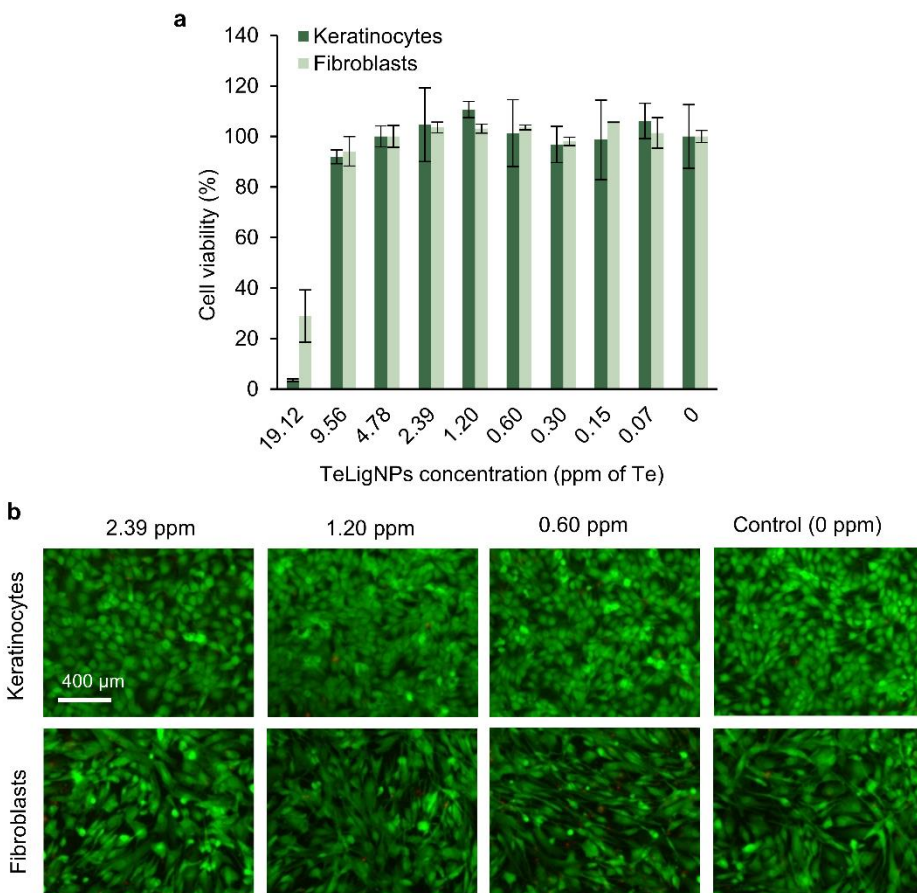


Figure 23. (a) Cell viability (%) of human keratinocytes and fibroblasts treated with different concentrations of TeLigNPs (ppm of Te) for 24 h assessed by the AlamarBlue assay. Results are reported as mean values \pm SD ($n=3$). (b) Live/dead assay of human keratinocytes and fibroblasts treated with different concentrations of TeLigNPs (ppm of Te). The assay stains the live cells in green and the dead ones in red.

following a safe-by-design approach using lignin as a reducing agent. This biopolymer has been innovatively used to reduce silver nitrate for the production of silver NPs (AgNPs),^{187,188} to decrease the cytotoxicity of metallic NPs¹⁰² and has been formulated in nanocomposites for improving the biocompatibility of biomedical devices.¹⁸⁹

The potential toxicity of the novel TeLigNPs was evaluated using human keratinocytes and fibroblasts as cell models. The cell viability of these cell lines upon incubation with tested antibacterial concentrations of TeLigNPs (Te concentrations ranging from 0.07 to 2.39 ppm) did not decrease compared to the untreated cells (**Figure 23a**). Remarkably, the cytotoxic effect was only observed when increasing 8-fold the concentration of TeLigNPs (19.12 ppm). Further evaluation by fluorescent microscopy of cell viability and morphology of human keratinocytes and fibroblasts incubated with TeLigNPs did not reveal cell morphology changes (**Figure 23b**). The biocompatibility of the TeLigNPs is associated with the presence of a natural, benign organic matrix that embeds the Te clusters.¹⁸⁶

Antibacterial mode of action of TeLigNPs

The bactericidal mechanism of TeNPs has not been completely elucidated, considering the production of ROS as one of the factors involved in their antibacterial capacity.¹⁸⁰ The toxicity of the tellurium oxyanion in bacteria has been related to superoxide-mediated oxidative stress causing cytoplasmic thiol oxidation, inactivation of iron-sulfur center-containing enzymes and peroxidation of the membrane lipids, which lead to cell death.^{162,190,191} Therefore, the generation of ROS induced by the TeLigNPs was evaluated in order to understand the antibacterial mechanism of these hybrid NPs (**Figure 24**). For both *E. coli* and *P. aeruginosa*, the incubation with TeLigNPs resulted in increase of the fluorescence emission after the addition of the H₂DCFDA probe, indicating the presence of ROS induced by the chemical activity of the tellurium oxyanion (**Figure 24a**). A fluorescence increase was not detected after incubation of *S. aureus* with TeLigNPs, indicating the absence of cellular damage,

in agreement with the previously obtained antimicrobial results (**Figure 19**). On the other hand, low fluorescence levels detected after incubation of human keratinocytes and fibroblasts with TeLigNPs, indicated that these NPs did not induce ROS in the studied cell lines (**Figure 24b**), in line with the biocompatibility results.

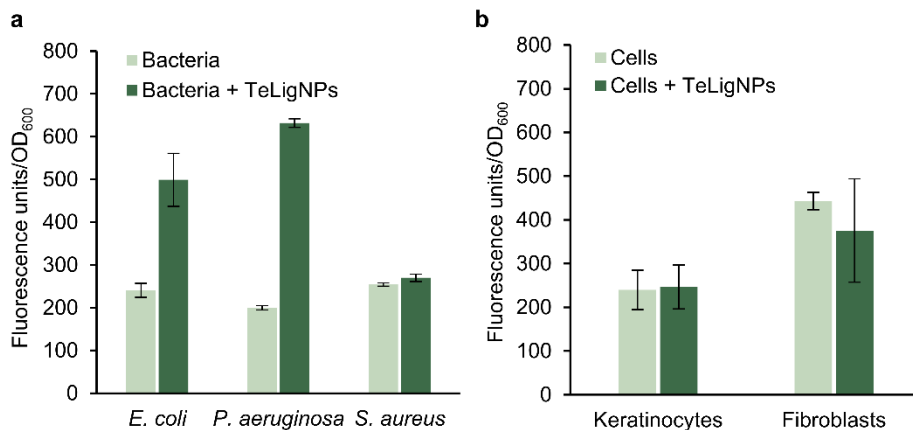


Figure 24. ROS generation assessment using the fluorescent probe H₂DCFDA after incubation of (a) bacteria (*S. aureus*, *E. coli* and *P. aeruginosa*) and (b) human keratinocytes and fibroblasts with TeLigNPs. Results are reported as mean values \pm SD (n=3).

Besides the production of ROS, the ability of TeLigNPs to disturb bacterial membranes was assessed using Langmuir technique. The injection of the TeLigNPs beneath the prepared Gram-negative model membrane induced an increase of the surface pressure indicating a membrane-disturbing effect due to the surface activity of the NPs (**Figure 25**).¹⁹² These results are supported by the observed irregularities in the cell envelope of the Gram-negative *E. coli* treated with TeLigNPs (**Figure 22b-c**). Different types of lignin have shown surface activity according to their origin or the processes employed for their purification,¹⁹³ while metallic particles without stabilizer have shown negligible surface activity. Thus, the observed surface activity was attributed to the lignin component of TeLigNPs, a role also previously described for lignin-capped silver NPs.¹⁹⁴

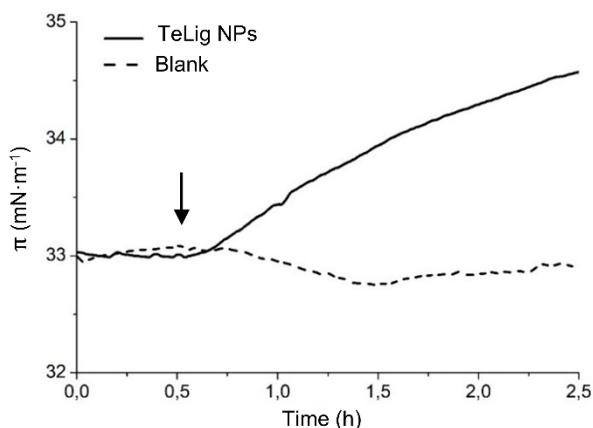


Figure 25. Kinetic adsorption process after the incorporation of the TeLigNPs into the air–water interface of the *E. coli* membrane lipids monolayer at $\pi=33$ mN·m⁻¹. The arrow indicates the injection of the TeLigNPs beneath the Langmuir film.

Based on the TeLigNPs mode of action and the observed different antimicrobial activities against the tested bacteria, we hypothesize that the bactericidal activity against Gram-negative bacteria is due to an insertion of the hybrid NPs to the outer membrane of these bacteria coupled to a membrane lipid peroxidation. The surface activity of TeLigNPs would allow the binding and insertion into the lipid bilayer of the outer membrane. In this sense, it has been reported that lignin particles adsorb at hydrophilic/hydrophobic interfaces,¹⁹⁵ and lignin-derived compounds can cross membrane bilayers due to hydroxyl-lipid interaction.^{196,197} Once inserted, ROS production by TeLigNPs generates lipid peroxides which decompose into highly reactive short-chain aldehydes able to diffuse in the cytoplasm and oxidize thiol and amino groups of proteins, thus affecting several cellular processes and leading to death.^{198,199} On the other hand, Gram-positive bacteria are characterized by a thick external peptidoglycan cell wall surrounding the cytoplasmic membrane which would prevent the access of the TeLigNPs to the cell membrane, which coupled to the intrinsic capacity of *S. aureus* to reduce tellurite, results in the observed low antimicrobial activity of TeLigNPs against this Gram-positive bacteria.

Phenolated lignin nanoparticles

Synthesis and characterization of PheLigNPs

The aim of this study was to enhance the antibacterial activity of lignin by increasing its phenolic content and formulating nanoparticles that could find applications as antibacterial agents in food packaging and biomedical fields. The rationale of the study is based on the enzymatic pre-activation of lignin using acetosyringone as a laccase mediator¹⁶⁷ to expand the oxidative action of laccase to molecules that are sterically inaccessible to the enzyme.²⁰⁰ Then, the addition of the phenolic compound TA in the presence of laccase, and the application of US would simultaneously (i) initiate cross-linking reactions between TA and lignin, and (ii) form NPs. Non-functionalized LigNPs and phenolated bulk lignin (PheLig) were also prepared to evaluate the contribution of the nano-form and the phenolic content to the antibacterial activity.

The combination of laccase/mediator system to graft the natural phenolic compound TA onto lignin under an ultrasonic field yielded PheLigNPs. The formation of PheLigNPs was evaluated by measuring the increase of phenols and the size of the resulting particles. Unmodified bulk lignin in suspension formed large microparticles observable by DLS with a phenolic content of 212.5 ± 5 mg GAE·g⁻¹, while after the sono-enzymatic treatment the phenolic content increased to 296.4 ± 14 mg·GAE g⁻¹ and the size of the particles was on the nanoscale (**Table 8**).

Table 8 Characterization of PheLigNPs, LigNPs, PheLig, and lignin in terms of phenolic content, size, PDI, and ζ -potential.

	Phenolic content (mg GAE ^a ·g ⁻¹ sample)	Hydrodynamic size (nm)	PDI	ζ -potential (mV)
PheLigNPs	340.4 ± 16	293.5	0.293	-34.0 ± 0.5
LigNPs	222.92 ± 18	292.2	0.245	-34.4 ± 0.4
PheLig	296.4 ± 14	> 4000	1	-31.1 ± 0.7
Lignin	212.5 ± 6	> 4000	1	-32.2 ± 1.8

This increase in the number of phenols confirmed the grafting of TA onto lignin, while the size of the particles confirmed the nanotransformation. TEM images revealed that the PheLigNPs with an average size of 217 ± 54 nm were formed by smaller clusters (**Figure 26**). The cavitation phenomena caused by the application of US waves can produce changes in lignin macromolecule, disintegrating mechanically the aggregated particles to nanoscale level.^{63,67} During this process, lignin most probably rearranged into NPs due to π - π interactions, van der Waals forces, and chain entanglement.^{21,201,202} The NPs maintained their size, PDI and ζ -potential after 6 months of storage at 4 °C, indicating their high stability (**Annex - Table S1**).

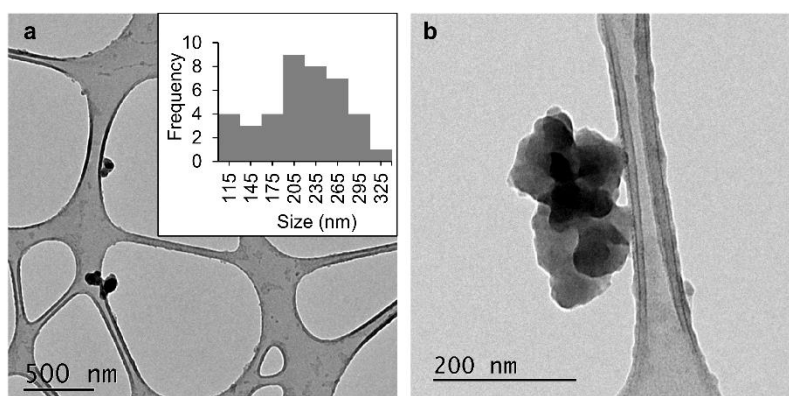


Figure 26. (a) TEM image of PheLigNPs at 4000X and size distribution of the particles (inset), and (b) TEM image of PheLigNPs at 20000X magnification.

In order to study the contribution of the nano-form and the phenolic content to the antibacterial activity of the PheLigNPs, non-functionalized lignin nanoparticles (LigNPs) and phenolated bulk lignin (PheLig) were prepared and characterized (**Figure 27**). PheLig presented a large particle size (>4000 nm) and phenolic content of 296.4 ± 14 mg GAE·g⁻¹, while LigNPs presented a hydrodynamic size of 292 nm and their phenolic content was 222.92 ± 18 mg GAE·g⁻¹ (**Table 8**, **Annex - Figure S2**).

The enzymatic phenolation of lignin was further characterized by FTIR to confirm that TA was grafted onto lignin (**Figure 28**). The characteristic bands of

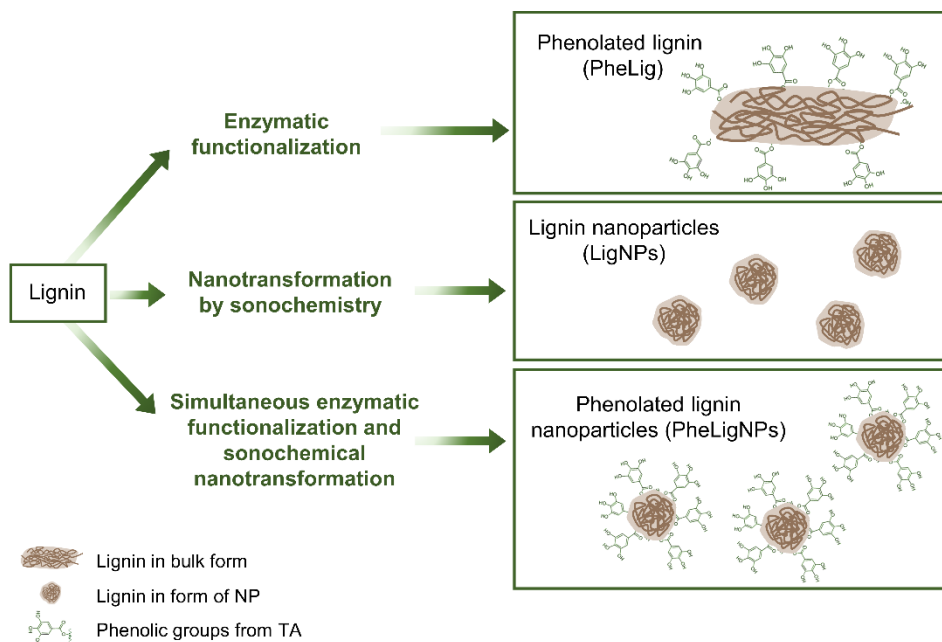


Figure 27. (a) Schematic representation of (1) phenolated lignin (PheLig), (2) lignin nanoparticles (LigNPs), and (3) phenolated lignin nanoparticles (PheLigNPs).

lignin appeared also in PheLigNPs, LigNPs, and phenolated lignin, reflecting the presence in the samples of the primary subunits of lignin, namely guaiacyl (G), syringyl (S), and p-hydroxyphenyl (H).⁶⁰ Upon phenolation, an increase in the intensity of the O–H stretching band at 3000–3600 cm^{-1} in the phenolated samples (PheLigNPs and PheLig) was observed, indicating an increase in the phenolic hydroxyl groups following the reaction with TA.^{156,157} This band was also observed in the TA spectra due to the presence of hydroxyl groups. The intensity of the O–H stretching band was slightly higher in the LigNPs than in the unmodified lignin, which was attributed to partial oxidation of lignin induced by the ultrasonication process.^{67,203} The signal at 1720 cm^{-1} , corresponding C=O stretching vibration of unconjugated carbonyl groups,²⁰⁴ was observed as a sharp peak in TA, and as a shoulder in the lignin samples. This peak was more accentuated in PheLigNPs and PheLig compared to their non-phenolated counterparts, confirming the presence of grafted TA. Further evidence for the successful phenolation of lignin is the appearance of the absorption band at 1366

cm^{-1} in PheLigNPs spectra corresponding to the presence of phenolic O-H.^{160,205,206} New characteristic peaks appeared at 922 and 760 cm^{-1} , associated to the C-H out-plane flexural vibration on aromatic rings.^{156,157,205} A strong band at 756 cm^{-1} was also observed in TA spectrum. The changes in these absorption bands were corroborated by the ratio A_x/A_{2090} (Annex – **Table S2**). These observations indicate that lignin's phenolic groups are oxidized to phenoxy radicals by the action of laccase²⁰⁰ and then undergo coupling reactions crosslinking with TA molecules, thus increasing the amount of phenolic groups (**Figure 13**).

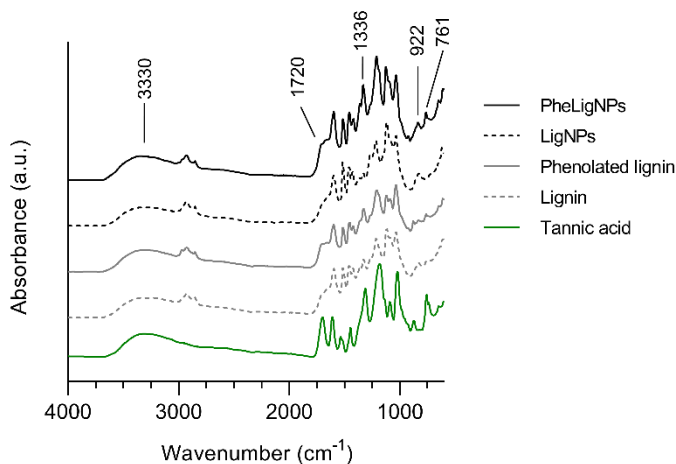


Figure 28. FTIR spectra of all the lignin samples and TA.

Antibacterial activity of PheLigNPs

In this work, the plant-derived polyphenol TA was used as a functional molecule to increase the antibacterial activity of LigNPs. The antibacterial activity of the PheLigNPs was determined by a standard broth dilution method against the Gram-positive *S. aureus* and *B. cereus*, and the Gram-negative *P. aeruginosa* and *E. coli*, which are relevant pathogenic bacteria causing medical- or food-related infections. In order to elucidate the factors contributing to the antibacterial effect of PheLigNPs, i.e., phenolic content and nanoform, the

antibacterial activity of non-functionalized lignin NPs (LigNPs), functionalized lignin in bulk form (PheLig), and pristine lignin was also studied. The MIC of PheLigNPs was 1.25 mg·mL⁻¹ for *S. aureus* and *B. cereus*, and 2.5 mg·mL⁻¹ for *P. aeruginosa* and *E. coli*, while the MICs of LigNPs, PheLig, and lignin for these bacteria were at least 2 times higher (**Table 9**). These results indicated that PheLigNPs presented higher antibacterial activity than their non-functionalized or bulk counterparts, which was attributed to both the higher phenolic content and the nanoform of PheLigNPs.

Table 9 MIC values (mg·mL⁻¹) of PheLigNPs, LigNPs, PheLig, and lignin assessed using the broth dilution method.

	<i>S. aureus</i>	<i>B. cereus</i>	<i>P. aeruginosa</i>	<i>E. coli</i>
PheLigNPs	1.25	1.25	2.50	2.50
LigNPs	5.00	2.50	5.00	5.00
PheLig	>5.00	5.00	>5.00	5.00
Lignin	>5.00	5.00	>5.00	>5.00

Further evidence of the improved antibacterial effect of PheLigNPs was obtained with the kinetic growth curves of bacteria. PheLigNPs at MIC (1.25 mg·mL⁻¹) were capable of inhibiting the growth of *S. aureus* and *B. cereus* (**Figure 29a–b**), as previously observed in the broth dilution method, while LigNPs, PheLig and lignin at the same concentration as PheLigNPs did not induce such growth inhibition. The antibacterial effect of PheLigNPs against the Gram-negative *P. aeruginosa* and *E. coli* was less pronounced, even at a higher concentration of NPs (2.5 mg·mL⁻¹) (**Figure 29c–d**). However, the growth rate of *P. aeruginosa* was reduced when it was incubated with PheLigNPs compared to the growth of this bacteria in contact with other lignin samples. The observation of the poor activity of lignin and plant polyphenols against Gram-negative bacteria has been previously reported.^{207,208} The different susceptibility of Gram-positive and Gram-negative bacteria to these compounds is still unclear,

since other studies did not found a correlation between the antibacterial effect of polyphenols and the Gram-staining.^{56,209,210}

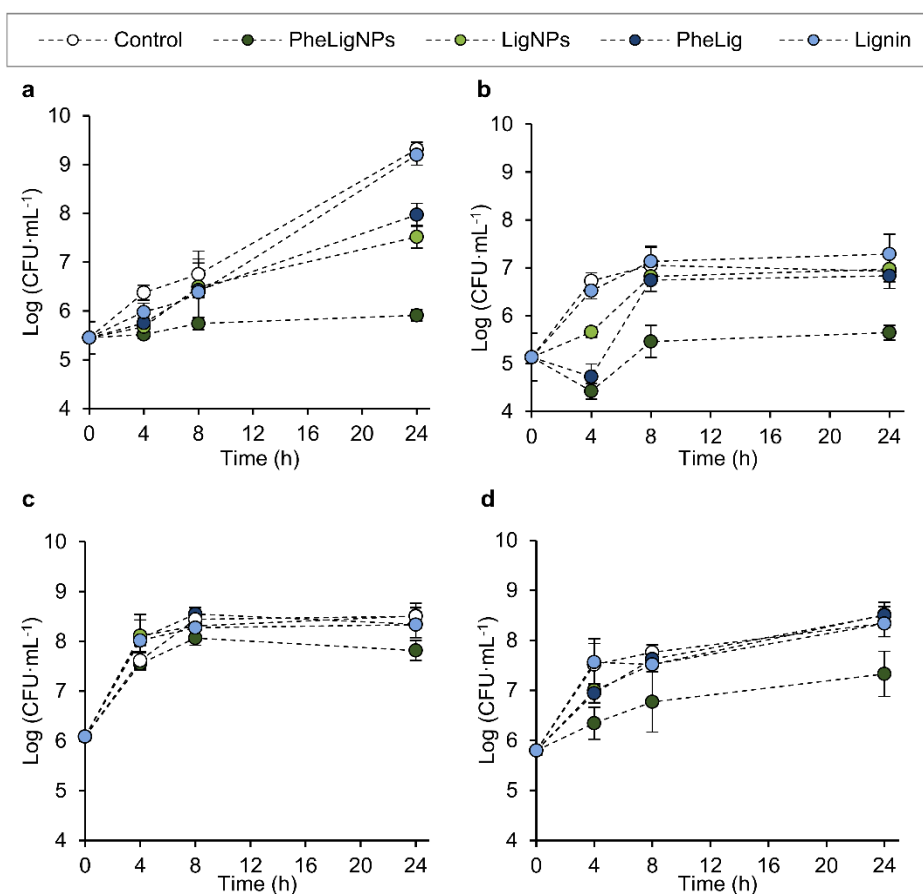


Figure 29. Kinetic growth curves of bacteria incubated with lignin samples at concentrations corresponding to MIC: (a) *S. aureus* (1.25 mg·mL⁻¹), (b) *B. cereus* (1.25 mg·mL⁻¹), (c) *P. aeruginosa* (2.5 mg·mL⁻¹) and (d) *E. coli* (2.5 mg·mL⁻¹). Results are reported as mean values \pm SD (n=3).

In vitro cytotoxicity assessment of PheLigNPs

A crucial requirement for the biomedical translation of nanomaterials is their biocompatibility. Natural plant-based molecules have been used to develop bioactive NPs with low toxicity, demonstrating suitability as active agents for biomedical applications.²¹¹ The cytotoxic effects of PheLigNPs were assessed *in vitro* using human cell lines (**Figure 30**). After 24 h incubation with PheLigNPs at antibacterial concentrations (2.50–1.25 mg·mL⁻¹), the cell viability of

keratinocytes and fibroblasts was above 80 % after incubation. Hence, the PheLigNPs are not considered toxic for human cells²¹² and have potential as antibacterial agents for applications in the field of biomedicine.

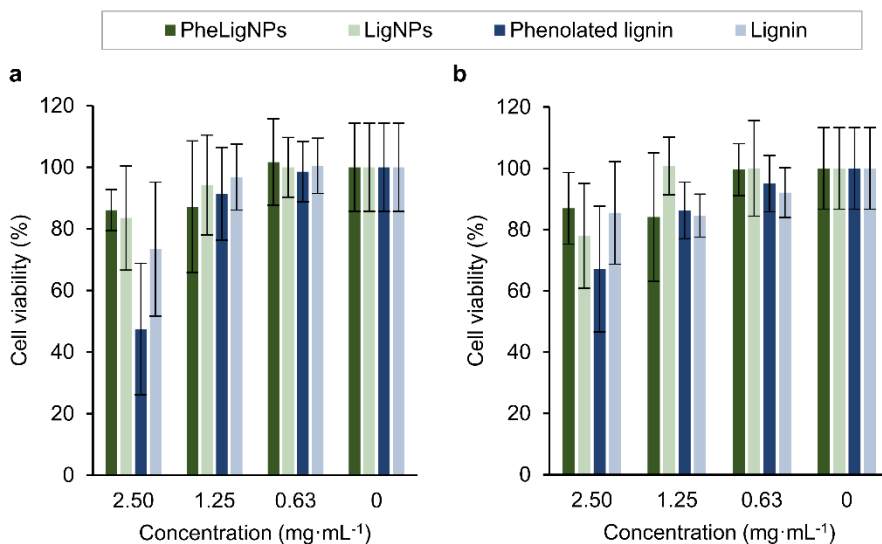


Figure 30. Cell viability (%) of (a) human keratinocytes and (b) fibroblasts exposed to PheLigNPs, LigNPs, PheLig, and lignin for 24 h assessed by the AlamarBlue assay. Results are reported as mean values \pm SD (n=3).

Antibacterial mechanism of action of PheLigNPs

The antibacterial mechanism of phenolic compounds is mainly attributed to (i) their ability to generate hydrogen peroxide, which coupled to metal ions complexation capacity, results in the inhibition of the activity of essential enzymes,⁵⁴ and (ii) their ability to destabilize bacterial membrane, causing an increase of its permeability.^{55,56} In this work, the antibacterial mechanism of action of PheLigNPs was investigated by measuring the metabolic activity of bacteria and the generated ROS under the presence of PheLigNPs and studying the interaction of the NPs with the bacterial membrane. Resazurin was used to determine the metabolic activity of bacteria incubated with sub-inhibitory concentrations of the NPs. Resazurin is a blue dye, which itself is non-fluorescent until it is reduced to the pink colored and fluorescent resorufin. In the cell,

resazurin can be reduced by the activity of the bacterial respiratory chain. Bacteria incubated with PheLigNPs presented a decrease in metabolic activity compared to the control (**Figure 31a**). Since sub-inhibitory concentrations of PheLigNPs were used for this assay, the lower fluorescence levels detected were attributed to the low metabolic activity of viable bacteria. Hence, bacterial metabolism was reduced after the incubation of PheLigNPs.

Despite phenolic compounds have been widely recognized as antioxidants, under certain conditions phenols can have a pro-oxidant behavior.⁷³ Indeed, polyphenols have shown the ability to react with dissolved oxygen, resulting in the generation of hydrogen peroxide, which is involved in the antibacterial activity of the molecule.⁵⁴ In this work, the ability of PheLigNPs to induce ROS in bacteria was studied using the fluorescent probe H₂DCFDA (**Figure 31b**), which is activated by intracellular oxidants including hydrogen peroxide and the hydroxyl radical.^{213,214} Incubation of bacteria with the NPs resulted in an increase of ROS causing oxidative stress in the cell, which would result in lipid peroxidation, DNA damage, and inactivation enzymes.²¹⁵

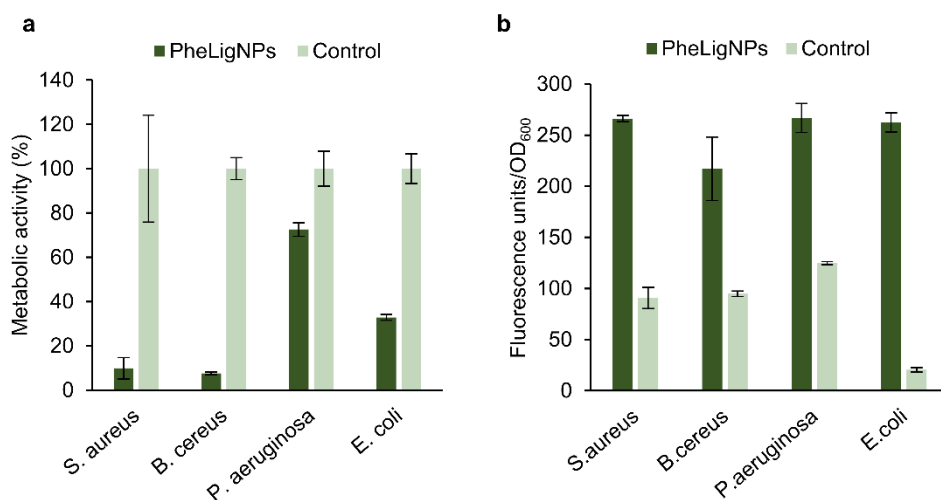


Figure 31. Antibacterial mechanism of action of PheLigNPs. (a) Evaluation of relative metabolic activity (%) of bacteria incubated with PheLigNPs by the resazurin assay. (b) ROS generation by bacteria in contact with PheLigNPs, assessed with the fluorescent probe H₂DCFDA. Controls refer to bacteria grown without PheLigNPs. Results are reported as mean values \pm SD (n=3).

Ultrastructural analysis of bacteria incubated with PheLigNPs allowed the study of the NP-bacteria interaction and the morphological changes of bacteria after being exposed to the NPs (**Figure 32**). Control bacteria, which were grown in normal conditions, presented non-damaged membranes. When bacteria were incubated with PheLigNPs, the NPs were attached to the bacteria, suggesting a possible interaction with the bacterial surface. *S. aureus* and *B. cereus*, the two Gram-positive bacteria, presented changes in the surface roughness but their shape did not present significant alterations in comparison to the control. The Gram-negative *P. aeruginosa* and *E. coli*, however, did change their morphology upon incubation with PheLigNPs. Despite cellular lysis or membrane cleavage was not observed, these bacteria were flattened, presenting several depressed areas.

Further evidence of the interaction between PheLigNPs and bacteria was obtained by QCM-D (**Figure 33a**), which provides real-time outputs of molecular adsorption and interactions taking place on the sensors. After establishing an initial baseline with PBS, *S. aureus* was circulated until its deposition on the sensor surface, which resulted in a constant frequency decrease coupled to an increase in dissipation. After removing the unbound materials by circulating PBS, a steady-state frequency measurement attributed to the deposited bacteria was obtained. Hence, the presence of *S. aureus* in the sensor was confirmed by the difference in the frequency between the initial and the second PBS baselines (≈ 65 Hz). The circulation of PheLigNPs followed by PBS caused a progressive frequency decrease (≈ 25 Hz) and dissipation increase, which was attributed to the interaction of PheLigNPs with bacteria and their subsequent deposition. The adhesion of PheLigNPs onto bacterial surface might be caused by multiple interactions between the phenolic moieties of the particle and the components of the cell envelope. According to previous studies, phenolic groups can interact with amino and thiol groups from membrane proteins,²¹⁶ and due to their hydrophobicity, phenolic moieties can interact with lipid membranes.²¹⁷

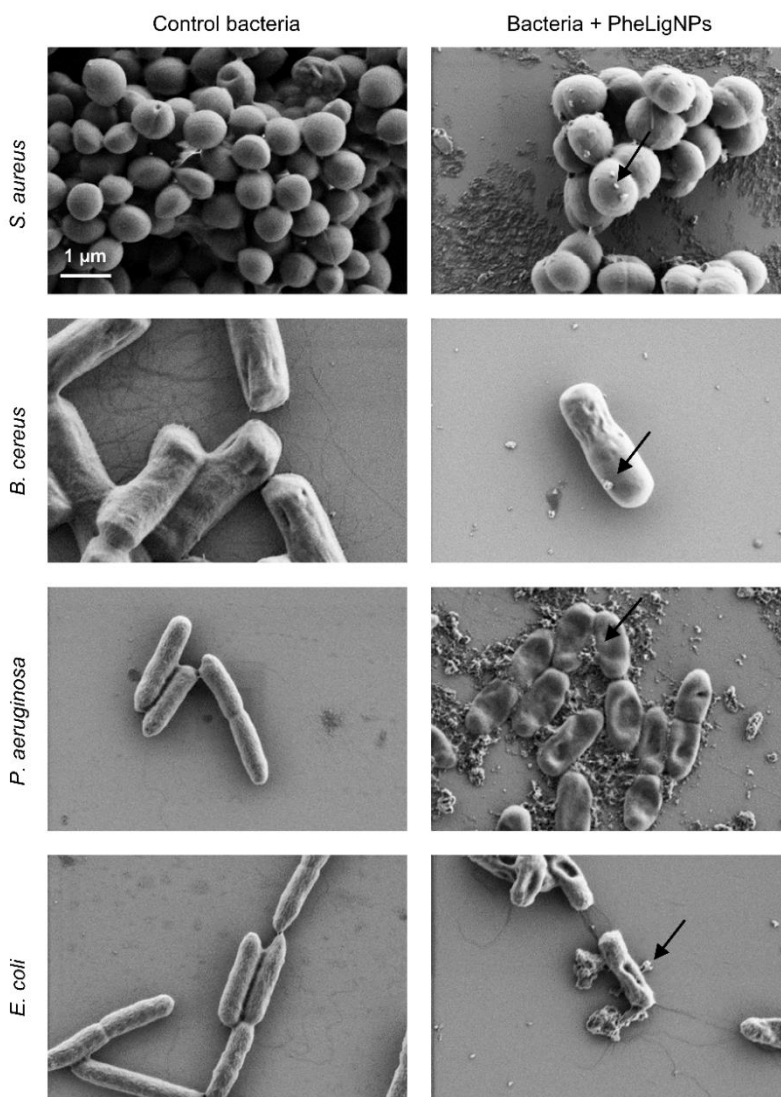


Figure 32. SEM images of *S. aureus*, *B. cereus*, *P. aeruginosa*, and *E. coli* before and after exposure to PheLigNPs. (b) QCM-D monitoring of normalized frequency (Δf) and dissipation (ΔD) obtained during the formation of a layer of *S. aureus* and its interaction with PheLigNPs. (c) Surface pressure-area isotherm of a PE:PG mixture monolayer in PBS, PheLigNPs in PBS, and PE:PG in PBS with PheLigNPs.

The interaction of PheLigNPs with a mimetic Gram-negative bacterial model membrane was investigated using Langmuir isotherms. The two main phospholipids of the *E. coli* outer membrane, PE and PG, were used to form a monolayer. The PE:PG surface pressure-area isotherm (**Figure 33b**) presented

a monotonic increase until the collapse pressure at $\sim 49 \text{ mN}\cdot\text{m}^{-1}$, as previously reported.²¹⁸ The PheLigNPs isotherm evidenced their high surface activity, which might contribute to their capacity to interact with bacterial membranes. Indeed, the isotherm of the model membrane containing PheLigNPs (PE:PG + PheLigNPs) was displaced to larger areas in comparison with PE:PG isotherm, and the collapse pressure decreased to $\sim 43 \text{ mN}\cdot\text{m}^{-1}$. Focusing on the physiological membrane pressure, $33 \text{ mN}\cdot\text{m}^{-1}$, PE:PG monolayers presented an area of $\sim 85 \text{ cm}^2$, while in PE:PG + PheLigNPs isotherm the area was $\sim 99 \text{ cm}^2$. The increase in the area recorded can be attributed to the intercalation of the NPs between the phospholipid chains, probably due to their hydrophobic nature.²¹⁹ Similar behavior has been reported for surface active lignin-capped silver NPs, which caused a membrane-disturbing effect.⁷⁶

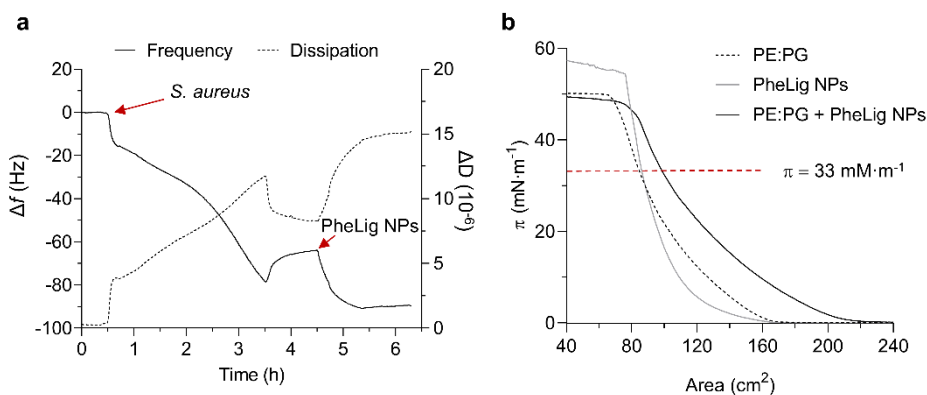


Figure 33. Study of the interaction of the PheLigNPs with bacteria. (a) QCM-D monitoring of normalized frequency (Δf) and dissipation (ΔD) obtained during the formation of a layer of *S. aureus* and its interaction with PheLigNPs. (b) Surface pressure-area isotherm of a PE:PG mixture monolayer in PBS, PheLigNPs in PBS, and PE:PG in PBS with PheLigNPs.

The integrity of the bacterial membranes was also studied using two fluorescent dyes: SYTO 9, which stains the cells with intact membranes in fluorescence green, and propidium iodide, which stains the cells in fluorescent red only after penetrating through damaged membranes. The control bacteria appeared mostly in green, revealing the integrity of their cytoplasmic membrane. Contrarily, when bacteria were incubated with PheLigNPs red cells

predominated, indicating that their membrane was damaged (**Figure 34**). Moreover, the fluorescence ratio SYTO 9/propidium iodide was higher for control bacteria than for bacteria incubated with PheLigNPs, indicating the increasing number of damaged cells after the treatment (**Annex –Table S3**). The obtained images and the fluorescence ratio SYTO 9/propidium iodide supported the membrane disturbing effect of PheLigNPs observed by Langmuir studies.

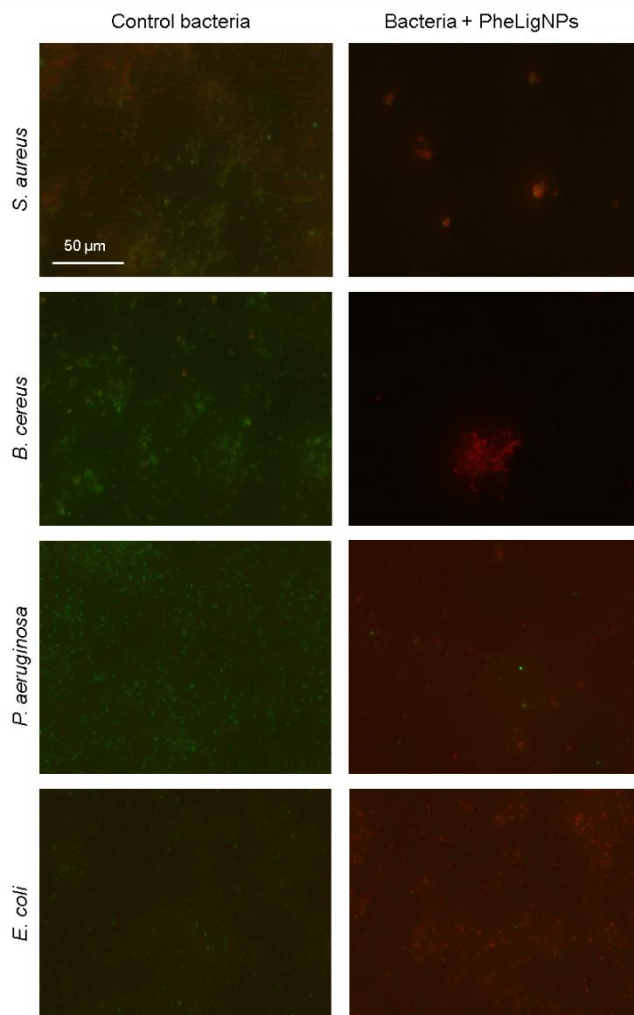


Figure 34. Fluorescence microscopy images of *S. aureus*, *B. cereus*, *P. aeruginosa*, and *E. coli* after 24 h treatment with PheLigNPs ($0.6 \text{ mg}\cdot\text{mL}^{-1}$), or without NPs (control). Bacteria were stained using the green fluorescent SYTO 9 that labels in green the bacteria with intact membrane, and red fluorescent propidium iodide that labels bacteria with damaged membranes.

On the basis of the reported evidence, we assume that PheLigNPs have affinity to the bacteria surface, being capable of interacting with proteins and intercalating into lipids, leading to membrane disturbance, inhibition of the respiratory chain, and formation of ROS that results in oxidative damage in the cells and hamper the bacterial proliferation. However, additional studies need to be performed to completely elucidate the antibacterial modes of action of phenolic NPs. The fact that the NPs affect the bacteria at different levels might hamper the acquisition of resistance by bacteria, which evidence the suitability of PheLigNPs as alternative plant-based antibacterial agents.

Resistance development of PheLigNPs by bacteria

Since PheLigNPs have shown multiple antibacterial modes of action, we hypothesized that they might avoid the development of resistance in bacteria. AMR is a natural phenomenon taking place when bacteria acquire the capacity of tolerating a certain antimicrobial agent after long exposure. In case of conventional antibiotics, their target are specific pathways or molecules essential for the viability of bacteria. Under the selective pressure of an antibiotic, susceptible bacteria are inhibited or eradicated, while the cells that acquire antibiotic-resistant traits are able to survive. According to the World Health Organization, AMR is one of the main global health threats and needs to be urgently addressed.²²⁰ After exposing *S. aureus* and *E. coli* to conventional antibiotics for 30 days, the MIC significantly increased by 1281 for ciprofloxacin and by 96 for ampicillin (**Table 10**). This indicates that bacteria developed antimicrobial resistance in response to antibiotics. On the contrary, almost no increase in the MIC was observed when *S. aureus* was incubated with PheLigNPs (an increase of 1.5) and no change in the MIC was observed for *E. coli*, indicating that resistance was not developed. Efforts have been made to develop alternative bactericidal compounds such as AgNPs and metal oxide NPs, however, some reports already reported the surge of bacterial strains resistant to ionic silver and even AgNPs.²²¹ Therefore, developing effective antibacterial agents that avoid the appearance of resistant strains is still challenging. In this work, given

the multiple and non-specific antibacterial modes of action of the PheLigNPs, including direct contact with the bacterial surface, these NPs are less prone to induce resistance than traditional antibiotics.

Table 10 MIC values changes of *S. aureus* and *E. coli* following a 30-days exposure to antibiotics or PheLigNPs

Bacteria	Antibiotic	PheLigNPs
<i>S. aureus</i>	1281 (ciprofloxacin)	1.5
<i>E. coli</i>	96 (ampicillin)	0

Chapter 2

Lignin-based nanoparticles in composite materials for wound healing

This chapter is based on the following publications:

Morena A G, Stefanov I, Ivanova K, Pérez-Rafael S, Sánchez-Soto M, Tzanov T. “Antibacterial Polyurethane Foams with Incorporated Lignin-Capped Silver Nanoparticles for Chronic Wound Treatment”. *Industrial and Engineering Chemistry Research*, 2020, doi: 10.1021/acs.iecr.9b06362

Morena A G, Pérez-Rafael S, Tzanov T. “Lignin-Based Nanoparticles as Both Structural and Active Elements in Self-Assembling and Self-Healing Multifunctional Hydrogels for Chronic Wound Management”. *Pharmaceutics*, 2022, licensed under CC-BY 4.0, doi: <https://doi.org/10.3390/pharmaceutics14122658>

Chapter 2. Lignin-based NPs in composite materials for wound healing

Introduction

Chronic wounds are injuries that do not show signs of healing within 4 to 6 weeks¹³⁹ and are characterized by a prolonged inflammatory stage, elevated load of pathogenic bacteria, poor blood supply, and alteration on immune function and overactivation of deleterious enzymes.²²² High morbidity of these wounds is observed, especially in patients with diabetes.²²³ Complications related to diabetic ulcers are the major cause of nontraumatic amputation.²²⁴ In addition, a demographically aging population further increases the health concern associated with chronic wounds. The management of these non-healable wounds comprises removing the non-viable tissue and applying wound dressings to absorb the excess of exudate from the wound bed, but at the same time to maintain the beneficial for healing moisture environment. Following this rationale, hydrogels, hydrocolloids, and synthetic foam dressings have been developed to promote wound healing.¹⁵³

Despite the fact that the dressing acts as a physical barrier between the wound and the environment, chronic wounds are susceptible to infection caused by endogenous and pathogenic bacteria. Several approaches have been studied to develop wound dressings that effectively reduce bacterial load, such as the use of quaternary ammonium,²²⁵ antibacterial chitosan,¹⁵⁰ and the addition of metal and metal oxide NPs in the dressing matrix.^{226,227} Considering the complex physiology of chronic wounds, an efficient wound dressing material should simultaneously inhibit the growth of pathogenic bacteria, reduce oxidative stress and promote wound healing by reducing the activity of deleterious enzymes.²²⁸

Lignin-based NPs are promising multifunctional agents for chronic wound management given their antibacterial and antioxidant activities, their

biocompatibility and their ability to attach to proteins, in addition to avoiding the development of resistance in bacteria.

This chapter describes the preparation and characterization of polymeric scaffolds with embedded lignin-based nanoparticles as wound dressing materials (**Figure 35**). Concretely, the particles described in Chapter 1 were used as multifunctional actives in polyurethane foams and biopolymer hydrogels with potential for chronic wound management. AgPheLigNPs and PheLigNPs were selected to prepare the composite materials for their higher reactivity accounting on their large phenolic content. The nanomaterials developed in this chapter are described below:

- **Flexible polyurethane foams (PUFs)** were prepared by incorporating the AgPheLigNPs into the polyol component, and mixing with isocyanate. The NPs were intended as active fillers and are expected to provide antibacterial and antioxidant properties to an inert polymeric matrix. Additionally, the AgPheLigNPs may act as polyols during polyurethane synthesis, forming covalent bonds in the foam structure.
- **Biopolymer-based hydrogels** were developed by mixing thiolated hyaluronic acid (HA-SH) and silk fibroin (SF) with PheLigNPs as both structural and functional elements. The NPs were the driving elements for the self-assembling since they established multiple non covalent interactions with both polymers and allowed the gelation.

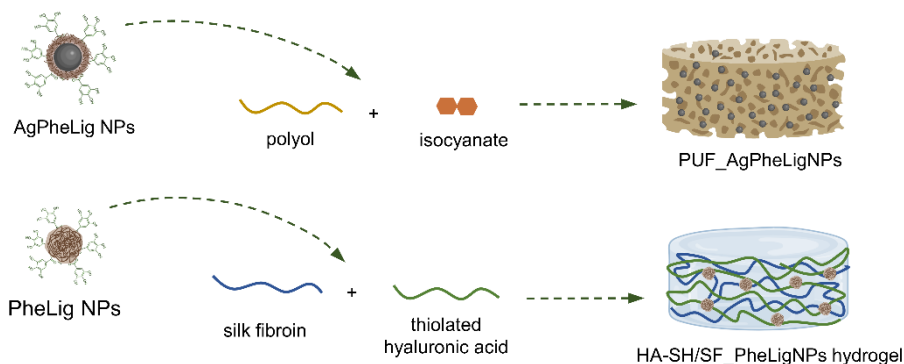


Figure 35. Schematic representation of the synthesis of nanocomposite materials for wound healing.

Materials and methods

Reagents, cells, and enzymes

Pharmaceutical grade HA sodium salt from *Streptococcus equi* (MW=600 kDa) was obtained from Lehvoss Iberia (Barcelona, Spain). N-(3-dimethylaminopropyl)-N'-ethylcarbodiimide (EDC), 2-iminothiolane hydrochloride (Traut's reagent), adipic acid dihydrazide (ADH), 6-hydroxy-2,5,7,8-tetramethylchroman-2-carboxylic acid (Trolox), 2,4,6-trinitrobenzenesulfonic acid (TNBSA) solution at 5 w/v % in methanol was purchased from Thermo Fisher Scientific (Spain). Silk fibroin solution (5 w/v %, 100–150 kDa), Ellman's reagent (5,5'-dithiobis-(2-nitrobenzoic acid)), 1,1-diphenyl-2-picrylhydrazyl (DPPH), 4,4'-methylenebis(phenyl isocyanate) (MDI), poly(ethylene glycol) (PEG, average $M_n=1000$), 1,4-diazabicyclo(2.2.2)octane (DABCO), glycerol, guaiacol, 2,2-diphenyl-1-picrylhydrazyl (DPPH), 2,2'-azino-bis(3-ethylbenzothiazoline-6-sulfonic acid) diammonium salt (ABTS), ascorbic acid, PBS, NB, LB with agar, Coliform ChromoSelect agar, Cetrimide agar, and Dulbecco's Modified Eagle's Medium (DMEM) were obtained from Sigma-Aldrich (Spain). DC 5179 Additive (a cell-regulating silicone surfactant for flexible foams) was obtained from Dow (USA). Commercial polyurethane foam Askina® was provided by B. Braun (Germany). AlamarBlue cell viability reagent, Live/Dead BacLight kit (Molecular probes L7012), and EnzChek Gelatinase/Collagenase Assay Kit were purchased from Invitrogen, Life Technologies Corporation (Spain).

MPO from human leukocytes with an activity of 1550 U/mg solid defined as the amount of enzyme producing an increase of 1.0 absorbance unit per min at 470 nm at pH 7.0 and 25 °C, using guaiacol as a substrate, was purchased from Planta Natural Products (Vienna, Austria). Hyaluronidase with an activity of 443 U/mg solid defined as the amount of enzyme causing a change in the transmittance at 600 nm of 0.330 per min at pH 5.35 at 37 °C in a 2.0 mL reaction mixture), was purchased from Sigma-Aldrich (Spain).

Bacterial strains *S. aureus* (ATCC 25923) and *P. aeruginosa* (ATCC 10145), human fibroblast cells (ATCC-CRL-4001, BJ-5ta), and human keratinocyte cells (HaCaT cell line) were obtained from the American Type Culture Collection (ATCC LGC Standards, Spain). The water used in all experiments was purified by MilliQ plus system (Millipore) with 18.2 M Ω -cm resistivity prior to its use.

Preparation of polyurethane foams embedded with AgPheLigNPs

The pre-foam solution was prepared by mixing 2.4 g (2.4 mmol) of PEG, 0.095 g (1.0 mmol) of glycerol, and 0.15 g of DC 5179 additive, under stirring for 10 min at 60 °C. Freeze-dried AgPheLigNPs (5, 7.9, and 10 mg) were dispersed in the polyol mixture by stirring and sonication in an US bath for 20 min at 60 °C (Table 11). Then, 25 μ L of H₂O was added, and the reaction mixture was stirred again for 10 min at 60 °C. The polyol formulation was then mixed with 1.3 g (5.20 mmol) of MDI until the system became homogeneous. The polymerization reaction was initiated by adding 25 mg (0.22 mmol) of DABCO. The mixture was manually stirred to obtain the foam that was further kept in the vessel for 24 h at room temperature for curing. The isocyanate index for the synthesized foams was 94.14.

Table 11 Nomenclature of the synthesized PUFs and the content of AgPheLigNPs (%) added to prepare of the PUFs.

Foam	AgPheLigNPs (%)
PUF-0	0
PUF-0.12%NP	0.12
PUF-0.20%NP	0.20
PUF-0.25%NP	0.25

Characterization of PUFs

FTIR analysis of the foams

FTIR spectra of the foams were recorded by a PerkinElmer Spectrum 100 FTIR spectrometer (PerkinElmer, MA, USA) in the 600–4000 cm⁻¹ range, performing

64 scans for each spectrum at 4 cm⁻¹ resolution. The spectrometer was equipped with an ATR accessory of germanium crystal with a high-resolution index (4.0).

SEM and energy dispersive X-ray spectroscopy analysis

The cell morphology of the foams was observed by scanning electron microscopy (SEM) using a JEOL JSM 7100 F microscope. The diameter of the cells was obtained by measuring 200 cells in each sample using ImageJ software (version 1.52a). EDX analysis was performed to evaluate the chemical composition of the nanoparticles.

Mechanical properties of the foams

The apparent density of the samples was calculated from the mass and the actual specimen dimensions using a precision balance and a digital Vernier calliper, respectively. Compression testing was carried out at room temperature (25 °C) along the vertical direction of samples on a Galdabini (Italy) universal testing machine equipped with a load cell of 1 KN and following the ISO 604 standard. The crosshead rate was set to 1 mm·min⁻¹. The Young's modulus was calculated from the slope of the stress–strain curves. The specific modulus was then obtained by dividing the average values by the apparent density.

Swelling kinetics

Swelling kinetics of PUFs was characterized by monitoring the mass changes during incubation in physiological fluid. Cubic pieces of foams of known weight (W_1) were immersed in PBS (0.01M, pH 7.4) and incubated at 37 °C. The swollen foams were removed, and the excess of fluid was absorbed with filter paper. The swollen foams were weighted (W_2), and the swelling index (%) at different check points was calculated as follows:

$$\text{Swelling index (\%)} = (W_2 - W_1)/W_1 \quad (\text{Eq. 6})$$

Silver content and silver release from the PUFs

In order to determine the silver content of the foams, three replicates of PUF cubes of known weight were digested with 20 % HNO₃ at 100 °C for 1 h. The

resulting solutions were analyzed by inductively coupled plasma mass spectrometry (ICP-MS 7800, Agilent Technologies) calibrated by an internal standard with ^{45}Rh and a standard curve of ^{107}Ag . The cumulative silver release profiles were evaluated by soaking 50 mg of foam in PBS pH 7.4 at 37 °C. Samples collected at different time intervals were appropriately diluted and analyzed by ICP-MS. The results are shown in terms of silver release (%) regarding the total silver content in each foam sample.

Antibacterial activity of PUFs

The antibacterial activity of the PUFs was assessed by release- and contact-killing tests. For both assays, bacterial suspensions were prepared by growing *S. aureus* and *P. aeruginosa* in MHB culture medium overnight at 37 °C. After reaching the exponential growth phase, the cultures were diluted in sterile PBS pH 7.4 to obtain a microbial suspension with an optical density $\text{OD}_{600}=0.01$ ($3 \cdot 10^6$ CFU·mL⁻¹). The release-killing test consisted of soaking one portion of cubic PUF (50 mg), which was previously sterilized by UV light for 30 min, in 2 mL of microbial suspension and incubating at 37 °C. After 24 h, the suspension was vortexed for 2 min to detach bacteria. After appropriate dilutions, the samples were inoculated in Petri agar dishes for CFU counting and incubated overnight at 37 °C to calculate the logarithm reduction of bacteria in contact with the foams. For the antimicrobial contact-killing test, 200 μL of bacterial suspension was added to sterile PUF cubes (50 mg). The foam was incubated at 37 °C in an oscillatory incubator. After 24 h, 1.8 mL of PBS pH 7.4 was added to the foam and vortexed for 2 min to detach bacteria. Logarithm reduction was obtained after plating an appropriate dilution of the suspension in agar plates. In all experiments, PUFs without nanoparticles were used as controls. The bacterial reduction was calculated following Eq. 3.

Ex vivo evaluation of MPO inhibition

Wound exudate was extracted from the dressing (UrgoCleans, Urgo Medical) of a patient with venous leg ulcer (Hospital de Terrassa, Spain). After removing

the dressing from patient's limb, 1 g of sample containing wound exudate, was soaked in 5 mL MilliQ water for 10 min. Then, the mixture was vortexed for 3 min and centrifuged for 5 min at 15000g. The extracted liquid was collected and centrifuged once again for 5 min at 15000g to remove the sludge from the wound dressing, and finally stored in the fridge at 4 °C for further use. The inhibitory activity of the PUFs against MPO in the wound fluid was determined by a colorimetric assay using guaiacol as a substrate. Briefly, 50 mg of foam was soaked in 1 mL of wound fluid diluted 1:8 in PBS pH 7.4. After 1 h incubation at 37 °C, the dressing was removed and 150 µL of sample was mixed with 10 µL of guaiacol (167 mM) and 22 µL of H₂O₂ (1 mM). The increase of absorbance at 470 nm was monitored for 10 min. Wound exudate samples incubated in the absence of the dressings were taken as the reference for calculating the percentage inhibition of MPO.

Antioxidant activity of PUFs

The antioxidant activity of the foams was evaluated spectrophotometrically measuring the decrease of ABTS radical absorbance at 417 nm. The ABTS radical was formed by mixing 2.45 mM potassium persulfate with ABTS (final concentration 7 mM) allowing the mixture to stand in the dark at room temperature for 16 h. Cubic pieces of PUF (50 mg) were incubated in 1 mL of ABTS radical solution at 37 °C in the dark for 30 min. Ascorbic acid was used as the reference (100 % inhibition) for calculating the inhibition percentage of absorbance.

In vitro cytotoxicity evaluation

The potential cytotoxicity of the PUFs was tested toward human fibroblasts (cell line BJ5ta) and human keratinocytes (cell line HaCaT). The cells were grown in 0.5 mL of DMEM in a 24-well plate (120000 cells per well) at 37 °C in a humidified atmosphere with 5 % CO₂ for 24 h. At pre-confluence, 1.5 mL of fresh medium and 50 mg of PUFs (previously sterilized by UV light) were added to each well. After 24 h incubation, the foams were removed from the wells, and the

cells were recovered for 24 h in 0.5 mL of fresh culture medium. The cell viability assessment was performed using the AlamarBlue assay as described in Chapter 1 (*Materials and methods*, section *Cytotoxicity assay*) and was calculated following Eq. 5.

Modification and characterization of HA

HA was modified with ADH and Traut's reagent in a two-step process as previously described¹⁰⁵ with some modifications. Briefly, HA salt (600 kDa) was dissolved in MilliQ water (2.5 mg·mL⁻¹) and ADH (45-fold molar excess) was added. After 30 min, the pH was adjusted to 4.8 with 1M HCl and EDC (4-fold molar excess) was added to the mixture. The pH was monitored and maintained at 4.8 by adding 1 M HCl for 2 h. Afterward, the reaction was stopped by raising the pH to 7.0 with 1 M NaOH. The solution was dialyzed in water for one day using 13 kDa cut-off membranes, and then freeze-dried. For the second step, the resulting HA-ADH was dissolved in MilliQ water (2.5 mg·mL⁻¹) and Traut's reagent dissolved in 0.1 M pH 8 phosphate buffer was added at a molar ratio of 1:2 (ADH : Traut's). The reaction took place for 2 h under a nitrogen atmosphere. The modified polymer was purified by dialysis against acidified water for one day. Finally, the resulting HA-SH was lyophilized and stored at 4 °C under a nitrogen atmosphere.

FTIR spectra of HA, HA-ADH and HA-SH were recorded by a PerkinElmer Spectrum 100 FTIR spectrometer (PerkinElmer, MA, USA) in the 600–4000 cm⁻¹ range, performing 64 scans for each spectrum at 4 cm⁻¹ resolution. The spectrometer was equipped with an ATR accessory of germanium crystal with a high-resolution index (4.0).

The amount of primary amines in HA-ADH was assessed using the TNBSA assay. Briefly, 0.25 mL of a solution of HA-ADH was added to 0.5 mL of a 0.01 w/v % solution of TNBSA in 0.1 M of sodium bicarbonate at pH 8.5. After incubating the mixture for 2 h at 37 °C, 0.25 mL of 10 w/v % SDS and 0.125 mL of 1 N HCl were added. Then, the absorbance was measured at 335 nm. ADH standards

were used to build the calibration curve and non-functionalized HA was used as a control.

The thiol content of HA-SH was determined espectrophotometrically using Ellman's reagent. Briefly, a solution of HA-SH in 0.2 M pH 8 phosphate buffer was mixed with 0.3 mg·mL⁻¹ Ellman's reagent at a volume ratio of 1:1. After 2 h incubation in the dark, the absorbance was measured at 412 nm. The calibration curve was built using L-cysteine, and unmodified HA was used as a control.

Synthesis of HA-SH/SF hydrogels

HA-SH was dissolved in sodium 0.1 M pH 5.5 acetate buffer under a nitrogen atmosphere. Then, silk fibroin solution was added and stirred for 1 min. The final concentration of each polymer in the solution was 1.0 or 1.5 w/v %. PheLigNPs at different concentrations (20, 10, and 5 mg·mL⁻¹) were added to the polymer mixture at a volume ratio of 20:3 (polymers : PheLigNPs). The formulations of the hydrogels are summarized in **Table 12**. The concentration of PheLigNPs used in the hydrogel formulations were chosen taking into account the antibacterial properties of the particles described in Chapter 1 (*Results and Discussion, section Phenolated lignin nanoparticles*).

Table 12 Hydrogel formulations

Hydrogel	Composition	
	Polymers	PheLigNPs (mg·mL ⁻¹)
1.5%_20	HA-SH (1.5 w/v %), SF (1.5 v/v %)	20
1.5%_10	HA-SH (1.5 w/v %), SF (1.5 v/v %)	10
1.5%_5	HA-SH (1.5 w/v %), SF (1.5 v/v %)	5
1.0%_20	HA-SH (1.0 w/v %), SF (1.0 v/v %)	20
1.0%_10	HA-SH (1.0 w/v %), SF (1.0 v/v %)	10
1.0%_5	HA-SH (1.0 w/v %), SF (1.0 v/v %)	5

Characterization of HA-SH/SF hydrogels

Rheological characterization

Rheological characterization of the hydrogels was performed with an MCR302 rheometer (Anton Paar, Austria), equipped with electrically heated plates. The assays were carried out using a 25 mm parallel, sandblasted plate. Strain-dependent oscillatory measurements were performed at a fixed frequency (1 s^{-1}) and in a range of increasing strains (0.1 to 10000 %). Continuous flow curves were obtained by monitoring the viscosity of the materials at increasing shear rates ($0.01\text{--}100 \text{ s}^{-1}$). The self-healing properties of the gels were studied using a 3-interval thixotropic test (3iTt) consisting of strain-dependent oscillatory measurements at a fixed frequency (1 s^{-1}) with an alternating strain (5 and 2000 %). All experiments were performed at $25 \text{ }^\circ\text{C}$ using a solvent trap in order to prevent dehydration during the tests.

Cryogenic Scanning Electron Microscopy (Cryo-SEM)

For cryo-SEM, the 1.5%₁₀ hydrogel and the control (polymer mixture at 1.5 % without PheLigNPs) were mounted on aluminum stubs and plunged into liquid nitrogen slush. Once the materials were frozen, they were transferred under vacuum conditions to a cryo-preparation chamber Quorum PP3000T (Quorum Technologies, Ltd., UK). The preparation chamber was under high vacuum and fitted with a cold stage where the samples were cold fractured, sublimed at $-90 \text{ }^\circ\text{C}$ for 4 min, sputter coated with platinum and transferred to a cold-stage in the chamber of the Hitachi S-3500N scanning electron microscope (Hitachi High-Tech Co., Japan) in the Institute of Marine Sciences of the Spanish Research Council facilities. The samples were maintained at $-130 \text{ }^\circ\text{C}$ during the observation at an acceleration voltage of 5 kV. The average size of the pores was obtained from imaging 50 pores using ImageJ software (version 1.52a).

Swelling capacity

The swelling of hydrogels was determined gravimetrically by immersing 100 mg of hydrogel in 20 mL PBS (0.1 M, pH 7.4) at room temperature. After different

incubation times, the weight of the hydrogel was determined after removing the excess water with filter paper. The swelling index was calculated following Eq. 6 (Chapter 2, *Materials and methods*, section *Characterization of PUFs*):

Stability in PBS

The hydrogel sample 1.0%₁₀ was chosen to study the stability of the gels in PBS (0.1 M, pH 7.4). Samples of 300 mg of gels were immersed in 1 mL of PBS for 1, 3, and 7 days. Every 24 h, the liquid was carefully removed and replaced with fresh PBS. After the established time intervals four samples were withdrawn from PBS and freeze-dried. The stability of the hydrogel was reported as the mean of the dry weight of the gels at each incubation time (n=5). The statistical significance was determined using a one-way ANOVA followed by Dunnett's multiple comparison test against time zero. P values less than 0.05 were considered statistically significant.

pH responsiveness of the hydrogels

The hydrogel sample 1.0%₁₀ was chosen to evaluate the behavior of the gels at different pH conditions. The mechanical properties of the gels were determined by the strain-dependent oscillatory test after incubating 500 mg of hydrogel in 1 mL of 0.1M Britton-Robinson buffer (pH 4.0, 5.0, 6.0, 7.0, 8.0, and 9.0) for 24 h. Hydrogels incubated in water were assigned as the reference. The rheological test was performed at a fixed frequency (1 s^{-1}) and in a range of increasing strains (0.1 to 10000 %).

The release of PheLigNPs from the polymeric matrix under different pH conditions was studied by measuring the fluorescence of the liquid in which the gels were incubated. Prior to the tests, the fluorescent excitation and emission peaks of PheLigNPs were determined. The release assay consisted in immersing 60 mg of the 1.0%₁₀ hydrogel in 0.2 mL of 0.1 M Britton-Robinson buffer (pH 4.0, 5.0, 6.0, 7.0, 8.0, and 9.0). After different time sets, the liquid was removed, and the fluorescence was measured at $\lambda_{\text{ex/em}}=480/610\text{ nm}$. Results are shown as the mean of three replicates \pm SD.

Biodegradability and NPs release in the presence of hyaluronidase

The biodegradability of the hydrogels was assessed by incubating 250 mg of the 1.0%₁₀ hydrogel with 1 mL of PBS (0.1 M, pH 7.4) containing 10 U·mL⁻¹ of hyaluronidase for 24 h at 37 °C and 230 rpm shaking. Afterward, the liquid was carefully removed and the tubes containing the hydrogels were freeze-dried. The control group were gels incubated only with PBS. The biodegradability of the hydrogels was reported as the mean of the dry weight of the gels (n=4). The statistical significance was determined using a one-way ANOVA followed by Dunnett's multiple comparison test. P values less than 0.05 were considered statistically significant.

The release of PheLigNPs in the presence of hyaluronidase was studied by measuring the fluorescence at $\lambda_{ex/em}=480/610$ nm in the supernatant of the hydrogels (300 mg) incubated with 1 mL of PBS (0.1 M, pH 7.4) containing 10 U·mL⁻¹ of hyaluronidase for 24 h at 37 °C and 230 rpm shaking. Results are shown as the mean of three replicates \pm SD.

Antioxidant activity

The antioxidant activity of the hydrogels was studied by measuring the decrease in absorbance of the free DPPH radical. Briefly, 30 mg of each hydrogel was incubated in 1 mL of 100 μ M DPPH solution in methanol at room temperature in the dark. At different incubation times, the supernatant was collected and the absorbance at 517 nm was measured. The assay was performed in triplicate and expressed relative to Trolox in terms of Trolox equivalent antioxidant capacity, TEAC (μ mol Trolox equiv·g⁻¹ hydrogel).

Antibacterial activity

The capacity of the hydrogels to inhibit bacterial proliferation was evaluated against *S. aureus* and *P. aeruginosa* by the standard flask shake method (ASTM-E2149-01) with some modifications. Briefly, 30 mg of hydrogel was immersed in a bacterial dispersion in PBS at OD₆₀₀=0.005 (corresponding to $\sim 10^5$ – 10^6 colony forming units per mL, CFU·mL⁻¹) and incubated for 24 h at 37 °C and 230 rpm.

The number of viable cells before and after the treatment with the gels was determined by the serial dilution method. The percent of bacterial reduction was calculated following Eq. 4 (Chapter 1, *Materials and methods*, section *Growth inhibition of bacteria by the lignin-based NPs*).

Morphology of bacterial cells

Morphological changes of *S. aureus* and *P. aeruginosa* treated with hydrogel were examined by SEM. Overnight bacterial cultures grown in NB were diluted to an $OD_{600}=0.01$, and 200 μL of the suspension were treated with 60 mg of the 1.5%₁₀ hydrogel for 24 h at 37 °C and 230 rpm shaking. The bacterial suspension was then transferred to a 48-well plate containing silicon wafers. After 24 h at room temperature, the liquid was removed and the bacteria remaining in the wafers were fixed overnight in a 2 % paraformaldehyde and 2.5 % glutaraldehyde-buffered solution. Bacteria were dehydrated by incubating the wafers with increasing concentrations of ethanol for 1 h each (25, 50, 75, and 100 %). The samples were observed using a field-emission SEM (Merlin Zeiss) operating at 1 kV.

Evaluation of MPO and MMPs inhibition

The inhibition of the MMPs activity in the presence of the hydrogels was studied using the Gelatinase/Collagenase Assay Kit. Briefly, 30 mg of hydrogel was incubated with 400 μL of collagenase ($1.5 \text{ U}\cdot\text{mL}^{-1}$) for 24 h at 37 °C. After the incubation, 40 μL of gelatin substrate ($125 \mu\text{g}\cdot\text{mL}^{-1}$) was added to 100 μL of reaction and the fluorescence was read at $\lambda_{\text{ex/em}}=493/528 \text{ nm}$. The percent of MMPs inhibition was calculated by taking the control values as 100 % activity. To avoid any background caused by the presence of the hydrogels, buffer solutions containing hydrogels in the absence of collagenase were used as blanks. Controls were tubes containing only collagenase or only buffer.

The capacity of the hydrogels to inhibit the activity of MPO was studied using guaiacol as a substrate. The hydrogels (30 mg) were immersed in 200 μL of 0.1 M pH 7.5 phosphate buffer containing 48 μL of guaiacol (167 mM) and 32 μL of

MPO ($0.063 \text{ U}\cdot\text{mL}^{-1}$). After 1 h in contact with the enzyme and the substrate, the hydrogel was withdrawn and 200 μL of the liquid were mixed with 10 μL of 1 mM H_2O_2 to start the reaction. Immediately after, the absorbance at 476 nm was measured every 2 min. The activity was determined by the rate of absorbance increase per min and expressed as a percentage of enzyme inhibition compared to the control (reaction mixture with enzyme and substrate, without hydrogel). All measurements were carried out using four replicates.

Cytotoxicity toward human cells

The cytotoxicity of the hydrogels was assessed *in vitro* using human fibroblasts (BJ5ta cell line) and keratinocytes (HaCaT cell line). The cells were grown in DMEM supplemented with 200 mM of L-glutamine, 1 % penicillin, and 10 % (v/v) fetal bovine serum, at 37 °C in a humidified atmosphere with 5 % CO_2 . The cells were harvested at pre-confluence and seeded at a density of 62000 cells per well on a 24-well plate containing permeable supports of tissue culture-treated polyester membrane (0.4 μm pore size). After 24 h of incubation, the cells were incubated with 30 mg of hydrogels, previously sterilized by UV, for 1 and 7 days at 37 °C. The samples and the medium were then removed, and the cell viability was assessed using 150 μL of the AlamarBlue reagent diluted in culture medium (10 % v/v). After 4 h incubation, the fluorescence was read at $\lambda_{\text{ex/em}}=550/590 \text{ nm}$. Wells containing only cells were used as the reference (growth control), while the blank was the AlamarBlue reagent incubated in the absence of cells. The percentage of cell viability was calculated following Eq. 5 (Chapter 1, *Materials and methods*, section *Cytotoxicity assay*). The results are reported as mean of values of cell viability (%) ($n=3$) \pm SD.

Cell viability was further studied with fluorescence microscopy using the Live/Dead Viability/Cytotoxicity kit (Thermo Fisher Scientific) that stains the live cells in green and the dead ones in red. After 7 days in contact with the hydrogels, the medium and the hydrogels were removed, and the cells were stained for 20 min with a PBS solution containing 0.1 v/v % calcein acetoxymethyl and 0.1 v/v % ethidium homodimer-1. The cells were observed

using a fluorescence microscope (Nikon/Eclipse Ti- S, the Netherlands) at $\lambda_{\text{ex/em}}=494/517$ nm for calcein acetoxymethyl and at $\lambda_{\text{ex/em}}=517/617$ nm for ethidium homodimer-1.

Data analysis

Data were analyzed using Graph Pad Prism version 8.0.1 (Graph Pad Software, CA, USA). Statistical significances were determined using the unpaired two-tailed Student's t-test or one-way ANOVA. *P* values less than 0.05 were considered statistically significant.

Results and discussion

Antibacterial polyurethane foams with incorporated lignin-capped silver NPs for chronic wound treatment

Structural and mechanical characterization of PUFs

Flexible PUFs were prepared by mixing MDI with a pre-foam solution where AgPheLigNPs were previously dispersed. Different concentrations of AgPheLigNPs were used to synthesize the foams (PUF-0.12%NP, PUF-0.20%NP and PUF-0.25%NP). The AgPheLigNPs content in each foam was selected according to the MIC results in order to obtain foams with antimicrobial properties (Chapter 1, *Results and discussion*, section *Silver phenolated lignin nanoparticles*). The brownish color of the foams containing NPs was attributed to the lignin component as constituent of the AgPheLigNPs (**Figure 37**, insets). Foam without NPs (PUF-0) was used as a control in these studies.

FTIR analysis of the foams revealed the characteristic bands for the main functional groups (**Figure 36a–b**). The peak related to N-H vibrational stretching was observed at 3323 cm^{-1} , probably overlapping the O-H band. The vibration of C-N and in plane bending of N-H from the urethane linkage were observed at 1511 cm^{-1} , and the C-H stretching of the aliphatic chains appeared at 2925 and 2855 cm^{-1} .^{229,230} The band related to the carbonyl group (C=O) from

the urethane linkage was observed at 1726 cm^{-1} .²³⁰ The absence of the characteristic vibration peak of $\text{N}=\text{C}=\text{O}$ at 2270 cm^{-1} suggested the consumption of isocyanate associated to the urethane linkage formation during the PUF synthesis.²³¹ The aromatic ring vibration of MDI was observed at 1595 cm^{-1} . The signals below 1600 cm^{-1} are fingerprints of polyurethane.²³² The presence of lignin could not be detected by FTIR, probably due to the low amount of AgPheLigNPs in the PUFs.

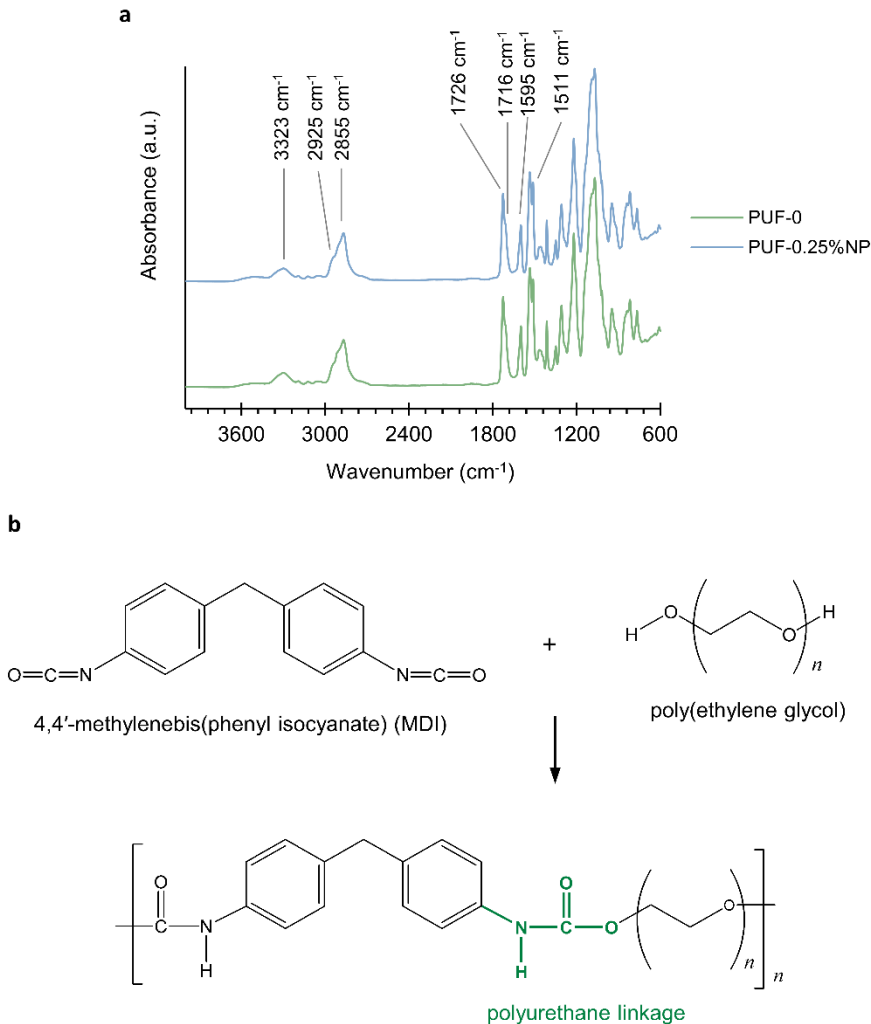


Figure 36. (a) FTIR spectra of control polyurethane foam (PUF-0) and polyurethane foam containing 0.25 wt% of AgPheLigNPs (PUF-0.25%NP). (b) Simplified polyurethane foam structure synthesized from 4,4'-methylenebis(phenyl isocyanate) (MDI) and poly(ethylene glycol).

SEM images of transversal cuts (**Figure 37a-d**) revealed an open-cell structure of PUFs, characteristic of soft foams.²³³ The cell diameter was uniform for each foam and decreased when the concentration of the NPs increased. In particular, significant difference in the cell size was found between PUF-0 and PUF-0.25%NP having the highest AgPheLigNPs content. Similar tendency was observed in previous works, where increasing the concentration of lignin²³⁰ and nanoparticles⁹ reduced the size of PUF cells. Decrease of the cell size may be explained by cross-linking of PUF structure due to: i) involvement of the lignin shell of the AgPheLigNPs in polymerization with the isocyanate component, and ii) coordination of the polyurethane chains by H-bonds with the lignin-capped NPs.²³⁴ The presence of AgPheLigNPs in PUF-0.25%NP was confirmed by SEM and EDX (**Figure 37e-f**). AgPheLigNPs were not detected in PUF-0.12%NP and PUF-0.20%NP samples, probably due to the low concentration of NPs and the three-dimensional structure of the foams. The total Ag content of the foams measured by ICP-MS was 217.9 ± 13.8 , 274.7 ± 25.8 , and 340.9 ± 21.0 ppb Ag/mg PUF for PUF-0.12%NP, PUF-0.20%NP, and PUF-0.25%NP, respectively.

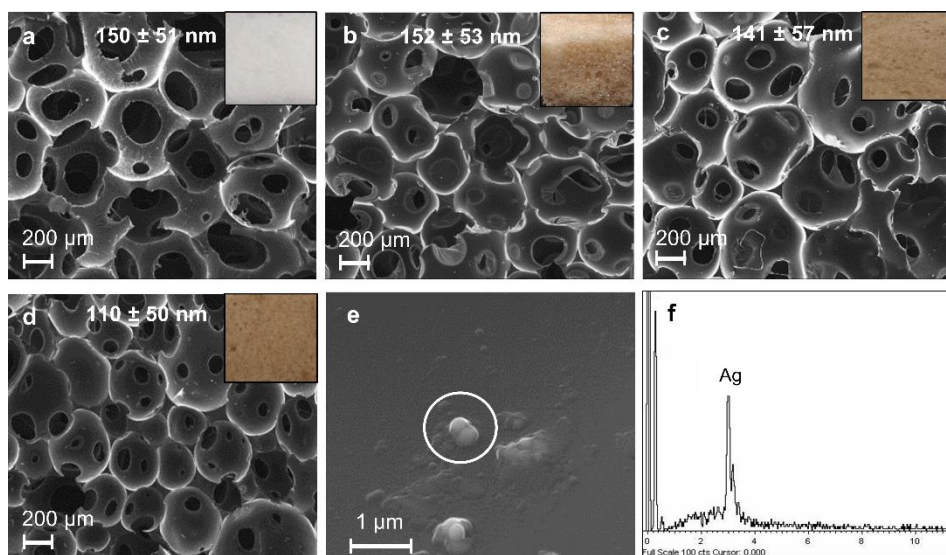


Figure 37. SEM images of transversal cuts of (a) PUF-0, (b) PUF-0.12%NP, (c) PUF-0.20%NP, and (d) PUF-0.25%NP at $\times 50$ magnification with their corresponding average cell size and representative photographs. (e) SEM image of PUF-0.25%NP at $\times 20000$ magnification, and (f) EDX spectrum for PUF-0.25%NP.

The density and compression modulus of the foams were measured to describe their mechanical properties. The foams completely recovered their initial shape after applying a compressive load at 50 % deformation. Foam density increased by 27 % when the AgPheLigNPs content was 0.25 % (**Figure 38a**). Incorporation of NPs chemically cross-linked with polyurethane has been described to improve the mechanical performance of the foams.²³⁵ In this study, the addition of AgPheLigNPs to the foams resulted in 40 % increase of their compression modulus, i. e. from 55 kPa for the reference PUF-0 to 78 kPa for PUF-0.20%NP and PUF-0.25%NP (**Figure 38b**). The results obtained from mechanical characterization of the PUFs suggested that the NPs are part of their structure and the lignin from the NPs may be covalently crosslinked with the polyols. However, further analysis of the structure of PUFs containing AgPheLigNPs is needed to elucidate the type of interactions between the NPs and the polyurethane chain.

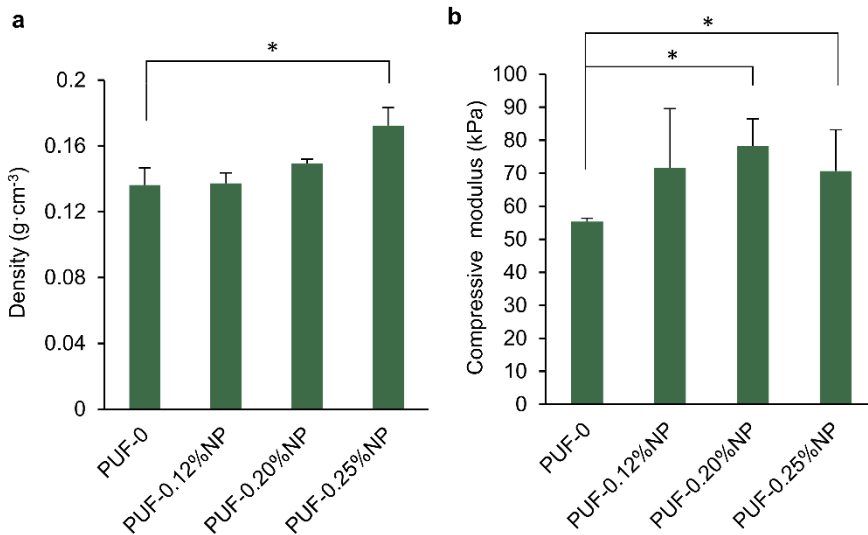


Figure 38. Density (g·cm⁻³) and compression modulus (kPa) of the synthesized polyurethane foams. Results are reported as mean values \pm SD (n=3).

Swelling profiles of PUFs containing AgPheLigNPs

Maintaining moist environment is crucial for wound healing. Moisture promotes the action of growth factors, fibroblasts and keratinocytes, thus

facilitating the growth of new tissue.²³⁶ However, excessive or insufficient wound moisture hinders the wound repair, causing tissue alterations and promoting bacterial colonization.²³⁷ Some chronic wounds generate large amounts of exudate that can overhydrate the wound bed. Additionally, the deleterious enzymes in the exudates degrade the ECM necessary for healing.¹⁴⁹ Therefore, an optimal dressing material should have the capacity to absorb the excess of exudate while keeping the moisture in wound bed and avoiding drying out.

The swelling of PUF-0 and Askina®, a benchmark commercial dressing, in physiological fluid at 37 °C presented similar kinetics, where ca. 1150 % was the maximum swelling index for both foams (**Figure 39**). All PUFs reached the maximum liquid uptake after 10 min of incubation, except for PUF-0.25%NP, which reached this maximum after 60 min. The high swelling ratios of the PUFs suggested that these materials would be able to absorb the excess of liquid in highly exudating wounds.

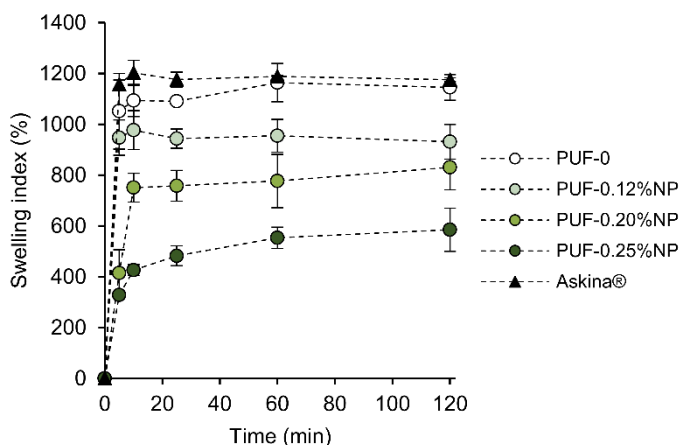


Figure 39. Swelling index (%) over time of PUFs in PBS (pH 7.4) at 37 °C. Results are reported as mean values \pm SD (n=5).

The AgPheLigNPs content in the foams clearly influenced their swelling capacity. The incorporation of AgPheLigNPs in the foams led to lower swelling ratios, suggesting an increase of PUFs' cross-linking density.^{230,238} The swelling index decreases from 1145 % to 585 % when the concentration of AgPheLigNPs

rises from 0.12 to 0.25 %. Hydroxyl groups of lignin present in the AgPheLigNPs may have reacted with isocyanate to generate urethane bonds involving the lignin shell of the NPs, thus increasing the cross-linking density of the foams.^{230,234,239,240} Customization of the swelling profiles of these PUFs by modulating their AgPheLigNPs content would allow for their use as absorbing materials for moderately to highly exuding wounds.

Silver release kinetics

A sustained release of the antimicrobial agent is required for obtaining a wound dressing with durable antimicrobial efficiency. However, achieving a constant release of the antimicrobial agent remains a major challenge. The cumulative silver release behavior of the AgPheLigNPs-loaded PUFs was followed for 24 h at 37 °C in PBS. The total amount of silver released after 24 h did not exceed 1 % in any of the foams (**Figure 40**). Initial burst release of the antimicrobial agent, which is a common issue when using polyurethane foams,^{241–243} was not observed in this assay. AgNPs can act as reservoirs of Ag⁺ that are released in a sustained fashion, which is advantageous over free Ag⁺ in terms of prolonged antibacterial action. This is especially beneficial in materials for biomedical applications requiring long-term antibacterial effect (e.g.,

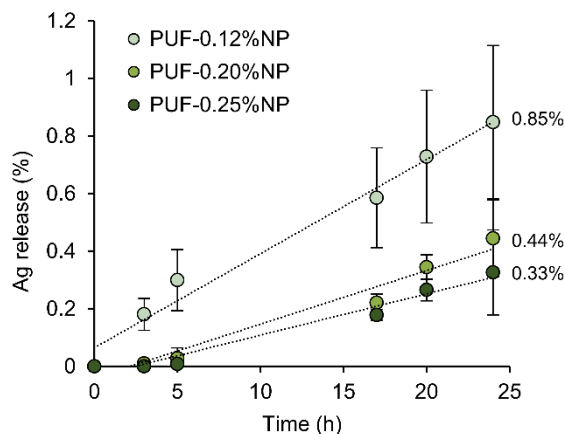


Figure 40. Silver release profile of PUFs in PBS (pH 7.4) at 37 °C. The results are expressed as percentage of released Ag relative to the total Ag content of each sample, and are reported as mean values \pm SD (n=3).

implants, wound dressings, urinary catheters). The lignin matrix embedded with AgNPs has possibly reacted with isocyanate to integrate into urethane bonds in the polymer structure. Such covalent interaction in addition to formation of hydrogen bonds between the lignin shell of the nanoparticles and the polyurethane macromolecules would prevent the burst release of silver. Increasing the concentration of AgPheLigNPs in the foams resulted in a slower Ag⁺ release, probably due to a higher cross-linking of lignin in the PUF structure.^{230,239,240}

Antibacterial activity of PUFs

The antimicrobial activity of the foams containing different amounts of AgPheLigNPs was evaluated against the Gram-positive *S. aureus* and the Gram-negative *P. aeruginosa*, two clinically relevant bacteria found in chronic wounds.¹⁴⁶ The capacity of the PUFs to kill these bacterial strains was assessed by contact-killing and release-killing methods (**Figure 41**). Only the PUFs containing AgPheLigNPs were able to reduce the bacterial load. The increase of the AgPheLigNPs content in the foams lead to higher bacterial reduction of *S.*

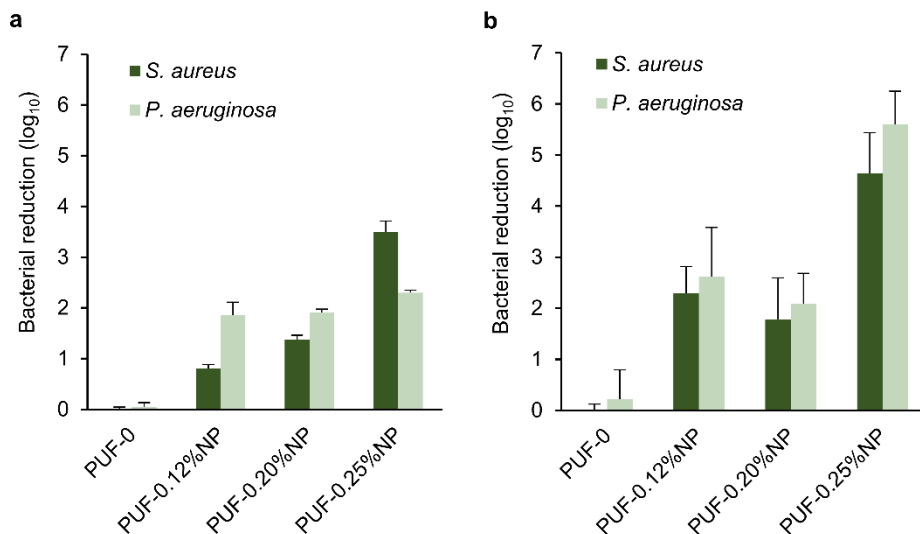


Figure 41. Antibacterial activity of the PUFs against *S. aureus* and *P. aeruginosa*. (a) release-killing test and (b) contact-killing test. Results are reported as mean values \pm SD (n=3).

aureus in the release-killing test, whereas similar bacterial log reduction of *P. aeruginosa* was found for all samples (**Figure 41a**). Higher antimicrobial effect was observed in the contact-killing experiments, achieving over 4.6 and 5.6 log reduction with PUF-0.25%NP against *S. aureus* and *P. aeruginosa*, respectively (**Figure 41b**). Enhanced antibacterial effect of immobilized AgNPs on contact-killing principle has been previously described.²⁴⁴ In our work, the results indicated that the PUFs containing AgPheLigNPs were able to eradicate bacteria through both contact and release mechanisms, suggesting that the antibacterial property of the foams can be attributed to the combined effect of Ag⁺ release and nanoparticles/bacteria interaction.²⁴⁵ The sustained silver release from the foams together with the antibacterial effect of the NPs suggested a long-term antibacterial efficiency of these materials.

Antioxidant property

During the inflammatory phase of wound healing, immune cells produce reactive oxygen species (ROS), which in low concentrations provide defense against microorganisms. However, the elevated levels of ROS in chronic wounds lead to oxidative stress,²⁴⁶ which damages ECM and cells, resulting in a delay of wound healing.²⁴⁷ It has been reported that reducing ROS using strong antioxidants decrease the chronicity of wounds in an animal model.¹⁴⁷ A simpler approach is to absorb ROS by the wound dressing itself, thereby reducing ROS concentration in the wound bed and reestablishing the prooxidant-antioxidant homeostasis.

The capacity of PUFs to scavenge radical species was assessed with the ABTS assay. All PUFs showed a radical scavenging activity of above 85 % (**Figure 42**). However, the increase of AgPheLigNPs content in the foams, associated with a decrease of their liquid uptake capacity (**Figure 39**), caused a decrease of the radical scavenging activity as well. Hence, the radical scavenging activity of the PUFs was associated rather to the capacity of the PUFs to absorb and retain ROS than to the reducing capacity of the lignin component of the NPs.

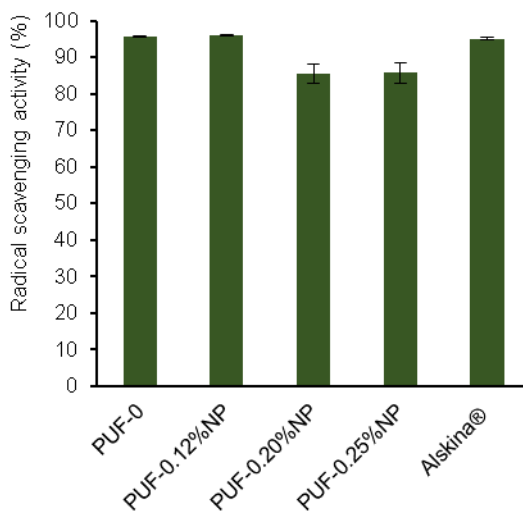


Figure 42. ABTS radical scavenging activity (%) of PUFs. Results are reported as mean values \pm SD (n=3).

In our group, wound dressing materials with antioxidant properties have been developed by incorporating natural phenolic compounds, such as GA and chicoric acid.^{150,248,249} It has been reported that lignin, as a polyphenolic molecule, possesses intrinsic antioxidant properties.²⁰⁴ However, in this work, the increase of lignin content, i.e. the amount of AgPheLigNPs in the PUFs, was not reflected in an increase of the antioxidant capacity of the foams. We hypothesized that the lignin present in the PUFs has been first partially oxidized to form the AgPheLigNPs and may also have reacted with isocyanate to form urethane linkages, thus reducing its free phenolic content and its radical scavenging capacity, respectively. This hypothesis was corroborated by the decrease of lignin phenol content after AgPheLigNPs formation, discussed in Chapter 1 (*Results and Discussion*, section *Silver phenolated lignin nanoparticles*). Additionally, the reduction of the foam cell size and swelling capacity could be related to the increase of cross-linking density.

Ex vivo inhibition activity of PUFs against deleterious wound enzyme

MPO and MMP are major enzymes related with the prolonged inflammatory phase of chronic wounds. The oxidative enzyme MPO catalyzes the generation of

the most potent bactericidal agent in humans, HClO, that effectively kills bacterial pathogens. Nevertheless, excessive amounts of HClO found in chronic wounds and subsequent formation of chlorine, hydroxyl radicals and singlet oxygen,²⁵⁰ could result in the oxidation of beneficial for healing biomolecules, thus impeding the healing process. On the other hand, MPO contributes to the proteolytic misbalance in chronic wounds by activating the latent MMPs and inhibiting the TIMMPs. Therefore, sequestering the MPO by a simple absorption in the foams and its partial removal from the wound bed may be beneficial for wound healing.

The ability of the PUFs to reduce MPO activity in wound exudate was tested *ex vivo* with the exudate of a venous leg ulcer exudate (**Figure 43**). PUF-0, PUF-0.12%NP and Alskina® commercial dressing showed 83–92 % inhibition of MPO. Contrarily, PUF-0.20%NP and PUF-0.25%NP presented up to 44 % MPO inhibition. The PUFs with the highest MPO inhibition capacity were those that presented the highest swelling ratios. The results suggested that MPO may have been trapped inside the PUFs, thus reducing its activity in the wound exudate.

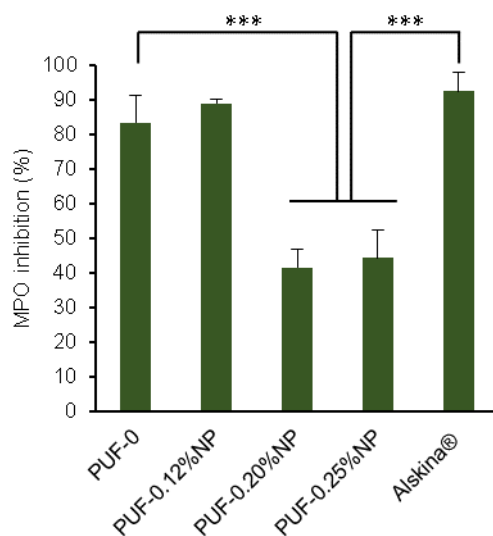


Figure 43. *Ex vivo* MPO inhibition (%) of the PUFs against MPO. The results are expressed in percentage of MPO inhibition relative to the baseline (samples without PUF). Results are reported as mean values \pm SD ($n=3$).

Cytotoxicity evaluation of the PUFs

Fibroblasts and keratinocytes play an essential role during the inflammatory phase in the cutaneous repair.²⁵¹ Fibroblasts synthesize collagen and promote the formation of ECM.²⁵² In chronic wounds, however, the proliferation of fibroblasts is considerably reduced.²⁵³ Hence, biocompatible wound dressing materials are required in order to reduce further damage on these cells. In this work, the AgPheLigNPs were synthesized following a safe-by-design approach employing a reducing agent, e. g. lignin, that also attenuated the toxicity of silver.⁹⁷ The potential cytotoxicity of the PUFs containing AgPheLigNPs was evaluated *in vitro* using human keratinocytes (HaCaT) and fibroblasts (BJ5ta) as cell models. The viability of keratinocytes and fibroblasts in contact with PUF-0 was 80 and 100 %, respectively (**Figure 44**). These low cytotoxicity levels did not vary when AgPheLigNPs were incorporated into the foams. Such low cytotoxicity may be attributed to the biocompatibility of lignin and to the low amount of Ag⁺ released over the studied period (below 1 % of the total silver content in 24 h).

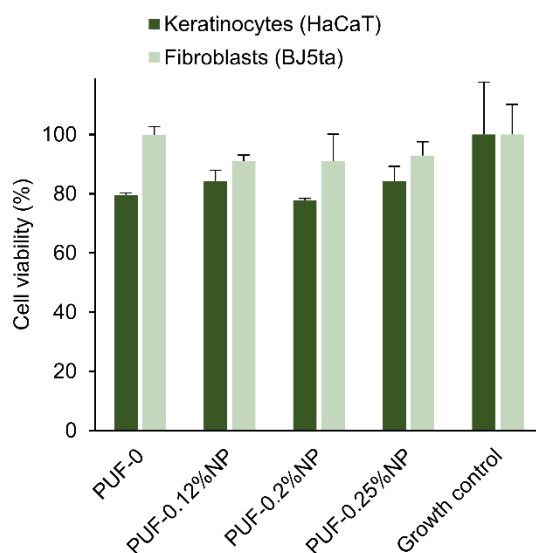


Figure 44. Cell viability (%) of human keratinocytes and fibroblasts exposed to PUFs for 24 h assessed by the AlamarBlue assay. Results are reported as mean values \pm SD (n=3).

Nano-enabled hydrogels self-assembled with phenolated lignin NPs

Synthesis of Self-assembling HA-SH/SF PheLigNPs hydrogels

Nano-enabled hydrogels were formed by self-assembling HA-SH, SF, and PheLigNPs. HA-SH and SF were chosen as hydrophilic polymers for the hydrogel's matrix, on account of their high solubility, molecular weight, functionality, and biocompatibility, while PheLigNPs served as gelation promoters and active agents. HA is an important component of the ECM, it is biocompatible and plays an important role in influencing cellular responses.²⁵⁴ On the other hand, SF, a natural structural protein derived from the silkworm, is an FDA-approved structural protein, safe in humans, and degradable that has been used in medical devices and for synthesizing mechanically robust materials,²⁵⁵ which is an essential requirement for materials used in the biomedical field.²⁵⁶ The crosslinking agents were lignin NPs enriched with natural phenolic compounds that have shown antioxidant and antibacterial properties and did not induce resistance in pathogenic bacterial strains (Chapter 1, *Results and Discussion*, section *Phenolated lignin nanoparticles*)

In order to increase the possible polymer-NP self-assembling interactions, HA was modified with ADH and Traut's reagent in a two-step process. The FTIR spectra of modified HA-ADH showed additional absorption at 1705 cm^{-1} (carbonyl group), and an increase in the amide I and amide II bands at 1648 cm^{-1} and 1550 cm^{-1} , respectively, from the coupled hydrazide molecule (**Figure 45**). The absorption peaks of HA at 1406 cm^{-1} corresponding to carboxylic groups decreased after modification with ADH, while the peak at 1376 cm^{-1} corresponding to carboxyl C=O stretching increased. The successful modification was also corroborated by TNBSA assay, with primary amines content of $159\pm 52\text{ mg ADH}\cdot\text{g}^{-1}$ sample. Finally, the HA-ADH was modified with Traut's reagent to produce HA-SH with a thiol content of $12.6\pm 0.5\text{ mg SH}\cdot\text{g}^{-1}$ sample.

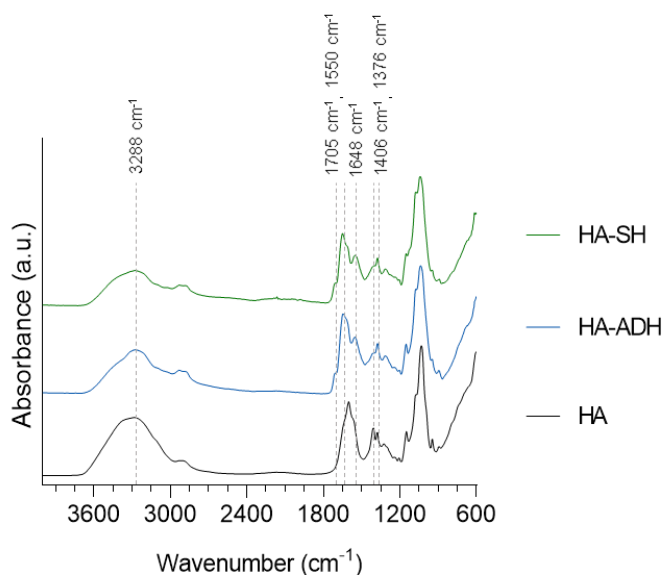


Figure 45. FTIR spectra of unmodified hyaluronic acid (HA), HA modified with adipic acid dihydrazide (HA-ADH) and thiolated HA (HA-SH).

The hydrogels were formed in an aqueous solution under environmental conditions, and gelation of the mixture was observed immediately after mixing the polymers with PheLigNPs. Because of the presence of catechol groups in lignin, many non-covalent interactions with HA-SH and SF are possible via hydrogen bonds, π - π , and thiol- π interactions^{257–259} forming a physically crosslinked network (**Figure 46a**). The strongest interactions in HA-SH are most likely between the cationic amino group from modified HA and with the phenolic groups from PheLigNPs (cation- π), whereas the strongest interaction in SF (5 % tyrosine content) is most likely between the tyrosine and the phenolic group of PheLigNPs (π - π).²⁶⁰ Even if the gelation occurred within seconds, the final mechanical properties of the gels were obtained after 2 h incubation at 37 °C. This suggests that the first interactions occurring in the gels are non-covalent bonds, but during incubation, spontaneous oxidation and covalent crosslinking of phenolic groups may also occur, as well as the formation of disulfide bonds from HA-SH. Apparently, mixing HA-SH with SF did not result in a gel, which confirmed the need for PheLigNPs to form the hydrogel network (**Figure 46b**).

CryoSEM images of the hydrogel showed a microporous structure with pore size of $\sim 3\text{--}4\ \mu\text{m}$, while the polymer mixture in the absence of PheLigNPs (control) presented larger pores ($\sim 10\ \mu\text{m}$) (**Figure 46c**). Such porous structure can improve the dispersibility and stability of PheLigNPs.¹¹¹ The decrease in pore size after the addition of PheLigNPs indicates a higher crosslinking degree in the hydrogel in comparison with the polymer mixture.^{9,261}

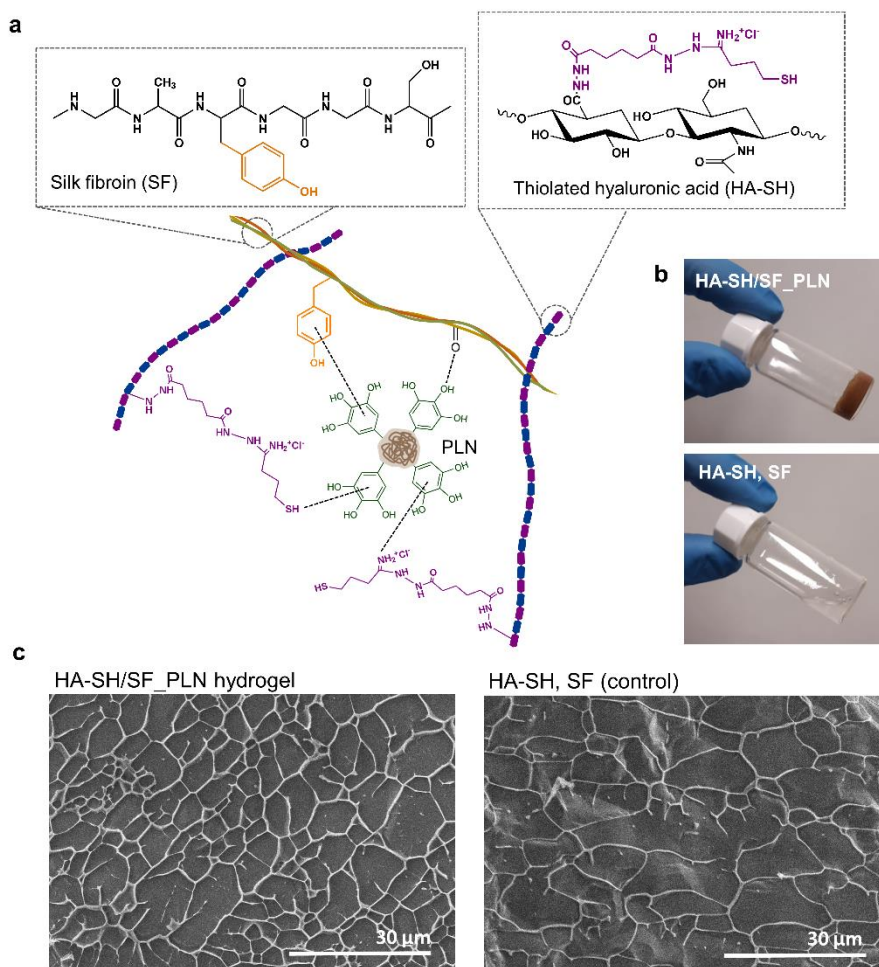


Figure 46. (a) Schematic representation of the non-covalent interactions forming the self-assembling HA-SH/SF_PheLigNPs hydrogel, (b) pictures of the gel obtained by mixing HA-SH, SF and PheLigNPs, and the non-gelating HA-SH and SF mixture, and (c) cryo-SEM images of the hydrogel (HA-SH/SF_PheLigNPs) and the control without PheLigNPs (mixture of HA-SH and SF).

Rheological properties of HA-SH/SF PheLigNPs hydrogels

The viscoelastic properties of the self-assembling hydrogels prepared with different concentrations of polymers and NPs were evaluated using a strain-dependent oscillatory test where the storage (G') and loss (G'') moduli in a range of increasing strains were recorded (**Figure 47a–b**). All the tested formulations presented higher G' values than G'' , confirming their gel-like behavior. The hydrogels presented a broad linear viscoelastic region since G' and G'' values were constant with varying deformation strains (0.1–100 %). The mechanical properties of the hydrogels clearly depended on the polymers and PheLigNPs concentration in the formulations. The gels formed with 20 and 10 mg·mL⁻¹ of PheLigNPs presented G' values of 102 and 78 Pa for hydrogels containing 1.5 % HA-SH and SF, and 67 and 35 in the case of 1.0 % hydrogels, respectively, which are at least 2-times higher than the gels formed with the lowest concentration of PheLigNPs (5 mg·mL⁻¹), suggesting a reinforced structure owing to an increased number of interactions between the polymers and the phenolic groups from PheLigNPs (Annex – **Table S4**).²⁶² The concentration of polymers also affected the storage and loss moduli of the gels. As expected, an increase in G' was observed at higher concentrations of HA-SH and SF, indicating that the hydrogels with 1.5 % of polymers were tougher than the ones prepared with 1.0 %.

For the rheological studies, $\tan \delta$, which is the ratio of the G'' over the G' ($\tan \delta = G''/G'$), and flow point, corresponding to the strain at which the sol-gel transition occurs ($G' = G''$), were used as a measure of the degree of crosslinking and elasticity in the nanocomposite hydrogels (Annex – **Table S4** and **Table S5**).²⁶² The flow point showed dependence on the PheLigNPs content. Increasing concentrations of PheLigNPs resulted in lower flow points, which can be related to a more structured material. Similarly, increasing the NPs concentration decrease the hydrogel elasticity, declining the $\tan \delta$ values from 0.212 to 0.124 for 1.0 % hydrogels and 0.195 to 0.145 for 1.5 % hydrogels. These results outlined the role of PheLigNPs as promoters for the gelation of HA-SH and SF where the NPs concentration results in a greater number of entanglements and

physical nodes enhancing the rheological properties of the nano-enabled hydrogel matrix.¹⁰⁵

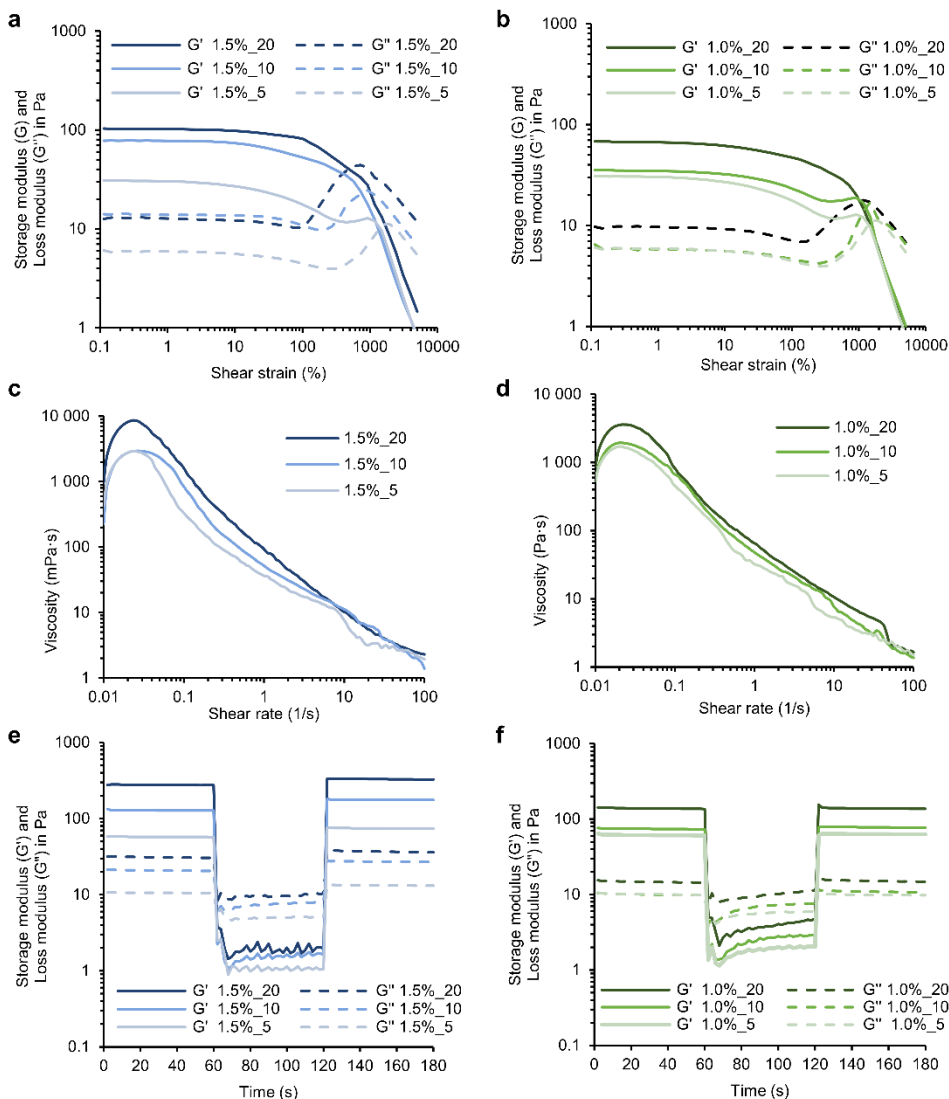


Figure 47. Rheological properties of the HA-SH/SF hydrogels. Strain-dependent oscillatory measurements were performed at 1 s^{-1} and increased shear strains of hydrogels prepared with (a) 1.5% or (b) 1.0% of polymers with varying PheLigNPs content. Viscosity vs. shear rate of hydrogels prepared with (c) 1.5% or (d) 1.0% of polymers, varying PheLigNPs content. 3iTT with intervals combining 5 and 2000% strains at 1 s^{-1} of hydrogels prepared with (e) 1.5% or (f) 1.0% of polymers with varying PheLigNPs content. All the tests were performed at $25 \text{ }^\circ\text{C}$ using a solvent trap. For simplification of the data interpretation, one representative sample per experimental group ($n = 3$) is shown.

Although mixing HA-SH and SF in the absence of PheLigNPs did not visually form a hydrogel (**Figure 46b**), the strain-dependent oscillatory test showed a G' higher than G'' (**Figure 48**). However, G' values were significantly lower than those obtained with the HA-SH/SF_PheLigNPs hydrogels (up to 13- and 14-fold lower for 1.0 and 1.5 % formulations, respectively), the viscoelastic region was narrower, and $\tan \delta$ was ~ 0.4 – 0.6 . This indicated that the PheLigNPs were the main responsible for hydrogel formation, although the interactions between HA-SH and SF also contributed to the hydrogel's structure.

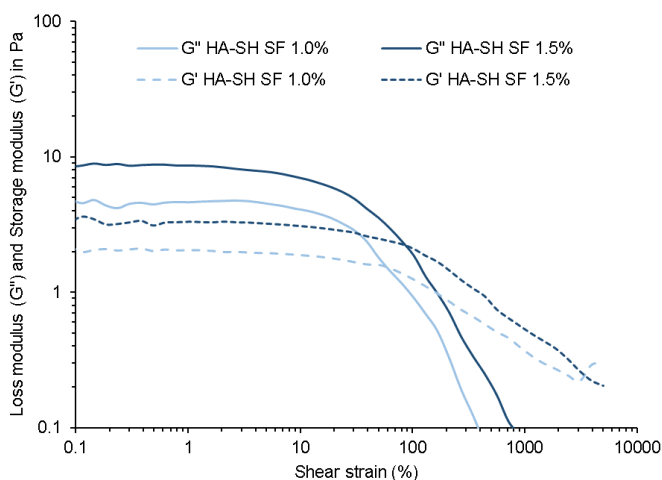


Figure 48. Strain-dependent oscillatory tests performed at 1 s^{-1} and $25 \text{ }^\circ\text{C}$ of mixtures containing a mixture of HA-SH and SF at 1.0 and 1.5 % after 2 h incubation at $37 \text{ }^\circ\text{C}$.

Due to the multiple possible reversible interactions proposed for these nano-enabled materials, such as cation- π , hydrogen bonds, thiol- π , and π - π interactions, the hydrogels are expected to possess shear-thinning properties. The viscosity of the hydrogels decreased upon increasing shear rates (**Figure 47c-d**), which confirmed their ability to flow on applied stress (e.g., injection through a syringe) which ensures their potential for minimally invasive delivery and conformal application. The concentration of PheLigNPs and polymers slightly affected the viscosity of the hydrogels. Concretely, increasing concentrations of PheLigNPs resulted in higher viscosity values, however,

varying the concentration of polymers did not result in significant viscosity changes (Annex – **Table S6**).

A critical parameter for the injectability of the gels is their recovery capacity after network rupture at high strains. Step-strain measurements were then performed by combining a low strain (5 %), and a high strain (2000 %) that allowed the network failure (**Figure 47e–f**), according to previously performed strain-dependent oscillatory tests (**Figure 47a–b**). After applying high strains, all the hydrogels recovered their initial G' and G'' values at low strains. This indicated that the hydrogels could recover to their initial properties after network rupture, which can be attributed to the reversible and robust nature of the non-covalently crosslinked hydrogel structure.

Swelling capacity

Appropriate swelling behavior of wound dressings would ensure the absorption of the excessive wound exudate while maintaining moisture, which is crucial for cell growth and proliferation.¹⁴² The swelling index of the different hydrogel formulations was studied (**Figure 49**) monitoring the weight variation after immersion in PBS at pH 7.4 and room temperature. A rapid increase in the swelling was observed during the first 8 h, followed by stabilization. As expected, the swelling depended on the concentration of PheLigNPs used to prepare the gels. The formulations with less amount of PheLigNPs (1.5%₅ and 1.0%₅) presented higher swelling, achieving values up to ~200 and ~120 % for hydrogels containing 1.5 and 1.0 % of biopolymers, respectively. This behavior was previously observed for hydrogels containing NPs²⁶³ and correlates with the rheological characterization of the gels where a higher degree of crosslinking was observed at increasing PheLigNPs content (**Figure 47a–b**). Indeed, a higher swelling index can be correlated to a weaker structure.²⁶⁴ The amount of HA-SH and SF in the hydrogel formulation also affected the swelling index, where at increasing polymer concentration and constant PheLigNPs content, a higher capacity to swell was observed. Higher swelling capacity upon increasing

concentrations of biopolymer has been previously reported.²⁶⁵ HA is a highly hydrophilic polymer capable of retaining large amounts of water and might be the main responsible for the high swelling capacity of the hydrogels.²⁶³ In short, the swelling capacity of these hydrogels can be tuned by varying the concentration of polymers (HA-SH, SF) and PheLigNPs.

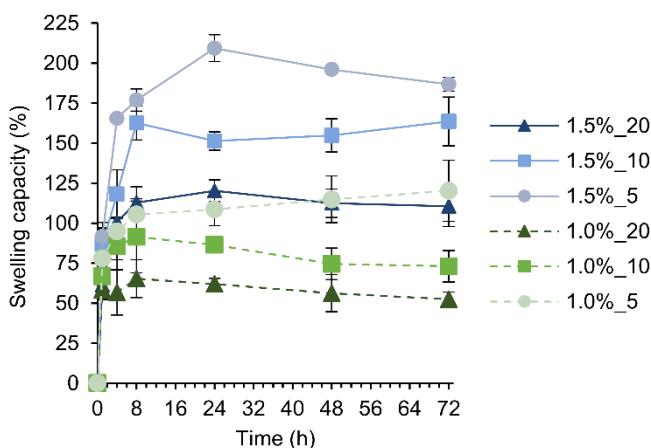


Figure 49. Swelling index (%) of hydrogels prepared with different concentrations of PheLigNPs and (a) 1.5% or (b) 1.0% of HA-SH and SF. Results are reported as mean values of swelling capacity (%) ($n=3$) \pm SD.

Stability of the hydrogels

The long-term stability of physically crosslinked hydrogels is challenging and limits their application in the medical field.^{256,263} Evaluation of hydrogel stability is crucial since the physical nature of crosslinking may cause uncontrolled leaching of NPs and degradation of polymeric matrix which may cause toxicity. After incubating the hydrogels in PBS for 7 days, a decrease in the dry mass was not observed (**Table 13**). One-way ANOVA test revealed that the dry mass of the hydrogels at days 1–7 was not significantly different from the initial mass. The results demonstrated the high long-term stability of the hydrogels. Achieving high stability in self-assembling hydrogels with non-covalent interactions is challenging. In the case of HA-SH/SF_PheLigNPs hydrogels, the combination of multiple interactions, i.e., π - π , thiol- π , and hydrogen bonding, might increase the

stability of the gels and reduce the possible degradation in physiological conditions. Moreover, covalent crosslinking with oxidized phenols from PheLigNPs and the polymers from the matrix may also occur, which would further increase the stability of the material.

Table 13 Stability of the hydrogels in PBS at 37 °C. Dry mass (mg) of samples 1.0%₁₀ at time 0, 1, 3 and 7 days, and statistical significance assessed using a multiple comparison one-way ANOVA test against time 0. Results are reported as the mean of five replicates \pm standard deviation (SD)

Time (days)	0	1	3	7
Dry mass (mg)	10.2 \pm 0.6	11.2 \pm 0.3	10.8 \pm 1.0	9.8 \pm 0.6
Statistical significance (One-way ANOVA)		ns ^a	ns	ns

^ans = not significant

Release of PheLigNPs and hydrogel stability in response to the pH and hyaluronidase

The pH of healthy skin ranges from 4.2 to 6.0.^{266,267} In acute wounds the pH oscillates during healing, often shifting from neutral to acidic with the regeneration of the epidermis. Contrarily, chronic wounds persist in an elevated alkaline environment (pH 7.2–8.9) that contributes in delayed healing.^{268,269} In order to guarantee the functionality of wound dressing materials, their properties need to be maintained when exposed to different physiological changes associated with pathologies, such as elevated pH. On the other hand, the alkaline pH of chronic wounds can be used as a trigger to release active agents from dressing materials, including growth factors,²⁷⁰ drug-loaded polymeric NPs,²⁷¹ antibiotics,²⁷² and other drugs.²⁷³ Controlled drug delivery systems enable the release of an active molecule under specific internal or external stimuli, which enhances the drug efficiency and avoids risks of overdosing.²⁷⁴

In this work, the behavior of the hydrogels at different pH was studied in terms of rheological stability and release of PheLigNPs as active agents. Strain-

dependent oscillatory tests showed that the hydrogels maintained the gel-like behavior ($G' > G''$) in all the tested pH (4.0–9.0) (**Figure 50a**). This confirms that the rheological properties of the hydrogels did not significantly vary after being exposed to acid, neutral and alkaline conditions. The hydrogels at neutral to basic pH (7, 8, and 9) displayed lower G'' in comparison with the reference (non-treated), while G' was maintained. Contrarily, G' of hydrogels at acid pH was lower, while G'' decreased. Differences in the flow point were observed with increasing alkalinity, raising from 917 % (reference) to 1170 %. Such increase could be correlated to a weaker structure in the hydrogel network.

The release rate and amount of PheLigNPs was clearly dependent on the pH since higher release rates with increasing pH values were observed (**Figure 50b**). A biphasic pattern characterized the release of PheLigNPs at alkaline and neutral pH, which consisted of an initial rapid release during the first 6 h and a slower sustained release phase. A similar profile with a significantly lower release rate resulted in acid pH. The higher release rates of PheLigNPs at alkaline pH coupled to the weaker structure of the hydrogels observed by rheology indicate that polymer-NP interactions are altered, which provokes changes in the hydrogel structure. Probably, at alkaline pH auto-oxidation of thiol and phenol groups occur, which weakens the polymer-NP interactions and facilitates PheLigNPs release. Moreover, the carboxylic groups from hyaluronic acid are ionized at alkaline pH, which increases the water uptake capacity and swelling, and facilitates the release of NPs.²⁷⁵ Despite PheLigNPs release and loss of some polymer-NP interactions, the hydrogels preserved their gel-like behavior. These results suggest that the hydrogels could be used as stimuli-responsive delivery materials triggered by the alkaline pH in chronic ulcers. Loading the PheLigNPs with specific active substances, such as growth factors or anti-inflammatory drugs, would provide additional functionalities to the NPs related to efficient wound healing.

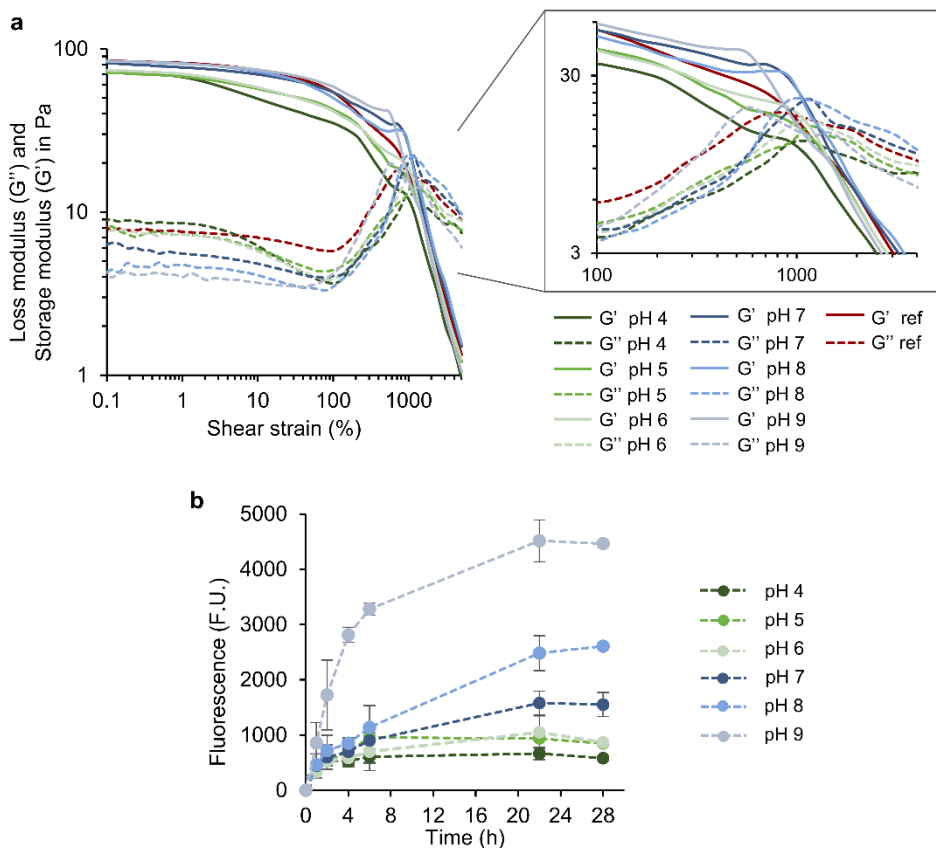


Figure 50. pH responsiveness of the hydrogels. (a) Rheological stability of the hydrogels after incubation at different pH measured using an oscillatory test (frequency 1 s^{-1} , shear strains 0.1–10000%). For simplification of the data interpretation, one representative sample per experimental group ($n=3$) is shown. (b) Release of PheLigNPs from the hydrogels incubated at different pH. Results are reported as mean fluorescence values ($n=3$) \pm SD.

The PheLigNPs release and biodegradability of the hydrogels in presence of hyaluronidase, a hydrolytic wound enzyme that degrades HA, was also studied (Table 14). The dry mass of the hydrogels after incubation with hyaluronidase did not present significant differences with that of reference hydrogel, indicating that the hydrolytic enzyme did not degrade the hydrogel. On the other hand, higher PheLigNPs release from the hydrogels was observed in the presence of hyaluronidase in comparison with the control group (treated with PBS). Probably, hyaluronidase weakens the hydrogel structure and facilitates the

release of PheLigNPs, but the presence of SF in the formulation enhances the stability of the hydrogel and delays the biodegradability.²⁷⁶

Table 14 Hydrogel stability and PheLigNPs release in response to hyaluronidase. The stability was reported as dry mass (mg) of the 1.0%₁₀ hydrogel at time 0 and 24 h with hyaluronidase or buffer, and the statistical significance was assessed using a multiple comparison one-way ANOVA test against time 0. PheLigNPs release is reported as fluorescence units (F.U.) measured in the supernatant. All results are reported as mean values (n = 4) ± SD.

Time (h)	0	24	
		Hyaluronidase	Buffer
Dry mass (mg)	8.4 ± 0.1	8.0 ± 0.5	8.6 ± 0.4
Dry mass statistical significant (One-way ANOVA)		ns ^a	ns
Fluorescence (F.U.)	0	3234 ± 497	1932 ± 375

^ans = not significant

Multiple features of the hydrogels for promoting wound healing

The presence of pathogenic and skin bacteria contributes to the non-healing state of a wound; thus an efficient management of bacterial load is essential to progress through healing. On the other hand, chronic wounds are characterized by elevated oxidative stress and high activity of MPO and MMPs. Specific control over deleterious wound enzymes and bacterial load would enhance the healing process.

The radical scavenging capacity of the hydrogels was assessed using the DPPH assay. All gel formulations were able to reduce the DPPH radical, confirming their antioxidant capacity (**Figure 51a**). According to the results, the antioxidant activity depended on the concentration of NPs, i.e. higher PheLigNPs yielded hydrogels with higher antioxidant capacity. The main antioxidant component of the formulations are PheLigNPs, which numerous phenolic groups provide the modified lignin with high antioxidant capacity.⁷³ Differences were also observed

varying the concentration of polymers. HA-SH could also contribute to the antioxidant capacity of the formulations.²⁷⁷

The capacity of the hydrogels to reduce the viability of bacteria was assessed using two common bacteria found in wounds, the Gram-positive *S. aureus* and the Gram-negative *P. aeruginosa* (**Figure 51b**). The viability of *S. aureus* was reduced by 95.87–99.72 %, with small differences between hydrogel formulations. The highest antibacterial formulations were those containing 1.0 % of polymers while varying the concentrations of PheLigNPs did not result in any trend. The lowest antibacterial capacity was found for 1.5%_20 hydrogel. In

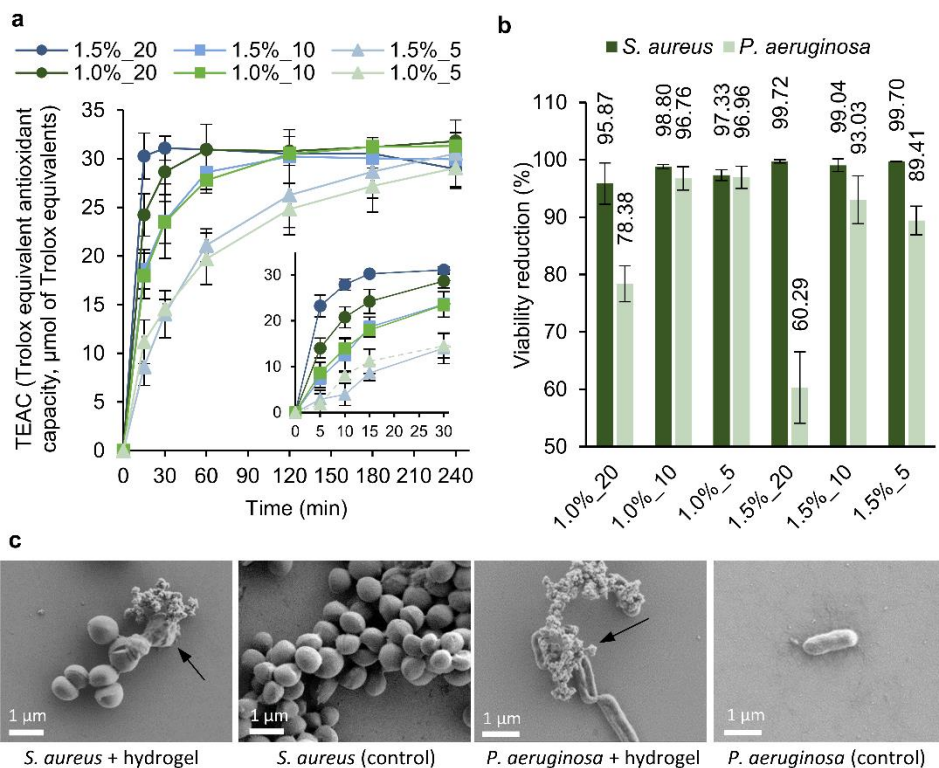


Figure 51. (a) Antioxidant activity of the hydrogels measured using the DPPH assay. Detail of the first 30 min of assay (inset). (b) Antibacterial capacity of the hydrogels against *S. aureus* and *P. aeruginosa* expressed as percent of viability reduction (%). Results are reported as mean values of bacterial viability reduction (%) (n=3) ± SD. (c) SEM images of *S. aureus* and *P. aeruginosa* treated with the hydrogels and respective controls (without treatment).

general, the effect on *P. aeruginosa* was lower, achieving values ranging from 60.29 to 96.96 %. The higher antibacterial activity of PheLigNPs against Gram-positive bacteria in comparison to Gram-negative ones was previously observed (Chapter 1, *Results and Discussion*, section *Phenolated lignin nanoparticles*). Contrary to what was expected, the gels containing the highest concentration of PheLigNPs (20 mg·mL⁻¹) exhibited notably lower antibacterial capacity against *P. aeruginosa* than those prepared with 10 and 5 mg·mL⁻¹. This difference can be attributed to the distinct swelling index of these hydrogels - higher swelling results in the absorption of bacteria into the hydrogel, which may contribute to the higher antibacterial effect. However, the released PheLigNPs to the medium are also expected to contribute to the antibacterial activity of the gels. The morphology of the bacterial cells treated with the hydrogels was evaluated by SEM (**Figure 51c**). After incubation with the hydrogels, some of the *S. aureus* cells presented irregular shapes and wrinkled surface that differed from the smooth and regular untreated *S. aureus*. Treated *P. aeruginosa* cells were flattened and presented depressed areas, whereas control cells were smooth and rounded. Structures formed of several particles were observed on the surface of the treated *S. aureus* and *P. aeruginosa*, which may correspond to PheLigNPs released from the hydrogels.

The advantage of using lignin as an antibacterial agent in biomedical applications is that it has unspecific and multiple antibacterial modes of action, and subsequently the surge of AMR can be avoided. In this line, PheLigNPs are suitable antibacterial agents for controlling bacterial load and avoiding bacterial infection in materials for wound healing, while preventing AMR appearance.

The deregulation of enzymes and other factors in chronic wounds results in excessive proteolytic activity that provokes ECM degradation and delays healing. Thus, the control over these enzymes, i.e. MPO and MMPs, would be crucial for effective chronic wound treatment. Phenolic groups are able to act as HClO scavengers or can be directly involved in the peroxidase cycle as substrates, thereby inhibiting the chlorination activity of the enzyme.²⁷⁸ Moreover, the

hydrogels' capacity to absorb fluids and proteins is also expected to diminish the activity of such enzymes in the wound bed. The capacity of the hydrogels of inhibiting the MPO and MMPs activities was assessed *in vitro* (**Figure 52**). All the formulations except for the 1.5%_5 hydrogel were capable of significantly reduce the enzymes' activities (by 20 to 52 %) as a function of the amount of PheLigNPs (Annex – **Table S7**). The most significant MPO inhibition capacity (~34 %) was achieved by the 1.5%_20 and 1.0%_20 hydrogels, independently of the amount of HA-SH and SF employed. The MPO inhibition by the gels can be attributed to the release of PheLigNPs or the absorption of the enzyme into the negatively charged hydrogel matrix following inhibition by the thiol and phenol groups in the polymeric matrix.^{105,279} A tendency was observed for MPO activity to decrease with increasing concentrations of PheLigNPs in the hydrogel's formulation, therefore, the reduced MPO activity is probably due to the action of released PheLigNPs. The same tendency was observed for MMPs inhibition, and the highest inhibition capacity was found for the 1.0%_20 hydrogel (52 % inhibition). The inhibition of MMPs activity is most likely due to the intermolecular interaction of MMPs with the polyphenolic PheLigNPs.^{216,259,280}

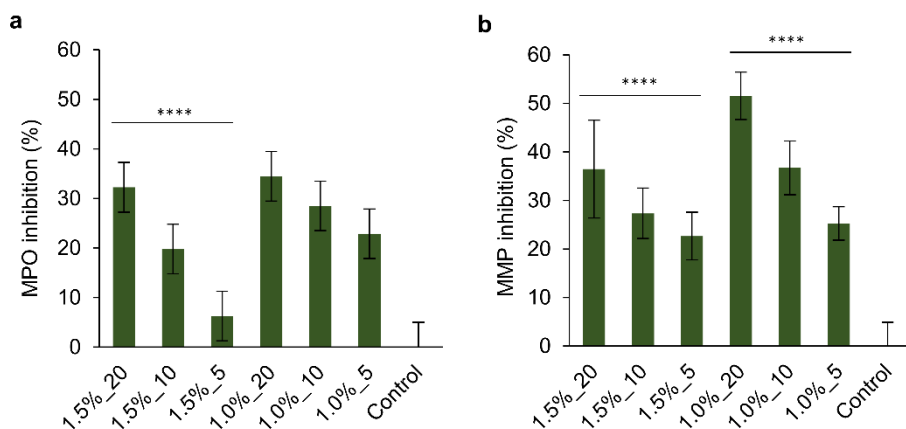


Figure 52. *In vitro* (a) MPO and (b) MMPs inhibition (%) by the hydrogels. Results are expressed in percentage of enzyme inhibition relative to the control (enzyme without hydrogel). Results are reported as mean values of enzyme inhibition (%) ($n=4$) \pm SD. A one-way ANOVA analysis was used to confirm the difference in MPO and MMPs inhibition capacity among the different hydrogel formulations.

Cytotoxicity evaluation of the hydrogels

In this study, the cell viability of human skin cells in contact with the hydrogels for 1 and 7 days was assessed. In chronic wounds, the proliferation of fibroblasts is significantly reduced in comparison with healing wounds, which deregulates tissue homeostasis and delays healing.²⁸¹ Materials used in the treatment of chronic wounds need to be biocompatible in order to minimize the loss of skin cells' function.²⁸² The hydrogels did not show cytotoxicity after 1 or 7 days in

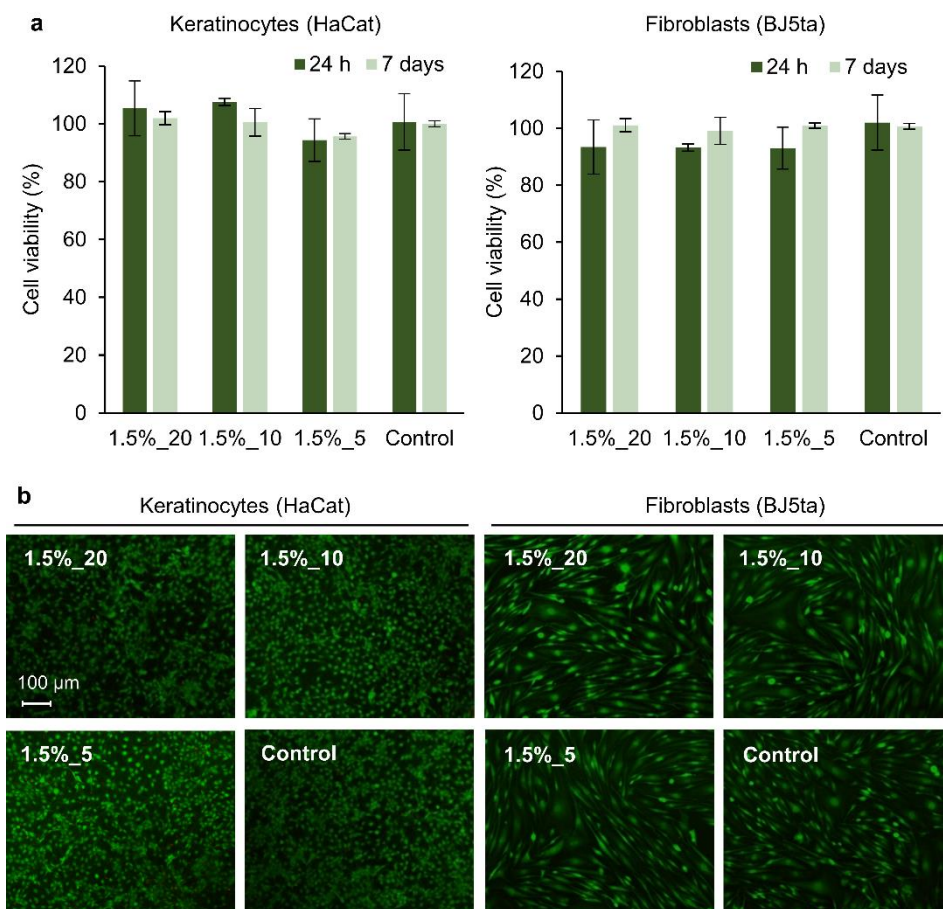


Figure 53. (a) Cell viability (%) of human keratinocytes and fibroblasts incubated with hydrogels (1.5%_20, 1.5%_10, and 1.5%_5) for 24 h assessed by the AlamarBlue assay. Results are reported as mean values of cell viability (%) \pm SD ($n=3$) and their statistical significance was calculated using one-way ANOVA ($p<0.05$). (b) Live/dead assay of human keratinocytes and fibroblasts treated with the hydrogels for 7 days. The assay stains the live cells in green and the dead ones in red.

contact with the cells, and the cell viability of keratinocytes and fibroblasts was no lower than 93 and 99 %, respectively (**Figure 53a**). Statistical analysis showed no significant differences between any of the samples ($p < 0.05$) This indicated that the materials potentially released from the hydrogels did not induce cytotoxicity. From the perspective of biocompatibility, the advantage of using metal-free PheLigNPs as the only crosslinking agent in the green synthesis of hydrogels is that toxic crosslinkers and catalysts are avoided. Live/dead staining further indicated the high viability of the cells incubated with the gels, and their morphology did not suffer changes in comparison with control cells (**Figure 53b**). The results suggested that the application of these hydrogels for the treatment of wounds may not imply biocompatibility concerns, however, *in vivo* studies should be performed previous to clinical application.

General discussion

General discussion

Nanoformulation of lignin in antibacterial materials is an emerging valorization approach for this underutilized biopolymer. Using lignin as a largely available renewable biomass material for the synthesis of antibacterial NPs reduces the environmental impact of these products. Moreover, avoiding the use of toxic solvents, chemical crosslinkers, or chemical reducing agents in the synthesis of nanomaterials minimizes both human toxicity and environmental hazard risks. In this thesis, different antibacterial lignin-based NPs and nanomaterials for biomedical applications were developed under a green chemistry concept. Pristine lignin or enzymatically phenolated lignin were used alone or as reducing agents of metal and metalloids to produce antibacterial AgPheLigNPs, TeLigNPs, and PheLigNPs through sonochemistry. Lignin was demonstrated to be a versatile polymer than can be either enzymatically modified or combined with metals and metalloids to enhance its antibacterial activity.

Lignin was the reducing agent of silver and tellurite ions in AgPheLigNPs and TeLigNPs, respectively. Lignin-mediated synthesis of AgNPs is possible due to the phenolic hydroxyl groups of the polymer, which are believed to interact with Ag^+ via cation–hydroxyl and cation– π bonding and reduce them into metallic AgNPs.^{111,132} Even if the reduction of tellurite by lignin has not been previously studied, this mechanism may also occur in the reduction of Te^{4+} to Te^0 .¹⁷⁸ In general, Ag^+ are more effective as antibacterial agents in comparison to AgNPs. However, once functionalized, AgNPs have shown superior antibacterial properties.²⁸³ The AgPheLigNPs described in this thesis presented a higher antibacterial effect than Ag^+ and AgNPs. Similarly, TeLigNPs were more antibacterial than their precursor (tellurite ion). These results revealed the improvement of the bactericidal properties due to the presence of lignin.

Despite the three lignin-based NPs presenting antibacterial properties, the ones containing Ag and Te showed significantly higher efficiency than those

prepared only with phenolated lignin. For instance, the MIC of AgPheLigNPs and TeLigNPs against *P. aeruginosa* was 5.4 ppb Ag and 2.39 ppm Te, respectively, while the MIC of PheLigNPs was 2.5 mg·mL⁻¹. As expected, the combination of lignin with metals and metalloids significantly enhances the antibacterial activity of the particles. Nevertheless, other properties should be considered for selecting the most convenient NP type such as the spectrum of susceptible bacteria, biocompatibility, biodegradability, and persistence in the environment and the human body. For instance, TeLigNPs were not active against *S. aureus* due to intrinsic resistance mechanisms against the tellurite ion, but were highly active against *E. coli*, presenting a MIC of 0.07 ppm Te. AgPheLigNPs were active against Gram-positive and Gram-negative bacteria even at low concentrations. However, concerns have been raised about the environmental persistence of AgNPs and their potential effects on human health.^{100,101} On the other hand, PheLigNPs did not show extraordinary antibacterial efficacy, but the absence of metals in this formulation reduces both environmental and health concerns, and enables their use in a broader range of applications such as additives for food packaging. Hence, the selection of an appropriate NP will depend on the desired antibacterial efficiency (bactericidal vs. bacteriostatic), the targeted bacteria, and the final application.

Despite the potential of these lignin-based NPs, lignin structure varies depending on the plant source and extraction method, which may hinder the production of NPs with homogeneous and reproducible properties. Another important aspect to consider is the sustainability of the production process. In this thesis, commercial lignin extracted from agricultural fibrous feedstock was used to synthesize the NPs. However, in order to minimize the impact of the process and drive towards a circular economy, it would be interesting to use residual lignin from the pulp and paper manufacturing industry as a raw material.

Besides the production of lignin based NPs, investigating the antibacterial mode of action of these particles was also an objective of the thesis. Acquiring a

comprehensive knowledge of how LigNPs inhibit the growth of microorganisms is crucial for developing effective antimicrobial composites for a broad range of applications. AgNPs exert their action against bacteria via different mechanisms, including (i) attachment to the bacterial cells, increasing their permeability,²⁸⁴ and (ii) the release of silver ions that penetrate into the bacteria and produce free radicals.^{285,286} The simultaneous action of AgNPs and the ions released leads to high levels of ROS, DNA damage, and cell death. Some studies report an improved antibacterial effect of lignin-capped AgNPs in comparison with non-capped AgNPs. Slavin *et al.* observed a 25-fold decrease in the MIC of AgLigNPs against MDR *S. aureus* in comparison with commercial AgNPs.⁷⁶ Such enhancement is attributed to the ability of lignin to interact and disturb bacterial membranes, hence facilitating the penetration of Ag⁺ ions inside the cell. Interestingly, such interaction was only found with bacterial model membranes, while no effect was observed in mammalian model membranes.¹⁹⁴ This proves the contribution of lignin to the reduction of silver toxicity, as described by previous works.^{102,287} The superior antibacterial properties of the AgPheLigNPs in comparison with Ag⁺ and AgNPs were also observed in the present study, since the concentration of silver needed to inhibit bacterial growth was reduced by at least 10-fold in the hybrid NPs.

The mechanism of action of TeNPs is not completely elucidated, but the generation of ROS is considered the main factor involved in their antibacterial activity.¹⁸⁰ Tellurite is extremely toxic for most Gram-negative bacteria as a result of generation of ROS, damage to metabolic enzymes, and glutathione depletion.²⁸⁸ TeLigNPs showed the capacity to induce ROS in *E. coli* and *P. aeruginosa*, but not in *S. aureus* or in mammalian cells. Moreover, TeLigNPs were capable of disturbing bacterial membranes, which may also contribute to their antibacterial action. In the case of PheLigNPs, besides the generation of ROS in bacteria, they also exhibited the capacity to strongly interact with bacterial surfaces and intercalate between the lipid membranes. The high affinity of lignin toward bacteria may explain the improvement of the antibacterial activity of

AgPheLigNPs and TeLigNPs in comparison with their precursors. Further studies on the penetration capacities of LigNPs inside bacterial cells would be useful to completely elucidate the mechanism of action of such particles.

The lignin-based NPs described in the first chapter of this thesis were used as active agents in materials for the treatment of chronic wounds. In particular, AgPheLigNPs were used as active fillers in polyurethane foams and PheLigNPs were used as active and structural elements in hydrogels. Considering the multiple factors involving wound chronicity, an advanced dressing should not only maintain the moisture, but also keep a bacteria-free environment and reduce the activity of deleterious wound enzymes.

PUF was chosen as wound dressing material for its resilience, flexibility, adaptability to different shapes and low cost.²⁸⁹ However, the majority of commercially available PUF dressings are inert or loaded with silver ions by absorption, which results in rapid release of Ag⁺ and short-term antibacterial effect.²⁹⁰ The AgPheLigNPs-loaded PUFs described in Chapter 2 of this thesis displayed high antibacterial capacity against two pathogenic bacteria commonly found in wounds, *S. aureus* and *P. aeruginosa*. Moreover, the foams presented a low and sustained release of silver over-time, which would diminish the toxic effects of silver and extends the antibacterial effect of the material. On the other hand, biopolymer hydrogels are biodegradable, present adaptability to different wounds, excellent ability to absorb fluids –which helps maintaining the moisture in the wound bed– and capacity to load active agents.²⁸⁹ The PheLigNPs described in Chapter 2 were the triggers for the gelation of thiolated HA and SF, and also conferred antibacterial and antioxidant properties to the material. The synthesis of hydrogels through self-assembling non covalent interactions between polymers and phenolic NPs¹⁰⁵ are currently in the process of patenting (Annex – Scientific contributions). Interestingly, the release of the active PheLigNPs was triggered by alkaline pH, which is the pH that most chronic wounds have.²⁶⁸ In both PUFs and hydrogels, the mechanical properties such as swelling capacity and density, as well as the antibacterial and antioxidant

properties, were controlled by particle content. This indicates that the materials' properties can be tuned by NPs content, making possible the design of the dressing as a function of the patients' need.

Despite the advantages of PUFs and hydrogels as dressing materials, their limitations should be also considered for selecting the appropriate dressing material. Polyurethane is a synthetic material requiring chemical catalysts and additives for its production, which can remain in the material and cause toxicity.²⁹¹ Moreover, the permeability of foams may result in excessive evaporation of moisture, so the addition of an occlusive layer is often necessary.²⁹² On the other hand, hydrogels can effectively retain moisture but their poor mechanical properties limit their application, so strategies such as addition of NPs reinforcement are needed.²⁹³ To improve hydrogels mechanical stability, they can be combined with other type of dressing materials, e.g., films and gauzes, that would enhance the mechanical properties of the dressing while maintaining hydrogel's properties. Both AgPheLigNPs and PheLigNPs showed promising suitability as active NPs in wound dressings, however, further studies on the materials' behavior during a prolonged period of time are needed to evaluate their potential in clinical practice.

AgPheLigNPs were not only used as antibacterial agents in PUFs for chronic wound management, but also in zirconia 3D-printed polymer-infiltrated ceramic networks.²⁹⁴ These materials containing AgPheLigNPs reduced the growth of *S. aureus* and *P. aeruginosa* in their surface by 90 and 73 %, respectively, in comparison with the pristine ceramic network. This work further demonstrates the versatility of lignin-based nanoparticles and their compatibility with multiple materials.

In order to bring the nanolignin-based materials to the market, their synthetic procedures should be simplified and upscaled, while maintaining low manufacturing costs. Overcoming the problem of lignins' intrinsic heterogeneity is a critical issue for obtaining reproducible materials. Despite studies showing

the advantages of highly antibacterial lignin materials for food and biomedical applications, safety data and clinical experience are required before their commercialization.²⁹⁵ Although lignin has been approved as a food additive by some regulatory bodies, its use in the form of NPs as a food contact substance (e.g., in food packaging) has not been regulated so far. In the case of lignin-based materials for wound healing, their classification in the proper medical device class is primordial for performing the appropriate clinical evaluation.²⁹⁶ Nevertheless, there is still a lack of specific regulatory guidance over nanomaterials in general and lignin-based materials, in particular, for biomedicine, which may hinder their entry into the market.^{297,298} It is thus important to focus future research on the physicochemical characteristics of nanoscale materials and understanding their interaction with biological systems, which is crucial for their approval by the regulatory bodies.

Overall, in this thesis, we highlighted the versatility of antibacterial LigNPs in terms of synthetic procedures, their multiple functionalities due to the nanoformulation, and their compatibility with different polymeric materials, demonstrating the enormous potential of these natural antibacterial agents.

Conclusions

Conclusions

In view of the tendency to move toward a circular economy model and sustainable processes, the use of renewable feedstock as an alternative to conventional petroleum-based sources has increased. LigNPs have raised interest in the scientific community for their sustainability, biodegradability, biocompatibility, and antibacterial capacity. The aim of this thesis was to engineer novel antibiotic-free, lignin-based NPs with antibacterial properties to be applied in the biomedical field. For this purpose, different hybrid LigNPs have been designed by combining this polymer with metals, metalloids, and natural phenolic compounds. Such particles were used as active and structural elements in materials for biomedical applications, especially for chronic wound treatment.

Antibacterial lignin-based nanoparticles

- Enzymatically synthesized phenolated lignin was used as a reducing and capping agent of silver to obtain AgPheLigNPs under high-intensity US
 - AgPheLigNPs were able to inhibit the growth of Gram-positive and negative bacteria at lower concentrations than Ag⁺ and AgNPs, which evidenced the enhancing effect of lignin.
 - The viability of human keratinocytes and fibroblasts was above 80 % for all the tested AgPheLigNPs concentrations, and the cell morphology incubated with the particles did not differ from the control cells. The presence of a biocompatible polymer surrounding the Ag core may contribute to decrease the toxicity of AgNPs and the released Ag⁺.
- Lignin was the reducing and capping agent of tellurium in the synthesis of TeLigNPs under high-intensity US
 - TeLigNPs completely inhibited the growth of *E. coli* and *P. aeruginosa* at a lower concentration than when using the tellurite salt, showing the advantages of the nanoformulation strategy. Moreover, the particles completely eradicated these bacteria within 4 h.

- Investigation of the antimicrobial mode of action revealed the capacity of TeLigNPs to induce a membrane-disturbing effect due to surface activity and the generation of ROS in the tested Gram-negative bacteria, but were not active against *S. aureus* or human cells.
- TeLigNPs did not induce cytotoxic effects or morphological changes to human cell lines, demonstrating that lignin can be used to develop safe-by-design tellurium-based nanomaterials.
- Plant-derived phenolic compounds were enzymatically grafted onto lignin and subjected to high-intensity US to obtain PheLigNPs
 - The antibacterial effect of PheLigNPs was demonstrated against *S. aureus*, *B. cereus*, *P. aeruginosa*, and *E. coli*. Both the higher phenolic content and the nanosize of the particles were responsible for the enhanced antibacterial effect of PheLigNPs in comparison with their nonfunctionalized or bulk counterparts (lignin, phenolated lignin, and LigNPs).
 - Studies on the antibacterial mode of action of PheLigNPs demonstrated the bacterial surface–particle interaction and membrane destabilization, coupled with increased levels of ROS, and reduced metabolic activity.
 - Bacteria in contact with PheLigNPs did not induce resistance, probably due to the multiple and unspecific targets, hence contributing to overcoming the growing concern of multidrug-resistant bacteria.

Lignin-based nanoparticles in composite materials for wound healing

- Antibacterial PUFs with potential for wound dressings were obtained by using AgPheLigNPs as active fillers.
 - The foams presented an open-cell structure where the cell diameter decreased with the increase of the AgPheLigNPs content. Their

swelling capacity, density, and mechanical properties can be tuned as a function of AgPLigNPs concentration.

- The PUFs containing AgPheLigNPs demonstrated sustained silver release over time, and eradicated up to 4 and 5 logs the medically relevant *S. aureus* and *P. aeruginosa*, respectively. Moreover, the foams were antioxidant and capable of inhibiting the activity of the deleterious oxidative wound enzyme myeloperoxidase.
- The PUFs did not show cytotoxicity to human keratinocytes and fibroblasts.
- Hydrogels were synthesized by combining HA-SH and SF as polymer matrix, and PheLigNPs as active NPs and gelation promoters.
 - The pore size of the polymer matrix was reduced after the addition of PheLigNPs, evidencing the crosslinking between the polymers and the NPs. This would allow an accurate control of the hydrogels' properties (e.g., swelling).
 - Rheological studies demonstrated that PheLigNPs were the primary cause of gelation. Depending on the PheLigNPs amount in the formulation, it was possible to obtain hydrogels with different rheological performances and swelling capacities to suit the final application.
 - The non-covalent reversible polymer-NP interactions provided the hydrogels with injectability and rapid self-healing properties without compromising the stability of the gels, which ensures their adaptability to complex wound architectures and recovery after subjecting to mechanical stress (bend, shear etc.).
 - The release of active PheLigNPs was triggered in chronic wounds with alkaline pHs, while the mechanical properties of the hydrogels at this pH were not compromised.

- The viability of *S. aureus* and *P. aeruginosa* was reduced by the gels up to 99.7 % and 99.0 %, respectively. Moreover, the gels presented high antioxidant capacity.
- In addition, the hydrogels demonstrated the ability to control the activity of deleterious wound enzymes (MPO and MMPs) as a function of PheLigNPs content, which is favorable for wound healing.
- The absence of cytotoxicity in fibroblasts and keratinocytes suggests that the hydrogels could be used as materials for the treatment of chronic wounds.

Bibliography

Bibliography

- (1) Hu, B.; Wang, K.; Wu, L.; Yu, S. H.; Antonietti, M.; Titirici, M. M. Engineering Carbon Materials from the Hydrothermal Carbonization Process of Biomass. *Adv. Mater.* **2010**, *22* (7), 813–828. <https://doi.org/10.1002/adma.200902812>.
- (2) Vanneste, J.; Ennaert, T.; Vanhulsel, A.; Sels, B. Unconventional Pretreatment of Lignocellulose with Low-Temperature Plasma. *ChemSusChem* **2017**, *10* (1), 14–31. <https://doi.org/10.1002/cssc.201601381>.
- (3) Ragauskas, A. J.; Beckham, G. T.; Bidy, M. J.; Chandra, R.; Chen, F.; Davis, M. F.; Davison, B. H.; Dixon, R. A.; Gilna, P.; Keller, M.; et al. Lignin Valorization: Improving Lignin Processing in the Biorefinery. *Science (80-.)*. **2014**, *344* (6185), 1246843. <https://doi.org/10.1126/science.1246843>.
- (4) Koch, G. Raw Material for Pulp. In *Handbook of Pulp*; John Wiley & Sons, Ltd, 2008; Vol. 1, pp 21–68. <https://doi.org/10.1002/9783527619887.ch2>.
- (5) Mansouri, N. E. El; Salvadó, J. Structural Characterization of Technical Lignins for the Production of Adhesives: Application to Lignosulfonate, Kraft, Soda-Anthraquinone, Organosolv and Ethanol Process Lignins. *Ind. Crops Prod.* **2006**, *24* (1), 8–16. <https://doi.org/10.1016/j.indcrop.2005.10.002>.
- (6) Upton, B. M.; Kasko, A. M. Strategies for the Conversion of Lignin to High-Value Polymeric Materials: Review and Perspective. *Chem. Rev.* **2016**, *116* (4), 2275–2306. <https://doi.org/10.1021/acs.chemrev.5b00345>.
- (7) Grossman, A.; Wilfred, V. Lignin-Based Polymers and Nanomaterials. *Curr. Opin. Biotechnol.* **2019**, *56*, 112–120. <https://doi.org/10.1016/j.copbio.2018.10.009>.
- (8) Zhang, Z.; Terrasson, V.; Guénin, E. Lignin Nanoparticles and Their Nanocomposites. *Nanomaterials* **2021**, *11* (5), 1336. <https://doi.org/10.3390/nano11051336>.
- (9) Del Saz-Orozco, B.; Oliet, M.; Alonso, M. V; Rojo, E.; Rodríguez, F. Formulation Optimization of Unreinforced and Lignin Nanoparticle-Reinforced Phenolic Foams Using an Analysis of Variance Approach. *Compos. Sci. Technol.* **2012**, *72* (6), 667–674. <https://doi.org/10.1016/j.compscitech.2012.01.013>.
- (10) Mishra, P. K.; Wimmer, R. Aerosol Assisted Self-Assembly as a Route to Synthesize Solid and Hollow Spherical Lignin Colloids and Its Utilization in Layer by Layer Deposition. *Ultrason. Sonochem.* **2017**, *35*, 45–50. <https://doi.org/10.1016/j.ultsonch.2016.09.001>.
- (11) Cavallo, E.; He, X.; Luzi, F.; Dominici, F.; Cerrutti, P.; Bernal, C.; Foresti, M. L.; Torre, L.; Puglia, D. UV Protective, Antioxidant, Antibacterial and Compostable Polylactic Acid Composites Containing Pristine and Chemically Modified Lignin Nanoparticles. *Molecules* **2020**, *26* (1), 126. <https://doi.org/10.3390/molecules26010126>.
- (12) Tortora, M.; Cavalieri, F.; Mosesso, P.; Ciaffardini, F.; Melone, F.; Crestini, C. Ultrasound Driven Assembly of Lignin into Microcapsules for Storage and Delivery of Hydrophobic Molecules. *Biomacromolecules* **2014**, *15* (5), 1634–1643. <https://doi.org/10.1021/bm500015j>.
- (13) Shu, F.; Jiang, B.; Yuan, Y.; Li, M.; Wu, W.; Jin, Y.; Xiao, H. Biological Activities and Emerging Roles of Lignin and Lignin-Based Products-A Review.

- Biomacromolecules* **2021**, *22* (12), 4905–4918. <https://doi.org/10.1021/acs.biomac.1c00805>.
- (14) Ndaba, B.; Roopnarain, A.; Daramola, M. O.; Adeleke, R. Influence of Extraction Methods on Antimicrobial Activities of Lignin-Based Materials: A Review. *Sustain. Chem. Pharm.* **2020**, *18*, 100342. <https://doi.org/10.1016/j.scp.2020.100342>.
- (15) Sugiarto, S.; Leow, Y.; Tan, C. L.; Wang, G.; Kai, D. How Far Is Lignin from Being a Biomedical Material? *Bioact. Mater.* **2022**, *8*, 71–94. <https://doi.org/10.1016/j.bioactmat.2021.06.023>.
- (16) Duarah, P.; Haldar, D.; Purkait, M. K. Technological Advancement in the Synthesis and Applications of Lignin-Based Nanoparticles Derived from Agro-Industrial Waste Residues: A Review. *Int. J. Biol. Macromol.* **2020**, *163*, 1828. <https://doi.org/10.1016/j.ijbiomac.2020.09.076>.
- (17) Tang, Q.; Qian, Y.; Yang, D.; Qiu, X.; Qin, Y.; Zhou, M. Lignin-Based Nanoparticles: A Review on Their Preparations and Applications. *Polymers (Basel)*. **2020**, *12* (11), 1–22. <https://doi.org/10.3390/polym12112471>.
- (18) Hussin, M. H.; Appaturi, J. N.; Poh, N. E.; Latif, N. H. A.; Brosse, N.; Ziegler-Devin, I.; Vahabi, H.; Syamani, F. A.; Fatriasari, W.; Solihat, N. N.; et al. A Recent Advancement on Preparation, Characterization and Application of Nanolignin. *Int. J. Biol. Macromol.* **2022**, *200* (1), 303–326. <https://doi.org/10.1016/j.ijbiomac.2022.01.007>.
- (19) Beisl, S.; Miltner, A.; Friedl, A. Lignin from Micro- to Nanosize: Production Methods. *Int. J. Mol. Sci.* **2017**, *18* (6), 1244. <https://doi.org/10.3390/ijms18061244>.
- (20) Iravani, S.; Varma, R. S. Greener Synthesis of Lignin Nanoparticles and Their Applications. *Green Chem.* **2020**, *22* (3), 612–636. <https://doi.org/10.1039/c9gc02835h>.
- (21) Mishra, P. K.; Ekielski, A. The Self-Assembly of Lignin and Its Application in Nanoparticle Synthesis: A Short Review. *Nanomaterials* **2019**, *9* (2), 243. <https://doi.org/10.3390/nano9020243>.
- (22) Schneider, W. D. H.; Dillon, A. J. P.; Camassola, M. Lignin Nanoparticles Enter the Scene: A Promising Versatile Green Tool for Multiple Applications. *Biotechnol. Adv.* **2021**, *47*, 107685. <https://doi.org/10.1016/j.biotechadv.2020.107685>.
- (23) Sipponen, M. H.; Lange, H.; Crestini, C.; Henn, A.; Österberg, M. Lignin for Nano- and Microscaled Carrier Systems: Applications, Trends, and Challenges. *ChemSusChem* **2019**, *12* (10), 2039. <https://doi.org/10.1002/cssc.201900480>.
- (24) Chen, K.; Wang, S.; Qi, Y.; Guo, H.; Guo, Y.; Li, H. State-of-the-Art: Applications and Industrialization of Lignin Micro/Nano Particles. *ChemSusChem* **2021**, *14* (5), 1284. <https://doi.org/10.1002/cssc.202002441>.
- (25) Piccinino, D.; Capecchi, E.; Tomaino, E.; Gabellone, S.; Gigli, V.; Avitabile, D.; Saladino, R. Nano-structured Lignin as Green Antioxidant and Uv Shielding Ingredient for Sunscreen Applications. *Antioxidants* **2021**, *10* (2), 274. <https://doi.org/10.3390/antiox10020274>.
- (26) Beisl, S.; Friedl, A.; Miltner, A. Lignin from Micro- to Nanosize: Applications. *Int. J. Mol. Sci.* **2017**, *18* (11), 2367. <https://doi.org/10.3390/ijms18112367>.
- (27) Lizundia, E.; Sipponen, M. H.; Greca, L. G.; Balakshin, M.; Tardy, B. L.; Rojas, O.

- J.; Puglia, D. Multifunctional Lignin-Based Nanocomposites and Nanohybrids. *Green Chem.* **2021**, *23* (18), 6698–6760. <https://doi.org/10.1039/d1gc01684a>.
- (28) Barros, J.; Serk, H.; Granlund, I.; Pesquet, E. The Cell Biology of Lignification in Higher Plants. *Ann. Bot.* **2015**, *115* (7), 1053–1074. <https://doi.org/10.1093/aob/mcv046>.
- (29) Ruiz-Dueñas, F. J.; Martínez, Á. T. Microbial Degradation of Lignin: How a Bulky Recalcitrant Polymer Is Efficiently Recycled in Nature and How We Can Take Advantage of This. *Microb. Biotechnol.* **2009**, *2* (2), 164–177. <https://doi.org/10.1111/j.1751-7915.2008.00078.x>.
- (30) Lee, M.; Jeon, H. S.; Kim, S. H.; Chung, J. H.; Roppolo, D.; Lee, H.-J.; Cho, H. J.; Tobimatsu, Y.; Ralph, J.; Park, O. K. Lignin-based Barrier Restricts Pathogens to the Infection Site and Confers Resistance in Plants. *EMBO J.* **2019**, *38* (23), e101948. <https://doi.org/10.15252/embj.2019101948>.
- (31) Calvo-Flores, F. G.; Dobado, J. A.; Isac-García, J.; Martín-Martínez, F. J. Structure and Physicochemical Properties. In *Lignin and Lignans as Renewable Raw Materials*; John Wiley & Sons, Ltd, 2015; pp 9–48. <https://doi.org/10.1002/9781118682784.ch2>.
- (32) Capanema, E.; Balakshin, M.; Katahira, R.; Chang, H. M.; Jameel, H. How Well Do MWL and CEL Preparations Represent the Whole Hardwood Lignin? *J. Wood Chem. Technol.* **2014**, *35* (1), 17–26. <https://doi.org/10.1080/02773813.2014.892993>.
- (33) Stark, N. M.; Yelle, D. J.; Agarwal, U. P. Techniques for Characterizing Lignin. In *Lignin in Polymer Composites*; Elsevier Inc., 2016; pp 49–66. <https://doi.org/10.1016/B978-0-323-35565-0.00004-7>.
- (34) Lu, Y.; Lu, Y. C.; Hu, H. Q.; Xie, F. J.; Wei, X. Y.; Fan, X. Structural Characterization of Lignin and Its Degradation Products with Spectroscopic Methods. *J. Spectrosc.* **2017**, *2017*, 1–15. <https://doi.org/10.1155/2017/8951658>.
- (35) Boerjan, W.; Ralph, J.; Baucher, M. Lignin Biosynthesis. *Annu. Rev. Plant Biol.* **2003**, *54*, 519–546. <https://doi.org/10.1146/annurev.arplant.54.031902.134938>.
- (36) Katahira, R.; Elder, T. J.; Beckham, G. T. Chapter 1: A Brief Introduction to Lignin Structure. In *RSC Energy and Environment Series*; 2018; Vol. 2018-Janua, pp 1–20. <https://doi.org/10.1039/9781788010351-00001>.
- (37) Laurichesse, S.; Avérous, L. Chemical Modification of Lignins: Towards Biobased Polymers. *Prog. Polym. Sci.* **2014**, *39* (7), 1266–1290. <https://doi.org/10.1016/j.progpolymsci.2013.11.004>.
- (38) Vanholme, R.; Demedts, B.; Morreel, K.; Ralph, J.; Boerjan, W. Lignin Biosynthesis and Structure. *Plant Physiol.* **2010**, *153* (3), 895–905. <https://doi.org/10.1104/pp.110.155119>.
- (39) Anderson, E. M.; Stone, M. L.; Katahira, R.; Reed, M.; Muchero, W.; Ramirez, K. J.; Beckham, G. T.; Román-Leshkov, Y. Differences in S/G Ratio in Natural Poplar Variants Do Not Predict Catalytic Depolymerization Monomer Yields. *Nat. Commun.* **2019**, *10* (1), 2033. <https://doi.org/10.1038/s41467-019-09986-1>.
- (40) Lange, H.; Decina, S.; Crestini, C. Oxidative Upgrade of Lignin - Recent Routes Reviewed. *Eur. Polym. J.* **2013**, *49* (6), 1151–1173. <https://doi.org/10.1016/j.eurpolymj.2013.03.002>.

- (41) Chung, H.; Washburn, N. R. Extraction and Types of Lignin. In *Lignin in Polymer Composites*; Elsevier Inc., 2016; pp 13–25. <https://doi.org/10.1016/B978-0-323-35565-0.00002-3>.
- (42) Crestini, C.; Lange, H.; Sette, M.; Argyropoulos, D. S. On the Structure of Softwood Kraft Lignin. *Green Chem.* **2017**, *19* (17), 4104–4121. <https://doi.org/10.1039/c7gc01812f>.
- (43) Aro, T.; Fatehi, P. Production and Application of Lignosulfonates and Sulfonated Lignin. *ChemSusChem* **2017**, *10* (9), 1861–1877. <https://doi.org/10.1002/cssc.201700082>.
- (44) Lobato-Peralta, D. R.; Duque-Brito, E.; Villafán-Vidales, H. I.; Longoria, A.; Sebastian, P. J.; Cuentas-Gallegos, A. K.; Arancibia-Bulnes, C. A.; Okoye, P. U. A Review on Trends in Lignin Extraction and Valorization of Lignocellulosic Biomass for Energy Applications. *J. Clean. Prod.* **2021**, *293*, 126123. <https://doi.org/10.1016/j.jclepro.2021.126123>.
- (45) Fernandes, C.; Melro, E.; Magalhães, S.; Alves, L.; Craveiro, R.; Filipe, A.; Valente, A. J. M.; Martins, G.; Antunes, F. E.; Romano, A.; et al. New Deep Eutectic Solvent Assisted Extraction of Highly Pure Lignin from Maritime Pine Sawdust (*Pinus Pinaster* Ait.). *Int. J. Biol. Macromol.* **2021**, *177*, 294–305. <https://doi.org/10.1016/j.ijbiomac.2021.02.088>.
- (46) Owhe, E. O.; Kumar, N.; Lynam, J. G. Lignin Extraction from Waste Biomass with Deep Eutectic Solvents: Molecular Weight and Heating Value. *Biocatal. Agric. Biotechnol.* **2021**, *32*, 1878–18181. <https://doi.org/10.1016/j.bcab.2021.101949>.
- (47) Chen, Z.; Ragauskas, A.; Wan, C. Lignin Extraction and Upgrading Using Deep Eutectic Solvents. *Ind. Crops Prod.* **2020**, *147*, 112241. <https://doi.org/10.1016/j.indcrop.2020.112241>.
- (48) Ahmed, M. A.; Lee, J. H.; Raja, A. A.; Choi, J. W. Effects of Gamma-Valerolactone Assisted Fractionation of Ball-Milled Pine Wood on Lignin Extraction and Its Characterization Aswell as Its Corresponding Cellulose Digestion. *Appl. Sci.* **2020**, *10* (5), 1599. <https://doi.org/10.3390/app10051599>.
- (49) Jampa, S.; Puente-Urbina, A.; Ma, Z.; Wongkasemjit, S.; Luterbacher, J. S.; Van Bokhoven, J. A. Optimization of Lignin Extraction from Pine Wood for Fast Pyrolysis by Using a γ -Valerolactone-Based Binary Solvent System. *ACS Sustain. Chem. Eng.* **2019**, *7* (4), 4058–4068. <https://doi.org/10.1021/acssuschemeng.8b05498>.
- (50) Shen, X. J.; Wen, J. L.; Mei, Q. Q.; Chen, X.; Sun, D.; Yuan, T. Q.; Sun, R. C. Facile Fractionation of Lignocelluloses by Biomass-Derived Deep Eutectic Solvent (DES) Pretreatment for Cellulose Enzymatic Hydrolysis and Lignin Valorization. *Green Chem.* **2019**, *21* (2), 275–283. <https://doi.org/10.1039/c8gc03064b>.
- (51) Lê, H. Q.; Pokki, J. P.; Borrega, M.; Uusi-Kyyny, P.; Alopaeus, V.; Sixta, H. Chemical Recovery of γ -Valerolactone/Water Biorefinery. *Ind. Eng. Chem. Res.* **2018**, *57* (44), 15147–15158. <https://doi.org/10.1021/acs.iecr.8b03723>.
- (52) Radotić, K.; Mičić, M. Methods for Extraction and Purification of Lignin and Cellulose from Plant Tissues. In *Sample Preparation Techniques for Soil, Plant, and Animal Samples*; Humana Press, New York, NY, 2016; pp 365–376. https://doi.org/10.1007/978-1-4939-3185-9_26.
- (53) Wang, G.; Xia, Y.; Liang, B.; Sui, W.; Si, C. Successive Ethanol–Water

- Fractionation of Enzymatic Hydrolysis Lignin to Concentrate Its Antimicrobial Activity. *J. Chem. Technol. Biotechnol.* **2018**, 93 (10), 2977–2987. <https://doi.org/10.1002/jctb.5656>.
- (54) Arakawa, H.; Maeda, M.; Okubo, S.; Shimamura, T. Role of Hydrogen Peroxide in Bactericidal Action of Catechin. *Biol. Pharm. Bull.* **2004**, 27 (3), 277–281. <https://doi.org/10.1248/bpb.27.277>.
- (55) Cushnie, T. P. T.; Lamb, A. J. Recent Advances in Understanding the Antibacterial Properties of Flavonoids. *Int. J. Antimicrob. Agents* **2011**, 38 (2), 99–107. <https://doi.org/10.1016/j.ijantimicag.2011.02.014>.
- (56) Bouarab-Chibane, L.; Forquet, V.; Lantéri, P.; Clément, Y.; Léonard-Akkari, L.; Oulahal, N.; Degraeve, P.; Bordes, C. Antibacterial Properties of Polyphenols: Characterization and QSAR (Quantitative Structure-Activity Relationship) Models. *Front. Microbiol.* **2019**, 10 (APR), 829. <https://doi.org/10.3389/fmicb.2019.00829>.
- (57) Xu, Y. H.; Zeng, P.; Li, M. F.; Bian, J.; Peng, F. γ -Valerolactone/Water System for Lignin Fractionation to Enhance Antibacterial and Antioxidant Capacities. *Sep. Purif. Technol.* **2021**, 279, 1383–5866. <https://doi.org/10.1016/j.seppur.2021.119780>.
- (58) Zeb, A. Concept, Mechanism, and Applications of Phenolic Antioxidants in Foods. *J. Food Biochem.* **2020**, 44 (9), e13394. <https://doi.org/10.1111/jfbc.13394>.
- (59) Espinoza-Acosta, J. L.; Torres-Chávez, P. I.; Ramírez-Wong, B.; López-Saiz, C. M.; Montaña-Leyva, B. Antioxidant, Antimicrobial, and Antimutagenic Properties of Technical Lignins and Their Applications. *BioResources* **2016**, 11 (2), 5452–5481. https://doi.org/10.15376/biores.11.2.Espinoza_Acosta.
- (60) Wang, B.; Sun, D.; Wang, H. M.; Yuan, T. Q.; Sun, R. C. Green and Facile Preparation of Regular Lignin Nanoparticles with High Yield and Their Natural Broad-Spectrum Sunscreens. *ACS Sustain. Chem. Eng.* **2019**, 7 (2), 2658–2666. <https://doi.org/10.1021/acssuschemeng.8b05735>.
- (61) Qian, Y.; Zhong, X.; Li, Y.; Qiu, X. Fabrication of Uniform Lignin Colloidal Spheres for Developing Natural Broad-Spectrum Sunscreens with High Sun Protection Factor. *Ind. Crops Prod.* **2017**, 101, 54–60. <https://doi.org/10.1016/j.indcrop.2017.03.001>.
- (62) Frangville, C.; Rutkevičius, M.; Richter, A. P.; Velez, O. D.; Stoyanov, S. D.; Paunov, V. N. Fabrication of Environmentally Biodegradable Lignin Nanoparticles. *ChemPhysChem* **2012**, 13 (18), 4235–4243. <https://doi.org/10.1002/cphc.201200537>.
- (63) Gilca, I. A.; Popa, V. I.; Crestini, C. Obtaining Lignin Nanoparticles by Sonication. *Ultrason. Sonochem.* **2015**, 23, 369–375. <https://doi.org/10.1016/j.ultsonch.2014.08.021>.
- (64) Freitas, F. M. C.; Cerqueira, M. A.; Gonçalves, C.; Azinheiro, S.; Garrido-Maestu, A.; Vicente, A. A.; Pastrana, L. M.; Teixeira, J. A.; Michelin, M. Green Synthesis of Lignin Nano- and Micro-Particles: Physicochemical Characterization, Bioactive Properties and Cytotoxicity Assessment. *Int. J. Biol. Macromol.* **2020**, 163, 1798–1809. <https://doi.org/10.1016/j.ijbiomac.2020.09.110>.
- (65) Paul, S.; Thakur, N. S.; Chandna, S.; Reddy, Y. N.; Bhaumik, J. Development of a Light Activatable Lignin Nanosphere Based Spray Coating for Bioimaging and Antimicrobial Photodynamic Therapy. *J. Mater. Chem. B* **2021**, 9 (6), 1592–

1603. <https://doi.org/10.1039/d0tb02643c>.
- (66) Moradipour, M.; Chase, E. K.; Khan, M. A.; Asare, S. O.; Lynn, B. C.; Rankin, S. E.; Knutson, B. L. Interaction of Lignin-Derived Dimer and Eugenol-Functionalized Silica Nanoparticles with Supported Lipid Bilayers. *Colloids Surfaces B Biointerfaces* **2020**, *191*, 111028. <https://doi.org/10.1016/j.colsurfb.2020.111028>.
- (67) Garcia Gonzalez, M. N.; Levi, M.; Turri, S.; Griffini, G. Lignin Nanoparticles by Ultrasonication and Their Incorporation in Waterborne Polymer Nanocomposites. *J. Appl. Polym. Sci.* **2017**, *134* (38), 45318. <https://doi.org/10.1002/app.45318>.
- (68) Yang, W.; Fortunati, E.; Gao, D.; Balestra, G. M.; Giovanale, G.; He, X.; Torre, L.; Kenny, J. M.; Puglia, D. Valorization of Acid Isolated High Yield Lignin Nanoparticles as Innovative Antioxidant/Antimicrobial Organic Materials. *ACS Sustain. Chem. Eng.* **2018**, *6* (3), 3502–3514. <https://doi.org/10.1021/acssuschemeng.7b03782>.
- (69) Yang, W.; Ding, H.; Qi, G.; Guo, J.; Xu, F.; Li, C.; Puglia, D.; Kenny, J.; Ma, P. Enhancing the Radical Scavenging Activity and UV Resistance of Lignin Nanoparticles via Surface Mannich Amination toward a Biobased Antioxidant. *Biomacromolecules* **2021**, *22*, 2693. <https://doi.org/10.1021/acs.biomac.1c00387>.
- (70) Kim, S.; Fernandes, M. M.; Matamá, T.; Loureiro, A.; Gomes, A. C.; Cavaco-Paulo, A. Chitosan-Lignosulfonates Sono-Chemically Prepared Nanoparticles: Characterisation and Potential Applications. *Colloids Surfaces B Biointerfaces* **2013**, *103*, 1–8. <https://doi.org/10.1016/j.colsurfb.2012.10.033>.
- (71) Akiyama, H.; Fujii, K.; Yamasaki, O.; Oono, T.; Iwatsuki, K. Antibacterial Action of Several Tannins against *Staphylococcus Aureus*. *J. Antimicrob. Chemother.* **2001**, *48* (4), 487–491. <https://doi.org/10.1093/jac/48.4.487>.
- (72) Renzetti, A.; Betts, J. W.; Fukumoto, K.; Rutherford, R. N. Antibacterial Green Tea Catechins from a Molecular Perspective: Mechanisms of Action and Structure-Activity Relationships. *Food Funct.* **2020**, *11* (11), 9370–9396. <https://doi.org/10.1039/d0fo02054k>.
- (73) Castaneda-Arriaga, R.; Pérez-González, A.; Reina, M.; Alvarez-Idaboy, J. R.; Galano, A. Comprehensive Investigation of the Antioxidant and Pro-Oxidant Effects of Phenolic Compounds: A Double-Edged Sword in the Context of Oxidative Stress? *J. Phys. Chem. B* **2018**, *122* (23), 6198–6214. <https://doi.org/10.1021/acs.jpcc.8b03500>.
- (74) Panda, L.; Duarte-Sierra, A. Recent Advancements in Enhancing Antimicrobial Activity of Plant-Derived Polyphenols by Biochemical Means. *Horticulturae* **2022**, *8* (5), 401. <https://doi.org/10.3390/horticulturae8050401>.
- (75) Plaper, A.; Golob, M.; Hafner, I.; Oblak, M.; Šolmajer, T.; Jerala, R. Characterization of Quercetin Binding Site on DNA Gyrase. *Biochem. Biophys. Res. Commun.* **2003**, *306* (2), 530–536. [https://doi.org/10.1016/S0006-291X\(03\)01006-4](https://doi.org/10.1016/S0006-291X(03)01006-4).
- (76) Slavin, Y. N.; Ivanova, K.; Hoyo, J.; Perelshtein, I.; Owen, G.; Haegert, A.; Lin, Y.-Y.; LeBihan, S.; Gedanken, A.; Häfeli, U. O.; et al. Novel Lignin-Capped Silver Nanoparticles against Multidrug-Resistant Bacteria. *ACS Appl. Mater. Interfaces* **2021**, *13* (19), 22098–22109.

- <https://doi.org/10.1021/acsami.0c16921>.
- (77) Slavina, Y. N.; Ivanova, K.; Tang, W. L.; Tzanov, T.; Li, S. D.; Bach, H. Targeting Intracellular Mycobacteria Using Nanosized Niosomes Loaded with Antibacterial Agents. *Nanomaterials* **2021**, *11* (8), 1984. <https://doi.org/10.3390/nano11081984>.
- (78) Saratale, R. G.; Saratale, G. D.; Ghodake, G.; Cho, S. K.; Kadam, A.; Kumar, G.; Jeon, B. H.; Pant, D.; Bhatnagar, A.; Shin, H. S. Wheat Straw Extracted Lignin in Silver Nanoparticles Synthesis: Expanding Its Prophecy towards Antineoplastic Potency and Hydrogen Peroxide Sensing Ability. *Int. J. Biol. Macromol.* **2019**, *128*, 391–400. <https://doi.org/10.1016/j.ijbiomac.2019.01.120>.
- (79) Saratale, R. G.; Cho, S. K.; Saratale, G. D.; Kadam, A. A.; Ghodake, G. S.; Magotra, V. K.; Kumar, M.; Bharagava, R. N.; Varjani, S.; Palem, R. R.; et al. Lignin-Mediated Silver Nanoparticle Synthesis for Photocatalytic Degradation of Reactive Yellow 4G and In Vitro Assessment of Antioxidant, Antidiabetic, and Antibacterial Activities. *Polymers (Basel)*. **2022**, *14* (3), 648. <https://doi.org/10.3390/polym14030648>.
- (80) Pletzer, D.; Asnis, J.; Slavina, Y. N.; Hancock, R. E. W.; Bach, H.; Saatchi, K.; Häfeli, U. O. Rapid Microwave-Based Method for the Preparation of Antimicrobial Lignin-Capped Silver Nanoparticles Active against Multidrug-Resistant Bacteria. *Int. J. Pharm.* **2021**, *596*, 120299. <https://doi.org/10.1016/j.ijpharm.2021.120299>.
- (81) Marulasiddeshwara, M. B.; Dakshayani, S. S.; Sharath Kumar, M. N.; Chethana, R.; Raghavendra Kumar, P.; Devaraja, S. Facile-One Pot-Green Synthesis, Antibacterial, Antifungal, Antioxidant and Antiplatelet Activities of Lignin Capped Silver Nanoparticles: A Promising Therapeutic Agent. *Mater. Sci. Eng. C* **2017**, *81*, 182. <https://doi.org/10.1016/j.msec.2017.07.054>.
- (82) Tran, N. T.; Nguyen, T. T. T.; Ha, D.; Nguyen, T. H.; Nguyen, N. N.; Baek, K.; Nguyen, N. T.; Tran, C. K.; Tran, T. T. Van; Le, H. Van; et al. Highly Functional Materials Based on Nano-Lignin, Lignin, and Lignin/Silica Hybrid Capped Silver Nanoparticles with Antibacterial Activities. *Biomacromolecules* **2021**, *22* (12), 5327. <https://doi.org/10.1021/acs.biomac.1c01250>.
- (83) Aadil, K. R.; Pandey, N.; Mussatto, S. I.; Jha, H. Green Synthesis of Silver Nanoparticles Using Acacia Lignin, Their Cytotoxicity, Catalytic, Metal Ion Sensing Capability and Antibacterial Activity. *J. Environ. Chem. Eng.* **2019**, *7* (5), 103296. <https://doi.org/10.1016/j.jece.2019.103296>.
- (84) Zevallos Torres, L. A.; Woiciechowski, A. L.; Oliveira de Andrade Tanobe, V.; Zandoná Filho, A.; Alves de Freitas, R.; Nosedá, M. D.; Saito Szameitat, E.; Faulds, C.; Coutinho, P.; Bertrand, E.; et al. Lignin from Oil Palm Empty Fruit Bunches: Characterization, Biological Activities and Application in Green Synthesis of Silver Nanoparticles. *Int. J. Biol. Macromol.* **2021**, *167*, 1499–1507. <https://doi.org/10.1016/j.ijbiomac.2020.11.104>.
- (85) Wang, Y.; Li, Z.; Yang, D.; Qiu, X.; Xie, Y.; Zhang, X. Microwave-Mediated Fabrication of Silver Nanoparticles Incorporated Lignin-Based Composites with Enhanced Antibacterial Activity via Electrostatic Capture Effect. *J. Colloid Interface Sci.* **2021**, *583*, 80. <https://doi.org/10.1016/j.jcis.2020.09.027>.
- (86) Li, Y.; Yang, D.; Li, P.; Li, Z. Lignin as a Multi-Functional Agent for the Synthesis

- of Ag Nanoparticles and Its Application in Antibacterial Coatings. *J. Mater. Res. Technol.* **2022**, *17*, 3211–3220. <https://doi.org/10.1016/j.jmrt.2022.02.049>.
- (87) Rocca, D. M.; Vanegas, J. P.; Fournier, K.; Becerra, M. C.; Scaiano, J. C.; Lanterna, A. E. Biocompatibility and Photo-Induced Antibacterial Activity of Lignin-Stabilized Noble Metal Nanoparticles. *RSC Adv.* **2018**, *8* (70), 40454–40463. <https://doi.org/10.1039/C8RA08169G>.
- (88) Li, P.; Lv, W.; Ai, S. Green and Gentle Synthesis of Cu₂O Nanoparticles Using Lignin as Reducing and Capping Reagent with Antibacterial Properties. *J. Exp. Nanosci.* **2016**, *11* (1), 18–27. <https://doi.org/10.1080/17458080.2015.1015462>.
- (89) Maldonado-Carmona, N.; Marchand, G.; Villandier, N.; Ouk, T. S.; Pereira, M. M.; Calvete, M. J. F.; Calliste, C. A.; Žak, A.; Piksa, M.; Pawlik, K. J.; et al. Porphyrin-Loaded Lignin Nanoparticles Against Bacteria: A Photodynamic Antimicrobial Chemotherapy Application. *Front. Microbiol.* **2020**, *11*, 606185. <https://doi.org/10.3389/fmicb.2020.606185>.
- (90) Amos-Tautua, B. M.; Songca, S. P.; Oluwafemi, O. S. Application of Porphyrins in Antibacterial Photodynamic Therapy. *Molecules* **2019**, *24* (13), 2456. <https://doi.org/10.3390/molecules24132456>.
- (91) Maldonado-Carmona, N.; Ouk, T. S.; Villandier, N.; Calliste, C. A.; Calvete, M. J. F.; Pereira, M. M.; Leroy-Lhez, S. Photophysical and Antibacterial Properties of Porphyrins Encapsulated inside Acetylated Lignin Nanoparticles. *Antibiotics* **2021**, *10* (5), 513. <https://doi.org/10.3390/antibiotics10050513>.
- (92) Chen, L.; Shi, Y.; Gao, B.; Zhao, Y.; Jiang, Y.; Zha, Z.; Xue, W.; Gong, L. Lignin Nanoparticles: Green Synthesis in a γ -Valerolactone/Water Binary Solvent and Application to Enhance Antimicrobial Activity of Essential Oils. *ACS Sustain. Chem. Eng.* **2020**, *8* (1), 714–722. <https://doi.org/10.1021/acssuschemeng.9b06716>.
- (93) Jose, L. M.; Kuriakose, S.; Mathew, T. Development of Photoresponsive Zinc Oxide Nanoparticle - Encapsulated Lignin Functionalized with 2-[(E)-(2-Hydroxy Naphthalen-1-Yl) Diazenyl] Benzoic Acid: A Promising Photoactive Agent for Antimicrobial Photodynamic Therapy. *Photodiagnosis Photodyn. Ther.* **2021**, *36*, 102479. <https://doi.org/10.1016/j.pdpdt.2021.102479>.
- (94) Zhong, J. F.; Xu, L.; Qin, X. L. Efficient Antibacterial Silver Nanoparticles Composite Using Lignin as a Template. *J. Compos. Mater.* **2015**, *49* (19), 2329–2335. <https://doi.org/10.1177/0021998314545192>.
- (95) Lü, Q. F.; Zhang, J. Y.; Yang, J.; He, Z. W.; Fang, C. Q.; Lin, Q. Self-Assembled Poly(N-Methylaniline)-Lignosulfonate Spheres: From Silver-Ion Adsorbent to Antimicrobial Material. *Chem. - A Eur. J.* **2013**, *19* (33), 10935–10944. <https://doi.org/10.1002/chem.201204113>.
- (96) Klapiszewski, Ł.; Rzemieniecki, T.; Krawczyk, M.; Malina, D.; Norman, M.; Zdarta, J.; Majchrzak, I.; Dobrowolska, A.; Czaczyk, K.; Jesionowski, T. Kraft Lignin/Silica-AgNPs as a Functional Material with Antibacterial Activity. *Colloids Surfaces B Biointerfaces* **2015**, *134*, 220–228. <https://doi.org/10.1016/j.colsurfb.2015.06.056>.
- (97) Richter, A. P.; Brown, J. S.; Bharti, B.; Wang, A.; Gangwal, S.; Houck, K.; Cohen Hubal, E. A.; Paunov, V. N.; Stoyanov, S. D.; Velev, O. D. An Environmentally Benign Antimicrobial Nanoparticle Based on a Silver-Infused Lignin Core. *Nat. Nanotechnol.* **2015**, *10* (9), 817–823.

- <https://doi.org/10.1038/nnano.2015.141>.
- (98) Lintinen, K.; Luiro, S.; Figueiredo, P.; Sakarinen, E.; Mousavi, Z.; Seitsonen, J.; Rivière, G. N. S.; Mattinen, U.; Niemelä, M.; Tammela, P.; et al. Antimicrobial Colloidal Silver-Lignin Particles via Ion and Solvent Exchange. *ACS Sustain. Chem. Eng.* **2019**, *7* (18), 15297–15303. <https://doi.org/10.1021/acssuschemeng.9b02498>.
- (99) Jiménez-González, C.; Constable, D. J. C.; Ponder, C. S. Evaluating the “Greenness” of Chemical Processes and Products in the Pharmaceutical Industry—a Green Metrics Primer. *Chem. Soc. Rev.* **2012**, *41* (4), 1485–1498. <https://doi.org/10.1039/c1cs15215g>.
- (100) Dobias, J.; Bernier-Latmani, R. Silver Release from Silver Nanoparticles in Natural Waters. *Environ. Sci. Technol.* **2013**, *47* (9), 4140–4146. <https://doi.org/10.1021/es304023p>.
- (101) Li, Y.; Cummins, E. Hazard Characterization of Silver Nanoparticles for Human Exposure Routes. *J. Environ. Sci. Heal. - Part A Toxic/Hazardous Subst. Environ. Eng.* **2020**, *55* (6), 704–725. <https://doi.org/10.1080/10934529.2020.1735852>.
- (102) Nix, C. E.; Harper, B. J.; Conner, C. G.; Richter, A. P.; Velev, O. D.; Harper, S. L. Toxicological Assessment of a Lignin Core Nanoparticle Doped with Silver as an Alternative to Conventional Silver Core Nanoparticles. *Antibiotics* **2018**, *7* (2), 40. <https://doi.org/10.3390/antibiotics7020040>.
- (103) Nevrez, L. A. M.; Casarrubias, L. B.; Celzard, A.; Fierro, V.; Muñoz, V. T.; Davila, A. C.; Lubian, J. R. T.; Snchez, G. G. Biopolymer-Based Nanocomposites: Effect of Lignin Acetylation in Cellulose Triacetate Films. *Sci. Technol. Adv. Mater.* **2011**, *12* (4), 45006–45022. <https://doi.org/10.1088/1468-6996/12/4/045006>.
- (104) Wang, Y. Y.; Meng, X.; Pu, Y.; Ragauskas, A. J. Recent Advances in the Application of Functionalized Lignin in Value-Added Polymeric Materials. *Polymers (Basel)*. **2020**, *12* (10), 2277. <https://doi.org/10.3390/polym12102277>.
- (105) Pérez-Rafael, S.; Ivanova, K.; Stefanov, I.; Puiggali, J.; del Valle, L. J.; Todorova, K.; Dimitrov, P.; Hinojosa-Caballero, D.; Tzanov, T. Nanoparticle-Driven Self-Assembling Injectable Hydrogels Provide a Multi-Factorial Approach for Chronic Wound Treatment. *Acta Biomater.* **2021**, *134* (15), 131–143. <https://doi.org/10.1016/j.actbio.2021.07.020>.
- (106) Gerbin, E.; Rivière, G. N.; Foulon, L.; Frapart, Y. M.; Cottyn, B.; Pernes, M.; Marcuello, C.; Godon, B.; Gainvors-Claisse, A.; Crônier, D.; et al. Tuning the Functional Properties of Lignocellulosic Films by Controlling the Molecular and Supramolecular Structure of Lignin. *Int. J. Biol. Macromol.* **2021**, *181*, 136. <https://doi.org/10.1016/j.ijbiomac.2021.03.081>.
- (107) Zhang, X.; Liu, W.; Sun, D.; Huang, J.; Qiu, X.; Li, Z.; Wu, X. Very Strong, Super-Tough, Antibacterial, and Biodegradable Polymeric Materials with Excellent UV-Blocking Performance. *ChemSusChem* **2020**, *13* (18), 4974. <https://doi.org/10.1002/cssc.202001075>.
- (108) Li, S.; Zhang, Y.; Ma, X.; Qiu, S.; Chen, J.; Lu, G.; Jia, Z.; Zhu, J.; Yang, Q.; Chen, J.; et al. Antimicrobial Lignin-Based Polyurethane/Ag Composite Foams for Improving Wound Healing. *Biomacromolecules* **2022**, *23* (4), 1622–1632. <https://doi.org/10.1021/acs.biomac.1c01465>.

- (109) Li, M.; Jiang, X.; Wang, D.; Xu, Z.; Yang, M. In Situ Reduction of Silver Nanoparticles in the Lignin Based Hydrogel for Enhanced Antibacterial Application. *Colloids Surfaces B Biointerfaces* **2019**, *177*, 370–376. <https://doi.org/10.1016/j.colsurfb.2019.02.029>.
- (110) Deng, P.; Chen, F.; Zhang, H.; Chen, Y.; Zhou, J. Conductive, Self-Healing, Adhesive, and Antibacterial Hydrogels Based on Lignin/Cellulose for Rapid MRSA-Infected Wound Repairing. *ACS Appl. Mater. Interfaces* **2021**, *13* (44), 52333–52345. <https://doi.org/10.1021/acsami.1c14608>.
- (111) Zhang, L.; Lu, H.; Chu, J.; Ma, J.; Fan, Y.; Wang, Z.; Ni, Y. Lignin-Directed Control of Silver Nanoparticles with Tunable Size in Porous Lignocellulose Hydrogels and Their Application in Catalytic Reduction. *ACS Sustain. Chem. Eng.* **2020**, *8* (33), 12655–12663. <https://doi.org/10.1021/acssuschemeng.0c04298>.
- (112) World Health Organization. *Health and Food Safety - 2015 Annual Activity Report*; 2016.
- (113) Jayakumar, A.; Radoor, S.; Kim, J. T.; Rhim, J. W.; Parameswaranpillai, J.; Siengchin, S. Lignin-Based Bionanocomposites for Food Packaging Applications. In *Bionanocomposites for Food Packaging Applications*; Woodhead Publishing, 2022; pp 323–337. <https://doi.org/10.1016/b978-0-323-88528-7.00025-3>.
- (114) Yang, W.; Owczarek, J. S.; Fortunati, E.; Kozanecki, M.; Mazzaglia, A.; Balestra, G. M.; Kenny, J. M.; Torre, L.; Puglia, D. Antioxidant and Antibacterial Lignin Nanoparticles in Polyvinyl Alcohol/Chitosan Films for Active Packaging. *Ind. Crops Prod.* **2016**, *94*, 800–811. <https://doi.org/10.1016/j.indcrop.2016.09.061>.
- (115) Yang, W.; Fortunati, E.; Dominici, F.; Giovanale, G.; Mazzaglia, A.; Balestra, G. M.; Kenny, J. M.; Puglia, D. Synergic Effect of Cellulose and Lignin Nanostructures in PLA Based Systems for Food Antibacterial Packaging. *Eur. Polym. J.* **2016**, *79*, 1–12. <https://doi.org/10.1016/j.eurpolymj.2016.04.003>.
- (116) Wang, X.; Wang, S.; Liu, W.; Wang, S.; Zhang, L.; Sang, R.; Hou, Q.; Li, J. Facile Fabrication of Cellulose Composite Films with Excellent UV Resistance and Antibacterial Activity. *Carbohydr. Polym.* **2019**, *225*, 115213. <https://doi.org/10.1016/j.carbpol.2019.115213>.
- (117) Lizundia, E.; Armentano, I.; Luzi, F.; Bertoglio, F.; Restivo, E.; Visai, L.; Torre, L.; Puglia, D. Synergic Effect of Nanolignin and Metal Oxide Nanoparticles into Poly(l-Lactide) Bionanocomposites: Material Properties, Antioxidant Activity, and Antibacterial Performance. *ACS Appl. Bio Mater.* **2020**, *3* (8), 5263. <https://doi.org/10.1021/acsabm.0c00637>.
- (118) Deng, L.; Cai, C.; Huang, Y.; Dong, Y.; Fu, Y. Ultralow Loading Mussel-Inspired Conductive Hybrid as Highly Effective Modifier for Function-Engineered Poly(Lactic Acid) Composites. *Int. J. Biol. Macromol.* **2021**, *185*, 513–524. <https://doi.org/10.1016/j.ijbiomac.2021.06.170>.
- (119) Hu, S.; Hsieh, Y. Lo. Synthesis of Surface Bound Silver Nanoparticles on Cellulose Fibers Using Lignin as Multi-Functional Agent. *Carbohydr. Polym.* **2015**, *131*, 134. <https://doi.org/10.1016/j.carbpol.2015.05.060>.
- (120) Shankar, S.; Rhim, J. W. Preparation and Characterization of Agar/Lignin/Silver Nanoparticles Composite Films with Ultraviolet Light Barrier and Antibacterial Properties. *Food Hydrocoll.* **2017**, *71*, 76–84. <https://doi.org/10.1016/j.foodhyd.2017.05.002>.

- (121) Shankar, S.; Rhim, J. W.; Won, K. Preparation of Poly(Lactide)/Lignin/Silver Nanoparticles Composite Films with UV Light Barrier and Antibacterial Properties. *Int. J. Biol. Macromol.* **2018**, *107*, 1724. <https://doi.org/10.1016/j.ijbiomac.2017.10.038>.
- (122) Lizundia, E.; Vilas, J. L.; Sangroniz, A.; Etxeberria, A. Light and Gas Barrier Properties of PLLA/Metallic Nanoparticles Composite Films. *Eur. Polym. J.* **2017**, *91*, 10–20. <https://doi.org/10.1016/j.eurpolymj.2017.03.043>.
- (123) Lambré, C.; Barat Baviera, J. M.; Bolognesi, C.; Chesson, A.; Cocconcelli, P. S.; Crebelli, R.; Gott, D. M.; Grob, K.; Lampi, E.; Mengelers, M.; et al. Safety Assessment of the Substance Silver Nanoparticles for Use in Food Contact Materials. *EFSA Journal*. John Wiley and Sons Inc August 1, 2021. <https://doi.org/10.2903/j.efsa.2021.6790>.
- (124) Capecchi, E.; Piccinino, D.; Tomaino, E.; Bizzarri, B. M.; Polli, F.; Antiochia, R.; Mazzei, F.; Saladino, R. Lignin Nanoparticles Are Renewable and Functional Platforms for the Concanavalin a Oriented Immobilization of Glucose Oxidase-Peroxidase in Cascade Bio-Sensing. *RSC Adv.* **2020**, *10* (48), 29031–29042. <https://doi.org/10.1039/d0ra04485g>.
- (125) Riley, M. K.; Vermerris, W. Delivery of DNA into Human Cells by Functionalized Lignin Nanoparticles. *Materials (Basel)*. **2022**, *15* (1), 303. <https://doi.org/10.3390/ma15010303>.
- (126) Ma, S.; Feng, X.; Liu, F.; Wang, B.; Zhang, H.; Niu, X. The Pro-Inflammatory Response of Macrophages Regulated by Acid Degradation Products of Poly(Lactide-Co-Glycolide) Nanoparticles. *Eng. Life Sci.* **2021**, *21* (10), 709–720. <https://doi.org/10.1002/elsc.202100040>.
- (127) Yang, W.; Fortunati, E.; Bertoglio, F.; Owczarek, J. S.; Bruni, G.; Kozanecki, M.; Kenny, J. M.; Torre, L.; Visai, L.; Puglia, D. Polyvinyl Alcohol/Chitosan Hydrogels with Enhanced Antioxidant and Antibacterial Properties Induced by Lignin Nanoparticles. *Carbohydr. Polym.* **2018**, *181*, 275–284. <https://doi.org/10.1016/j.carbpol.2017.10.084>.
- (128) Visan, A. I.; Popescu-Pelin, G.; Gherasim, O.; Grumezescu, V.; Socol, M.; Zgura, I.; Florica, C.; Popescu, R. C.; Savu, D.; Holban, A. M.; et al. Laser Processed Antimicrobial Nanocomposite Based on Polyaniline Grafted Lignin Loaded with Gentamicin-Functionalized Magnetite. *Polymers (Basel)*. **2019**, *11* (2), 283. <https://doi.org/10.3390/polym11020283>.
- (129) He, X.; Li, Z.; Li, J.; Mishra, D.; Ren, Y.; Gates, I.; Hu, J.; Lu, Q. Ultrastretchable, Adhesive, and Antibacterial Hydrogel with Robust Spinnability for Manufacturing Strong Hydrogel Micro/Nanofibers. *Small* **2021**, *17* (49), 2103521. <https://doi.org/10.1002/sml.202103521>.
- (130) Gan, D.; Xing, W.; Jiang, L.; Fang, J.; Zhao, C.; Ren, F.; Fang, L.; Wang, K.; Lu, X. Plant-Inspired Adhesive and Tough Hydrogel Based on Ag-Lignin Nanoparticles-Triggered Dynamic Redox Catechol Chemistry. *Nat. Commun.* **2019**, *10* (1), 1487. <https://doi.org/10.1038/s41467-019-09351-2>.
- (131) Deng, P.; Chen, F.; Zhang, H.; Chen, Y.; Zhou, J. Conductive, Self-Healing, Adhesive, and Antibacterial Hydrogels Based on Lignin/Cellulose for Rapid Mrsa-Infected Wound Repairing. *ACS Appl. Mater. Interfaces* **2021**, *13* (44), 52333. <https://doi.org/10.1021/acsami.1c14608>.
- (132) Jaiswal, L.; Shankar, S.; Rhim, J. W.; Hahm, D. H. Lignin-Mediated Green Synthesis of AgNPs in Carrageenan Matrix for Wound Dressing Applications.

- Int. J. Biol. Macromol.* **2020**, *159*, 859–869. <https://doi.org/10.1016/j.ijbiomac.2020.05.145>.
- (133) Yang, W.; Xu, F.; Ma, X.; Guo, J.; Li, C.; Shen, S.; Puglia, D.; Chen, J.; Xu, P.; Kenny, J.; et al. Highly-Toughened PVA/Nanocellulose Hydrogels with Anti-Oxidative and Antibacterial Properties Triggered by Lignin-Ag Nanoparticles. *Mater. Sci. Eng. C* **2021**, *129*, 112385. <https://doi.org/10.1016/j.msec.2021.112385>.
- (134) Chandna, S.; Thakur, N. S.; Kaur, R.; Bhaumik, J. Lignin-Bimetallic Nanoconjugate Doped PH-Responsive Hydrogels for Laser-Assisted Antimicrobial Photodynamic Therapy. *Biomacromolecules* **2020**, *21* (8), 3216. <https://doi.org/10.1021/acs.biomac.0c00695>.
- (135) Li, M.; Jiang, X.; Wang, D.; Xu, Z.; Yang, M. In Situ Reduction of Silver Nanoparticles in the Lignin Based Hydrogel for Enhanced Antibacterial Application. *Colloids Surfaces B Biointerfaces* **2019**, *177*, 370–376. <https://doi.org/10.1016/j.colsurfb.2019.02.029>.
- (136) Aadil, K. R.; Mussatto, S. I.; Jha, H. Synthesis and Characterization of Silver Nanoparticles Loaded Poly(Vinyl Alcohol)-Lignin Electrospun Nanofibers and Their Antimicrobial Activity. *Int. J. Biol. Macromol.* **2018**, *120*, 763–767. <https://doi.org/10.1016/j.ijbiomac.2018.08.109>.
- (137) Haider, M. K.; Ullah, A.; Sarwar, M. N.; Yamaguchi, T.; Wang, Q.; Ullah, S.; Park, S.; Kim, I. S. Fabricating Antibacterial and Antioxidant Electrospun Hydrophilic Polyacrylonitrile Nanofibers Loaded with Agnps by Lignin-Induced in-Situ Method. *Polymers (Basel)*. **2021**, *13* (5), 748. <https://doi.org/10.3390/polym13050748>.
- (138) Haider, M. K.; Ullah, A.; Sarwar, M. N.; Saito, Y.; Sun, L.; Park, S.; Kim, I. S. Lignin-Mediated in-Situ Synthesis of CuO Nanoparticles on Cellulose Nanofibers: A Potential Wound Dressing Material. *Int. J. Biol. Macromol.* **2021**, *173*, 315–326. <https://doi.org/10.1016/j.ijbiomac.2021.01.050>.
- (139) Sibbald, R. G.; Goodman, L.; Woo, K. Y.; Krasner, D. L.; Smart, H.; Tariq, G.; Ayello, E. A.; Burrell, R. E.; Keast, D. H.; Mayer, D.; et al. Special Considerations in Wound Bed Preparation 2011: An Update. *Adv. Skin Wound Care* **2011**, *24* (9), 415–436. <https://doi.org/10.1097/01.ASW.0000405216.27050.97>.
- (140) Eming, S. A.; Martin, P.; Tomic-Canic, M. Wound Repair and Regeneration: Mechanisms, Signaling, and Translation. *Sci. Transl. Med.* **2014**, *6* (265), 265sr6. <https://doi.org/10.1126/scitranslmed.3009337>.
- (141) Martinengo, L.; Olsson, M.; Bajpai, R.; Soljak, M.; Upton, Z.; Schmidtchen, A.; Car, J. Prevalence of Chronic Wounds in the General Population: Systematic Review and Meta-Analysis of Observational Studies. *Ann. Epidemiol.* **2019**, *29*, 8–15. <https://doi.org/10.1016/j.annepidem.2018.10.005>.
- (142) Han, G.; Ceilley, R. Chronic Wound Healing: A Review of Current Management and Treatments. *Adv. Ther.* **2017**, *34* (3), 599–610. <https://doi.org/10.1007/s12325-017-0478-y>.
- (143) Tavakoli, S.; Klar, A. S. Advanced Hydrogels as Wound Dressings. *Biomolecules* **2020**, *10* (8), 1–20. <https://doi.org/10.3390/biom10081169>.
- (144) Wilkinson, H. N.; Hardman, M. J. Wound Healing: Cellular Mechanisms and Pathological Outcomes: Cellular Mechanisms of Wound Repair. *Open Biol.* **2020**, *10* (9), 200223. <https://doi.org/10.1098/rsob.200223>.
- (145) Bessa, L. J.; Fazii, P.; Di Giulio, M.; Cellini, L. Bacterial Isolates from Infected Wounds and Their Antibiotic Susceptibility Pattern: Some Remarks about

- Wound Infection. *Int. Wound J.* **2015**, *12* (1), 47–52. <https://doi.org/10.1111/iwj.12049>.
- (146) Gjødsbøl, K.; Christensen, J. J.; Karlsmark, T.; Jørgensen, B.; Klein, B. M.; Kroghfelt, K. A. Multiple Bacterial Species Reside in Chronic Wounds: A Longitudinal Study. *Int. Wound J.* **2006**, *3* (3), 225–231. <https://doi.org/10.1111/j.1742-481X.2006.00159.x>.
- (147) Dhall, S.; Do, D. C.; Garcia, M.; Kim, J.; Mirebrahim, S. H.; Lyubovitsky, J.; Lonardi, S.; Nothnagel, E. A.; Schiller, N.; Martins-Green, M. Generating and Reversing Chronic Wounds in Diabetic Mice by Manipulating Wound Redox Parameters. *J. Diabetes Res.* **2014**, *2014*. <https://doi.org/10.1155/2014/562625>.
- (148) Fu, X.; Kassim, S. Y.; Parks, W. C.; Heinecke, J. W. Hypochlorous Acid Oxygenates the Cysteine Switch Domain of Pro-Matrilysin (MMP-7): A Mechanism for Matrix Metalloproteinase Activation and Atherosclerotic Plaque Rupture by Myeloperoxidase. *J. Biol. Chem.* **2001**, *276* (44), 41279–41287. <https://doi.org/10.1074/jbc.M106958200>.
- (149) Lazaro, J. L.; Izzo, V.; Meaume, S.; Davies, A. H.; Lobmann, R.; Uccioli, L. Elevated Levels of Matrix Metalloproteinases and Chronic Wound Healing: An Updated Review of Clinical Evidence. *J. Wound Care* **2016**, *25* (5), 277–287. <https://doi.org/10.12968/jowc.2016.25.5.277>.
- (150) Stefanov, I.; Pérez-Rafael, S.; Hoyo, J.; Cailloux, J.; Santana Pérez, O. O.; Hinojosa-Caballero, D.; Tzanov, T. Multifunctional Enzymatically Generated Hydrogels for Chronic Wound Application. *Biomacromolecules* **2017**, *18* (5), 1544–1555. <https://doi.org/10.1021/acs.biomac.7b00111>.
- (151) Haske-Cornelius, O.; Bischof, S.; Beer, B.; Jimenez Bartolome, M.; Olatunde Olakanmi, E.; Mokoba, M.; Guebitz, G. M.; Nyanhongo, G. S. Enzymatic Synthesis of Highly Flexible Lignin Cross-Linked Succinyl-Chitosan Hydrogels Reinforced with Reed Cellulose Fibres. *Eur. Polym. J.* **2019**, *120*, 109201. <https://doi.org/10.1016/j.eurpolymj.2019.08.028>.
- (152) Hu, W.; Wang, Z.; Xiao, Y.; Zhang, S.; Wang, J. Advances in Crosslinking Strategies of Biomedical Hydrogels. *Biomater. Sci.* **2019**, *7* (3), 843–855. <https://doi.org/10.1039/c8bm01246f>.
- (153) Zeng, Q.; Qi, X.; Shi, G.; Zhang, M.; Haick, H. Wound Dressing: From Nanomaterials to Diagnostic Dressings and Healing Evaluations. *ACS Nano*. American Chemical Society February 22, 2022, pp 1708–1733. <https://doi.org/10.1021/acsnano.1c08411>.
- (154) Sahraro, M.; Yeganeh, H.; Sorayya, M. Guanidine Hydrochloride Embedded Polyurethanes as Antimicrobial and Absorptive Wound Dressing Membranes with Promising Cytocompatibility. *Mater. Sci. Eng. C* **2016**, *59*, 1025–1037. <https://doi.org/10.1016/j.msec.2015.11.038>.
- (155) Bartzoka, E. D.; Lange, H.; Thiel, K.; Crestini, C. Coordination Complexes and One-Step Assembly of Lignin for Versatile Nanocapsule Engineering. *ACS Sustain. Chem. Eng.* **2016**, *4* (10), 5194–5203. <https://doi.org/10.1021/acssuschemeng.6b00904>.
- (156) Jiang, P.; Sheng, X.; Yu, S.; Li, H.; Lu, J.; Zhou, J.; Wang, H. Preparation and Characterization of Thermo-Sensitive Gel with Phenolated Alkali Lignin. *Sci. Rep.* **2018**, *8* (1), 14450. <https://doi.org/10.1038/s41598-018-32672-z>.
- (157) Luo, B.; Jia, Z.; Jiang, H.; Wang, S.; Min, D. Improving the Reactivity of

- Sugarcane Bagasse Kraft Lignin by a Combination of Fractionation and Phenolation for Phenol-Formaldehyde Adhesive Applications. *Polymers (Basel)*. **2020**, *12* (8), 1825. <https://doi.org/10.3390/POLYM12081825>.
- (158) Sternberg, J.; Sequerth, O.; Pilla, S. Green Chemistry Design in Polymers Derived from Lignin: Review and Perspective. *Prog. Polym. Sci.* **2021**, *113*, 101344. <https://doi.org/10.1016/j.progpolymsci.2020.101344>.
- (159) Vishwanath, R.; Negi, B. Conventional and Green Methods of Synthesis of Silver Nanoparticles and Their Antimicrobial Properties. *Current Research in Green and Sustainable Chemistry*. Elsevier January 1, 2021, p 100205. <https://doi.org/10.1016/j.crgsc.2021.100205>.
- (160) Taleb, F.; Ammar, M.; Mosbah, M. ben; Salem, R. ben; Moussaoui, Y. Chemical Modification of Lignin Derived from Spent Coffee Grounds for Methylene Blue Adsorption. *Sci. Rep.* **2020**, *10* (1), 11048. <https://doi.org/10.1038/s41598-020-68047-6>.
- (161) Pradenas, G. A.; Paillavil, B. A.; Reyes-Cerpa, S.; Pérez-Donoso, J. M.; Vásquez, C. C. Reduction of the Monounsaturated Fatty Acid Content of Escherichia Coli Results in Increased Resistance to Oxidative Damage. *Microbiology* **2012**, *158* (5), 1279–1283. <https://doi.org/10.1099/mic.0.056903-0>.
- (162) Pérez, J. M.; Calderón, I. L.; Arenas, F. A.; Fuentes, D. E.; Pradenas, G. A.; Fuentes, E. L.; Sandoval, J. M.; Castro, M. E.; Elías, A. O.; Vásquez, C. C. Bacterial Toxicity of Potassium Tellurite: Unveiling an Ancient Enigma. *PLoS One* **2007**, *2* (2). <https://doi.org/10.1371/journal.pone.0000211>.
- (163) Ivanova, K.; Ivanova, A.; Ramon, E.; Hoyo, J.; Sanchez-Gomez, S.; Tzanov, T. Antibody-Enabled Antimicrobial Nanocapsules for Selective Elimination of Staphylococcus Aureus. *ACS Appl. Mater. Interfaces* **2020**, *12* (32), 35918–35927. <https://doi.org/10.1021/acsami.0c09364>.
- (164) Hoyo, J.; Torrent-Burgués, J.; Tzanov, T. Physical States and Thermodynamic Properties of Model Gram-Negative Bacterial Inner Membranes. *Chem. Phys. Lipids* **2019**, *218*, 57–64. <https://doi.org/10.1016/j.chemphyslip.2018.12.003>.
- (165) Hoyo, J.; Guaus, E.; Torrent-Burgués, J.; Sanz, F. Biomimetic Monolayer Films of Digalactosyldiacylglycerol Incorporating Plastoquinone. *Biochim. Biophys. Acta - Biomembr.* **2015**, *1848* (6), 1341–1351. <https://doi.org/10.1016/j.bbmem.2015.03.003>.
- (166) Hilgers, R.; Vincken, J. P.; Gruppen, H.; Kabel, M. A. Laccase/Mediator Systems: Their Reactivity toward Phenolic Lignin Structures. *ACS Sustain. Chem. Eng.* **2018**, *6* (2), 2037–2046. <https://doi.org/10.1021/acssuschemeng.7b03451>.
- (167) Díaz-González, M.; Vidal, T.; Tzanov, T. Phenolic Compounds as Enhancers in Enzymatic and Electrochemical Oxidation of Veratryl Alcohol and Lignins. *Appl. Microbiol. Biotechnol.* **2011**, *89* (6), 1693–1700. <https://doi.org/10.1007/s00253-010-3007-3>.
- (168) Aracri, E.; Díaz Blanco, C.; Tzanov, T. An Enzymatic Approach to Develop a Lignin-Based Adhesive for Wool Floor Coverings. *Green Chem.* **2014**, *16* (5), 2597. <https://doi.org/10.1039/c4gc00063c>.
- (169) Slagman, S.; Zuilhof, H.; Franssen, M. C. R. Laccase-Mediated Grafting on Biopolymers and Synthetic Polymers: A Critical Review. *ChemBioChem* **2018**, *19* (4), 288–311. <https://doi.org/10.1002/cbic.201700518>.
- (170) Sun, Q.; Cai, X.; Li, J.; Zheng, M.; Chen, Z.; Yu, C. P. Green Synthesis of Silver

- Nanoparticles Using Tea Leaf Extract and Evaluation of Their Stability and Antibacterial Activity. *Colloids Surfaces A Physicochem. Eng. Asp.* **2014**, *444*, 226–231. <https://doi.org/10.1016/j.colsurfa.2013.12.065>.
- (171) Domínguez, A. V.; Algaba, R. A.; Canturri, A. M.; Villodres, Á. R.; Smani, Y. Antibacterial Activity of Colloidal Silver against Gram-Negative and Gram-Positive Bacteria. *Antibiotics* **2020**, *9* (1). <https://doi.org/10.3390/antibiotics9010036>.
- (172) Ahamed, M.; AlSalhi, M. S.; Siddiqui, M. K. J. Silver Nanoparticle Applications and Human Health. *Clin. Chim. Acta* **2010**, *411* (23–24), 1841–1848. <https://doi.org/10.1016/j.cca.2010.08.016>.
- (173) Cunningham, B.; Engstrom, A. E.; Harper, B. J.; Harper, S. L.; Mackiewicz, M. R. Silver Nanoparticles Stable to Oxidation and Silver Ion Release Show Size-Dependent Toxicity in Vivo. *Nanomaterials* **2021**, *11* (6), 1516. <https://doi.org/10.3390/nano11061516>.
- (174) Pankaj; Ashokkumar, M. *Theoretical and Experimental Sonochemistry Involving Inorganic Systems*; Springer Netherlands, 2011. <https://doi.org/10.1007/978-90-481-3887-6>.
- (175) Francesko, A.; Cano Fossas, M.; Petkova, P.; Fernandes, M. M.; Mendoza, E.; Tzanov, T. Sonochemical Synthesis and Stabilization of Concentrated Antimicrobial Silver-Chitosan Nanoparticle Dispersions. *J. Appl. Polym. Sci.* **2017**, *134* (30), 45136. <https://doi.org/10.1002/app.45136>.
- (176) Okoli, C. U.; Kuttiyiel, K. A.; Cole, J.; McCutchen, J.; Tawfik, H.; Adzic, R. R.; Mahajan, D. Solvent Effect in Sonochemical Synthesis of Metal-Alloy Nanoparticles for Use as Electrocatalysts. *Ultrason. Sonochem.* **2018**, *41*, 427–434. <https://doi.org/10.1016/j.ultrsonch.2017.09.049>.
- (177) Shimazaki, Y. Phenoxyl Radical-Metal Complexes. In *PATAI'S Chemistry of Functional Groups*; John Wiley & Sons, Ltd: Chichester, UK, 2012. <https://doi.org/10.1002/9780470682531.pat0603>.
- (178) Medina Cruz, D.; Tien-Street, W.; Zhang, B.; Huang, X.; Vernet Crua, A.; Nieto-Argüello, A.; Cholula-Díaz, J. L.; Martínez, L.; Huttel, Y.; González, M. U.; et al. Citric Juice-Mediated Synthesis of Tellurium Nanoparticles with Antimicrobial and Anticancer Properties. *Green Chem.* **2019**, *21* (8), 1982–1998. <https://doi.org/10.1039/c9gc00131j>.
- (179) Pugin, B.; Cornejo, F. A.; Muñoz-Díaz, P.; Muñoz-Villagrán, C. M.; Vargas-Pérez, J. I.; Arenas, F. A.; Vásquez, C. C. Glutathione Reductase-Mediated Synthesis of Tellurium-Containing Nanostructures Exhibiting Antibacterial Properties. *Appl. Environ. Microbiol.* **2014**, *80* (22), 7061–7070. <https://doi.org/10.1128/AEM.02207-14>.
- (180) Zonaro, E.; Lampis, S.; Turner, R. J.; Junaid, S.; Vallini, G. Biogenic Selenium and Tellurium Nanoparticles Synthesized by Environmental Microbial Isolates Efficaciously Inhibit Bacterial Planktonic Cultures and Biofilms. *Front. Microbiol.* **2015**, *6* (MAY), 584. <https://doi.org/10.3389/fmicb.2015.00584>.
- (181) Mohanty, A.; Kathawala, M. H.; Zhang, J.; Chen, W. N.; Loo, J. S. C.; Kjelleberg, S.; Yang, L.; Cao, B. Biogenic Tellurium Nanorods as a Novel Antivirulence Agent Inhibiting Pyoverdine Production in *Pseudomonas Aeruginosa*. *Biotechnol. Bioeng.* **2014**, *111* (5), 858–865. <https://doi.org/10.1002/bit.25147>.

- (182) Xu, Z.; He, H.; Zhang, S.; Wang, B.; Jin, J.; Li, C.; Chen, X.; Jiang, B.; Liu, Y. Mechanistic Studies on the Antibacterial Behavior of Ag Nanoparticles Decorated with Carbon Dots Having Different Oxidation Degrees. *Environ. Sci. Nano* **2019**, *6* (4), 1168–1179. <https://doi.org/10.1039/c8en01090k>.
- (183) Huang, Y. W.; Cambre, M.; Lee, H. J. The Toxicity of Nanoparticles Depends on Multiple Molecular and Physicochemical Mechanisms. *Int. J. Mol. Sci.* **2017**, *18* (12). <https://doi.org/10.3390/ijms18122702>.
- (184) Lewinski, N.; Colvin, V.; Drezek, R. Cytotoxicity of Nanoparticles. *Small* **2008**, *4* (1), 26–49. <https://doi.org/10.1002/sml.200700595>.
- (185) Rao, C. N. R.; Ramakrishna Matte, H. S. S.; Voggu, R.; Govindaraj, A. Recent Progress in the Synthesis of Inorganic Nanoparticles. *Dalt. Trans.* **2012**, *41* (17), 5089–5120. <https://doi.org/10.1039/c2dt12266a>.
- (186) Crua, A. V.; Medina, D.; Zhang, B.; González, M. U.; Huttel, Y.; Miguel García-Martín, J.; Cholula-Díaz, J. L.; Webster, T. J. Comparison of Cytocompatibility and Anticancer Properties of Traditional and Green Chemistry-Synthesized Tellurium Nanowires. *Int. J. Nanomedicine* **2019**, *14*, 3155–3176. <https://doi.org/10.2147/IJN.S175640>.
- (187) Milczarek, G.; Rebis, T.; Fabianska, J. One-Step Synthesis of Lignosulfonate-Stabilized Silver Nanoparticles. *Colloids Surfaces B Biointerfaces* **2013**, *105*, 335–341. <https://doi.org/10.1016/j.colsurfb.2013.01.010>.
- (188) Hu, S.; Hsieh, Y. Lo. Silver Nanoparticle Synthesis Using Lignin as Reducing and Capping Agents: A Kinetic and Mechanistic Study. *Int. J. Biol. Macromol.* **2016**, *82*, 856–862. <https://doi.org/10.1016/j.ijbiomac.2015.09.066>.
- (189) Figueiredo, P.; Lintinen, K.; Hirvonen, J. T.; Kostianen, M. A.; Santos, H. A. Properties and Chemical Modifications of Lignin: Towards Lignin-Based Nanomaterials for Biomedical Applications. *Progress in Materials Science.* 2018, pp 233–269. <https://doi.org/10.1016/j.pmatsci.2017.12.001>.
- (190) Chasteen, T. G.; Fuentes, D. E.; Tantaleán, J. C.; Vásquez, C. C. Tellurite: History, Oxidative Stress, and Molecular Mechanisms of Resistance. *FEMS Microbiol. Rev.* **2009**, *33* (4), 820–832. <https://doi.org/10.1111/j.1574-6976.2009.00177.x>.
- (191) Tremaroli, V.; Fedi, S.; Zannoni, D. Evidence for a Tellurite-Dependent Generation of Reactive Oxygen Species and Absence of a Tellurite-Mediated Adaptive Response to Oxidative Stress in Cells of *Pseudomonas Pseudoalcaligenes* KF707. *Arch. Microbiol.* **2007**, *187* (2), 127–135. <https://doi.org/10.1007/s00203-006-0179-4>.
- (192) Fernandes, M. M.; Ivanova, K.; Hoyo, J.; Pérez-Rafael, S.; Francesko, A.; Tzanov, T. Nanotransformation of Vancomycin Overcomes the Intrinsic Resistance of Gram-Negative Bacteria. *ACS Appl. Mater. Interfaces* **2017**, *9* (17), 15022–15030. <https://doi.org/10.1021/acsami.7b00217>.
- (193) Barros, A. M.; Dhanabalan, A.; Constantino, C. J. L.; Balogh, D. T.; Oliveira, O. N. Langmuir Monolayers of Lignins Obtained with Different Isolation Methods. *Thin Solid Films* **1999**, *354* (1), 215–221. [https://doi.org/10.1016/S0040-6090\(99\)00526-X](https://doi.org/10.1016/S0040-6090(99)00526-X).
- (194) Hoyo, J.; Ivanova, K.; Torrent-Burgues, J.; Tzanov, T. Interaction of Silver-Lignin Nanoparticles With Mammalian Mimetic Membranes. *Front. Bioeng. Biotechnol.* **2020**, *8*, 439. <https://doi.org/10.3389/fbioe.2020.00439>.
- (195) Nypelö, T. E.; Carrillo, C. A.; Rojas, O. J. Lignin Supracolloids Synthesized from

- (W/O) Microemulsions: Use in the Interfacial Stabilization of Pickering Systems and Organic Carriers for Silver Metal. *Soft Matter* **2015**, *11* (10), 2046–2054. <https://doi.org/10.1039/c4sm02851a>.
- (196) Vermaas, J. V.; Dixon, R. A.; Chen, F.; Mansfield, S. D.; Boerjan, W.; Ralph, J.; Crowley, M. F.; Beckham, G. T. Passive Membrane Transport of Lignin-Related Compounds. *Proc. Natl. Acad. Sci. U. S. A.* **2019**, *116* (46), 23117–23123. <https://doi.org/10.1073/pnas.1904643116>.
- (197) Boija, E.; Johansson, G. Interactions between Model Membranes and Lignin-Related Compounds Studied by Immobilized Liposome Chromatography. *Biochim. Biophys. Acta - Biomembr.* **2006**, *1758* (5), 620–626. <https://doi.org/10.1016/j.bbmem.2006.04.007>.
- (198) Pérez, J. M.; Arenas, F. A.; Pradenas, G. A.; Sandoval, J. M.; Vásquez, C. C. Escherichia Coli YqhD Exhibits Aldehyde Reductase Activity and Protects from the Harmful Effect of Lipid Peroxidation-Derived Aldehydes. *J. Biol. Chem.* **2008**, *283* (12), 7346–7353. <https://doi.org/10.1074/jbc.M708846200>.
- (199) Wang, T. Y.; Libardo, M. D. J.; Angeles-Boza, A. M.; Pellois, J. P. Membrane Oxidation in Cell Delivery and Cell Killing Applications. *ACS Chemical Biology*. 2017, pp 1170–1182. <https://doi.org/10.1021/acscchembio.7b00237>.
- (200) Mogharabi, M.; Faramarzi, M. A. Laccase and Laccase-Mediated Systems in the Synthesis of Organic Compounds. *Adv. Synth. Catal.* **2014**, *356* (5), 897–927. <https://doi.org/10.1002/adsc.201300960>.
- (201) Xiong, F.; Han, Y.; Wang, S.; Li, G.; Qin, T.; Chen, Y.; Chu, F. Preparation and Formation Mechanism of Size-Controlled Lignin Nanospheres by Self-Assembly. *Ind. Crops Prod.* **2017**, *100*, 146–152. <https://doi.org/10.1016/j.indcrop.2017.02.025>.
- (202) Qian, Y.; Deng, Y.; Qiu, X.; Li, H.; Yang, D. Formation of Uniform Colloidal Spheres from Lignin, a Renewable Resource Recovered from Pulping Spent Liquor. *Green Chem.* **2014**, *16*, 2156–2163. <https://doi.org/10.1039/c3gc42131g>.
- (203) McKenzie, T. G.; Karimi, F.; Ashokkumar, M.; Qiao, G. G. Ultrasound and Sonochemistry for Radical Polymerization: Sound Synthesis. *Chem. - A Eur. J.* **2019**, *25* (21), 5372–5388. <https://doi.org/10.1002/chem.201803771>.
- (204) Jiang, B.; Zhang, Y.; Gu, L.; Wu, W.; Zhao, H.; Jin, Y. Structural Elucidation and Antioxidant Activity of Lignin Isolated from Rice Straw and Alkali-oxygen Black Liquor. *Int. J. Biol. Macromol.* **2018**, *116*, 513–519. <https://doi.org/10.1016/j.ijbiomac.2018.05.063>.
- (205) Mou, H.; Huang, J.; Li, W.; Wu, X.; Liu, Y.; Fan, H. Study on the Chemical Modification of Alkali Lignin towards for Cellulase Adsorbent Application. *Int. J. Biol. Macromol.* **2020**, *149*, 794–800. <https://doi.org/10.1016/j.ijbiomac.2020.01.229>.
- (206) Hemmilä, V.; Hosseinpourpia, R.; Adamopoulos, S.; Eceiza, A. Characterization of Wood-Based Industrial Biorefinery Lignosulfonates and Supercritical Water Hydrolysis Lignin. *Waste and Biomass Valorization* **2020**, *11* (11), 5835–5845. <https://doi.org/10.1007/s12649-019-00878-5>.
- (207) Maisetta, G.; Batoni, G.; Caboni, P.; Esin, S.; Rinaldi, A. C.; Zucca, P. Tannin Profile, Antioxidant Properties, and Antimicrobial Activity of Extracts from Two Mediterranean Species of Parasitic Plant Cytinus. *BMC Complement.*

- Altern. Med.* **2019**, *19* (1), 82. <https://doi.org/10.1186/s12906-019-2487-7>.
- (208) Dong, X.; Dong, M.; Lu, Y.; Turley, A.; Jin, T.; Wu, C. Antimicrobial and Antioxidant Activities of Lignin from Residue of Corn Stover to Ethanol Production. *Ind. Crops Prod.* **2011**, *34* (3), 1629–1634. <https://doi.org/10.1016/j.indcrop.2011.06.002>.
- (209) Taguri, T.; Tanaka, T.; Kouno, I. Antibacterial Spectrum of Plant Polyphenols and Extracts Depending upon Hydroxyphenyl Structure. *Biol. Pharm. Bull.* **2006**, *29* (11), 2226–2235. <https://doi.org/10.1248/bpb.29.2226>.
- (210) Borges, A.; Ferreira, C.; Saavedra, M. J.; Simões, M. Antibacterial Activity and Mode of Action of Ferulic and Gallic Acids against Pathogenic Bacteria. *Microb. Drug Resist.* **2013**, *19* (4), 256–265. <https://doi.org/10.1089/mdr.2012.0244>.
- (211) Zhang, H.; Yi, Z.; Sun, Z.; Ma, X.; Li, X. Functional Nanoparticles of Tea Polyphenols for Doxorubicin Delivery in Cancer Treatment. *J. Mater. Chem. B* **2017**, *5* (36), 7622–7631. <https://doi.org/10.1039/c7tb01323j>.
- (212) ISO. ISO 10993-5:2009 - Biological Evaluation of Medical Devices- Part 5: Tests for in Vitro Cytotoxicity. **2009**, 1–34.
- (213) Rastogi, R. P.; Singh, S. P.; Häder, D. P.; Sinha, R. P. Detection of Reactive Oxygen Species (ROS) by the Oxidant-Sensing Probe 2',7'-Dichlorodihydrofluorescein Diacetate in the Cyanobacterium *Anabaena Variabilis* PCC 7937. *Biochem. Biophys. Res. Commun.* **2010**, *397* (3), 603–607. <https://doi.org/10.1016/j.bbrc.2010.06.006>.
- (214) Castro-Alfárez, M.; Polo-López, M. I.; Fernández-Ibáñez, P. Intracellular Mechanisms of Solar Water Disinfection. *Sci. Rep.* **2016**, *6*, 38145. <https://doi.org/10.1038/srep38145>.
- (215) Sakihama, Y.; Cohen, M. F.; Grace, S. C.; Yamasaki, H. Plant Phenolic Antioxidant and Prooxidant Activities: Phenolics-Induced Oxidative Damage Mediated by Metals in Plants. *Toxicology* **2002**, *177* (1), 67–80. [https://doi.org/10.1016/S0300-483X\(02\)00196-8](https://doi.org/10.1016/S0300-483X(02)00196-8).
- (216) Seczyk, L.; Swieca, M.; Kapusta, I.; Gawlik-Dziki, U. Protein–Phenolic Interactions as a Factor Affecting the Physicochemical Properties of White Bean Proteins. *Molecules* **2019**, *24* (3), 408. <https://doi.org/10.3390/molecules24030408>.
- (217) Phan, H. T. T.; Yoda, T.; Chahal, B.; Morita, M.; Takagi, M.; Vestergaard, M. C. Structure-Dependent Interactions of Polyphenols with a Biomimetic Membrane System. *Biochim. Biophys. Acta - Biomembr.* **2014**, *1838* (10), 2670–2677. <https://doi.org/10.1016/j.bbamem.2014.07.001>.
- (218) Ferreres, G.; Pérez-Rafael, S.; Torrent-Burgués, J.; Tzanov, T. Hyaluronic Acid Derivative Molecular Weight-Dependent Synthesis and Antimicrobial Effect of Hybrid Silver Nanoparticles. *Int. J. Mol. Sci.* **2021**, *22* (24), 13428. <https://doi.org/10.3390/ijms222413428>.
- (219) Yu, X.; Chu, S.; Hagerman, A. E.; Lorigan, G. A. Probing the Interaction of Polyphenols with Lipid Bilayers by Solid-State Nmr Spectroscopy. *J. Agric. Food Chem.* **2011**, *59* (12), 6783–6789. <https://doi.org/10.1021/jf200200h>.
- (220) WHO. Antimicrobial Resistance: Global Report on Surveillance 2014. *World Heal. Organ.* **2014**, 1–257. <https://doi.org/9789241564748>.
- (221) Panáček, A.; Kvítek, L.; Smékalová, M.; Večeřová, R.; Kolář, M.; Röderová, M.; Dyčka, F.; Šebela, M.; Pruček, R.; Tomanec, O.; et al. Bacterial Resistance to

- Silver Nanoparticles and How to Overcome It. *Nat. Nanotechnol.* **2018**, *13* (1), 65–71. <https://doi.org/10.1038/s41565-017-0013-y>.
- (222) Price, L. B.; Liu, C. M.; Melendez, J. H.; Frankel, Y. M.; Engelthaler, D.; Aziz, M.; Bowers, J.; Rattray, R.; Ravel, J.; Kingsley, C.; et al. Community Analysis of Chronic Wound Bacteria Using 16S rRNA Gene-Based Pyrosequencing: Impact of Diabetes and Antibiotics on Chronic Wound Microbiota. *PLoS One* **2009**, *4* (7). <https://doi.org/10.1371/journal.pone.0006462>.
- (223) Nussbaum, S. R.; Carter, M. J.; Fife, C. E.; DaVanzo, J.; Haught, R.; Nussgart, M.; Cartwright, D. An Economic Evaluation of the Impact, Cost, and Medicare Policy Implications of Chronic Nonhealing Wounds. *Value Heal.* **2018**, *21* (1), 27–32. <https://doi.org/10.1016/j.jval.2017.07.007>.
- (224) Brem, H.; Sheehan, P.; Rosenberg, H. J.; Schneider, J. S.; Boulton, A. J. M. Evidence-Based Protocol for Diabetic Foot Ulcers. *Plast. Reconstr. Surg.* **2006**, *117* (7 SUPPL.). <https://doi.org/10.1097/01.prs.0000225459.93750.29>.
- (225) Wang, C.; Zolotarskaya, O.; Ashraf, K. M.; Wen, X.; Ohman, D. E.; Wynne, K. J. Surface Characterization, Antimicrobial Effectiveness, and Human Cell Response for a Biomedical Grade Polyurethane Blended with a Mixed Soft Block PTMO-Quat/PEG Copolyoxetane Polyurethane. *ACS Appl. Mater. Interfaces* **2019**, *11* (23), 20699–20714. <https://doi.org/10.1021/acsami.9b04697>.
- (226) Bužarovska, A.; Dinescu, S.; Lazar, A. D.; Serban, M.; Pircalabioru, G. G.; Costache, M.; Gualandi, C.; Avérous, L. Nanocomposite Foams Based on Flexible Biobased Thermoplastic Polyurethane and ZnO Nanoparticles as Potential Wound Dressing Materials. *Mater. Sci. Eng. C* **2019**, *104*, 109893. <https://doi.org/10.1016/j.msec.2019.109893>.
- (227) Ye, D.; Zhong, Z.; Xu, H.; Chang, C.; Yang, Z.; Wang, Y.; Ye, Q.; Zhang, L. Construction of Cellulose/Nanosilver Sponge Materials and Their Antibacterial Activities for Infected Wounds Healing. *Cellulose* **2016**, *23* (1), 749–763. <https://doi.org/10.1007/s10570-015-0851-4>.
- (228) Farahani, M.; Shafiee, A. Wound Healing: From Passive to Smart Dressings. *Adv. Healthc. Mater.* **2021**, *10* (16), 2100477. <https://doi.org/10.1002/adhm.202100477>.
- (229) Carriço, C. S.; Fraga, T.; Pasa, V. M. D. Production and Characterization of Polyurethane Foams from a Simple Mixture of Castor Oil, Crude Glycerol and Untreated Lignin as Bio-Based Polyols. *Eur. Polym. J.* **2016**, *85*, 53–61. <https://doi.org/10.1016/j.eurpolymj.2016.10.012>.
- (230) Li, J.; Wang, B.; Chen, K.; Tian, X.; Zeng, J.; Xu, J.; Gao, W. The Use of Lignin as Cross-Linker for Polyurethane Foam for Potential Application in Adsorbing Materials. *BioResources* **2017**, *12* (4), 8653–8671. <https://doi.org/10.15376/biores.12.4.8653-8671>.
- (231) De Luca Bossa, F.; Santillo, C.; Verdolotti, L.; Campaner, P.; Minigher, A.; Boggioni, L.; Losio, S.; Coccia, F.; Iannace, S.; Lama, G. C. Greener Nanocomposite Polyurethane Foam Based on Sustainable Polyol and Natural Fillers: Investigation of Chemico-Physical and Mechanical Properties. *Materials (Basel)*. **2020**, *13* (1), 211. <https://doi.org/10.3390/ma13010211>.
- (232) Bernardini, J.; Anguillesi, I.; Coltelli, M. B.; Cinelli, P.; Lazzeri, A. Optimizing the Lignin Based Synthesis of Flexible Polyurethane Foams Employing Reactive Liquefying Agents. *Polym. Int.* **2015**, *64* (9), 1235–1244.

- <https://doi.org/10.1002/pi.4905>.
- (233) Ashjari, H. R.; Dorraji, M. S. S.; Fakhrzadeh, V.; Eslami, H.; Rasoulifard, M. H.; Rastgouy-Houjaghan, M.; Gholizadeh, P.; Kafil, H. S. Starch-Based Polyurethane/CuO Nanocomposite Foam: Antibacterial Effects for Infection Control. *Int. J. Biol. Macromol.* **2018**, *111*, 1076–1082. <https://doi.org/10.1016/j.ijbiomac.2018.01.137>.
- (234) Liu, W.; Fang, C.; Wang, S.; Huang, J.; Qiu, X. High-Performance Lignin-Containing Polyurethane Elastomers with Dynamic Covalent Polymer Networks. *Macromolecules* **2019**, *52* (17), 6474–6484. <https://doi.org/10.1021/acs.macromol.9b01413>.
- (235) Yarmohammadi, M.; Khalaf Adeli, A.; Zamani Pedram, M.; Shahidzadeh, M.; Pirouzfard, V. Improvement in Mechanical Properties of Polyurethane-Urea Nanocomposites by Using Modified SiO₂ Nanoparticles. *J. Appl. Polym. Sci.* **2018**, *135* (45). <https://doi.org/10.1002/app.46707>.
- (236) Okan, D.; Woo, K.; Ayello, E. A.; Sibbald, G. The Role of Moisture Balance in Wound Healing. *Adv. Skin Wound Care* **2007**, *20* (1), 39–53; quiz 53–55. <https://doi.org/10.1097/00129334-200701000-00013>.
- (237) Sibbald, R. G.; Woo, K.; Ayello, E. A. Increased Bacterial Burden and Infection: The Story of NERDS and STONES. *Adv. Skin Wound Care* **2006**, *19* (8), 447–461. <https://doi.org/https://doi.org/10.1097/00129334-200610000-00012>.
- (238) Tavares, L. B.; Boas, C. V.; Schleder, G. R.; Nacas, A. M.; Rosa, D. S.; Santos, D. J. Bio-Based Polyurethane Prepared from Kraft Lignin and Modified Castor Oil. *Express Polym. Lett.* **2016**, *10* (11), 927–940. <https://doi.org/10.3144/expresspolymlett.2016.86>.
- (239) Pan, X.; Saddler, J. N. Effect of Replacing Polyol by Organosolv and Kraft Lignin on the Property and Structure of Rigid Polyurethane Foam. *Biotechnol. Biofuels* **2013**, *6* (1), 12. <https://doi.org/10.1186/1754-6834-6-12>.
- (240) Chung, H.; Washburn, N. R. Improved Lignin Polyurethane Properties with Lewis Acid Treatment. *ACS Appl. Mater. Interfaces* **2012**, *4* (6), 2840–2846. <https://doi.org/10.1021/am300425x>.
- (241) Pyun, D. G.; Yoon, H. S.; Chung, H. Y.; Choi, H. J.; Thambi, T.; Kim, B. S.; Lee, D. S. Evaluation of AgHAP-Containing Polyurethane Foam Dressing for Wound Healing: Synthesis, Characterization, in Vitro and in Vivo Studies. *J. Mater. Chem. B* **2015**, *3* (39), 7752–7763. <https://doi.org/10.1039/c5tb00995b>.
- (242) Percival, S. L. Antimicrobial Efficacy of a Silver Impregnated Hydrophilic PU Foam. *Surg. Technol. Int.* **2018**, *32*, 67–74.
- (243) Sahuquillo Arce, J. M.; Iranzo Tatay, A.; Llácer Luna, M.; Sanchis Boix, Y.; Guitán Deltell, J.; González Barberá, E.; Beltrán Heras, J.; Gobernado Serrano, M. In Vitro Study of the Antimicrobial Properties of a Silver Ion-Releasing Polyurethane Foam. *Cir. Esp.* **2011**, *89* (8), 532–538. <https://doi.org/10.1016/j.ciresp.2011.02.015>.
- (244) Agnihotri, S.; Mukherji, S.; Mukherji, S. Immobilized Silver Nanoparticles Enhance Contact Killing and Show Highest Efficacy: Elucidation of the Mechanism of Bactericidal Action of Silver. *Nanoscale* **2013**, *5* (16), 7328–7340. <https://doi.org/10.1039/c3nr00024a>.
- (245) Siritongsuk, P.; Hongsing, N.; Thammawithan, S.; Daduang, S.; Klaynongsruang, S.; Tuanyok, A.; Patramanon, R. Two-Phase Bactericidal

- Mechanism of Silver Nanoparticles against *Burkholderia Pseudomallei*. *PLoS One* **2016**, *11* (12), e0168098. <https://doi.org/10.1371/journal.pone.0168098>.
- (246) Wlaschek, M.; Scharffetter-Kochanek, K. Oxidative Stress in Chronic Venous Leg Ulcers. *Wound Repair Regen.* **2005**, *13* (5), 452–461. <https://doi.org/10.1111/j.1067-1927.2005.00065.x>.
- (247) Frykberg, R. G.; Banks, J. Challenges in the Treatment of Chronic Wounds. *Adv. Wound Care* **2015**, *4* (9), 560–582. <https://doi.org/10.1089/wound.2015.0635>.
- (248) Antonio, F.; Guillem, R.; Sonia, T.; Mattu, C.; Gentile, P.; Chiono, V.; Ciardelli, G.; Tzanov, T. Cross-Linked Collagen Sponges Loaded with Plant Polyphenols with Inhibitory Activity towards Chronic Wound Enzymes. *Biotechnol. J.* **2011**, *6* (10), 1208–1218. <https://doi.org/10.1002/biot.201100194>.
- (249) Stefanov, I.; Hinojosa-Caballero, D.; Maspoch, S.; Hoyo, J.; Tzanov, T. Enzymatic Synthesis of a Thiolated Chitosan-Based Wound Dressing Crosslinked with Chicoric Acid. *J. Mater. Chem. B* **2018**, *6* (47), 7943–7953. <https://doi.org/10.1039/c8tb02483a>.
- (250) Klebanoff, S. J. Myeloperoxidase: Friend and Foe. *J. Leukoc. Biol.* **2005**, *77* (5), 598–625. <https://doi.org/10.1189/jlb.1204697>.
- (251) Wojtowicz, A. M.; Oliveira, S.; Carlson, M. W.; Zawadzka, A.; Rousseau, C. F.; Baksh, D. The Importance of Both Fibroblasts and Keratinocytes in a Bilayered Living Cellular Construct Used in Wound Healing. *Wound Repair Regen.* **2014**, *22* (2), 246–255. <https://doi.org/10.1111/wrr.12154>.
- (252) Heng, M. C. Y. Wound Healing in Adult Skin: Aiming for Perfect Regeneration. *Int. J. Dermatol.* **2011**, *50* (9), 1058–1066. <https://doi.org/10.1111/j.1365-4632.2011.04940.x>.
- (253) Mendez, M. V.; Stanley, A.; Park, H. Y.; Shon, K.; Phillips, T.; Menzoian, J. O. Fibroblasts Cultured from Venous Ulcers Display Cellular Characteristics of Senescence. *J. Vasc. Surg.* **1998**, *28* (5), 876–883. [https://doi.org/10.1016/S0741-5214\(98\)70064-3](https://doi.org/10.1016/S0741-5214(98)70064-3).
- (254) Becker, L. C.; Bergfeld, W. F.; Belsito, D. V.; Klaassen, C. D.; Marks, J. G.; Shank, R. C.; Slaga, T. J.; Snyder, P. W.; Andersen, F. A. Final Report of the Safety Assessment of Hyaluronic Acid, Potassium Hyaluronate, and Sodium Hyaluronate. *Int. J. Toxicol.* **2009**, *28* (4_suppl), 5–67. <https://doi.org/10.1177/1091581809337738>.
- (255) Pollini, M.; Paladini, F. Bioinspired Materials for Wound Healing Application: The Potential of Silk Fibroin. *Materials*. MDPI AG August 1, 2020, p 3361. <https://doi.org/10.3390/ma13153361>.
- (256) Roy, N.; Saha, N.; Saha, P. Stability Study of Novel Medicated Hydrogel Wound Dressings. *Int. J. Polym. Mater. Polym. Biomater.* **2013**, *62* (3), 150–156. <https://doi.org/10.1080/00914037.2011.641697>.
- (257) Fan, H.; Wang, J.; Gong, J. P. Barnacle Cement Proteins-Inspired Tough Hydrogels with Robust, Long-Lasting, and Repeatable Underwater Adhesion. *Adv. Funct. Mater.* **2020**, 2009334. <https://doi.org/10.1002/adfm.202009334>.
- (258) Krogsgaard, M.; Nue, V.; Birkedal, H. Mussel-Inspired Materials: Self-Healing through Coordination Chemistry. *Chem. - A Eur. J.* **2016**, *22* (3), 844–857. <https://doi.org/10.1002/chem.201503380>.

- (259) Le Bourvellec, C.; Renard, C. M. G. C. Interactions between Polyphenols and Macromolecules: Quantification Methods and Mechanisms. *Crit. Rev. Food Sci. Nutr.* **2012**, *52* (3), 213–248. <https://doi.org/10.1080/10408398.2010.499808>.
- (260) Hausken, K. G.; Frevol, R. L.; Dowdle, K. P.; Young, A. N.; Talusig, J. M.; Holbrook, C. C.; Rubin, B. K.; Murphy, A. R. Quantitative Functionalization of the Tyrosine Residues in Silk Fibroin through an Amino-Tyrosine Intermediate. *Macromol. Chem. Phys.* **2022**, *223* (17). <https://doi.org/10.1002/macp.202200119>.
- (261) Guerriero, M.; Castaldo, R.; Silvestri, B.; Avolio, R.; Cocca, M.; Errico, M. E.; Avella, M.; Gentile, G.; Ambrogio, V. Hyper-Crosslinked Polymer Nanocomposites Containing Mesoporous Silica Nanoparticles with Enhanced Adsorption towards Polar Dyes. *Polymers (Basel)*. **2020**, *12* (6). <https://doi.org/10.3390/polym12061388>.
- (262) Appel, E. A.; Tibbitt, M. W.; Webber, M. J.; Mattix, B. A.; Veisoh, O.; Langer, R. Self-Assembled Hydrogels Utilizing Polymer-Nanoparticle Interactions. *Nat. Commun.* **2015**, *6* (1), 1–9. <https://doi.org/10.1038/ncomms7295>.
- (263) Kostina, N. Y.; Sharifi, S.; De Los Santos Pereira, A.; Michálek, J.; Grijpma, D. W.; Rodriguez-Emmenegger, C. Novel Antifouling Self-Healing Poly(Carboxybetaine Methacrylamide-Co-HEMA) Nanocomposite Hydrogels with Superior Mechanical Properties. *J. Mater. Chem. B* **2013**, *1* (41), 5644–5650. <https://doi.org/10.1039/c3tb20704h>.
- (264) Byette, F.; Bouchard, F.; Pellerin, C.; Paquin, J.; Marcotte, I.; Mateescu, M. A. Cell-Culture Compatible Silk Fibroin Scaffolds Concomitantly Patterned by Freezing Conditions and Salt Concentration. *Polym. Bull.* **2011**, *67* (1), 159–175. <https://doi.org/10.1007/s00289-010-0438-z>.
- (265) Kowalski, G.; Kijowska, K.; Witzak, M.; Kuterasiński, L.; Lukasiewicz, M. Synthesis and Effect of Structure on Swelling Properties of Hydrogels Based on High Methylated Pectin and Acrylic Polymers. *Polymers (Basel)*. **2019**, *11* (1), 114. <https://doi.org/10.3390/polym11010114>.
- (266) Jones, E. M.; Cochrane, C. A.; Percival, S. L. The Effect of PH on the Extracellular Matrix and Biofilms. *Adv. Wound Care* **2015**, *4* (7), 431–439. <https://doi.org/10.1089/wound.2014.0538>.
- (267) Lambers, H.; Piessens, S.; Bloem, A.; Pronk, H.; Finkel, P. Natural Skin Surface PH Is on Average below 5, Which Is Beneficial for Its Resident Flora. *Int. J. Cosmet. Sci.* **2006**, *28* (5), 359–370. <https://doi.org/10.1111/j.1467-2494.2006.00344.x>.
- (268) Wallace, L. A.; Gwynne, L.; Jenkins, T. Challenges and Opportunities of PH in Chronic Wounds. *Ther. Deliv.* **2019**, *10* (11), 719–735. <https://doi.org/10.4155/tde-2019-0066>.
- (269) Percival, S. L.; McCarty, S.; Hunt, J. A.; Woods, E. J. The Effects of PH on Wound Healing, Biofilms, and Antimicrobial Efficacy. *Wound Repair Regen.* **2014**, *22* (2), 174–186. <https://doi.org/10.1111/wrr.12125>.
- (270) Banerjee, I.; Mishra, D.; Das, T.; Maiti, T. K. Wound PH-Responsive Sustained Release of Therapeutics from a Poly(NIPAAm-Co-AAc) Hydrogel. *J. Biomater. Sci. Polym. Ed.* **2012**, *23* (1–4), 111–132. <https://doi.org/10.1163/092050610X545049>.
- (271) Kiaee, G.; Mostafalu, P.; Samandari, M.; Sonkusale, S. A PH-Mediated

- Electronic Wound Dressing for Controlled Drug Delivery. *Adv. Healthc. Mater.* **2018**, 7 (18), 1800396. <https://doi.org/10.1002/adhm.201800396>.
- (272) Mirani, B.; Pagan, E.; Currie, B.; Siddiqui, M. A.; Hosseinzadeh, R.; Mostafalu, P.; Zhang, Y. S.; Ghahary, A.; Akbari, M. An Advanced Multifunctional Hydrogel-Based Dressing for Wound Monitoring and Drug Delivery. *Adv. Healthc. Mater.* **2017**, 6 (19), 1700718. <https://doi.org/10.1002/adhm.201700718>.
- (273) Jia, Y.; Zhang, X.; Yang, W.; Lin, C.; Tao, B.; Deng, Z.; Gao, P.; Yang, Y.; Cai, K. A PH-Responsive Hyaluronic Acid Hydrogel for Regulating the Inflammation and Remodeling of the ECM in Diabetic Wounds. *J. Mater. Chem. B* **2022**, 10 (15), 2875–2888. <https://doi.org/10.1039/d2tb00064d>.
- (274) Adepu, S.; Ramakrishna, S. Controlled Drug Delivery Systems: Current Status and Future Directions. *Molecules* **2021**, 26 (19), 5905. <https://doi.org/10.3390/molecules26195905>.
- (275) Hendi, A.; Hassan, M. U.; Elsherif, M.; Alqattan, B.; Park, S.; Yetisen, A. K.; Butt, H. Healthcare Applications of PH-Sensitive Hydrogel-Based Devices: A Review. *Int. J. Nanomedicine* **2020**, 15, 3887–3901. <https://doi.org/10.2147/IJN.S245743>.
- (276) Umuhuza, D.; Yang, F.; Long, D.; Hao, Z.; Dai, J.; Zhao, A. Strategies for Tuning the Biodegradation of Silk Fibroin-Based Materials for Tissue Engineering Applications. *ACS Biomater. Sci. Eng.* **2020**, 6 (3), 1290–1310. <https://doi.org/10.1021/acsbmaterials.9b01781>.
- (277) Mohammed, A. A.; Niamah, A. K. Identification and Antioxidant Activity of Hyaluronic Acid Extracted from Local Isolates of *Streptococcus Thermophilus*. *Mater. Today Proc.* **2022**, 60, 1523–1529. <https://doi.org/10.1016/j.matpr.2021.12.038>.
- (278) Díaz-González, M.; Rocasalbas, G.; Francesko, A.; Touriño, S.; Torres, J. L.; Tzanov, T. Inhibition of Deleterious Chronic Wound Enzymes with Plant Polyphenols. *Biocatal. Biotransformation* **2012**, 30 (1), 102–110. <https://doi.org/10.3109/10242422.2012.646676>.
- (279) Rocasalbas, G.; Touriño, S.; Torres, J. L.; Tzanov, T. A New Approach to Produce Plant Antioxidant-Loaded Chitosan for Modulating Proteolytic Environment and Bacterial Growth. *J. Mater. Chem. B* **2013**, 1 (9), 1241–1248. <https://doi.org/10.1039/c2tb00239f>.
- (280) Kim, Y. J.; Uyama, H.; Kobayashi, S. Inhibition Effects of (+)-Catechin-Aldehyde Polycondensates on Proteinases Causing Proteolytic Degradation of Extracellular Matrix. *Biochem. Biophys. Res. Commun.* **2004**, 320 (1), 256–261. <https://doi.org/10.1016/J.BBRC.2004.05.163>.
- (281) Monika, P.; Chandraprabha, M. N.; Murthy, K. N. C.; Rangarajan, A.; Waiker, P. V.; Sathish, M. Human Primary Chronic Wound Derived Fibroblasts Demonstrate Differential Pattern in Expression of Fibroblast Specific Markers, Cell Cycle Arrest and Reduced Proliferation. *Exp. Mol. Pathol.* **2022**, 127, 104803. <https://doi.org/10.1016/j.yexmp.2022.104803>.
- (282) Pastar, I.; Stojadinovic, O.; Yin, N. C.; Ramirez, H.; Nusbaum, A. G.; Sawaya, A.; Patel, S. B.; Khalid, L.; Isseroff, R. R.; Tomic-Canic, M. Epithelialization in Wound Healing: A Comprehensive Review. *Adv. Wound Care* **2014**, 3 (7), 445–464. <https://doi.org/10.1089/wound.2013.0473>.
- (283) Hamad, A.; Khashan, K. S.; Hadi, A. Silver Nanoparticles and Silver Ions as

- Potential Antibacterial Agents. *J. Inorg. Organomet. Polym. Mater.* **2020**, *30* (12), 4811–4828. <https://doi.org/10.1007/s10904-020-01744-x>.
- (284) Sondi, I.; Salopek-Sondi, B. Silver Nanoparticles as Antimicrobial Agent: A Case Study on E. Coli as a Model for Gram-Negative Bacteria. *J. Colloid Interface Sci.* **2004**, *275* (1), 177–182. <https://doi.org/10.1016/j.jcis.2004.02.012>.
- (285) Danilczuk, M.; Lund, A.; Sadlo, J.; Yamada, H.; Michalik, J. Conduction Electron Spin Resonance of Small Silver Particles. *Spectrochim. Acta - Part A Mol. Biomol. Spectrosc.* **2006**, *63* (1), 189–191. <https://doi.org/10.1016/j.saa.2005.05.002>.
- (286) Kim, J. S.; Kuk, E.; Yu, K. N.; Kim, J. H.; Park, S. J.; Lee, H. J.; Kim, S. H.; Park, Y. K.; Park, Y. H.; Hwang, C. Y.; et al. Antimicrobial Effects of Silver Nanoparticles. *Nanomedicine Nanotechnology, Biol. Med.* **2007**, *3* (1), 95–101. <https://doi.org/10.1016/j.nano.2006.12.001>.
- (287) Richter, A. P.; Bharti, B.; Armstrong, H. B.; Brown, J. S.; Plemmons, D.; Paunov, V. N.; Stoyanov, S. D.; Velev, O. D. Synthesis and Characterization of Biodegradable Lignin Nanoparticles with Tunable Surface Properties. *Langmuir* **2016**, *32* (25), 6468–6477. <https://doi.org/10.1021/acs.langmuir.6b01088>.
- (288) Pugin, B.; Cornejo, F. A.; García, J. A.; Díaz-Vásquez, W. A.; Arenas, F. A.; Vásquez, C. C. Thiol-Mediated Reduction of *Staphylococcus Aureus* Tellurite Resistance. *Adv. Microbiol.* **2014**, *04* (04), 183–190. <https://doi.org/10.4236/aim.2014.44024>.
- (289) Liang, Y.; Liang, Y.; Zhang, H.; Guo, B. Antibacterial Biomaterials for Skin Wound Dressing. *Asian J. Pharm. Sci.* **2022**, *17* (3), 353–384. <https://doi.org/10.1016/J.AJPS.2022.01.001>.
- (290) Mao, C.; Xiang, Y.; Liu, X.; Cui, Z.; Yang, X.; Yeung, K. W. K.; Pan, H.; Wang, X.; Chu, P. K.; Wu, S. Photo-Inspired Antibacterial Activity and Wound Healing Acceleration by Hydrogel Embedded with Ag/Ag@AgCl/ZnO Nanostructures. *ACS Nano* **2017**, *11* (9), 9010–9021. <https://doi.org/10.1021/acs.nano.7b03513>.
- (291) El Khezraji, S.; Thakur, S.; Raihane, M.; López-Manchado, M. A.; Belachemi, L.; Verdejo, R.; Lahcini, M. Use of Novel Non-Toxic Bismuth Catalyst for the Preparation of Flexible Polyurethane Foam. *Polymers (Basel)*. **2021**, *13* (24), 4460. <https://doi.org/10.3390/polym13244460>.
- (292) Dhivya, S.; Padma, V. V.; Santhini, E. Wound Dressings - A Review. *BioMedicine (Netherlands)*. 2015, pp 24–28. <https://doi.org/10.7603/s40681-015-0022-9>.
- (293) Dannert, C.; Stokke, B. T.; Dias, R. S. Nanoparticle-Hydrogel Composites: From Molecular Interactions to Macroscopic Behavior. *Polymers (Basel)*. **2019**, *11* (2), 275. <https://doi.org/10.3390/POLYM11020275>.
- (294) Hodásová, L.; Morena, A. G.; Tzanov, T.; Fargas, G.; Llanes, L.; Alemán, C.; Armelin, E. 3D-Printed Polymer-Infiltrated Ceramic Network with Antibacterial Biobased Silver Nanoparticles. *ACS Appl. Bio Mater.* **2022**, *5*, 4803–4813. <https://doi.org/10.1021/acsabm.2c00509>.
- (295) Yu, O.; Kim, K. H. Lignin to Materials: A Focused Review on Recent Novel Lignin Applications. *Appl. Sci.* **2020**, *10* (13), 4626. <https://doi.org/10.3390/app10134626>.

- (296) Hamdan, S.; Pastar, I.; Drakulich, S.; Dikici, E.; Tomic-Canic, M.; Deo, S.; Daunert, S. Nanotechnology-Driven Therapeutic Interventions in Wound Healing: Potential Uses and Applications. *ACS Cent. Sci.* **2017**, *3* (3), 163–175. <https://doi.org/10.1021/acscentsci.6b00371>.
- (297) Domínguez-Robles, J.; Cárcamo-Martínez, Á.; Stewart, S. A.; Donnelly, R. F.; Larrañeta, E.; Borrega, M. Lignin for Pharmaceutical and Biomedical Applications – Could This Become a Reality? *Sustain. Chem. Pharm.* **2020**, *18*, 2352–5541. <https://doi.org/10.1016/j.scp.2020.100320>.
- (298) Foulkes, R.; Man, E.; Thind, J.; Yeung, S.; Joy, A.; Hoskins, C. The Regulation of Nanomaterials and Nanomedicines for Clinical Application: Current and Future Perspectives. *Biomater. Sci.* **2020**, *8* (17), 4653–4664. <https://doi.org/10.1039/d0bm00558d>.
- (299) Calvo-Flores, F. G.; Dobado, J. A. Lignin as Renewable Raw Material. *ChemSusChem* **2010**, *3* (11), 1227–1235. <https://doi.org/10.1002/cssc.201000157>.
- (300) Liang, Y.; Li, Z.; Huang, Y.; Yu, R.; Guo, B. Dual-Dynamic-Bond Cross-Linked Antibacterial Adhesive Hydrogel Sealants with On-Demand Removability for Post-Wound-Closure and Infected Wound Healing. *ACS Nano* **2021**, *15* (4), 7078–7093. <https://doi.org/10.1021/acsnano.1c00204>.

Annex

Annex

Supplementary information of Chapter 1

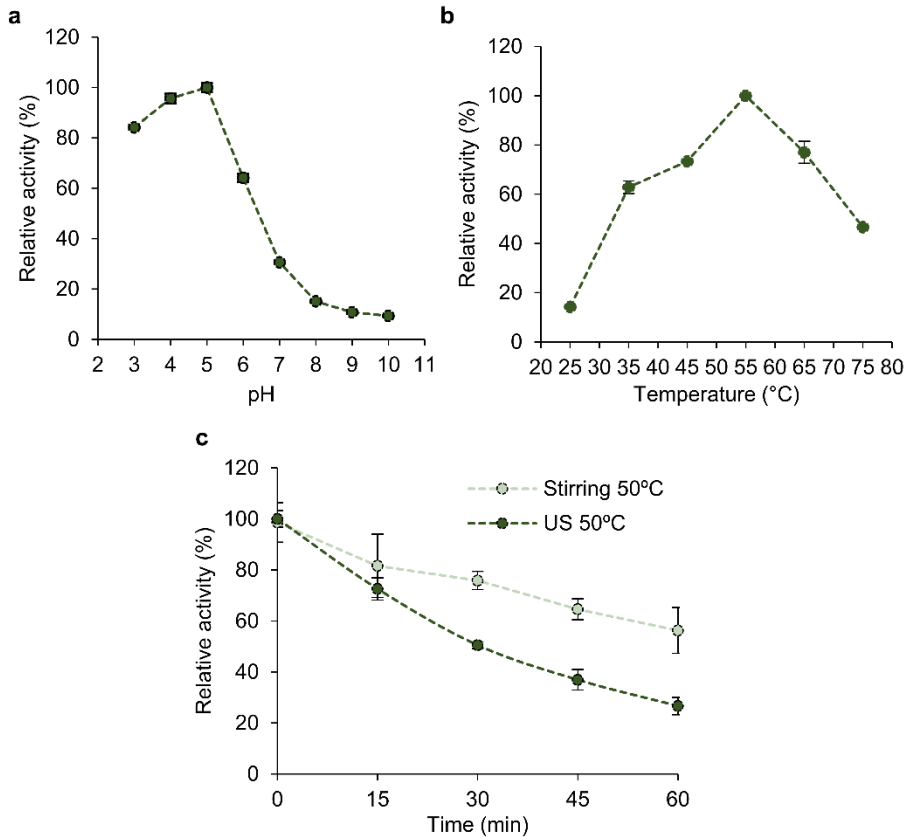


Figure S1. Relative activity of laccase (a) at different pH, (b) at different temperature, and (c) enzyme stability of laccase under 250 rpm stirring at 50 °C and under 50% amplitude ultrasound at 50 °C. The enzymatic activity of laccase was determined using ABTS as a substrate.

Table S1 Stability of PheLigNPs and LigNPs assessed by measuring the hydrodynamic size, PDI, and ζ -potential after 6 months of storage at 4 °C

	Hydrodynamic size (nm)	PDI	ζ -potential (mV)
PheLigNPs	300.1	0.271	-32.6 ± 0.6
LigNPs	282.5	0.255	-31.2 ± 0.5

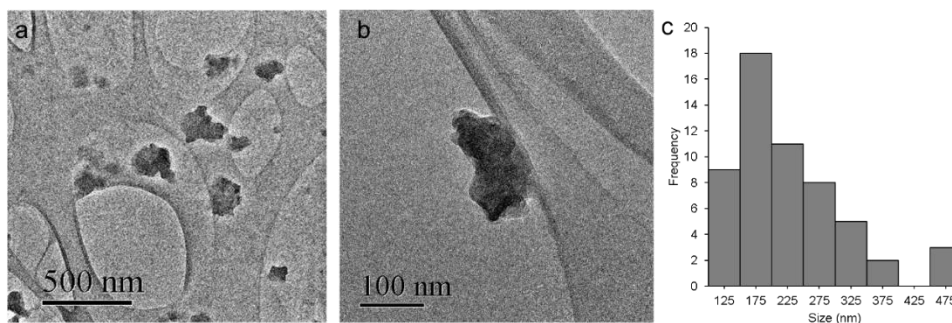


Figure S2. TEM images of LigNPs at (a) 6000X and (b) 30000X magnification and (c) size distribution of the particles.

Table S2 Signal assignments and peak ratio of lignin samples in the FTIR spectra

Assignments	Band (cm ⁻¹)	A_x/A_{2090} ratio			
		Lignin	PheLigNPs	LigNPs	PheLig
Phenolic and aliphatic O-H stretching	3280	0.40	3.02	1.70	2.61
C-H stretching in aromatic methoxyl groups	2920	1.00	1.00	1.00	1.00
Phenolic hydroxyl groups	1366	0.58	1.62	0.44	0.56
Aromatic C-H out of plane bending	922	0.2	1.40	0.17	0.24
Aromatic C-H out of plane flexural vibration	761	0.84	1.90	0.02	0.85

Table S3 Ratio of SYTO 9 to propidium iodide fluorescence emissions of bacteria incubated without PheLigNPs (control bacteria) and with PheLigNPs (bacteria + PheLigNPs) for 24 h.

	Control bacteria	Bacteria + PheLigNPs
<i>S. aureus</i>	34.8 ± 6.3	0.9 ± 0.3
<i>B. cereus</i>	7.8 ± 0.5	1.7 ± 0.2
<i>P. aeruginosa</i>	3.4 ± 0.4	1.1 ± 0.1
<i>E. coli</i>	8.4 ± 0.5	1.7 ± 0.2

Supplementary information of Chapter 2

Table S4 Storage modulus (G'), loss modulus (G'') and damping factor ($\tan \delta$) values at 1 % shear strain of different hydrogel formulations and polymer mixtures (controls)

Hydrogel sample	G' (Pa)	G'' (Pa)	$\tan \delta$
HA-SH, SF, PheLigNPs_1.5%_20	102.13	12.70	0.124
HA-SH, SF, PheLigNPs_1.5%_10	77.68	13.84	0.178
HA-SH, SF, PheLigNPs_1.5%_5	59.68	12.63	0.212
Control 1.5 % (HA-SH, SF)	8.6	3.32	0.385
HA-SH, SF, PheLigNPs_1.0%_20	66.70	9.67	0.145
HA-SH, SF, PheLigNPs_1.0%_10	34.73	5.82	0.168
HA-SH, SF, PheLigNPs_1.0%_5	30.34	5.92	0.195
Control 1.0 % (HA-SH, SF)	4.65	2.05	0.442

Table S5 Flow point or shear strain value (%) at which the hydrogel does not follow a gel-like behavior ($G' < G''$)

Hydrogel sample	Flow point (%)
HA-SH, SF, PheLigNPs_1.5%_20	564
HA-SH, SF, PheLigNPs_1.5%_10	917
HA-SH, SF, PheLigNPs_1.5%_5	149
HA-SH, SF, PheLigNPs_1.0%_20	917
HA-SH, SF, PheLigNPs_1.0%_10	1490
HA-SH, SF, PheLigNPs_1.0%_5	1900

Table S6 Viscosity values of hydrogels at 0.1 s⁻¹ and 1.0 s⁻¹ shear rate

Hydrogel sample	Viscosity (Pa·s) at 0.1 s ⁻¹	Viscosity (Pa·s) at 1.0 s ⁻¹
HA-SH, SF, PheLigNPs_1.5%_20	1552.2	88.3
HA-SH, SF, PheLigNPs_1.5%_10	812.3	49.9
HA-SH, SF, PheLigNPs_1.5%_5	321.9	35.8
HA-SH, SF, PheLigNPs_1.0%_20	798.7	64.0
HA-SH, SF, PheLigNPs_1.0%_10	658.5	46.4
HA-SH, SF, PheLigNPs_1.0%_5	445.7	31.5

Table S7 Statistical significance of the MPO and MMPs inhibition capacity of the hydrogels assessed using a multiple comparison one-way ANOVA followed by Dunnett's post-hoc test

	Mean difference	95 % confidence interval	Significant	Adjusted p-value
MPO inhibition				
Control vs. 1.5%_20	- 32.24	-42.97 to -21.52	Yes (****)	<0.0001
Control vs. 1.5%_10	-19.78	-29.66 to -9.906	Yes (****)	<0.0001
Control vs. 1.5%_5	-6.261	-16.14 to 3.618	No (ns) ^a	0.3662
Control vs. 1.0%_20	-34.48	-44.87 to -24.09	Yes (****)	<0.0001
Control vs. 1.0%_10	-28.48	-38.59 to -18.37	Yes (****)	<0.0001
Control vs. 1.0%_5	-22.86	-33.59 to -12.13	Yes (****)	<0.0001
MMPs inhibition				
Control vs. 1.5%_20	-36.46	-48.07 to -24.84	Yes (****)	<0.0001
Control vs. 1.5%_10	-27.34	-38.96 to -15.73	Yes (****)	<0.0001
Control vs. 1.5%_5	-22.66	-34.27 to -11.04	Yes (***)	0.0001
Control vs. 1.0%_20	-51.56	-63.18 to -39.95	Yes (****)	<0.0001
Control vs. 1.0%_10	-36.72	-48.33 to -25.10	Yes (****)	<0.0001
Control vs. 1.0%_5	-25.26	-36.88 to -13.64	Yes (****)	<0.0001

^ans = not significant

Scientific contribution

Peer reviewed publications

Recupido F, Lama G C, Ammendola M, De Luca Bossa F, Minigher A, Campaner P, **Morena A G**, Tzanov T, Ornelas M, Barros A, Gomes F, Bouça V, Malgueiro R, Sanchez M, Martinez M, Sorrentino L, Boggioni L, Perucca M, Anegalla S, Marzella R, Moimare P, Verdolotti L. Rigid enabled composite bio-based polyurethane foams: from synthesis to LCA analysis. *Polymer*, 2023, doi: 10.1016/j.polymer.2023.125674.

Morena A G, Pérez-Rafael S, Tzanov T. Lignin-Based Nanoparticles as Both Structural and Active Elements in Self-Assembling and Self-Healing Multifunctional Hydrogels for Chronic Wound Management. *Pharmaceutics*, 2022, doi: 10.3390/pharmaceutics14122658

Morena A G, Tzanov T. Antibacterial lignin-based nanoparticles and their use in composite materials. *Nanoscale Advances*, 2022, doi: 10.1039/d2na00423b

Hodásová L, **Morena A G**, Tzanov T, Fargas G, Llanes L, Alemán C, Armelin E. 3D-Printed Polymer-Infiltrated Ceramic Network with Antibacterial Biobased Silver Nanoparticles. *ACS Applied Bio Materials*, 2022, doi: 10.1021/acsabm.2c00509

Morena A G, Bassegoda A, Natan M, Jacobi G, Banin E, Tzanov T. Antibacterial Properties and Mechanisms of Action of Sonoenzymatically Synthesized Lignin-Based Nanoparticles. *ACS Applied Materials & Interfaces*, 2022, doi: 10.1021/acsami.2c05443

Morena A G, Bassegoda A, Hoyo J, Tzanov T. Hybrid Tellurium–Lignin Nanoparticles with Enhanced Antibacterial Properties, *ACS Applied Materials & Interfaces*, 2021, doi: 10.1021/acsami.0c22301

Morena A G, Stefanov I, Ivanova K, Pérez-Rafael S, Sánchez-Soto M, Tzanov T. Antibacterial Polyurethane Foams with Incorporated Lignin-Capped Silver

Nanoparticles for Chronic Wound Treatment. *Industrial and Engineering Chemistry Research*, 2020, doi: 10.1021/acs.iecr.9b06362

Book chapters

Morena A G, Ferreres G, Ivanova K, Pérez-Rafael S, Tzanov T, Antimicrobial Lightweight Materials and Components, in “Advanced Lightweight Multifunctional Materials” edited by Costa P, Costa C, and Lanceros-Mendez S, ISBN: 978-0-12-818501-8, Elsevier, 2020, 469-502.

Patents

Pérez Rafael S., Ivanova K., Ferreres Cabanes G., Morena A. G., Tzanov T. EP20383150.8 (2020). Method to produce in situ self-assembled multifunctional nanocomposite hydrogel and its uses thereof.

Communications to meetings

Puertas-Segura A, **Morena A G**, Pérez-Rafael S, Ciardelli G, Tzanov T (2022, November). Antimicrobial and antifouling nano-enabled hydrogel coating built on urinary catheters using a bottom up enzymatic approach. Oral communication presented at The European Summit of Industrial Biotechnology (esib 2022), Graz, Austria.

Crivello G, Orlandini G, **Morena A G**, Matu C, Boffito M, Tzanov T, Ciardelli G (2022, November). Dual-function nanoparticles enzymatically conjugated with a custom-made polyurethane hydrogel for chronic wound treatment. Oral communication presented at The European Summit of Industrial Biotechnology (esib 2022), Graz, Austria.

Morena A G, Pérez-Rafael S, Tzanov T (2022, March). Phenolated-lignin nanoparticles as crosslinking agents in nanocomposite hydrogels for biomedical applications. Oral communication presented at the 263th American Chemical Society National Meeting & Exposition, San Diego, California (USA).

Morena A G, Pérez-Rafael S, Tzanov T (2022, March). Sono-enzymatic fractioning of biomass for the production of bio-based wood adhesive. Oral communication presented at the 263th American Chemical Society National Meeting & Exposition, San Diego, California (USA).

Morena A G, Bassegoda A, Natan M, Banin E, Tzanov T (2021, December). Sono-enzymatic synthesis of phenolated lignin nanoparticles with antibacterial properties. Oral communication presented at Pacifichem (The International Chemical Congress of Pacific Basin Societies), virtual.

Morena A G, Bassegoda A, Hoyo J, Tzanov T (2020, April). Hybrid Tellurium-Lignin Nanoparticles with Enhanced Antibacterial Properties. Oral communication presented at the 259th American Chemical Society National Meeting & Exposition, virtual.

Morena A G, Stefanov I, Ivanova K, Pérez-Rafael S, Tzanov T (2019, September). Immobilized lignin-capped silver nanoparticles in a multifunctional polyurethane foam dressing for chronic wound treatment. Oral communication presented at E-MRS 2019 Fall Meeting, Warsaw, Poland.

Morena A G, Stefanov I, Tzanov T (2019, April). Antibacterial polyurethane foam with incorporated lignin-capped silver nanoparticles for chronic wound treatment. Oral communication presented at 257th ACS National Meeting, Orlando, Florida (USA).

Awards

Best student oral communication to the contribution entitled: “Antibacterial polyurethane foam with incorporated lignin-capped silver nanoparticles for chronic wound treatment” presented at the 257th ACS National Meeting, Orlando, Florida (USA), April 2019.

Selection of the article entitled “Antibacterial lignin-based nanoparticles and their use in composite materials” for inclusion in the Nanoscale Advances Popular Advances Collection 2022.